UNIVERSITÄT ZU LÜBECK

From the Institute of Biochemistry
of the University of Lübeck
Director: Prof. Dr. Dr. h.c. Rolf Hilgenfeld

Structural and biochemical characterization of chlamydial HtrA proteases

Dissertation
for Fulfillment of
Requirements
for the Doctoral Degree
of the University of Lübeck
from the Department of Natural Sciences

Submitted by
Ulrike Flügge
from Potsdam

Lübeck 2019

First referee:	PD Dr. rer. nat. Guido Hansen
Second referee:	Prof. Dr. rer. nat. Thomas Peters
Date of oral examination:	June 26$^{\text{th}}$, 2020
Approved for printing.	Lübeck, July 7$^{\text{th}}$, 2020

Declaration

I declare that I have written this dissertation completely on my own. Furthermore, I confirm that no other sources have been used than those specified in the dissertation itself. This dissertation, in same or similar form, has not been submitted to any other doctoral degree committee yet.

Lübeck,

Abstract

Protein quality control is essential for living cells to prevent accumulation of un- or misfolded proteins. Sophisticated mechanisms involving degradation and refolding have evolved to maintain cellular homeostasis. The periplasmic space of gram-negative bacteria is characterized by a special oxidizing milieu with high temperature requirement A (HtrA) proteins as key players in protein quality control. Several members of the HtrA-protein family are directly associated with infectious diseases. They promote bacterial survival under harsh conditions, bacterial invasion and processing of virulence factors. Consequently, HtrA proteins represent potential targets for antibacterial drug development.

In this thesis, the chlamydial HtrA protease from *S. negevensis* ($HtrA_{Sn}$) has been structurally and biochemically characterized. The crystal structures of the $HtrA_{Sn}$ 6- and 12-mer have been determined. $HtrA_{Sn}$, a homolog of DegP and DegQ from *E. coli*, is composed of a chymotrypsin-like serine protease domain and two N-terminal PDZ (post-synaptic density protein, disc large and zo-1 proteins) domains. PDZ domains are modular protein-interaction domains which possess the ability to specifically interact with the C-terminal residues of polypeptide chains. These domains enable self-compartmentalizing of $HtrA_{Sn}$ into an exceptional stable 6-mer *in vitro*. The presence of protease substrates induces the transformation into higher-order oligomers such as 12- or 24-mers. The 6-mer crystal structure reveals an inactive proteolytic center and is stabilized by extensive interactions of adjacent PDZ2 domains. Additional contacts of the PDZ2 to the PDZ1* and protease* domains of opposite protomers form a tightly interconnected cage which is fundamentally different from $DegP_{Ec}$ 6-mers. The structural integrity of the $HtrA_{Sn}$ 12-mer is also provided by PDZ2 interactions with the neighboring PDZ1* domain and suggests a conserved stabilization mechanism for $HtrA_{Sn}$ oligomers. The three-dimensional structure of the 12-mer displays a unique architecture among prokaryotic higher-order HtrA proteins which is mostly attributed to a different orientation and position of the PDZ2 domain. Two peptides are bound in the PDZ1 domain and in the active site. The latter is reorganized compared to the $HtrA_{Sn}$ 6-mer and enables substrate binding and cleavage. Similar to other members

of the HtrA-protein family, the proteolytic activity of $HtrA_{Sn}$ is allosterically activated by substrate binding.

$HtrA_{Ct}$, a virulence factor from *C. trachomatis*, promotes chlamydial survival in host cells during infection. $HtrA_{Ct}$ was biochemically characterized to allow for a detailed comparison to its homolog in *S. negevensis*. Interestingly, $HtrA_{Ct}$ forms many different oligomeric forms, ranging from 3- to 12-mers with diverse biochemical properties, in a concentration-dependent manner even in the absence of substrates. Whereas the $HtrA_{Ct}$ 6-mer features are comparable to the $HtrA_{Sn}$ 6-mer, the 3-mer state shows significant differences in e.g. oligomerization behaviour. As a consequence, $HtrA_{Sn}$ represents a suited model for the 6-mer oligomeric state but the complexity of the $HtrA_{Ct}$ oligomer regulation mechanism still awaits characterization.

Whereas unfolded proteins promote proteolytic activity in $HtrA_{Sn}$ and $HtrA_{Ct}$, the major outer membrane protein (MOMP) from both chlamydial species prevents substrate cleavage and has an inhibitory effect. The interaction between both proteins implies a physiological relevance which has to be further elucidated in the future.

The results of this thesis reveal crystal structures exhibiting new architectures of prokaryotic HtrA proteins. The three-dimensional models provide essential insights into the stabilization of 6- and 12-mer assemblies in chlamydial HtrAs and thus, represent a structural framework for rational development of antichlamydial compounds.

Zusammenfassung

Zelluläre Proteinqualitätskontrolle verhindert die Akkumulation von fehl- oder ungefalteten Proteinen und ist damit essentiell für das Überleben der Zelle. Verschiedene Abbau- und Rückfaltungsmechanismen haben sich entwickelt um die Homöostase der Zelle zu erhalten. Im periplasmatischen Raum von gramnegativen Bakterien tragen HtrA (high temperature requirement A)-Proteine entscheidend zu einer effektiven ATP-unabhängigen Proteinqualitätskontrolle bei. Mehrere Mitglieder der HtrA-Proteinfamilie sind direkt mit bakteriellen Infektionskrankheiten assoziiert. Sie gewährleisten das bakterielle Überleben, fördern den Eintritt in die Zelle und prozessieren Virulenzfaktoren. Dementsprechend bietet die selektive Enzyminhibition von HtrA-Proteinen eine vielversprechende Strategie zur Entwicklung antibakteriellen Medikamente.

Im Rahmen dieser Arbeit wurde die chlamydiale HtrA-Protease aus *S. negevensis* ($HtrA_{Sn}$) mittels biochemischen Analysen und Röntgenkristallographie näher untersucht. $HtrA_{Sn}$ ist ein Homolog zu den gut charakterisierten HtrA-Proteinen DegP und DegQ aus *E. coli* und verfügt über eine Chymotrypsin-artige Serinproteasedomäne und zwei N-terminale PDZ-Domänen (PDZ1 und PDZ2). PDZ-Domänen vermitteln Wechselwirkungen zwischen Proteinen und haben eine charakteristische Substratbindungsstelle, die mit den C-terminalen Aminosäureresten von Polypeptidketten interagiert. Diese Domänen ermöglichen Homooligomerisierung von $HtrA_{Sn}$ und führen dazu, dass das Protein *in vitro* als stabiles 6-mer vorliegt. Die Anwesenheit von ungefalteten Proteinen, die als Substrate für HtrA-Proteine dienen, induziert die Assemblierung von 12-mer-Komplexen. In dieser Arbeit wurden die dreidimensionalen Kristallstrukturen von $HtrA_{Sn}$ in 6- und 12-mer-Zustand erfolgreich bestimmt und die biochemischen Eigenschaften dieser Moleküle untersucht.

Das $HtrA_{Sn}$ 6-mer verfügt über ein inaktives proteolytisches Zentrum und wird durch Wechselwirkungen benachbarter PDZ2-Domänen stabilisiert. Zusätzliche Kontakte der PDZ2-Domäne mit der PDZ1*- und Proteasedomäne* des angrenzenden Protomers bilden einen eng miteinander verzahnten Komplex, welcher sich deutlich vom $DegP_{Ec}$ 6-mer unterscheidet. Die strukturelle Integrität des $HtrA_{Sn}$ 12-mers wird ebenfalls durch

Wechselwirkungen zwischen PDZ2- und benachbarter PDZ1*-Domäne gewährleistet und weist auf einen konservierten Stabilisierungmechanismus für $HtrA_{Sn}$-Oligomere hin. Die Orientierung und Position der PDZ2-Domänen variiert unter den prokaryotischen HtrA 12-mer-Proteinen und führt zu einer einzigartigen Domänenstruktur des $HtrA_{Sn}$ 12-mers. Im 12-mer sind Peptide in der PDZ1-Domäne und im katalytischen Zentrum gebunden. Letzteres ist in diesem Zustand frei zugänglich und aktiv. Die Proteaseaktivität von $HtrA_{Sn}$ wird ähnlich wie bei anderen HtrA-Proteinen allosterisch durch Substratbindung aktiviert.
Die homologe chlamydiale Protease aus *C. trachomatis* $HtrA_{Ct}$ wurde im Hinblick auf Gemeinsamkeiten und Unterschiede mit $HtrA_{Sn}$ biochemisch charakterisiert. $HtrA_{Ct}$ ist ein Virulenzfaktor, welcher essentiell für das Überleben des Bakteriums innerhalb der Wirtszelle ist. Im Gegensatz zu $HtrA_{Sn}$ bildet $HtrA_{Ct}$ konzentrationsabhängig verschiedene oligomere Komplexe auch in Abwesenheit von Substrat. Die biochemischen Eigenschaften unterscheiden sich, abhängig von der vorliegenden oligomeren Form des $HtrA_{Ct}$. Während sich das $HtrA_{Ct}$ 6-mer ähnlich verhält wie das $HtrA_{Sn}$ 6-mer, weisen die Trimere signifikante Unterschiede auf. Demnach ist das $HtrA_{Sn}$ 6-mer ein geeignetes Model für das $HtrA_{Ct}$ 6-mer. Die komplexen Regulationsmechanismen, die die Oligomerisierung des $HtrA_{Ct}$ steuern sind jedoch noch nicht vollständig verstanden.
Während ungefaltete Proteine die Geschwindigkeit der Proteaseaktivität von $HtrA_{Sn}$ und $HtrA_{Ct}$ positiv beeinflussen, verhindert MOMP (major outer membrane protein) die Substratspaltung und wirkt inhibierend. Diese Interaktionen zwischen MOMP und HtrA-Proteinen weisen auf eine physiologische Bedeutung hin, welche in der Zukunft genauer untersucht werden muss.
Die Ergebnisse dieser Arbeit umfassen die biochemische Charakterisierung von den chlamydialen HtrA-Proteinen $HtrA_{Sn}$ und $HtrA_{Ct}$, die eine einzigartige Domänenarchitektur aufweisen, was anhand der Kristallstrukturen gezeigt werden konnte. Diese liefern neue Einblicke in die Stabilisierungsmechanismen von 6- und 12-meren chlamydialen HtrA-Proteinen und deren Funktionsweise, und können folglich der rationalen Entwicklung antichlamydialer Therapeutika dienen.

Contents

1 Introduction **1**
1.1 *Chlamydiae* . . . 1
1.1.1 Incidence and Taxonomy . . . 1
1.1.2 Epidemiology of Chlamydia . . . 2
1.1.3 Pathogenesis of *C. trachomatis* . . . 3
1.1.4 Pathogenesis of *S. negevensis* . . . 6
1.2 High-temperature requirement protein A (HtrA) . . . 7
1.2.1 DegS - protease in σ^E stress response pathways . . . 8
1.2.2 DegP - a self-compartmentalizing protease . . . 10
1.2.3 DegQ - a periplasmic DegP homolog . . . 13
1.2.3.1 DegQ from *E. coli* . . . 13
1.2.3.2 DegQ from *Legionella* . . . 14
1.2.4 $HtrA_{Ct}$ . . . 14
1.2.5 HtrAs as virulence factors . . . 16
1.3 MOMP of *C. trachomatis* . . . 17
1.4 Objectives . . . 18

2 Material and Methods **21**
2.1 Material . . . 21
2.1.1 Equipment . . . 21
2.1.2 Chemicals . . . 23
2.1.3 Bacteria cells and DNA constructs . . . 25
2.2 Methods . . . 27
2.2.1 Cloning . . . 27
2.2.2 Mutagenesis . . . 27
2.2.3 Recombinant protein production . . . 28
2.2.4 Purification . . . 28
2.2.4.1 Cell lysis for purification of soluble proteins . . . 28
2.2.4.2 Cell lysis and membrane preparation for insoluble proteins 29
2.2.4.3 Membrane solubilization by detergents . . . 29
2.2.4.4 Histidine-tagged protein purification . . . 29
2.2.4.5 Maltose-binding protein-tagged protein purification . . 29
2.2.4.6 Size-exclusion chromatography (SEC) . . . 30
2.2.4.7 Preparative SEC . . . 30
2.2.4.8 Analytical SEC . . . 30
2.2.4.9 Ion exchange chromatography . . . 31
2.2.4.10 Protein purification under denaturing conditions . . . 33
2.2.4.11 Protein concentration determination . . . 34

2.2.5 Protein characterization . . . 34
2.2.5.1 SDS-PAGE . . . 34
2.2.5.2 Native PAGE . . . 35
2.2.6 Dynamic light scattering . . . 35
2.2.7 Circular Dichroism . . . 35
2.2.8 Thermal shift assay . . . 36
2.2.9 Fluorescence-based protein activity assay . . . 36
2.2.10 Small-angle X-ray scattering . . . 38
2.2.11 Crystallization, crystal optimization, diffraction data collection, structure determination, refinement and validation . . . 39

3 Results **41**
3.1 High-temperature requirement A protein from *S. negevensis* . . . 41
3.1.1 Purification of $HtrA_{Sn}$ . . . 41
3.1.2 Biochemical characterization of $HtrA_{Sn}$ . . . 43
3.1.2.1 Proteolytic activity of $HtrA_{Sn}$ . . . 43
3.1.2.2 Oligomerization behaviour of $HtrA_{Sn}$ . . . 46
3.1.2.3 Temperature dependency of $HtrA_{Sn}$ . . . 49
3.2 Crystallization and structure elucidation of $HtrA_{Sn}$ . . . 51
3.2.1 Optimization of the crystallization condition of the $HtrA_{Sn}$ 6-mer and 12-mer and structure elucidation . . . 51
3.2.2 Crystal structure model of $HtrA_{Sn}$ 6-mer . . . 53
3.2.3 Crystal structure of $HtrA_{Sn}$ 12-mer . . . 55
3.2.4 Comparison between the $HtrA_{Sn}$ 6-mer and 12-mer crystal structures . . . 59
3.2.4.1 LA loop . . . 59
3.2.4.2 LB loop . . . 62
3.2.4.3 LC loop . . . 63
3.2.4.4 LD loop . . . 64
3.2.4.5 LE Loop . . . 64
3.2.4.6 L1 loop . . . 65
3.2.4.7 L2 loop . . . 66
3.2.4.8 L3 loop . . . 67
3.2.5 AAC of $HtrA_{Sn}$ . . . 68
3.2.6 The interaction between Q290 and F477 stabilizes cages . . . 69
3.2.7 $HtrA_{Sn}$ 6- and 12-mer crystal structures reveal a unique architecture . . . 73
3.2.8 SAXS . . . 80
3.3 HtrA from *C. trachomatis* - $HtrA_{Ct}$ . . . 83
3.3.1 Purification of $HtrA_{Ct}$ . . . 83
3.3.2 Biochemical characterization of $HtrA_{Ct}$ . . . 85
3.3.2.1 Proteolytic activity of $HtrA_{Ct}$ . . . 85
3.3.2.2 Oligomerization behaviour of $HtrA_{Ct}$ . . . 88
3.3.2.3 Temperature dependency . . . 90
3.3.2.4 Crystallization of $HtrA_{Ct}$ . . . 92
3.3.2.5 SAXS . . . 93

3.4 Interactions between major outer membrane proteins (MOMPs) and HtrA 96
3.4.1 Purification of $MOMP_{Sn}$-MBP 96
3.4.2 Biochemical characterization of interactions between MOMP-MBP and HtrA 97
3.4.3 Purification of $MOMP_{Sn}$ and $MOMP_{Ct}$ 100
3.4.4 Biochemical characterization of interactions between MOMP-His_6 and HtrA 100

4 Discussion **103**
4.1 $HtrA_{Sn}$ - a self-compartimentizing protease 103
4.1.1 The importance of the PDZ2-PDZ1* interface in oligomer stabilization of HtrA proteins 106
4.1.2 The importance of the regulatory LA-loop in $HtrA_{Sn}$ 109
4.1.3 $HtrA_{Sn}$ reveals a unique architecture 110
4.1.4 $HtrA_{Ct}$ - a virulence factor with many faces 112
4.2 Interactions between chlamydial HtrA proteins and MOMPs 114
4.3 Concluding remarks and future perspectives 115

Appendix **117**

List of Figures **126**

List of Tables **128**

Abbreviations **129**

Bibliography **131**

Curriculum vitae **147**

Acknowledgements **149**

1 Introduction

1.1 *Chlamydiae*

The term «Chlamydia» was first used by Halberstaedter and Prowazek in 1907 (Halberstadter & Prowazek, 1907). Both scientists were members of an expedition to Java to study possible syphilis treatments. They used conjunctival scrapings of trachoma patients to infect orangutans which developed granulomas in their conjunctiva. Microscopic analysis showed intracytoplasmic inclusions consisting of numerous small particles. The scientists referred to these particles as «Chlamydozoa» from the Greek word for mantle (Pospischil, 2009). In 1932, Bedson and his co-worker Bland discovered and described for the first time the intracellular biphasic life-cycle of *Chlamydiae* (Bedson & Bland, 1932). On account of the small size, the infectious agent was called «trachoma virus» (Wang, 1999) until newer cell culture methods enabled identification of ribosomes and cell membranes, and thus, it was classified as a prokaryote. In 1971, the taxonomic order *Chlamydiales* was established (Storz & Page, 1971).

1.1.1 Incidence and Taxonomy

Chlamydiae are obligate intracellular gram-negative bacteria with a wide host range. Chlamydial and chlamydial-like infections have been described for humans, various bird species, rodents, koala, cats, cattle, sheep, horses, amphibian, reptiles, amoebae and arthropods (Vanrompay et al., 1993; Cislakova et al., 2004; Augustine, 1998; Regan et al., 1979; Borel et al., 2006; Longbottom et al., 1998; Theegarten et al., 2008; Berger et al., 1999; Soldati et al., 2004; Michel et al., 2005; Cislakova et al., 2004; Corsaro & Greub, 2006). Zoonosis can occur sporadically for *C. psittaci* (Petrovay & Balla, 2008) and *C. abortus* (Baud & Greub, 2011) but the infections are usually caused by human-to-human transmission.
A phylogenetic tree constructed from 16S and 23S rRNA sequences together with protein sequences of 424 core proteins revealed five families of the *Chlamydiales* or-

der: *Chlamydiaceae*, *Parachlamydiaceae*, *Waddliaceae*, *Simkaniaceae* and *Criblamydiaceae* (Pillonel et al., 2015). The latter four are mostly found in amoebae, however *Parachlamydiaceae*, *Waddliaceae* and *Simkaniaceae* are proposed to be emerging human pathogens (Corsaro & Greub, 2006). Bacteria belonging to the *Chlamydiaceae* family include animal and human pathogens which can be further classified in biovars and serotypes.

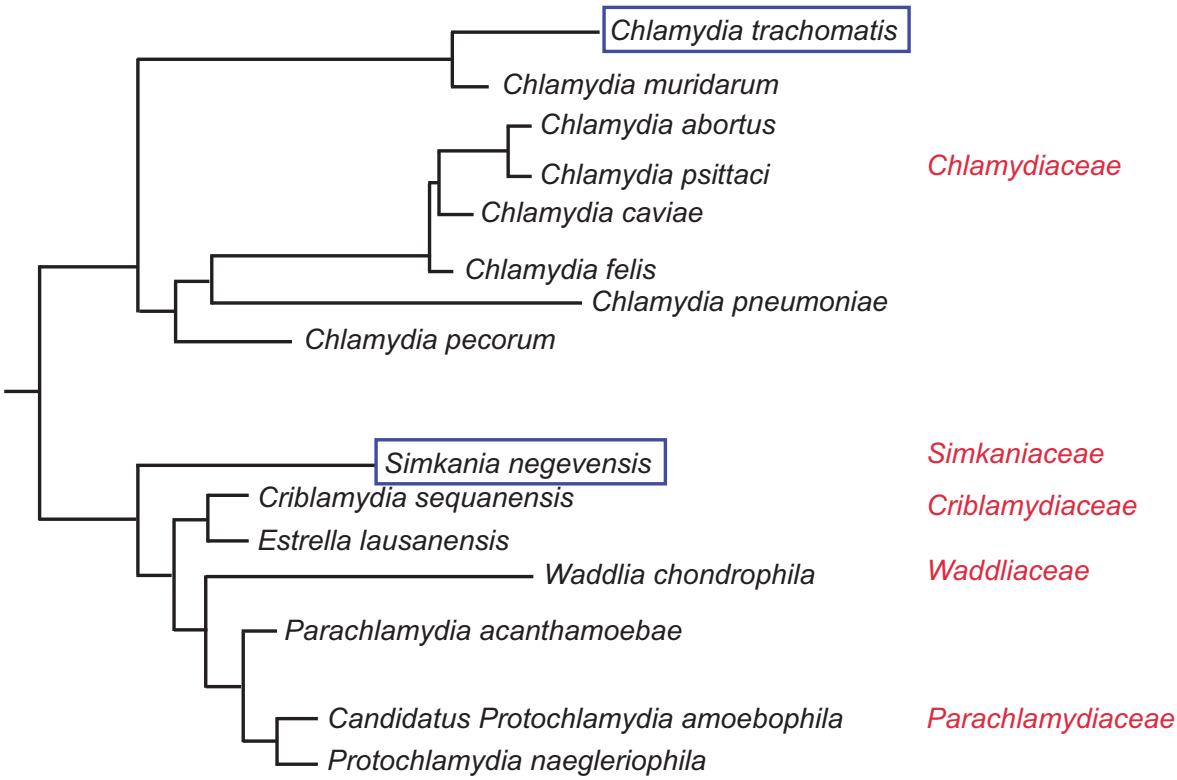

Figure 1.1: Phylogenetic tree of the *Chlamydiales* order based on 16S and 23S rRNA sequence and averaged identity of core genes. The five families are highlighted in red. Proteins of the blue bordered species are discussed in this study (modified from Pillonel et al., 2015).

1.1.2 Epidemiology of Chlamydia

The *Chlamydiaceae* family includes the human pathogens *C. trachomatis*, *C. pneumoniae* and *C. psittaci*.

C. trachomatis is the most commonly diagnosed sexually transmitted pathogen which leads to severe genital and ocular infections. Serotyping based on immunological analysis of the major outer membrane protein (MOMP)(Schaeffer & Henrich, 2008) of *C. trachomatis* reveals more than 20 serovars (Wang & Grayston, 1991; Dean et al., 2000) at present. Serovars A-C cause trachoma which can result in corneal opacity and blind-

ness by various re-infections (Mabey et al., 2003). Serovars D-K are etiological agents of oculo-genital infections. They usually are non-invasive (Schaeffer & Henrich, 2008) which means the bacteria remain in the mucosal epithelial cells. The infection often proceeds without symptoms and is thereby left untreated. For women, this can lead to pelvic inflammatory disease, chronic pelvic pain, ectopic pregnancy and preterm delivery. Complications for men result in epididymitis (and possible infertility), Reiter's syndrome or proctitis (Weir, 2004).
The serovars L1-L3 cause systemic infections leading to lymphogranuloma venerum (LGV). In Africa, South East Asia, South America, and the Caribbean (Thomson et al., 2008) these serovars occur often and can lead to critical conditions like chronic lymphangitis, genital elephantiasis and perirectal abscesses, anal fistulas and strictures when untreated (O'Byrne et al., 2016). The incidence of LGV in industrialized countries is low and so far restricted to homosexual men (Thomson et al., 2008).
C. pneumoniae is a common etiological agent of respiratory and cardiovascular tract infections. Besides bronchitis and pneumonia, it is linked to asthma, chronic obstructive pulmonary disease (COPD), atherosclerosis and even Alzheimer's disease, as several brain cell types serve as host cells for chlamydial infection (Belland et al., 2004; Choroszy-Król et al., 2014; Cosentini et al., 2008; Gérard et al., 2006).
The causative agent of human and avian psittacosis, *C. psittaci*, is transmitted to humans by zoonosis. It leads to severe influenza-like symptoms accompanied by pneumonia and in severe cases by encephalitis (Harkinezhad et al., 2009). Studies reveal that *C. psittaci* infection has been associated with ocular lymphoma (Ferreri et al., 2004).
Simkania negevensis has been associated with pneumonia and bronchiolitis (Vouga et al., 2017). Its importance as potential new human pathogen is still under discussion as new studies show a low human prevalence (Vouga et al., 2018). However, further evaluation of its implication may provide new insights into the biology of the *Chlamydiales* order.

1.1.3 Pathogenesis of *C. trachomatis*

A typical characteristic of *Chlamydiae* is a biphasic developmental cycle which they undergo during infection. They convert between two morphologically and functionally distinct forms: the highly infectious, metabolically inactive elementary bodies (EBs) and the noninfectious metabolically active reticulate bodies (RBs) (Bastidas et al., 2013). Using the example of *C. trachomatis*, the life cycle exhibits the following stages (Cocchiaro & Valdivia, 2009): (I) attachment of EBs and internalization into the host

cell; (II) transition from EBs to RBs; (III) parasitophorous vacoule (inclusion) remodelling and bacterial replication; (IV) inclusion growth and redifferentiation from RBs to EBs and (V) EBs release from host cell and infection of new target cells.

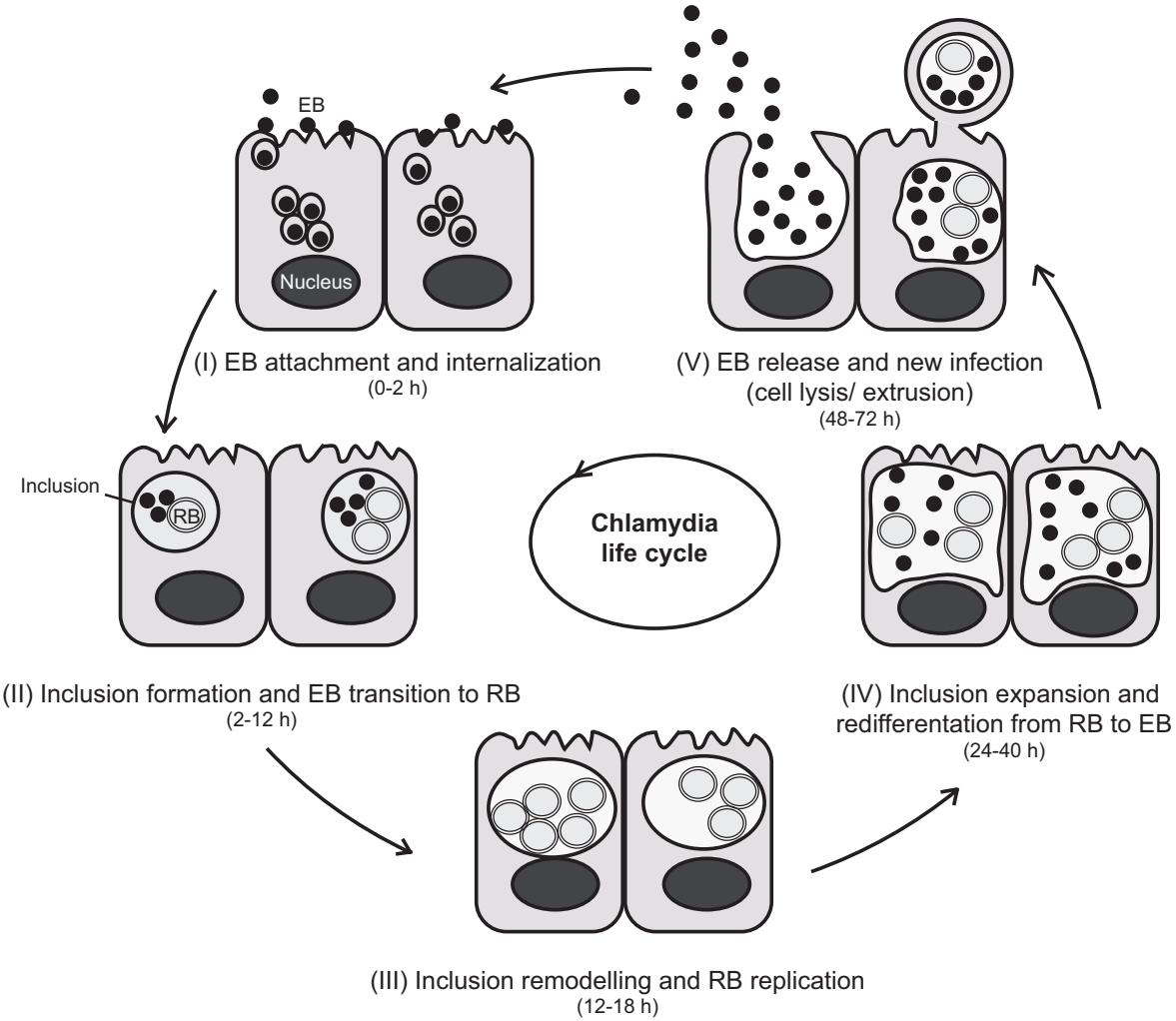

Figure 1.2: Life cycle of *C. trachomatis*. EBs penetrate epithel cells and after internalization an inclusion is formed. EBs differentiate into RBs which immediately start with replication. The inclusion expands and is remodelled by bacterial proteins. Between 18-24 hours postinternalization, RBs peak in numbers and start to transition back in EBs. EBs exit the cell by lysis or extrusion and start a new infection cycle.(modified from Bastidas et al., 2013)

Chlamydiae are able to invade most cultured cells suggesting multiple entry pathways using ubiquitous receptors. Various bacterial adhesins like MOMP, OmcB and PmpD (Su et al., 1996; Fadel & Eley, 2007; Swanson et al., 2009) have been proposed depending on host-cell type and chlamydial species (Dautry-Varsat et al., 2005). As possible host-cell receptors and ligands heparan sulfate, mannose receptor, mannose-6-receptor, estrogen receptor and platelet-derived growth factor receptor have been described (Cocchiaro & Valdivia, 2009). Attachment occurs in a two-step process in-

volving initial reversible electrostatic interactions between glycans on the EBs and host cell glycosaminoglycans (Menozzi et al., 2002), followed by irreversible binding to the host-cell surface by specific receptors (Bastidas et al., 2013). Additionally, a protein disulfide-isomerase (PDI) exposed on the host-cell surface is required for EBs bacterial entry. The EB outer membrane consists of a mesh of cysteine-rich proteins which form a disulfide cross-linked polymer layer providing osmotic stability and rigidity (Huang et al., 2010). The bacterium binds to a receptor which is associated with a PDI and the oxido-reductive function of the enzyme enables internalization into the host cell (Abromaitis & Stephens, 2009). The exact mechanism of bacterial uptake remains elusive as there are controversial studies by which strategy chlamydial species may enter the cell (Dautry-Varsat et al., 2005).

EBs entry in nonphagocytic cells induces actin reorganization at the attachment site via small GTPases (Carabeo et al., 2004, 2007). Other redundant mechanisms initiated by Ct694/TmeA also seem to play a role during cytoskeleton remodelling but are still under discussion (McKuen et al., 2017).

During internalization the stable disulfide-cross-linked protein layer of the EBs is reduced, followed by a decondensation of the nucleoid and initiation of bacterial transcription. The differentiation from EBs to RBs takes place in the inclusion where RBs replicate via binary fission (Cocchiaro & Valdivia, 2009).

The inclusion membrane initially resembles the host-cell plasma membrane. During the course of the infection several components are replaced by bacterial proteins enabling the transport of the inclusion to the Golgi apparatus via microtubules (Grieshaber et al., 2003) and the interaction with numerous host-cell molecules. A subset of these are Rab GTPases which are recruited to the inclusion and allow sphingomyelin and iron acquisition by Golgi fragmentation and interference of the transferrin pathway (Rzomp et al., 2003, 2006; Ouellette & Carabeo, 2010; Rejman Lipinski et al., 2009; Heuer et al., 2009). Sphingomyelin is necessary for inclusion expansion and stability (Carabeo et al., 2003). The uptake of nutrients is enabled via vesicular and non-vesicular transport by interactions with transfer proteins (Derré et al., 2011; Elwell et al., 2011), multivesicular bodies (Beatty, 2006), lipid droplets (Kumar et al., 2006) and lysosomes (Ouellette et al., 2011) facilitating bacterial replication.

In late stages of infection, the bacterial number increases drastically leading to inclusion expansion until almost the whole cytoplasmic space is occupied. RBs redifferentiate to EBs via an unknown mechanism and after 48-72 hours the EBs exit the host cell by cell lysis or extrusion. Cell lysis is induced by cysteine proteases which disrupt the inclusion, followed by a calcium-signalling-dependent cell death. Exit by extrusion leaves the host cell with a still intact bacterial vacuole and thereby maintains the infectious state of the cell (Hybiske & Stephens, 2008).

To maintain a replicative intracellular niche, *Chlamydiae* have evolved mechanisms to evade the host-cell immune response by preventing apoptosis. The chlamydial protease-like activating factor (CPAF) hinders formyl peptide receptor 2 (FPR2)-mediated activation of polymorphonuclear leukocytes by cleavage of FPR2 (Rajeeve et al., 2018). Additionally, CPAF is able to degrade antimicrobial peptides with antichlamydial activity like LL-37 (Tang et al., 2015), and thereby ensures extracellular EB survival. Messinger et al. (2015) described an inhibition of caspase-3-induced cell death for various chlamydial species. The inclusion membrane protein »*Chlamydia* promoter of Survival« (CpoS) seems to be crucial for blocking pro-death signals (Sixt et al., 2017). In addition to direct evasion processes from the host-cell immune response there is *in vitro* evidence for a chlamydial resting state which is not replicative and not infectious and thereby a form of persistence. Persistent forms of *C. trachomatis* are characterized by relatively small inclusions with morphologically altered RBs which are known as abberant bodies induced by antibiotics, cytokines, nutrient-deprivation and other stressors (Marsh et al., 2017; Hogan et al., 2004).

1.1.4 Pathogenesis of *S. negevensis*

S. negevensis is an obligate intracellular pathogen replicating in amoebae, human epithel cells and makrophages and has been associated with infectious of the respiratory tract of humans. With 2.5 Mbp, the genome is at least two times larger than that of other *Chlamydiae* (Kahane et al., 2002). The life cycle is comparable to *C. trachomatis* with a significantly longer infection duration of 5 – 12 days (Kahane et al., 2002). Instead of a spherical vacuole, *S. negevensis* forms a continuous membrane system spanning the host cell and forming extensive contact to the endoplasmic reticulum (ER) (Herweg et al., 2016). For nutrient acquisition the retrograde transport pathway from the Golgi apparatus to the ER seems to play a crucial role (Herweg et al., 2016). In late infection stages mitochondrial fragmentation has been observed (Kozjak-Pavlovic et al., 2017) but its function for the bacterium remains elusive.
Interestingly, *S. negevensis* infected cells exhibit a strong resistance to apoptosis which could serve as pathogenic strategy to promote its long-term relationship within the host cell (Karunakaran et al., 2011). Additionally, the bacterium has no visible cytotoxicity and does not induce cell lysis to the same extend as other members of the *Chlamydiales* order (Vouga et al., 2017). Consequently, *S. negevensis* is able to persistent for a prolonged time in infected cells. Further investigations of its exact survival mechanism and pathogenicity in humans are required to provide new insights into the biology of the *Chlamydiales* order.

1.2 High-temperature requirement protein A (HtrA)

Intracellular pathogens as *Chlamydia* developed a sophisticated system of protein-quality control to promote bacterial survival under harsh conditions as elevated temperatures, low pH, osmotic or oxidative stress which lead to protein aggregation (Skórko-Glonek et al., 1999). Mis- or unfolded proteins represent a serious hazard for the bacterium and to prevent cell death the gene expression of so called heat-shock proteins (HSP) are upregulated. One important HSP family are the HtrA proteins. They were first identified in *E. coli* as indispensable survival factors at temperatures above 42 °C. Bacteria carrying an insertion mutation in their *htrA* gene did not grow at elevated temperatures (Lipinska et al., 1988). Further studies revealed a null mutant which failed to degrade proteins in the periplasmic space and was accordingly named the *degP* mutant (Strauch et al., 1989). The periplasmic space exhibits special conditions like ATP-absence and an oxidizing milieu. Thereby it is dependent on an own protein-quality control system uncoupled from the one in the cytoplasm. HtrA proteins serve as essential ATP-independent protein-quality control factors which ensure cell viability under stress conditions by exhibiting proteolytic and chaperone activity (Clausen et al., 2002). This ability promotes survival of pathogenic bacteria and as a result establishes HtrA as important virulence factor (Ingmer & Brøndsted, 2009).

HtrA proteins harbor a serine-protease domain with a highly conserved chymotrypsin fold and a catalytic triade of His-Asp-Ser and at least one C-terminal PDZ domain (post-synaptic density protein, disc large and zo-1 proteins) (Morais Cabral et al., 1996; Doyle et al., 1996; Pallen & Ponting, 1997). PDZ domains are the most common protein-protein interaction modules, built of 80–100 amino-acid residues and specialized for binding the C-terminus of target proteins (Jeleń et al., 2003). The protease domain consists of two lobes, each forms a six-stranded β-barrel and the proteolytic cleft is positioned in between. Substrate binding at the active site is mediated via β-sheet augmentation (Perona & Craik, 1995). There are eight surface loops which are labeled according to the trypsin protease nomenclature: L1-L3 and LA-LE (Perona & Craik, 1995). The L1 loop harbors the oxyanion hole whereas the L2 loop in active protease forms the S1 specificity pocket. The L3, LA and LD loops are regulatory loops transmitting signals and thereby activating the protease. The roles of the LB and LE loop are not yet clearly identified (Krojer et al., 2008b). Protease activity is promoted when the N-terminal signal peptide is cleaved (Lipinska et al., 1988).
A multitude of HtrA proteases in various species has been detected including those of microorganisms, fungi, plants, frogs, birds, fish and mammals (Clausen et al., 2011). In *E. coli*, there are three well-studied HtrA proteins which serve as model proteins

and are further highlighted in the following subsections: DegP, DegQ and DegS. They exhibit a high amino-acid sequence identity in their protease domain, but whereas DegP and DegQ contain two PDZ domains, DegS harbors only one. A distinguishing feature of DegP and DegQ is the length of their LA loop, also called Q-linker as many Gln residues are found in DegP. With 40 amino-acid residues, the Q-linker of DegP encompasses twice the size of the Q-linker of DegQ (Kim & Kim, 2005).

1.2.1 DegS - protease in σ^E stress response pathways

Stress-response pathways sensing misfolded proteins in one cellular compartment and transducing signals to another compartment prevent dangerous protein aggregation. In *E. coli* there is an extracytoplasmic stress response which is induced by high amounts of unfolded proteins in the cell envelope, especially by unfolded outer membrane porins (OMPs) (Alba et al., 2002). Under stress conditions transcription factor σ^E is activated and associates with the RNA polymerase to increase gene expression of envelope-localized chaperones, proteases and proteins for lipopolysaccharide (LPS) synthesis and transport (Rhodius et al., 2006; Dartigalongue et al., 2001). RseA and RseB are negative regulators of σ^E encoded together with the *rpoE* (σ^E gene) in a single operon (Alba et al., 2002). RseA is an inner-membrane protein with one transmembrane domain, an N-terminal cytoplasmic and a C-terminal periplasmic domain (De Las Peñas et al., 1997). In the absence of a stress signal, RseA interacts tightly with σ^E on the cytoplasmic site and with RseB in periplasmic space. Proteolytic cleavage of RseA by DegS induces the signal transduction which leads to σ^E release. Under non-stress conditions, DegS exhibits an inactive resting state and additionally, the stress response is inhibited by masking the RseA cleavage site by RseB binding (Chaba et al., 2011; Kim, 2015).

The crystal structure of DegS (Wilken et al., 2004), PDB entry:1SOT) reveals a homotrimer with a funnel-like shape exposing fully accessible proteolytic sites (Fig. 1.3). To prevent uncontrolled RseA processing, the activation of DegS is tightly regulated. The ligand-free DegS structure displays the inactive state, exhibiting a blocked oxyanion hole and S1 binding pocket. The PDZ domain stabilizes the inactive protease domain conformation by interactions with the L3 loop. Unfolded OMP initiates DegS activation by binding to the PDZ binding pocket via an C-terminal YXF motif. This leads to a rearrangement of the L3 loop by 15 Å. The amino-acid residues at the X position of the substrate (P2) interacts directly with T184 from the L3 loop inducing the conformational change. Subsequently, the LD* loop from the neighboring monomer

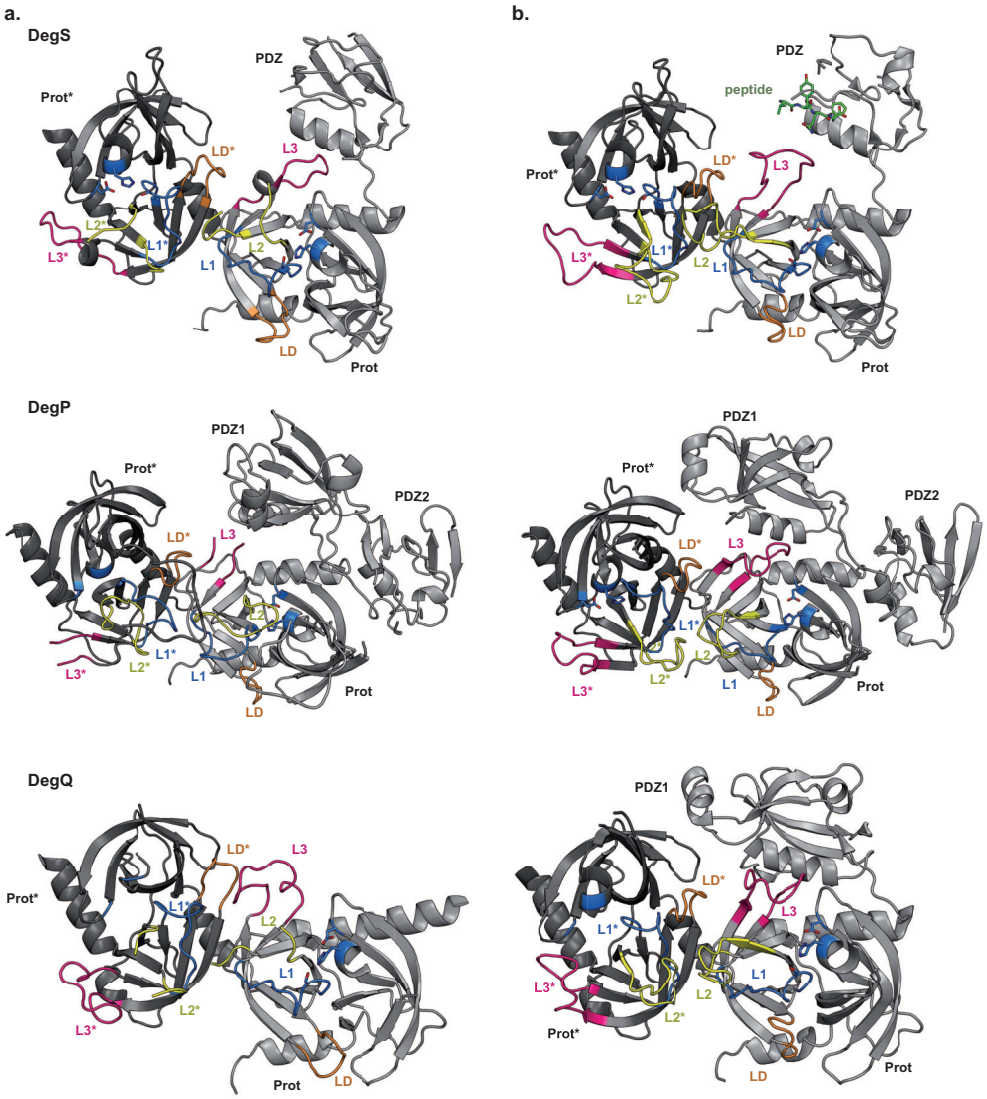

Figure 1.3: Allosteric activation cascade of *E.coli*-HtrA proteins. a) Crystal structures of DegS, DegP and DegQ in their proteolytic inactive state. In DegS and DegQ the L2 loop is too flexible to be traced whereas in DegP parts of the L3 loop are missing. One monomer with its adjacent protease domain (»Prot«) is depicted. b) Crystal structures of DegS, DegP and DegQ in their proteolytic active state. In DegS, a bound substrate in the PDZ binding cleft interacts directly with the regulatory L3 loop which is reoriented. This rearrangement leads to changes in the LD* loop of the adjacent monomer which in turn influences orientation of L2 and L1* loops. Blockade of the oxyanion hole is abolished and the S1 specificity pocket is correctly formed. In DegP and DegQ the signal transduction is initiated by re-orientation of helix $\alpha 6$ (PDZ1) which interacts with the L3 loop. Afterwards the signal is transmitted via LD* loop to L1* and L2 loop similar to DegS.

(the asterisk marks elements from the adjacent protomer in the trimer) changes its position and influences remodelling of the L2 and L1* loops thereby unblocking the oxyanion hole and the S1 specificity pocket. In contrast to other serine proteases, the

activation of DegS is a reversible process (Wilken et al., 2004).
DegS activation is the critical step in triggering the σ^E stress response. Additionally the interaction between RseB and RseA has to be disrupted. Studies showed that an increased level of LPS or LPS fragment leads to dissociation of RseB exposing the RseA cleavage site (Lima et al., 2013). After RseA cleavage by DegS, the cytoplasmic RseA domain bound to σ^E is released by RseP cleavage (Akiyama et al., 2004). This complex is further processed by cytoplasmic ATP-dependent proteases generating free σ^E (Flynn et al., 2004) and thus activating gene expression.

1.2.2 DegP - a self-compartmentalizing protease

In early biochemical studies defining proteases in *E. coli*, DegP was initially identified as protease Do, a serine protease with an unusually large molecular weight of 300-500 kDa (Swamy et al., 1983). The *degP* gene is upregulated by DegS-mediated σ^E activation of transcription (Strauch et al., 1989) or by the Cpx stress response pathway induced by protein folding stress in the periplasm of *E. coli* (Danese et al., 1995).
As an important factor for protein-quality control, DegP is responsible for maintaining periplasmic protein homeostasis by degrading un- or misfolded proteins and thereby preventing lethal aggregation. Studies also reported chaperone activity (Spiess et al., 1999) and a role in OMP biogenesis, as DegP binds to folded OMPs but does not degrade them (Krojer et al., 2008b). Current studies question the chaperone function in living cells and assume that the main function of DegP is to cleave unfolded proteins (Chang, 2016).

A special feature of DegP is the ability to form higher-order oligomers consisting of 6, 12, 15, 18 or 24 monomeric subunits (Krojer et al., 2008b; Jiang et al., 2008; Shen et al., 2009). The first crystal structure of DegP revealed a distorted 6-mer with two interlocked homotrimers arranged in a face-to-face manner (Fig. 1.4). Interactions between both 3-mers are mediated via LA loops which protrude pillar-like into the opposite 3-mer and interact with the L1* and L2* loop preventing formation of the S1 specificity pocket and blocking the entrance to the proteolytic site. The active proteolytic centers are located at the inner wall of the particle. DegP harbors two PDZ domains. Their overall fold resembles other PDZ domains but with an additional β-sheet and an α-helix which seem to be unique to PDZ domains of the HtrA family. Pores between protease and PDZ domains allow access into the cage-like particle. Consequently, the PDZ domains have the function of gate keepers (Krojer et al., 2002). The pore size limits the substrate entry and thus, regulates indirectly the proteolytic activity (Clausen et al., 2002). The self-association of DegP which leads to segregated compartments

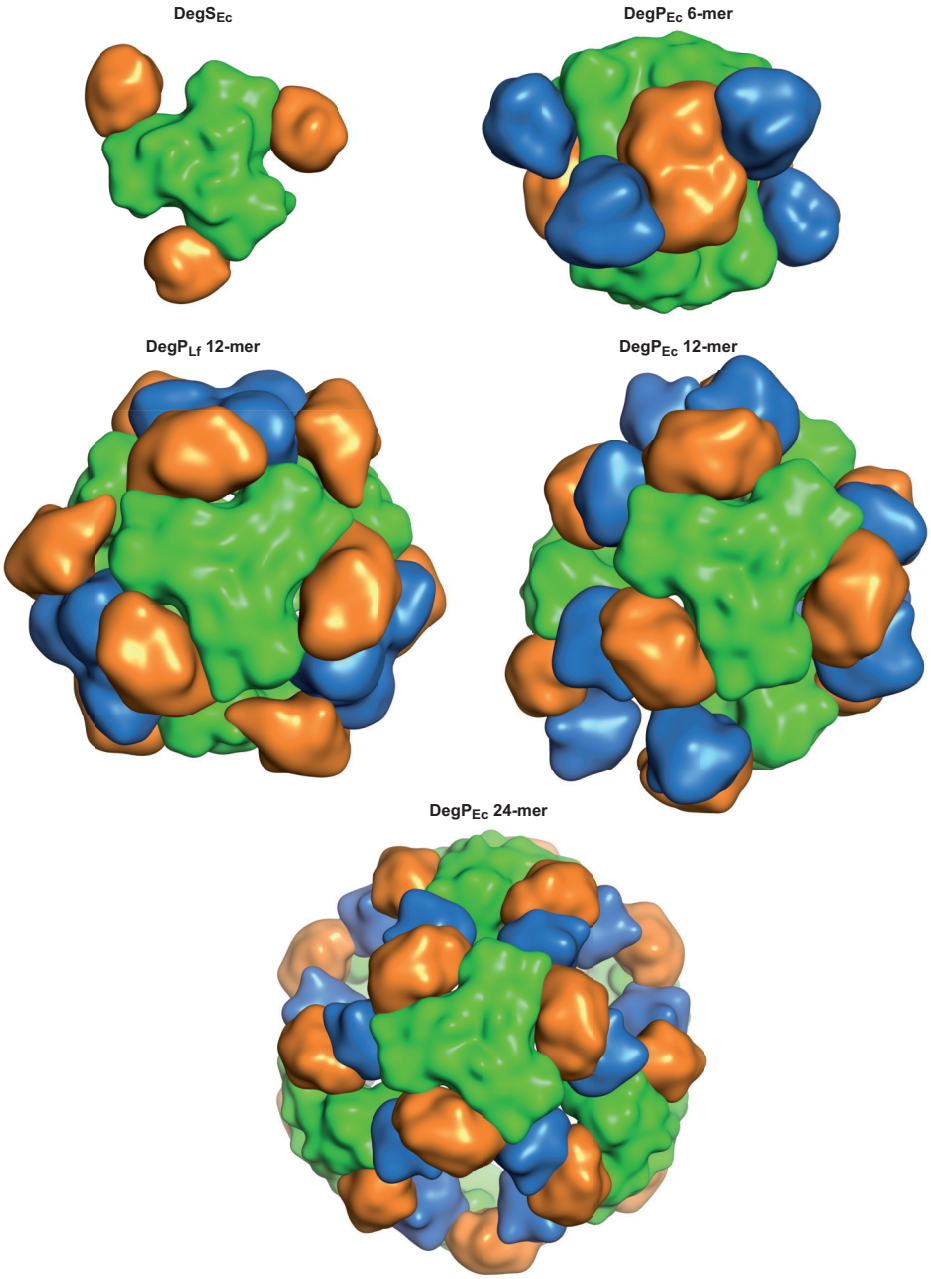

Figure 1.4: Three-dimensional crystal structures of prokaryotic HtrA proteins. The proteins are depicted in surface representation with the protease domain in green, PDZ1 in orange and PDZ2 domains in blue. The sizes of the molecules are not shown in scale in respect to each other.

with proteolytic active centers are properties of a self-compartmentalizing protease. Similar to DegS, substrate binding induces conformational changes which involve the L3, LD*, L1 and L2 loops (s. Fig.1.3). Additionally, the LA loop plays a regulatory role and inhibits proteolytic activity until reorientation of the PDZ1 domain extracts

it from the active site (Krojer et al., 2008b). Upon substrate binding, DegP assembles into higher order oligomers (12-/24-mers) (Krojer et al., 2008b). The cage size is adaptable depending on substrate size and concentration. Thus, small peptides induce 12-mer assembly whereas larger substrates such as bovine serum albumin (BSA) lead to the formation of 24-mers *in vitro* (Krojer et al., 2008b; Iwanczyk et al., 2011). For β-casein, denatured lysozyme and denatured BSA, an encapsulation of substrate could be observed before cleavage (Krojer et al., 2008b; Jiang et al., 2008). Similar to 6-mers, 12- and 24-mers also consist of trimeric building blocks and resemble highly symmetrical hollow spheres with an outer diameter of 160 and 195 Å, respectively (Krojer et al., 2008b; Kim et al., 2011). In contrast to earlier models which assumed a 6-meric resting state and a 12/24-meric activation state, cage assembly is not a prerequisite for proteolytic activity. Proteolytic inactive variants like $DegP^{S210A}$ are capable of forming higher order oligomers, and mutants ensuring exclusively trimer formation ($DegP^{Y444A}$) exhibit significant protease activity (Kim & Sauer, 2012). Nevertheless, the 12-meric state binds substrate peptides more tightly and cleaves more efficiently (Kim & Sauer, 2012). Allosteric binding of peptides shows a cooperative binding effect and drastically increases protease activity (Merdanovic et al., 2010). A strong activator of protease activity and oligomerization is the heptapeptide DPMFKLV which binds to DegP with high affinity ($K_D = 5\ \mu M$). The protease cleaves preferably residues with small hydrophobic side chains such as valine, alanine, isoleucine and threonine in P1 (Kolmar et al., 1996; Krojer et al., 2008a).
The oligomerization of DegP is a reversible process (Krojer et al., 2008b) which is a unique feature of HtrA proteases. The exact mechanism of oligomerization is still under investigation. Studies reported PDZ-PDZ interactions to be important for higher-order oligomerization. $DegP^{\Delta PDZ2}$ variants resemble DegS and form trimers only. More specific mutations with truncated PDZ2 domains revealed the significance of the last eight C-terminal residues for stabilizing higher-order oligomers. The $DegP^{\Delta 440\text{-}448}$ variant assembles into hexameric state but no conversion into 12- or 24-mer could be observed (Jiang et al., 2008). Additionally, the LA loop has a stabilizing role in 6-mer assembly. It interacts with the LA* and the L1* loop of the opposite protomer and thereby preserves the integrity of the HtrA oligomer. Furthermore, contacts to L2* loop and PDZ1 domain have been described and disruption of these lead to increased proteolytic activity. It was also proposed that the LA loop interacts with the regulatory L3 loop but until now there are no valid results confirming this theory (Figaj et al., 2014).

Interestingly, DegP shows the ability to bind liposomes. Structural investigations reveal positively charged clusters of Arg and Lys originating from PDZ1 and PDZ2 domains displaying candidate sites for membrane attachment (Krojer et al., 2008b). Via electron

microscopic studies bowl-shaped structures of DegP with 4-, 5- and 6-fold symmetry associated with lipid membranes could be identified. The self-assembly is independent of substrate binding and exhibit higher proteolytic activity than soluble DegP (Shen et al., 2009).

1.2.3 DegQ - a periplasmic DegP homolog

1.2.3.1 DegQ from *E. coli*

DegQ is another periplasmic HtrA protein with chaperone and protease activity. It resembles DegP in sequence (amino-acid sequence identity $\sim$ 60 % in *E. coli*) and domain organization (Wrase et al., 2011; Waller & Sauer, 1996; Kolmar et al., 1996). As described above, the biggest difference between both proteins is the length of the LA-loop. In contrast to *E. coli*, many prokaryotes only encode one HtrA protein which is usually a DegQ homologue emphasizing its importance for protein quality control in the periplasmic space of these species (Kim & Kim, 2005).
In *E. coli*, it has been observed that DegQ complements DegP under certain conditions (Waller & Sauer, 1996), as it has a similar substrate specificity (Kolmar et al., 1996). Substrate binding also induces the formation of 12- and 24-meric cage-like particles (Sawa et al., 2011) which are the proteolytic active form. The nature of the resting state is still under discussion. Whereas one group showed a 6-meric resting state (Malet et al., 2012) another group described a trimer (Bai et al., 2011). Similar to the other HtrA proteins, DegQ is activated by an allosteric activation cascade initiated by substrate binding to the PDZ1 domain, influencing the L3 loop which in turn transmits the signal via LD* to L1* and L2* loops (Sawa et al., 2011), rendering the protease active (Fig. 1.3).
A special feature of DegQ is its pH sensitivity. In acidic pH (pH 4.5 – 6) proteolytic substrate cleavage is most efficient with an optimum at pH 5.5. This is corroborated by the fact, that the oligomeric state at pH 5.5 is mainly 12-meric whereas at higher pH smaller oligomers predominate. Additional studies showed that this feature enables cell survival and growth in an environment with lower pH (Sawa et al., 2011).
It is assumed that DegQ exhibits a more prominent chaperone activity than DegP. In electromocroscopic studies it could be shown that lysozyme molecules which were added in an unstructured, reduced state bound to the DegQ 12-mer and are located within the cage-like particle. As the bound molecules are in state which is close to the native folded state of lysozyme this is strong evidence for the refolding capacity of DegQ. As ordered parts of the LA loop are directed towards the lysozyme, a new

substrate binding function for this loop has been proposed (Malet et al., 2012). The overall geometry of the 12-mer and 24-mer DegQ cage-like particle diverges from DegP crystal structures in terms of PDZ1 and 2 domains (Malet et al., 2012).

1.2.3.2 DegQ from *Legionella*

Interestingly, there are two additional prokaryotic DegQs with known crystal structures. DegQ from *Legionella fallonii* (Lf) and *Legionella pneumophila* (Lp) resemble each other but show clear differences to the architecture and function of the $DegQ_{Ec}$ 12-mer (Wrase et al., 2011; Schubert et al., 2015). *Legionella* are interacellular parasites of free-living protozoa usually found in fresh water. *L. pneumophila* is the causative agent of Legionnaires' disease, a severe pneumonia with a high fatality rate (Fields et al., 2002). $DegQ_{Lf/Lp}$ shows a trimeric resting state which assembles into 12- or 24-mers upon substrate binding. Proteolytic activity is dependent on cage assembly. Engineered protein variants with impaired ability to form high-order oligomers show no cleavage capacity (e.g. $DegQ_{Lf}^{\Delta PDZ2}$, $DegQ_{Lf}^{\Delta C9}$ a variant lacking the last 9 C-terminal residues). Interestingly in *E. coli*, the $DegQ^{\Delta PDZ2}$ variant is still able to form 12-mers upon substrate binding and exhibits proteolytic activity (Sawa et al., 2011; Malet et al., 2012). In this case, 12-mer integrity is provided by PDZ1 interactions (Sawa et al., 2011).
For *Legionella*, proteolytic activity was measured by the release of a fluorogenic reporter 7-amino-4-methylcoumarin (AMC) coupled to a substrate peptide (DPMFKLV). It shows, that cleavage efficiency is very low. Allosteric binding of β-casein or suitable peptide substrates dramatically increases proteolytic activity in a dose-dependent manner (Schubert et al., 2015). Thus, the proteolytic activity is modulated by the presence of substrates.

1.2.4 $HtrA_{Ct}$

In *C. trachomatis* there is only one HtrA homologue, $HtrA_{Ct}$ which is expressed constitutively throughout the developmental cycle from approximately 8 hours after infection to its highest level between 24-40 hours (Huston et al., 2008). As the *htrA* gene of *C. trachomatis* can complement the heat stress phenotype in *E. coli htrA*$^-$, similar functions as $DegP_{Ec}$ in heat shock response have been proposed (Huston et al., 2008). Supporting this assumption, studies in chlamydial-infected human HEp-2 cell

showed an increased $HtrA_{Ct}$ level under heat stress (Huston et al., 2008). Additionally, $HtrA_{Ct}$ is detected in high amounts during penicillin-induced persistence, presumably to maintain extracytoplasmic protein functionality required for ongoing viability (Huston et al., 2008).
Biochemical studies reveal $HtrA_{Ct}$ as a serine protease with proposed chaperone function similar to other HtrA proteins (Huston et al., 2007). Addition of the unique $HtrA_{Ct}$ protease inhibitor JO146 during the replicative phase of *C. trachomatis* resulted in diminished inclusion size and inability to form viable EB. During heat stress the inhibitor was completely lethal (Gloeckl et al., 2013). This implies an essential role for $HtrA_{Ct}$ in *Chlamydiae* survival in host cells.
$HtrA_{Ct}$ is proteolytically active over a wide pH range from 6 to 10 with an optimum at pH 6.5 (Huston et al., 2007). It forms 6-mers which assemble into higher-order oligomers upon binding of unfolded substrate (Huston et al., 2011). Similar to other HtrA proteins, an allosteric activation cascade is proposed which could in parts be confirmed by mutational analysis. Mutations in the PDZ1-binding cleft ($HtrA_{Ct}^{L302N}$) leave the protein unable to perform proteolytic cleavage and higher-order oligomer assembly (Huston et al., 2011). Substitution of highly conserved arginines R224 (L3-LD* interactions) and R362 (PDZ1-L3 interactions) by alanine and leucine, respectively, abolishes proteolytic activity completely (Marsh et al., 2013).
$HtrA_{Ct}$ cleaves after small hydrophobic residues like isoleucine, alanine and valine and clearly prefers isoleucine at the P1 position. Additionally, the preference of a large positively charged residue at P3 (K/R) may indicate the formation of a salt bridge in substrate binding (Huston et al., 2011).
Like for DegP and other HtrAs (*Shigella flexneri*, Purdy et al., 2007) interactions with OMPs have been reported for $HtrA_{Ct}$ (Sklar et al., 2007; Huston et al., 2011). Chlamydial OMPs such as MOMP and the polymorphic membrane protein C (PmpC) exhibit a C-terminal sequence which stimulates the proteolytic activity of $HtrA_{Ct}$ (Huston et al., 2011). Studies with MBP-MOMP fusion proteins, either full-length or degraded to peptides, revealed a dramatic increase in proteolytic activation. The intact MBP-MOMP fusion protein has been shown to induce oligomerization whereas the peptides did not (Huston et al., 2011). These are first indications for the importance of $HtrA_{Ct}$ interactions with MOMP *in vitro*.

Since $HtrA_{Ct}$ is essential for chlamydial survival in cells, it represents a novel therapeutic target for antichlamydial therapy. During the replication cycle it is located in periplasmic space of *C. trachomatis*. Additionally, secretion into the host cell cytoplasm has been reported (Wu et al., 2011), suggesting a role in manipulation of host-cell signaling. However, host-cell targets of $HtrA_{Ct}$ are still unknown.

1.2.5 HtrAs as virulence factors

For a long time, the role of bacterial HtrAs in pathogenesis has been primarily attributed to survival under stress conditions during infection. Current studies reveal that HtrA proteins are also directly involved in pathogen-host interaction as they are released into the environment by mostly unknown pathways (Backert et al., 2018). Species-dependent, prokaryotic HtrAs are located either membrane-bound to the bacterial cell wall (*Bacillus anthracis* (Sela-Abramovich et al., 2009); *C. pneumoniae*, (Montigiani et al., 2002)) or in the periplasm (most gram-negativ HtrAs). One proposed secretion mechanism is the incorporation of HtrAs in outer-membrane vesicles (OMV) (Bartolini et al., 2013). The production of OMVs is often associated with envelope stress as a mechanism to discard harmful waste (McBroom & Kuehn, 2007) suggesting a contribution of HtrAs in this process.
Extracellular and cytoplasmic HtrAs can directly target host cell or bacterial proteins to promote virulence. One mode of action is the disruption of the epithel barrier by cleaving proteins involved in adherens junctions and tight junctions. HtrAs from *E. coli*, *H. pylori*, *Proteus mirabilis*, *Salmonella enterica*, *Shigella flexneri*, *Campylobacter jejuni*, *Borrelia burgdorferi* and *Yersinia enterocolitica* have been reported to cleave E-cadherin and thereby facilitate bacterial invasion (Hoy et al., 2010, 2012; Russell & Johnson, 2013; Russell et al., 2013; Boehm et al., 2012; Abfalter et al., 2016). Additionally, cleavage of structural components like occludin (*H. pylori*, *C. jejuni*), and claudin-8 (*H. pylori*) might intensify this effect (Tegtmeyer et al., 2017; Elmi et al., 2016). Surface-exposed HtrAs can also degrade extracellular matrix proteins like fibronectin, aggrecan and proteoyglycans to increase invasiveness (Russell & Johnson, 2013; Russell et al., 2013; Tegtmeyer et al., 2017).
Processing of bacterial virulence factors for example for surface presentation of adhesins (*S. flexneri*) or regulation of secretion of virulence proteins (*B. anthracis*) (Purdy et al., 2007; Chitlaru et al., 2011) is also associated with HtrA proteases.
Due to their pathogenic function, HtrA proteins are regarded as new potential targets for antibacterial therapeutics. The first lead compounds that were tested are based on typical active site serin inhibitors and targeted the catalytic center of $DegP_{Ec}$. A chloromethyl ketone was attached to a substrate imitating peptide which successfully inhibits proteolytic activity but with a rather low specificity (Hauske et al., 2009). For inhibition of the proteolytic activity of $HtrA_{Ct}$, a similar approach was followed modifying a tripeptid V-P-V or A-P-V with a reactive phosphonate that irreversibly binds serine. With JO146 and JCP83, two effective inhibitors were obtained with no obvious cell toxicity and a specificity for chlamydial HtrA proteins only (Gloeckl et al., 2013; Lawrence et al., 2016).

For *H. pylori*, a nonpeptidic rhodamine derivative scaffold was identified as effective active site inhibitor (Hoy et al., 2010). Another compound targeting *H. pylori* HtrA was generated which binds the putative allosteric site and could thereby completely inhibit proteolytic activity towards E-cadherin *in vitro* (Perna et al., 2014), showing a novel approach for HtrA inhibition.

1.3 MOMP of *C. trachomatis*

Gram-negative bacteria contain two lipid bilayer membranes confining the periplasmic space. Whereas the cytoplasmic membrane shows an even distribution of phospholipids among the inner and outer leaflet, the outer membrane is highly asymmetric, containing phospholipids in the inner leaflet and LPS exposed to the cell surface. The outer membrane is a permeability barrier enabling nutrient import via integral outer-membrane proteins (OMP). In contrast to other membrane proteins, OMPs form β-barrels composed of antiparallel amphipathic β-strands (Koebnik et al., 2000) with a hydrophobic surface and a polar interior. These β-barrel structures are very stable and highly resistant to proteases. OMPs are synthesized in the cytoplasm as a precursor with an N-terminal signal sequence mediating inner membrane transport via the Sec system. In *E. coli*, three chaperones, Skp, SurA and DegP, have been reported to be involved in OMP transport through the periplasmic space to the Bam folding complex (Tommassen, 2010).
In *C. trachomatis*, the outer-membrane β-barrel data base (OMPdb) (Tsirigos et al., 2011) identified 13 outer-membrane β-barrels, with the most abundant one, MOMP, contributing to almost 60 % of the total chlamydial protein mass (Hepler et al., 2018). MOMP is a 40 kDa cysteine rich ion channel (Hughes et al., 2001) encoded by the *ompA* gene with a very unique amino-acid sequence. An extensive intermolecular network is formed via disulfide bonds with other cysteine-rich proteins, probably as substitute for the missing peptidoglycan layer increasing structural integrity of the outer membrane (Yen et al., 2005). In RBs disulfide bonds are reduced allowing higher flexibility and an increase in diameter to facilitate replication (Elwell et al., 2011).
Due to the high abundance and accessibility of MOMP, it has been a focus of subunit vaccine development for many years (Pal et al., 2001, 2005; Kari et al., 2009; Poston et al., 2017). However, the recombinant production of MOMP is difficult due to several complications such as solubility issues, incorrect folding and low yield. One approach to gain immunogenicity is the use of MOMP peptides as koala vaccination which shows first successful triggering of an immune response towards *Chlamydia peco-*

rum infections (Nyari et al., 2018). Other studies investigated variable domains (VD) of MOMP containing B- and T-cell epitopes and revealed promising results by production of neutralizing antibodies in mice (Olsen et al., 2015). Vaccination with fusion protein containing VD4 of MOMP in cationic liposomes ensures partial protection in minipigs and mice by inducing a robust antibody response (Bøje et al., 2016). Current investigations are centered on a vaccine for Phase 1 testing.

1.4 Objectives

Despite their high sequence homology the HtrA protein family shows a surprising variety in function and structure. Most prokaryotic HtrA proteins are involved in periplasmic protein quality control and thereby enabling cell survival in harsh environment. However, several prokaryotic members are directly associated with infectious diseases. Their pathogenicity has been attributed primarily to maintenance of bacterial fitness. Current studies also reveal direct involvement in pathogen-host interactions as in some species HtrA proteins have been shown to be released into cytoplasm or extracellular space (Backert et al., 2018). They can promote bacterial invasion by disruption of the epithel barrier (Hoy et al., 2010; Russell & Johnson, 2013; Boehm et al., 2012; Abfalter et al., 2016) and degradation of extracellular matrix proteins (Russell et al., 2013; Tegtmeyer et al., 2017) or process and regulate secretion of virulence factors (Purdy et al., 2007; Chitlaru et al., 2011). Consequently, HtrA proteins represent a new potential target for antibacterial treatment.
The groundwork for HtrA protein research was laid by extensive studies of DegP, DegQ and DegS from *E. coli* which serve as model proteins for many prokaryotic HtrA proteins. Recent studies covering various HtrA proteins from different species reveal the diversity in structure and function and show that they do not conform in all aspects to the *E. coli* models. There are fundamental features which are found in most HtrA proteins with two PDZ domains such as their ability to form higher-order oligomers. However, the mechanism and initiation of oligomerization are still not well understood and await characterization.

In *C. trachomatis*, the causative agent of the most prevalent sexually transmitted infection world wide, $HtrA_{Ct}$ has been identified as virulence factor essential for bacterial survival. The protease has been associated with heat-stress response and chlamydial persistence, and a role in RB-to-EB-transition and OMP assembly has been discussed, too (Marsh et al., 2017). However, *in vivo* substrates of $HtrA_{Ct}$ and the corresponding cellular mechanisms which could promote pathogenicity are still under investigation.

The aim of this study was the structural and biochemical characterization of chlamydial HtrA proteins. $HtrA_{Ct}$ and the close relative $HtrA_{Sn}$ from *S. negevensis*, a potential new human pathogen associated with pneumonia and bronchiolitis (Vouga et al., 2017), have been investigated. As there are no three-dimensional models of chlamydial HtrA proteins available so far, the main focus was the crystallization and determination of high-resolution three-dimensional structures. These structural data might help to understand the species-specific properties and are thereby a valuable prerequisite for rational drug design. Additionally, the structures are analyzed with focus on new insights into the mechanism of oligomerization and stabilization of higher-order oligomers.
To gain insights into the physiological role of chlamydial HtrA proteins, the interaction with MOMP has been characterized. As chlamydial MOMPs are in focus of vaccination research for many years, their interaction with HtrA proteins may shed light on new approaches to attack chlamydial cells.

2 Material and Methods

2.1 Material

2.1.1 Equipment

Instrument	**Manufacturer**
ÄKTA FPLC	GE Healthcare, Freiburg
ÄKTAprime plus	GE Healthcare, Freiburg
Agarose gel electrophoresis chamber *Mini-Sub cell GT*	BioRad, Munich
BRANDplates®, PureGrade™	Brand, Wertheim
Centrifugal filters *Amicon® Ultra-4, 10 K*	Merck, Darmstadt
Centrifugal filters *Amicon® Ultra-15, 10 K*	Merck, Darmstadt
Centrifugal filters *Amicon® Ultra-15, 30 K*	Merck, Darmstadt
Centrifuge Avanti J-26 XP	Beckman-Coulter, Krefeld
Centrifuge Biofuge 13	Heraeus Instr., Hamburg
Centrifuge Optima L-90K Ultracentrifuge	Beckman-Coulter, Krefeld
Centrifuge Sigma 3-18K	Sigma, Göttingen
Crystallization plates *Cryschem™S Plate*	Hampton Research, USA
Crystallization plates *Intelli plate 96-2*	Art Robbins Instr., USA
Crystallization Robot *Crystal Phoenix*	Art Robbins Instr., USA
Eppendorf μCuvette® G1.0	Eppendorf, Hamburg
EPS 3002	Life Technologies, USA
EPS 3501 XL	Amersham Biosciences, UK
FLx800™	BioTek, Bad Friedrichshall
French® Pressure Cell Press	Thermo IEC, USA
HiLoad™Superdex™200 pg	GE Healthcare, Freiburg
HisTrap™HP 5 mL	GE Healthcare, Freiburg

Instrument	Manufacturer
Hoefer SE 250 Mini-Vertical Gel Electrophoresis Units	Amersham, UK
Incubation shaker *Aqua-Shaker*	A. Kühne AG, Switzerland
Incubation shaker *Innova4230*	NewBrunswick Sci., USA
Laboklav 55-195	SHP Steriltechnik, Detzel Schloss/Satuelle
Magnet stirrer *MR 2002*	Heidolph Instr., Schwabach
MBPTrap HP	GE Healthcare
Microscope *SZX12*	Olympus, Hamburg
Reax top Vortex Mixer	Heidolph, Schwabach
TGradient Thermocycler	Biometra, Göttingen
Peristaltic pump *EconoPump*	BioRad, Munich
Scales *1419*	Satorius, Göttingen
Scales *572*	Kern, Balingen
Scales *TP-3101*	Denver Instr., Göttingen
Shaking Incubator 3032	GFL, Burgwedel
Sonifier W-250 D	Branson Ultrasonics, USA
Superdex 200 10/300 GL	GE Healthcare
Spectrophotometer *BioPhotometer plus*	Eppendorf, Hamburg
Spectrophotometer *BioPhotometer D30*	Eppendorf, Hamburg
Spectrophotometer *Cary 50 conc*	Varian, USA
StepOne Real-Time PCR System	Applied Biosystems (AB), USA
Techne® Dri-Block® heater DB 3D	Sigma, Göttingen
Thermomixer *1.5 mL comfort*	Eppendorf, Hamburg
Ultracel® 10kDa Ultrafiltration Discs (25 mm)	Merck, Darmstadt
Ultracel® 10kDa Ultrafiltration Discs (44.5 mm)	Merck, Darmstadt
UV transilluminator	biostep®, Burkhardtsdorf
Vacuum pump	Brand, Wertheim

2.1.2 Chemicals

Chemical	Manufacturer
AccuPrime™ *Pfx*	Invitrogen, USA
Agar Agar Standard Grade	Gerbu, Heidelberg
Alcohol Dehydrogenase (ADH)	Sigma-Aldrich, Seelze
Ampicillin Sodium Salt	Gerbu, Heidelberg
APS	Serva, Heidelberg
Bacto Peptone	BD, Belgium
Bacto Yeast Extract	BD, Belgium
Biozyme LE Agarose	Biozym, Oldendorf
Blue dextran	Sigma-Aldrich, Seelze
Bromphenol blue	Sigma-Aldrich, Seelze
BSA-Type H1	Gerbu, Heidelberg
Cytochrome c	Sigma-Aldrich, Seelze
cOmpleteTablets EDTA-free Protease inhibitor, EASY Pack	Roche, Mannheim
D(+)-Glucose Monohydrate	Merck, Darmstadt
D(+)-Maltose Monohydrate	Merck, Darmstadt
Dodecyl Maltoside (DDM)	Gerbu, Heidelberg
Dodecylsulfate-Na-salt	Serva, Heidelberg
Dimethyl sulfoxide	Merck, Darmstadt
di-Sodium hydrogen phosphate dihydrate	Merck, Darmstadt
DTT High purity	Gerbu, Heidelberg
EDTA-Disodium	Gerbu, Heidelberg
Ethanol ROTIPURAN® p.a.	Roth, Karlsruhe
Ethidiumbromide	Roth, Karlsruhe
10x Fast Digest Buffer	ThermoScientific, Darmstadt
10x Fast Digest Green Buffer	ThermoScientific, Darmstadt
FastDigest DpnI # FD1703	ThermoScientific, Darmstadt
FastDigest SalI # FD0664	ThermoScientific, Darmstadt
FastDigest BamHI # FD0054	ThermoScientific, Darmstadt
Ferritin	Pharmacia, Sweden
GeneJET Gel Extraction Kit # K0691	ThermoScientific, Darmstadt
GeneJet Plasmid Miniprep Kit # K0503	ThermoScientific, Darmstadt
GeneRuler™ 1 kb DNA Ladder # SM0311	ThermoScientific, Darmstadt

Chemical	Manufacturer
GeneRuler™ 100 bp DNA Ladder # SM0241	ThermoScientific, Darmstadt
Glycerol, 99.5 %	Gerbu, Heidelberg
Guanidinium hydrochloride, minimum 99 %	Sigma-Aldrich, Seelze
HEPES PUFFERAN® $\geq$ 99.5 %,p.a.	Roth, Karlsruhe
Hydrochloric acid (HCl) 37%	Merck, Darmstadt
Imidazole	Merck, Darmstadt
IPTG-b, Biotechnical Grade	Gerbu, Heidelberg
Izit Crystal Dye	Hampton Research, USA
Kanamycin sulfate	Gerbu, Heidelberg
L-Arginine base	Serva, Heidelberg
Lithium chloride	Roth, Karlsruhe
Lysozyme	Sigma-Aldrich, Seelze
MES	Gerbu, Heidelberg
Magnesium formate	Sigma-Aldrich, Seelze
NativeMark™Unstained Protein Standard	ThermoScientific
N-Dodecyl-N,N-dimethylammonio-3-propane sulfonate (SB-12)	Sigma-Aldrich, Seelze
N-Lauroylsarcosine sodium salt	Sigma-Aldrich, Seelze
Nickel(II) chloride hexahydrate	Merck, Darmstadt
Octyl β-D-glucopyranoside (OG)	Sigma-Aldrich
Ovalbumin	Gerbu, Heidelberg
PageRuler™Unstained Protein Ladder # 26614	ThermoScientific, Darmstadt
Poly(ethylene glycol) (PEG) 3350	Sigma-Aldrich, Seelze
Potassium citrate tribasic monohydrate	Sigma-Aldrich, Seelze
Rapid DNA Ligation Kit # K1423	ThermoScientific, Darmstadt
Rotiphorese® Gel 30 (37; 5:1)	Roth, Karlsruhe
Sodium acetate trihydrate (NaAc)	Roth, Karlsruhe
Sodium chloride, p.a., ACS, ISO	Roth, Karlsruhe
Sodium citrate tribasic dihydrate	Sigma-Aldrich, Seelze
Sodium dihydrogen phosphate monohydrate	Merck, Darmstadt
Sodium formate	Sigma-Aldrich, Seelze
Sodium hydroxide (NaOH)	Roth, Karlsruhe
Sodium potassium tartrate tetrahydrate ACS reagent, 99 %	Sigma-Aldrich, Seelze

Chemical	Manufacturer
Sodium thiocyanate	Sigma-Aldrich, Seelze
SYPRO® Orange Protein Gel Stain	Sigma-Aldrich, Seelze
TEMED	Serva, Heidelberg
Triton X-100	Fluka, Switzerland
Tris(2-carboxyethyl)phosphine hydrochloride (TCEP)	Sigma-Aldrich, Seelze
Tris(hydroxymethyl)aminomethane-HCl (Tris)	Gerbu, Heidelberg
Urea	Gerbu, Heidelberg
2x YT Broth	Roth, Karlsruhe
Peptides	
DPMFKLV-AMC	
DPMFKLA-AMC	
DPMFKLV	
Crystallization Screens	
Additive Screen	Hampton Research, USA
Index™1-96	Hampton Research, USA
PACT *premier*™	Molecular Dimensions, UK
PEG/Ion Screen™ 1& 2	Hampton Research, USA
Structure Screen™ 1& 2	Molecular Dimensions, UK

2.1.3 Bacteria cells and DNA constructs

Bacteria	geno type	function
DH5α	fhuA2 lacΔU169 phoA glnV44 Φ80' lacZΔM15 gyrA96 recA1 relA1 endA1 thi-1 hsdR17	plasmid preparation
Ku98 (Harnasch et al., 2004)	degP::kan treA::spec ΔmalF3 ΔphoA (PvuII) phoR araD139 Δ(ara-leu)7697 ΔlacX74 galE galK thi rpsL F′ lacI^{Q}pro)	expression
BL21Gold	B F- dcm+ Hte ompT hsdS(rB mB) gal λ(DE3) endA Tet^{r}	expression

Table 2.1: Primers for cloning and mutagenesis. All primers were produced by MWG Eurofins. Restriction site and mutated areas are shown in bold, stop codon is red. For some construct one primer only is shown as the corresponding primer is the wild type one.(f:forward, r:reverse)

Contructs	**Primer (5'-3')**
$HtrA_{Sn}$	f:GG**GGATCC**ATGGGGAAAATTCCCGCGGCC
	r:GG**GTCGAC**TTATTTCGTCGTTTTTAACGA
$HtrA_{Sn}$ S230A	f:CCAGGAAAT**GCG**GGTGGCCCCTTAGTTGATCTAG
	ATGGAAAC
	r:GGGGCCACC**CGC**ATTTCCTGGGTTTATCGCTGCATC
$HtrA_{Sn}$ F218A	f:CTCGAAGAC**GCG**CTTCAGACTGATGCAGCG
	r:AGTCTGAAG**CGC**GTCTTCGAGGTCGGTGATTTG
$HtrA_{Sn}$ F218Y	f:CTCGAAGAC**TAT**CTTCAGACTGATGCAGCG
	r:AGTCTGAAG**ATA**GTCTTCGAGGTCGGTGATTTG
$HtrA_{Sn}$ Q290A	f:GGTGTTTCACTT**GCG**CCGATTGATCGG
	r:CCGATCAATCGG**CGC**AAGTGAAACACC
$HtrA_{Sn}$ F477A	r:GG**GTCGAC**TTATTTCGTCGTTTTTAACGAGTA
	CGCCCGCAC
$HtrA_{Sn}^{\Delta 69\text{-}100/2G}$	f:GGAGGAGCACCCCAACCTCAACTTAGTC
	r:GGGGTGCTCCTCCATCTGAAACCCC
$HtrA_{Sn}^{\Delta 69\text{-}100/3G}$	f:GGAGGAGGACCTCAACTTAGTC
	r:TCCTCCTCCTGAAACCCCTTC
$HtrA_{Ct}$	f:GG**GGATCC**ATGTCGCCAATGCTAGGCTAT
	r:GG**GTCGAC**CTACTCGTCTGATTTCAAGAC
$HtrA_{Ct}$ S247A	f:AATCCTGGGAATGCAG**GCG**GTCCA
	r:CAATGGAC**CGC**CTGCATTCCCAGGATT
$HtrA_{Ct}{}^{0}\Delta N34$	f:GCG**GGATCC**CTTGCAGTATCCTCAGGAGATC
$MOMP_{Sn}$	f:AT**GGATCC**TTGTATAACGGCAATCCAAG
	r:AT**GTCGAC**TTACTAGAACTTCACTTCGCC
$MOMP_{Ct}$	f:AT**GGATCC**CTGCCTGTGGGGAATCCTGC
	r:AT**GTCGAC**TTAGAAGCGGAATTGTGC

2.2 Methods

2.2.1 Cloning

Genomic DNA of *C. trachomatis* and *S. negevensis* was used as DNA template. Gene amplification was done by polymerase chain reaction (PCR) using corresponding primer pairs (stock concentration: 100 μM, s.Tab.2.1) and AccuPrime^{TM}*Pfx* DNA Polymerase (Thermo Scientific) according to product information sheet. The PCR product was purified by the GeneJET gel extraction kit (Thermo Scientific) and cleaved by SalI for 30 min at 37 °C. BamHI was added and the solution was further incubated for another 15 min. The target DNA construct was purified by preparative agarose gel electrophoresis (0.8 % agarose gel, 70V for 45-60 min) and GeneJET gel extraction kit (Thermo Scientific). DNA fragments were inserted in the corresponding vector with rapid DNA ligation kit (Thermo Scientific). For constructs with N-terminal His-tag, the pQE30 vector was used. Cloning of target genes for recombinant proteins with N-terminal MBP-tag was done with the pMAL-c2x vector (NEB). Both vectors carry the ampicillin-resistance gene. Restriction-enzyme cleavage and purification of the vector was done as described for the PCR product but with doubled incubation time (SalI 1 h, BamHI 30 min).
After ligation, *E. coli* DH5α cells were transformed with plasmid DNA and positive clones were selected by ampicillin resistance. All constructs were confirmed by sequencing before use (MWG Eurofins).

2.2.2 Mutagenesis

Amino-acid substitutions were performed by using the QuikChange II Site-directed mutagenesis kit (Agilent Technologies). For contructs with low success rate, a site-directed mutagenesis approach with two PCR cycles and two primer pairs was used. Two primers contain the desired mutation (X1 (rev), X2 (fwd)) whereas the other two are the usual forward and reverse primer (F, R) for the DNA construct. In the first PCR cycle two different approaches were set up, one with primer pair F+X1, the other with X2+R. Both PCR products were purified by agarose gel eletrophoresis and GeneJET gel extraction kit (Thermo Scientific). For the second PCR, 50 ng of each fragment was used as new template and together with primer pair F+R the construct was amplified. After anew purification by agarose gel electrophoresis and GeneJET gel extraction kit (Thermo Scientific) the restriction digest, ligation and transformation

was done as previously described.

2.2.3 Recombinant protein production

For recombinant protein production, competent cells were transformed with target construct and a few colonies were picked for over-night culture. 100 mL pre-culture of 1xTY medium containing 100 μg/mL ampicillin was used. For Ku98 cell the addition of 34 μg/mL kanamycin was necessary. The main culture (2 L, 2xTY medium,100 μg/mL ampicillin, 34 μg/mL kanamycin (Ku98)) was inoculated with 1:200 of the pre-culture. At an OD_{600} of 0.6-0.8, gene expression was induced by 1 mM IPTG. Optimized production conditions for the different target proteins are listed in Tab.2.2. Cell harvest was done at 4°C by centrifugation for 10 min 7000 x g in Beckman Coulter Avanti J-26XP. Cell pellet was frozen in -80 °C.

Table 2.2: Optimized conditions for recombinant protein production.

Contruct	**compentent cells**	T(°C)	time (h)
$HtrA_{Sn}$ and variants	Ku98	22	16
$HtrA_{Ct}$ and variants	Ku98	22	16
$MOMP_{Sn}$	BL21Gold	30	4
$MOMP_{Sn}$-MBP	BL21Gold	20	16
$MOMP_{Ct}$	BL21Gold	30	4
$MOMP_{Ct}$-MBP	BL21Gold	20	16

2.2.4 Purification

2.2.4.1 Cell lysis for purification of soluble proteins

The cell pellet was thawed in lysis buffer on ice and the cells were disrupted by two rounds of sonication. The first step lasted 5 min with 5 s pulse on (amplitude $\sim$ 40%) and 10-15 s pulse off. After mixing the cell suspension, a second sonication step of 3 min with an amplitude of 45% was conducted. Separation of supernatant and cell debris was done by ultracentrifugation for 1 h at 120000 x g, 4°C. After filtration (pore size 0.45 μm), the sample was ready for loading on the desired column for protein purification.

2.2.4.2 Cell lysis and membrane preparation for insoluble proteins

The cell pellet was thawed in lysis buffer and the cells were disrupted by a high-pressure homogenizer (3x 1500 psi). Removal of undisrupted cells was done by centrifugation for 30 min at 5500 x g (4°C). The supernatant was further separated by ultracentrigation for 1.5 h at 135000 x g, 4°C. After homogenization of the pellet, a subsequent wash step with lysis buffer containing 0.5 % Triton X-100 (incubation time: 1-2 h) followed by another ultracentrifugation removed the bacterial inner membrane. The pellet was homogenized in storage buffer for further use.

2.2.4.3 Membrane solubilization by detergents

For extraction of membrane proteins $MOMP_{Sn}$ and $MOMP_{Ct}$, the membrane was solubilized using a buffer containing 1% sarkosyl and 10 mM DTT (incubation time: 1-2 h, RT, gentle stirring). After ultracentrifugation for 1.5 h at 135000 x g (4 °C) and filtration of the supernatant (pore size 0.45 μm), the sample was ready for protein purification.

2.2.4.4 Histidine-tagged protein purification

Most recombinant proteins in this study carry a N-terminal Histidine(His)-tag and were purified by immobilized metal ion affinity chromatography (IMAC). 5 mL HisTrap^{TM}(GE Healthcare) columns were thoroughly washed with at least 10 column volumes (CV) of water and equilibrated in buffer A (10 CV). Protein samples were loaded onto the column by a peristaltic pump with 1 mL/min. After a subsequent rinsing with 10 CV of buffer A, a 2-4% buffer B wash step was included before the protein was eluted by an imidazole gradient. Fractions were loaded on 15% polyacrylamide gels and pooled according to the result.

2.2.4.5 Maltose-binding protein-tagged protein purification

Solubility of hydrophobic membrane proteins can be increased by generating fusion proteins with maltose-binding protein (MBP). This fusion protein is then extracted by amylose affinity chromatography (AmyAC).
The MBPTrap^{TM}column was equilibrated in buffer A before the supernatant was loaded with 0.5 mL/min onto the column. After a subsequent wash with buffer A,

the target protein was eluted by adding 10 mL buffer B containing 50 mM maltose. Before re-use, the column is cleaned using 5 mL 0.5M NaOH. Fractions were loaded on 15% polyacrylamide gels and pooled according to the result.

2.2.4.6 Size-exclusion chromatography (SEC)

2.2.4.7 Preparative SEC

For preparative gel-filtration, a 120 mL column (Superdex 200, GE Healthcare) was rinsed with water and equilibrated on running buffer. The protein sample was concentrated by centrifugal filter units (Merck) to a volume of 2.5-3 mL and loaded on the column via a 5-mL-loop. Fractions were collected, analyzed by sodium dodecyl sulfate-polyacrylamide gel electrophoresis (SDS-PAGE) and pooled for further use.

2.2.4.8 Analytical SEC

Analytical gel-filtration was performed with a 25 mL column (Superdex 200 10/300 GL, GE Healthcare) exhibiting a resolution range of 10-600 kDa. The column was equilibrated with running buffer. The maximum sample volume was 500 μL. To analyze the molecular weight (MW) of the target protein, a calibration curve was obtained using standard proteins (Tab.2.3). Blue dextran was used to mark the void volume of the column. As the elution volume was dependent on pH and salt concentration of the running buffer separate calibration runs were performed for each buffer used (Fig.2.1).

Table 2.3: Standard proteins for calibration of the analytic gel-filtration column.

protein	**MW (kDa)**
Cytochrome C	12.5
Ovalbumin	45
BSA (monomer)	67
BSA (dimer)	134
ADH	150
Ferritin	440
Blue dextran	2000

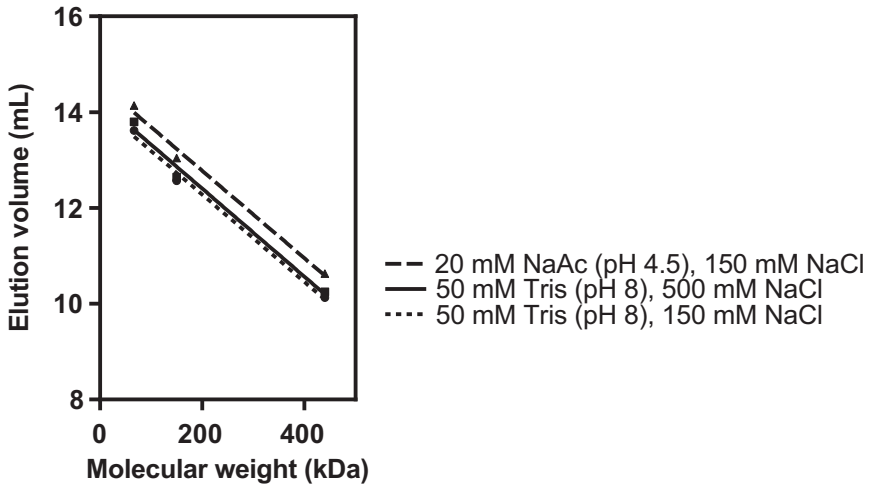

Figure 2.1: Calibration curves of Superdex 200 10/300. A calibration curve containing BSA, ADH and Ferritin was done for acidic and basic buffers with different salt concentrations.

2.2.4.9 Ion exchange chromatography

Ion exchange chromatography was performed as second purification step to remove impurities that could not be separated by preparative SEC. For $HtrA_{Sn}$, a cation exchange (CatIEx) was done. Pooled fractions after affinity chromatography were dialyzed over-night (4°C) against 5 L 50 mM sodium phosphate pH 5.3, 100 mM NaCl (low-salt buffer) and loaded on HiTrap^{TM}SP column (GE Healthcare). After a washing step with low-salt buffer, the protein was eluted by a NaCl gradient (high-salt buffer: 50 mM sodium phosphate pH 5.3, 1 M NaCl).
$MOMP_{Sn}$-MBP was further purified by anion exchange chromatography (AnIex). The protein sample after Dextrin affinity chromatography was diluted to a buffer composition of 20 mM Tris pH 8, 50 mM NaCl. A HiTrap^{TM}Q (GE Healthcare) column was used. After sample loading and a thorough washing step with low-salt buffer (20 mM Tris pH 8, 50 mM NaCl), the target protein was eluted by a NaCl gradient (high-salt buffer: 20 mM Tris pH 8, 1 M NaCl).

Table 2.4: Optimized conditions for recombinant protein purification.

Target protein		**Purification step**	**Buffer A**	**Buffer B**
$HtrA_{Sn}$	1	IMAC	20 mM Hepes pH 8, 500 mM NaCl, 10 mM Imidazole	20 mM Hepes pH 8, 500 mM NaCl, 500 mM Imidazole

Target protein		Purification step	Buffer A	Buffer B
	2	CatIEx	50 mM sodium phosphate pH 5.3, 100 mM NaCl	50 mM sodium phosphate pH 5.3, 1 M NaCl
	3	SEC	20 mM Tris pH 7, 150 mM NaCl	
$HtrA_{Sn}{}^{0}$	1	IMAC	20 mM Hepes pH 8, 500 mM NaCl, 10 mM Imidazole	20 mM Hepes pH 8, 500 mM NaCl, 500 mM Imidazole
	2	Dialysis	20 mM NaAc 4.5, 150 mM NaCl	
$HtrA_{Sn}$ F218A/ F218Y/ F477A	1	IMAC	20 mM Hepes pH 8, 500 mM NaCl, 10 mM Imidazole	20 mM Hepes pH 8, 500 mM NaCl, 500 mM Imidazole
	2	SEC	20 mM NaAc 4.5, 150 mM NaCl	
$HtrA_{Sn}$ Q290A	1	IMAC	20 mM Hepes pH 8, 500 mM NaCl, 10 mM Imidazole	20 mM Hepes pH 8, 500 mM NaCl, 500 mM Imidazole
	2	SEC	20 mM Tris 8.5, 500 mM NaCl	
$HtrA_{Ct}$/ $HtrA_{Ct}{}^{0}$	1	IMAC	50 mM sodium phosphate pH 8.5, 500 mM NaCl, 10 mM Imidazole	50 mM sodium phosphate pH 8.5, 500 mM NaCl, 500 mM Imidazole
	2	SEC	20 mM NaAc 4.5,150 mM NaCl, 1 mM DTT	
$HtrA_{Ct}{}^{0}$ ΔN34	1	IMAC	50 mM sodium phosphate pH 8, 500 mM NaCl, 10 mM Imidazole	50 mM sodium phosphate pH 8, 500 mM NaCl, 500 mM Imidazole
	2	SEC	20 mM Tris pH 7, 150 mM NaCl	

Target protein	Purification step	Buffer A	Buffer B
$MOMP_{Sn}$-MBP	1 AmyAC	20 mM Tris pH 8, 200 mM NaCl, 1 mM EDTA	20 mM Tris pH 8, 200 mM NaCl, 1 mM EDTA, 50 mM Maltose
	2 AnIEx	20 mM Tris pH 8	20 mM Tris pH 8, 1 M NaCl
$MOMP_{Sn}$	1 IMAC	20 mM Hepes pH 7, 500 mM NaCl, 5 % Glycerol, 1% Sarkosyl	20 mM Hepes pH 7, 500 mM NaCl, 500 mM Imidazole, 5 % Glycerol, 0.2% DDM
$MOMP_{Ct}$-MBP	1 AmyAC	20 mM Tris pH 7.4, 200 mM NaCl, 1 mM EDTA	20 mM Tris pH 7.4, 200 mM NaCl, 1 mM EDTA, 50 mM Maltose
	2 AnIEx	20 mM Tris pH 8	20 mM Tris pH 8, 1 M NaCl
$MOMP_{Ct}$	1 IMAC	20 mM Hepes pH 7, 500 mM NaCl, 1% Sarkosyl	20 mM Hepes pH 7, 500 mM NaCl, 500 mM Imidazole, 1.5% OG

2.2.4.10 Protein purification under denaturing conditions

$HtrA_{Sn}$, $HtrA_{Ct}$ and corresponding variants have been purified under denaturing conditions. Usually the first purification step, the IMAC was the same as before. The exception is the $HtrA_{Ct}{}^{0}\Delta N34$ variant, were 6 M urea is already added to buffer A and B to increase protein yield. The eluted target protein was then denatured by addition of 8 M urea to a final concentration of at least 5-6 M urea. To improve purity, a preparative SEC with running buffer containing 6 M urea was conducted. The pooled fraction were dropwise added to 400 mL ice-cold refolding buffer (100 mM Hepes pH 8, 400 mM Arginine, 1 mM EDTA, 30 % Glycerol (w/v)) and incubated under gentle stirring over-night at 4 °C. The sample was concentrated to a volume of $\sim$ 100 mL and dialyzed against storage buffer. For $HtrA_{Sn}{}^{\#}$ the storage buffer was 20 mM Tris pH 7, 150 mM NaCl whereas for all the other refolded proteins were stored in 20 mM NaAc 4.5, 150 mM NaCl.

2.2.4.11 Protein concentration determination

The protein concentration was determined by UV absorption at 280 nm and the theoretical absorption coefficient given by ExPASy ProtParam (Gasteiger et al., 2005) using the Lambert-Beer law.

Table 2.5: MW and theoretical absorption coefficient determined by ExPASy ProtParam.

protein	**$MW_{1\text{-}mer}$(kDa)**	**$A_{0.1\%}$**	**protein**	**$MW_{1\text{-}mer}$(kDa)**	**$A_{0.1\%}$**
$HtrA_{Sn}$	51.376	0.426	$HtrA_{Ct}$	53.671	0.380
$HtrA_{Sn}{}^{0}$	51.231	0.427	$HtrA_{Ct}{}^{0}$	53.655	0.38
$HtrA_{Sn}$F218A	51.171	0.428	$HtrA_{Ct}{}^{0}\Delta$N34	51.074	0.37
$HtrA_{Sn}$F218Y	51.263	0.456	$MOMP_{Sn}$	28.619	1.534
$HtrA_{Sn}$Q290A	51.190	0.428	$MOMP_{Sn}$-MBP	70.828	1.556
$HtrA_{Sn}$F477A	51.171	0.428	$MOMP_{Ct}$	41.803	1.349
			$MOMP_{Ct}$-MOMP	83.883	1.463

2.2.5 Protein characterization

2.2.5.1 SDS-PAGE

Protein identification and evaluation of purity was done by SDS-PAGE analysis. Samples were denatured by adding 6x loading dye and heating to 95 °C for 2 min. For most experiments 15 % separating gels were casted with a 5% stacking gel. The electrophoresis was performed at a constant current of 25 mA for 1 h 15 min. Running buffer composition was prepared according to Hoefer manual for SE250 gel electrophoresis units.

Table 2.6: Buffer composition for SDS-PAGE analysis.

Buffer component	**6x Loading dye**	**4x stacking buffer**	**4x separating buffer**
Tris	0.35 M (pH 6.8)	0.5 M (pH 6.8)	1.5 M (pH 8.8)
SDS	0.35 M	0.4 %	0.4 %
Glycerol	30 %(v/v)		
DTT	0.6 M		
Bromphenol Blue	0.175 mM	0.035 mM	

Table 2.7: Gel casting instruction for 15% separating polyacrylamide gels with 5% stacking gels.

Compound	Volume	Compound	Volume
15 % separating gel		5 % stacking gel	
4x separating buffer	2.5 mL	4x stacking buffer	1.5 mL
H_2O	2.5 mL	H_2O	3.5 mL
Acrylamide/Bis-acrylamide (30%)	5 mL	Acrylamide/Bis-acrylamide (30%)	1 mL
APS (10 %)	100 μL	APS (10 %)	50 μL
Temed	8 μ	APS (10 %)	100 μL

2.2.5.2 Native PAGE

Electrophoretic mobility of proteins in the absence of SDS depends on the charge, pH and folding of native proteins. In this study 10 % gels were casted with the same composition as previously described without SDS. Running buffer consists of 25 mM Tris-HCl and 192 mM glycine. Electrophoresis was performed at 4 °C and 120 V for 7 h.

2.2.6 Dynamic light scattering

Monodispersity of protein samples was determined by dynamic light scattering (DLS). Samples were centrifuged for 5 min at highest speed. 20 μL of the sample were transferred into a DLS cuvette. 3x 10 measurements (10 s) were performed to determine the hydrodynamic radius.

2.2.7 Circular Dichroism

Circular dichroism (CD) is a method to analyze secondary structure composition and protein folding. Measurements were done at the Jasco-715 CD photometer in a CD cuvette with a diameter of 0.1 cm (Hellma Analytics). Samples were analyzed in 10 mM sodium phosphate buffer pH 8 and $\sim$ 200 μL were used for measurements. CD spectra were measured with parameters as given in Tab.2.8 at a constant temperature over a wavelength range of 195-260 nm or at a constant wavelength over a specific temperature range. The baseline of the instrument was measured for each setting by using the according buffer for the experiment. For melting temperature (T_m) determination, the temperature was increased 1 °C/min and the data was analyzed by equation 2.1. Θ_{max} is the averaged value of the starting plateau whereas Θ_{min} is the average of the ending

plateau.
For analysis of the CD spectra, the baseline was subtracted and the raw data converted to mean residue ellipticity by equation 2.2. An important value for this equation was the mean residue weight (MRW) which was calculated from MW and the number of amino acids in the target protein. The secondary structure composition was calculated by the online software K2D3 (Louis-Jeune et al., 2011).

$$a = \frac{\Theta - \Theta_{max}}{\Theta_{min} - \Theta_{max}} \qquad (2.1)$$

$$MRW = \frac{MW(Da)}{No.amino\,acids - 1}$$

$$[\Theta]_\lambda = \frac{\Theta * MRW * 0.1cm}{c(mg/mL)} \qquad (2.2)$$

Table 2.8: Instrument settings of Jasco J-715 for CD spectra measurement (wavelength scan).

Parameter	
sensitivity standard	100 mdeg
start wavelength	260 nm
end wavelength	195 nm
data pitch	0.1 nm
Scanning mode	continous
Scanning speed	20 $\frac{nm}{min}$
response	8s
band width	1 nm
accumulation	3

2.2.8 Thermal shift assay

Thermal shift assay (TSA) is a biochemical method to measure protein stability and folding at different temperatures. SYPRO® Orange Protein Gel Stain (Sigma-Aldrich) was used at 2x concentration for measurements. 49 μL of the target protein sample was transferred in a 48-well plate and mixed with 1 μL of 100x dye. The samples were measured at the StepOne Real-Time PCR System (AB) using the ROX dye filter. The starting temperature was 25 °C, increasing continuously to 95 °C.

2.2.9 Fluorescence-based protein activity assay

To determine proteolytic activity and ensure enzyme functionality, a fluorescence-based assay was used. Substrates are marked by C-terminal 7-amino-4-methylcoumarin

(AMC). Free AMC is excited at 360 nm and emits at 460 nm. The measurements were done in 96-well plates using the FLx800^{TM}Multi-Detection Microplate Reader (BioTek). The enzyme activity was usually determined at 37 °C over a time of 35 min in reaction buffer (50 mM Tris pH 8 with 150 mM NaCl). For measurement of the temperature dependency, the temperature was continuously increased starting at 20 °C. The thermostat of the instrument was able to heat up to 50 °C. For higher temperatures, the protein was pre-incubated at a thermomixer for 30 min and after substrate addition, the AMC release was measured at 50 °C. The relative activity was retrieved from the slope of fluorescence variation per unit (relative fluorescence units (RFU)) of time (ΔRFU/s) and was converted to free AMC release per second by a calibration curve of free AMC in assay buffer (0 - 1.5 mM free AMC, s. Fig. 2.2). The correlation factor for RFU to AMC conversion was 5.651. That means, the release of 1 nM free AMC corresponds to a signal of 5.651 RFU.
Optimization of protein and substrate concentration lead to a use of 5 μM protein and 50 μM substrate in a sample volume of 60 μL.

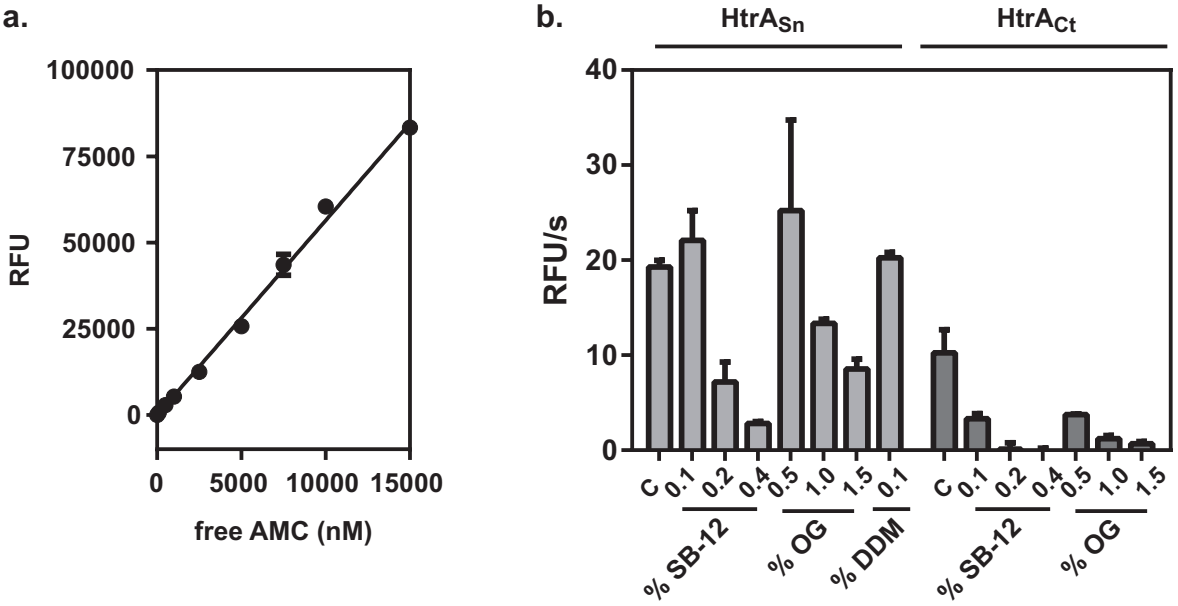

Figure 2.2: a) Calibration curve for RFU/free AMC correlation coefficient determination. The regression line exhibits a slope of 5.651 with an R^2 of 0.99. b) Detergent test of $HtrA_{Sn}$ (light grey) and $HtrA_{Ct}$ (dark grey). (C: Control)

To investigate interactions between MOMPs and HtrA proteins, it was necessary to use detergents in the proteolytic assay. Preliminary test with different detergents were performed in order to find one which ensures the solubility of MOMP and protease activity of $HtrA_{Sn}$ and $HtrA_{Ct}$ (Tab. 2.2b). $HtrA_{Sn}$ was very robust and showed substrate cleavage at various detergents. However, $MOMP_{Sn}$ was soluble only in 0.1%

DDM. $HtrA_{Ct}$'s proteolytic activity is dramatically influenced by detergent addition and a very low fluorescence signal was measured. As a result, the substrate concentration was increased to 150 μM which increased the signal-to-noise ratio significantly. The reaction buffer for the enzyme assay of $HtrA_{Ct}$ was supplemented with 1% OG to ensure the solubility of $MOMP_{Ct}$.

2.2.10 Small-angle X-ray scattering

Small-angle X-ray scattering (SAXS) measurements allow the determination of the gyration radius (R_G), the maximal particle dimension (D_{max}) and the particle volume (Porod volume (PV)) which are used to analyze the molecular weight and the particle shape of a molecule. To generate appropriate samples for SAXS measurements, monodispersity has to be ensured. This was done by DLS and analytical SEC. Before and after every sample measurements, the sample buffer was measured to monitor the signal-to-noise ratio of the instrument. The sample buffer had to have exactly the same composition as the analyzed sample without protein. Samples were measured at the beamline P12 (EMBL, DESY Hamburg). Settings are shown in Tab.2.9.

Table 2.9: SAXS settings for diffraction data collection.

Parameter	
λ	1.241 nm
Exposure time	0.045 s
Temperature	20 °C
Sample volume	20 μL
Detector	Pilatus 2M Pixel Detector

Initial processing of diffraction data was done with PRIMUS (Konarev et al., 2003). Extrapolation of I(0) enables molecular weight determination (s. equation2.3) by comparison to I(0) of a standard protein (Std) with known concentration, e. g. BSA or glucose isomerase.

$$MW = \frac{I_0(sample)}{c(sample)} * \frac{MW_{Std}}{\frac{I_0(Std)}{c_{Std}}} \tag{2.3}$$

2.2.11 Crystallization, crystal optimization, diffraction data collection, structure determination, refinement and validation

For initial crystallization screening commercial kits from Hampton Research (PegIon™, Index™) and Molecular Dimensions (Structure, PACT *premier*™) were used. Preparation of screening plates was carried out by the Phoenix crystallization robot with a dropsize of 0.3 μL. After identification of optimal crystallization conditions, crystallization was done in Cryschem S sitting-drop plates (Hampton Research) with 500 μL reservoir and a dropsize of 10 μL with equal volumes of 10 mg/mL protein and reservoir.

Glycerol was used as cryoprotectant. Crystals were transferred from plates into drops with reservoir solution containing increasing glycerol concentrations of 5%, 10 %, 15%, 20% and 25% before flash-cooling in liquid nitrogen.

Diffraction data were collected at 100 K with λ=1.0332 Å at the beamline P11 at PETRAIII (DESY) using a Pilatus 6MF (DECTRIS) detector. Initial data was processed by XDS (Kabsch, 2010) and scaled using SCALA from CCP4 suite (Evans, 2011; Winn et al., 2011). Phaser (McCoy et al., 2007) was used for molecular replacement and the model building programs ArpWarp (Morris et al., 2002) and Autobuild (Terwilliger et al., 2007) helped to improve the initial structures. Search models were predicted and generated by the Fold & Function Assignment (FFAS) web side (Jeffery, 2004). Side chain residues were manually fitted in the electron density map with COOT (Emsley et al., 2010) and automatically refined by phenix.refine (Afonine et al., 2012). Validation and improvement of structural models was carried out by WHAT IF-Server and wwPDB Validation Service.

3 Results

3.1 High-temperature requirement A protein from *S. negevensis*

3.1.1 Purification of $HtrA_{Sn}$

To get a first insight into potential function and biochemical properties of $HtrA_{Sn}$ the amino-acid sequence was analyzed by ProtParam (Gasteiger et al., 2005) which reveals a monomer size of 51 kDa and an isoelectric point at 6.32. Sequence alignment with homologs in *E. coli* (Ec), *Chlamydia trachomatis* (Ct) and *Chlamydia pneumoniae* (Cp) (Fig. 4.4) shows a high sequence identity to $HtrA_{Ct}$ (54 %), $HtrA_{Cp}$ (50 %), $DegQ_{Ec}$ (42 %) and $DegP_{Ec}$ (40%) (Madden, 2003). This suggests a similar structural arrangement and mode of action. DegP and DegQ proteins can be distinguished by the length of the LA loop (Kim & Kim, 2005). In *E. coli*, the LA loop encompasses 48 amino-acid residues in $DegP_{Ec}$ and 25 amino-acid residues in $DegQ_{Ec}$. With a length of 35 amino acids the LA loop of $HtrA_{Sn}$ is of intermediate size and thus $HtrA_{Sn}$ is difficult to classify as either DegP or DegQ protein.

For biochemical characterization and crystallization, $HtrA_{Sn}$ and $HtrA_{Sn}$ variants were successfully produced in *E. coli* Ku98 cells and subsequently purified. The purification of $HtrA_{Sn}$ wild type is described in more detail. The recombinantly produced protein contains an N-terminal His-tag, enabling a first purification step by affinity chromatography yielding high amounts of target protein. Results from a following cation exchange chromatography displays two prominent peaks (P1+P2) both comprising the target protein (Fig. 3.1a). In preparative SEC, P1 elutes with an apparent molecular weight of approximately 340 kDa, whereas in P2 an additional peak with an apparent mass of 540 kDa is detectable (Fig. 3.1c). The molecule sizes determined by analytical gelfiltration indicate 6-mer and 12-mer assembly of $HtrA_{Sn}$ (Fig. 3.2c). Two liters of bacteria culture yield around 100 mg of $HtrA_{Sn}$ in hexameric and 10 mg

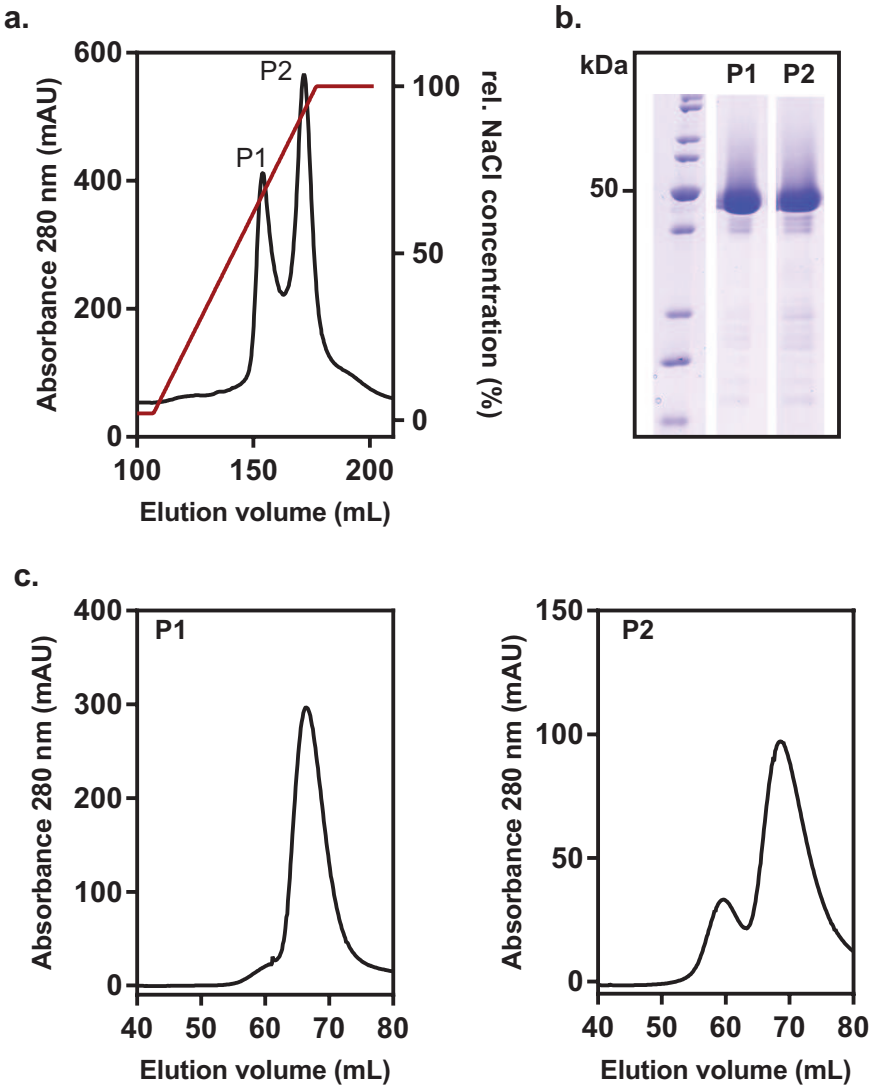

Figure 3.1: Purification of $HtrA_{Sn}$. a) Chromatogram of cation exchange chromatography of $HtrA_{Sn}$ shows two peaks (P1+P2). b) Results from SDS-PAGE for P1+P2 reveal a prominent band at around 50 kDa matching the size of a $HtrA_{Sn}$ monomer. c) SEC profiles displaying for P1 a monodisperse sample with a molecular weight of 340 kDa whereas P2 has an additional peak with an apparent mass of 540 kDa.

in dodecameric form, highlighting the preference for a 6-mer state in solution at physiological pH. 12-mers form probably due to the presence of co-purified peptides from *E. coli*. To eliminate the influence of the latter, $HtrA_{Sn}$ was purified under denaturing conditions and subsequently refolded ($HtrA_{Sn}{}^{\#}$). Results from DLS and SEC indicate that refolded protein assembles essentially as 6-mer (Fig. 3.2). Other $HtrA_{Sn}$ variants were purified using a similar protocol with minor modifications in buffer composition and usually without the ion exchange chromatography step.

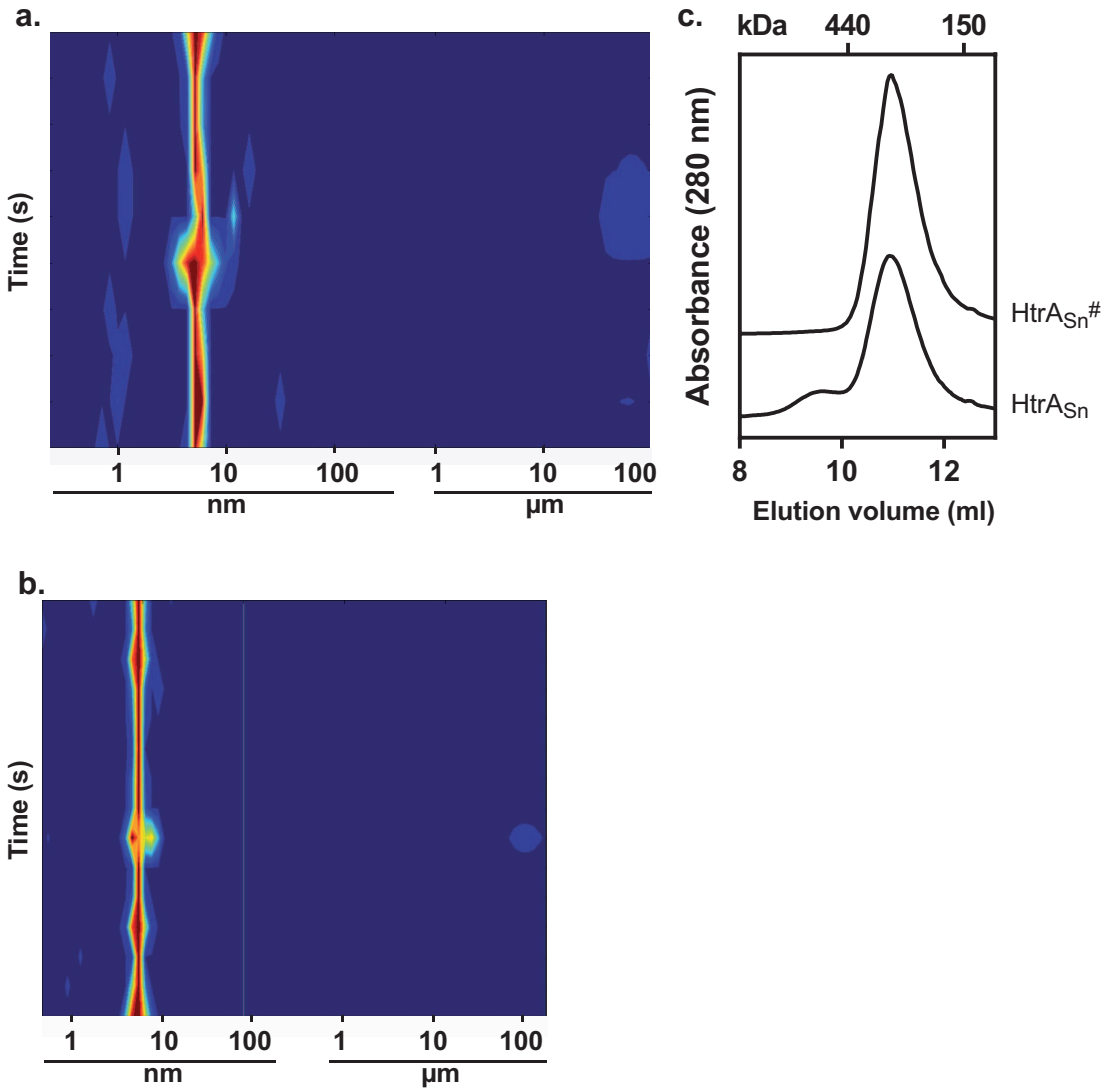

Figure 3.2: Refolded $HtrA_{Sn}{}^{\#}$ shows essentially 6-mer assembly. a) DLS spectrum of $HtrA_{Sn}$ displays a main fraction with an hydrodynamic radius R_h of 6.32 nm. b) R_h of $HtrA_{Sn}{}^{\#}$ is 5.79 nm and the refolded protein shows a monodisperse distinct band. c) Results from analytical SEC demonstrate that $HtrA_{Sn}$ and $HtrA_{Sn}{}^{\#}$ are predominantly forming 6-mers in solution. $HtrA_{Sn}$ also assembles into 12-mers in small amounts.

.

3.1.2 Biochemical characterization of $HtrA_{Sn}$

3.1.2.1 Proteolytic activity of $HtrA_{Sn}$

To verify the functionality of $HtrA_{Sn}$ and $HtrA_{Sn}{}^{\#}$, proteolytic activity was quantified by AMC release from the fluorogenic reporter heptapeptide DPMFKLV(pept1)-AMC, an established $DegP_{Ec}$ substrate (Hauske et al., 2009). $HtrA_{Sn}$ (5 μM) shows a basal substrate (50 μM) cleavage rate of 0.35 $\frac{nM}{s}$ which is slightly increases (0.5 $\frac{nM}{s}$) in the

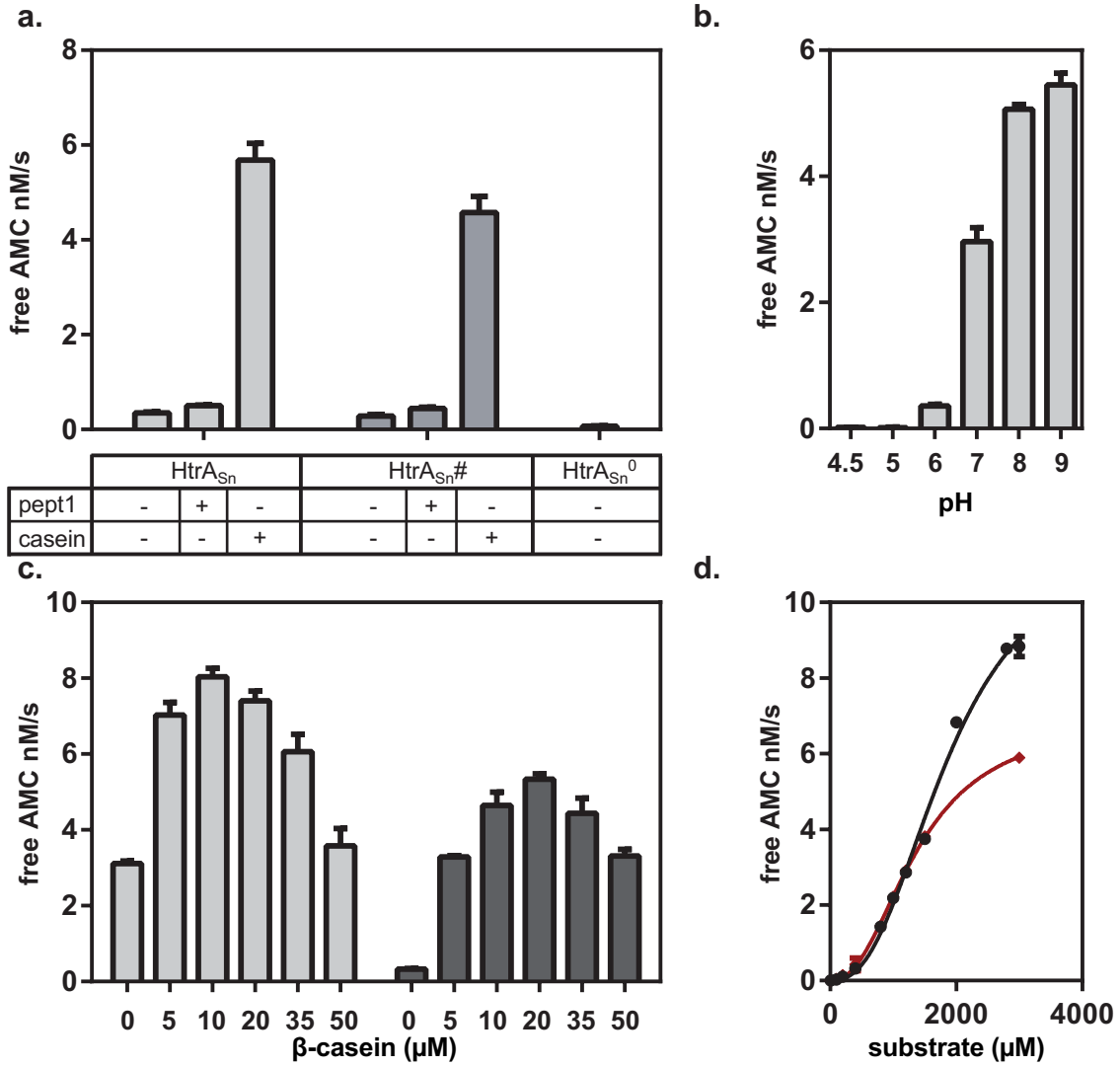

Figure 3.3: Proteolytic activity of HtrA$_{Sn}$. a) Protease activity measurements of HtrA$_{Sn}$, HtrA$_{Sn}$$^{\#}$ and HtrA$_{Sn}$^{0} by monitoring of AMC release. HtrA$_{Sn}$ shows basal substrate cleavage which is slightly more effective in presence of pept1. Addition of β-casein increases activity dramatically. HtrA$_{Sn}$$^{\#}$ behaves similar whereas HtrA$_{Sn}$^{0} shows no activity. b) β-casein addition leads to an increase in protease activity in a dose-dependent manner. The highest activity is detected for HtrA$_{Sn}$$^{\#}$ at 20 μM and for HtrA$_{Sn}$ at 10 μM. At higher concentrations competitive effects diminish fluorogenic substrate cleavage. c) Proteolytic activity of HtrA$_{Sn}$ is pH-dependent. Substrate cleavage occurs at pH >6. d) Monitoring fluorescence of HtrA$_{Sn}$ degradation of pept1-AMC (black) and DPMFKLA-AMC (red) at increasing peptide concentrations. For both substrates a sigmoidal curve is measured indicating positive cooperativity.

presence of free pept1 (50 μM, Fig. 3.3a). Intrinsically unfolded β-casein functions as activator and remarkably increases proteolytic activity. HtrA$_{Sn}$ and HtrA$_{Sn}$$^{\#}$ exhibit comparable protease activity, verifying the correct refolding of HtrA$_{Sn}$$^{\#}$. Consequently, experiments where co-purified peptides could have an impact were conducted with the

refolded protein.
Replacement of active-site serine (Ser230) by alanine converts the protease into an inactive state ($HtrA_{Sn}{}^{0}$) and represents a valid negative control (Fig. 3.3a).
Activation of $HtrA_{Sn}$ is β-casein concentration dependent (Fig. 3.3c). The highest activity has been detected for $HtrA_{Sn}{}^{\#}$ at 20 μM β-casein and for $HtrA_{Sn}$ at 10 μM as most likely co-purified peptides already occupied binding site and active center promoting proteolytic activity. At higher β-casein concentrations the detected fluorescence diminishes due to competitive effects.
To determine the sensibility of the proteolytic activity of $HtrA_{Sn}$ to pH variations the protein functionality assay was conducted at different buffers from pH 4.5–9 (Fig. 3.3b). In acidic range there is no activity detectable but at pH above 6 the protease is activated and shows high cleavage rates at pH 7–9.

In contrast to $DegP_{Ec}$ and $DegQ_{Lp}$ (Hauske et al., 2009; Schubert et al., 2015), pept1 does not significantly increase proteolytic activity of $HtrA_{Sn}$ (Fig. 3.3a). To analyze the kinetic parameters, protease assays with 1 μM $HtrA_{Sn}$ and increasing fluorogenic reporter peptide concentration up to 3 mM were measured. The substrate concentrations was limited by the ability of the substrate to dissolve in the assay buffer. While HtrA proteins prefer non-polar amino-acid residues in prime site, two peptides with alanine and valine in P1 position (pept1-AMC, DPMFKLA-AMC) were tested and compared. Both substrates show a sigmoidal curve implying positive cooperativity without reaching a saturation plateau. However, analysis with GraphPad Prism 6.0 software (nonlinear regression - one site specific binding with Hill slope) allows an estimation of kinetic parameters. In low substrate-concentration range the slope is comparable for both but pept1-AMC reaches higher fluorescence emission conceivably leading to a higher v_{max}. The latter suggests a higher efficacy of pept1-AMC cleavage than for DMPFKLA-AMC. Consequently, valine is preferably cleaved in $HtrA_{Sn}$.

Besides β-casein, there are other reported substrates for HtrA proteins such as BSA and lysozyme in denatured states (Krojer et al., 2008b). Both proteins significantly increase protease activity of $HtrA_{Sn}$. Interestingly, lysozyme is not degraded to the same extend by $HtrA_{Sn}$ as denatured BSA (Fig. 3.4).

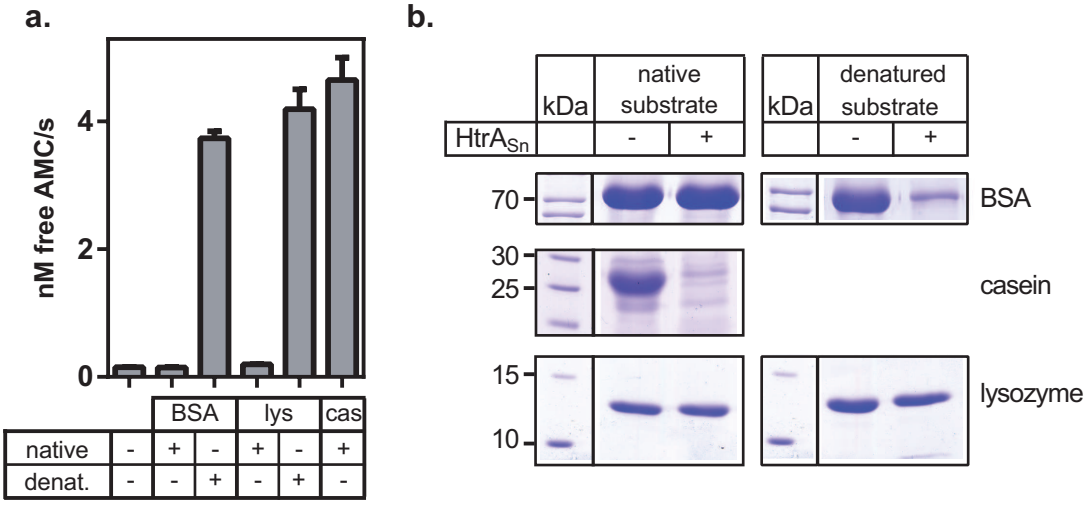

Figure 3.4: The influence of unfolded proteins on proteolytic activity of $HtrA_{Sn}$. a) Denatured BSA and lysozyme increase $HtrA_{Sn}$ proteolytic activity to the same extend as β-casein. b) SDS-PAGE analysis displays that β-casein and unfolded BSA are degraded by $HtrA_{Sn}$ whereas denatured lysozyme is not.

3.1.2.2 Oligomerization behaviour of $HtrA_{Sn}$

An outstanding property of HtrA proteins is the ability to form higher-order oligomers. The basic building block is a pyramidal homotrimer which can assemble into complex oligomers consisting of up to 30 molecules (Kim et al., 2011). The oligomerization behaviour of $HtrA_{Sn}$ has been analyzed by analytical SEC and native PAGE (Fig. 3.5). $HtrA_{Sn}$ assembles predominantly into 6-mers with a small amount of 12-mers whereas the refolded protein $HtrA_{Sn}{}^{\#}$ exclusively forms 6-mers (Fig. 3.5a).
For $DegQ_{Lf}$ it has been reported that pept1 addition at an 4x molar excess induces oligomerization (Schubert et al., 2015). Interestingly, pept1 does not lead to the assembly of higher-order oligomer in $HtrA_{Sn}{}^{\#}$ (Fig. 3.5a,c) even at an 20-fold excess. This suggests differences in the activation mode of oligomerization between prokaryotic HtrA proteins.

Oligomerization is substrate-concentration dependent (Fig. 3.6). An increase in β-casein concentration shifts the 6-mer peak towards the 12-mer peak in SEC (Fig. 3.6a). At very high substrate concentrations small amounts of 24-mer were detectable (data not shown). Intriguingly, the shift in molecular weight is continuous (Fig. 3.6a). This effect could indicate stepwise substrate binding to $HtrA_{Sn}$ 6-mer and an assembly into 12-mer cages at a critical concentration. Alternatively, a transient intermediate state with an apparent molecular weight of 450 kDa (9-mer) might be present. Oligomerization is a transient process which occurs in the presence of unfolded substrates and is

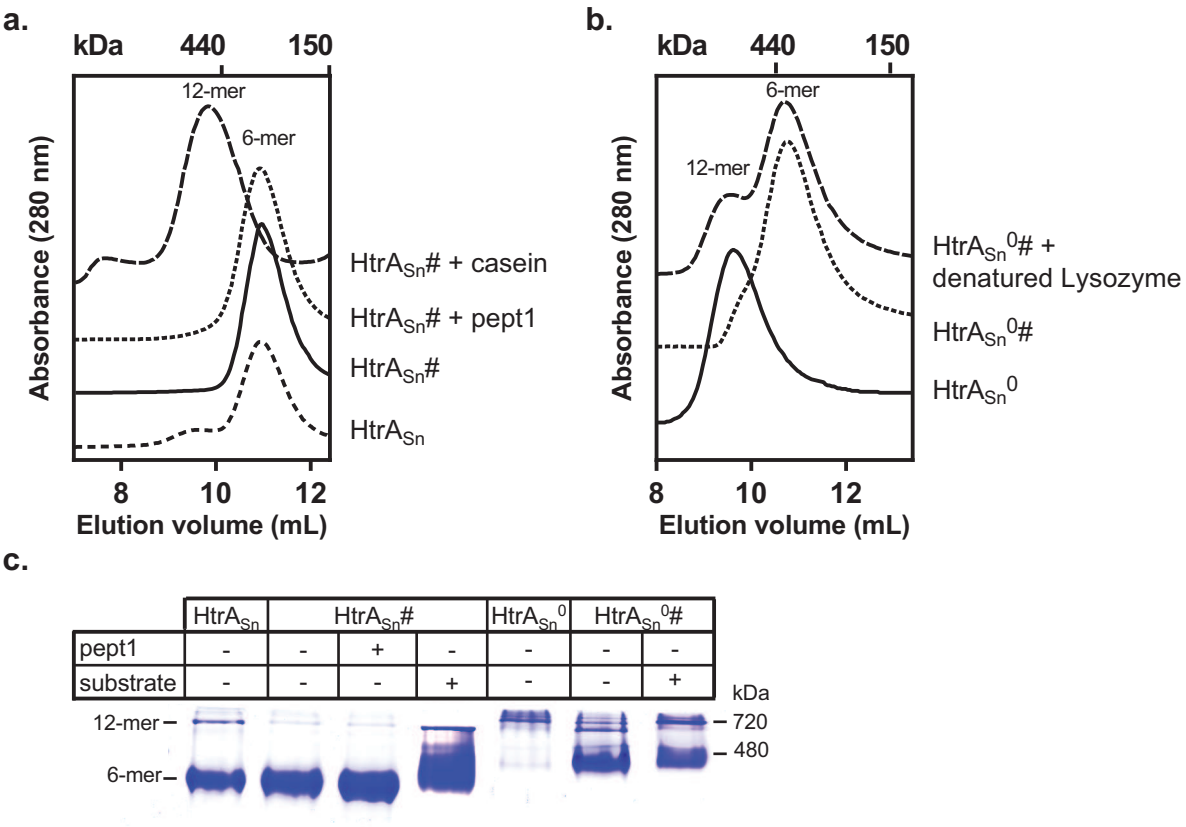

Figure 3.5: $HtrA_{Sn}$ proteins form higher-order oligomers in the presence of unfolded proteins. a) Results from analytical SEC show that $HtrA_{Sn}$ and $HtrA_{Sn}{}^{\#}$ (50 μM) form predominantly 6-mers. Addition of pept1 (1.25 mM) has no impact on the oligomeric state while the presence of casein (250 μM) results in 12-mer assembly. Elution volume markers are depicted on top. b) $HtrA_{Sn}{}^{0}$ elutes as 12-mer and $HtrA_{Sn}{}^{0\#}$ as 6-mer in SEC. Upon addition of denatured lysozyme, $HtrA_{Sn}{}^{0\#}$ assembles partially into 12-mers. c) In native PAGE $HtrA_{Sn}$, $HtrA_{Sn}{}^{\#}$ and $HtrA_{Sn}{}^{0\#}$ appear predominantly as 6-mers. The presence of pept1 has no effect on $HtrA_{Sn}{}^{\#}$ whereas β-casein addition leads to assembly of 12-mers and a shift in 6-mer band. For $HtrA_{Sn}{}^{0}$ almost exclusively 12-mer is visible. The shift of bands between $HtrA_{Sn}$ and $HtrA_{Sn}{}^{0\#}$ 6-mer is an effect of the acidic pH which influences electrophoretic mobility.

reversed when the substrate is depleted by proteolytic cleavage (Fig. 3.6b).

The pH-dependency of $HtrA_{Sn}$ oligomer assembly was analyzed by analytical SEC (Fig. 3.6c) at pH 4.5, 7 and 9. As mentioned above, the oligomerization into higher-order oligomers is a transient process which is reversed when bound substrate is depleted. Due to the proteolytic activity of $HtrA_{Sn}$ in neutral to basic pH (Fig. 3.3), the $HtrA_{Sn}$ 12-mers are unstable and the protein forms mainly 6-mers. At acidic pH, the lack of proteolysis stabilizes the $HtrA_{Sn}$ 12-mer. This enabled the isolation of $HtrA_{Sn}$ 12-mer for SAXS experiments.

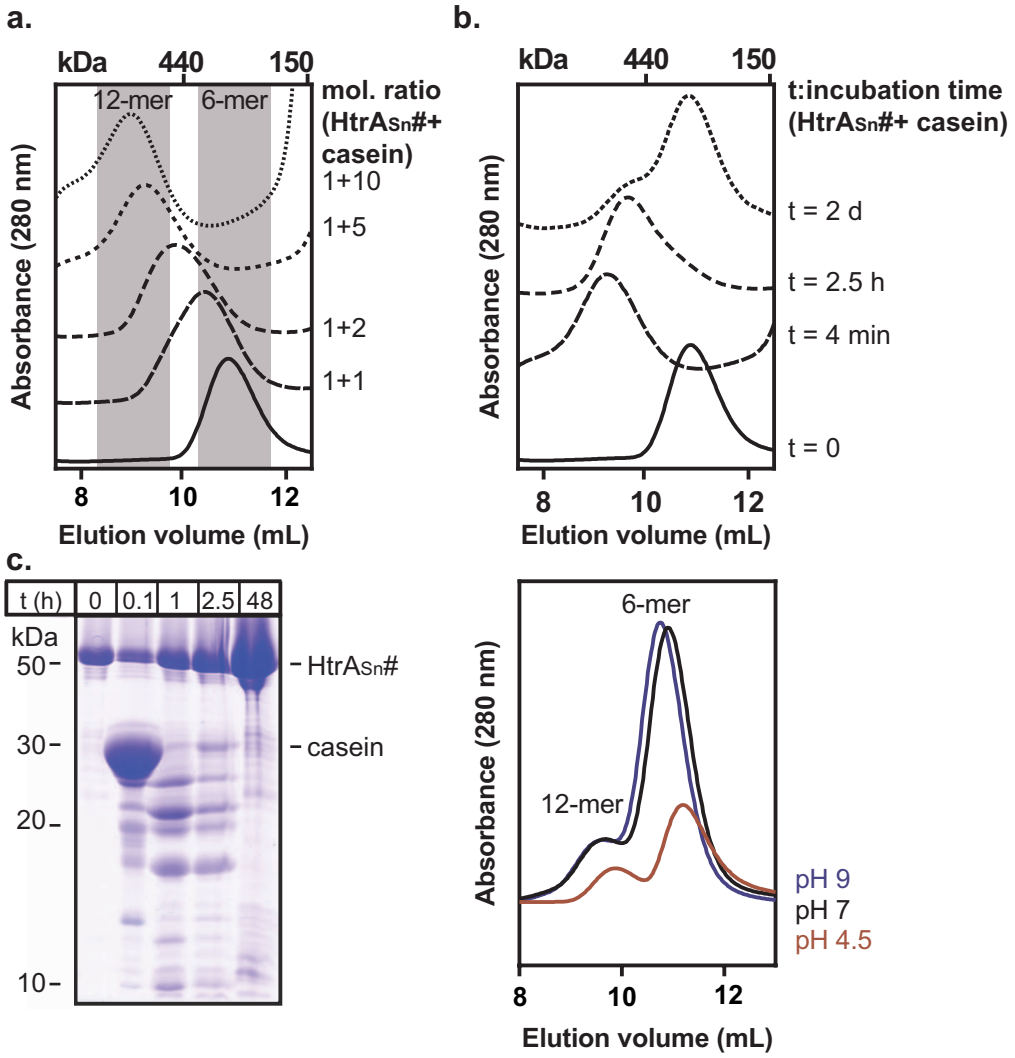

Figure 3.6: Higher-order oligomer assembly is a substrate-concentration dependent transient process. a) Oligomerization of $HtrA_{Sn}$ is substrate-concentration dependent. At higher β-casein concentration the 6-mer peak diminishes and the fraction of 12-mer increases. b) Results from SEC reveal that $HtrA_{Sn}$ assembles rapidly into higher-order oligomers in the presence of 5-fold β-casein excess. This process is reversed over time. After substrate depletion $HtrA_{Sn}$ appears mainly as 6-mer again. The degradation of substrate was monitored by SDS-PAGE analysis. c) The $HtrA_{Sn}$ 6-mer is stable at physiological pH (black) and in basic milieu (blue). At acidic pH (red), the protein precipitates but there is still 6-mer detectable.

The inactive variant $HtrA_{Sn}{}^{0}$ forms 12-mers after purification probably due to co-purified peptides (Fig. 3.5b). Therefore the inactive variant was also purified under denaturing conditions ($HtrA_{Sn}{}^{0\#}$). $HtrA_{Sn}{}^{0\#}$ elutes as 6-mer in SEC. Native PAGE analysis additionally reveals a small amount of 12-mer in $HtrA_{Sn}{}^{0\#}$. Assembly into higher-order oligomers might be due to incomplete refolded proteins which are encapsulated by correctly folded $HtrA_{Sn}{}^{0\#}$. $HtrA_{Sn}{}^{0}$ and $HtrA_{Sn}{}^{0\#}$ are not stable at higher pH values. Hence experiments with these variants were conducted at pH 4.5 which

causes a shift of the bands in native PAGE and also changes the elution volume in SEC. As β-casein precipitates at low pH, denatured lysozyme was used as substrate to induce oligomerization (Jomaa et al., 2007) in $HtrA_{Sn}{}^{0\#}$. As $HtrA_{Sn}{}^{0}$ assembles into higher-order oligomers in the presence of unfolded protein substrates, oligomerization is not dependent on proteolytic activity.

3.1.2.3 Temperature dependency of $HtrA_{Sn}$

As HtrA proteins are heat-shock proteases enabling cell survival at elevated temperatures, biochemical experiments at different temperatures were conducted. The $HtrA_{Sn}$ 12-mer shows proteolytic activity over a wide temperature range with a highest substrate cleavage rate at 50 °C (3.7a). In contrast to the $DegP_{Ec}$ 6-mer which dissociates into trimers at temperatures >42 °C (Krojer et al., 2008b), the $HtrA_{Sn}$ 6-mer is even stable at 55 °C (3.7b,c). CD spectra recorded at 25 °C and 55 °C with minima at 209 and 222 nm show little changes for the $HtrA_{Sn}$ 6-mer. The signal for the 12-mer state decreases significantly from 25 °C to 55 °C but also shows minima at 209, 215 and 221 nm. At 85 °C especially the 12-mer curve displays big changes indicating disintegration of secondary structure. Analysis of secondary structure content results in 25 % α-helix, 20 % β-sheet and 55 % random coil for the 6-mer at 25 °C. The 12-mer contains 23 % α-helix, 22 % β-sheet and 55 % random coil at 25 °C. At 85 °C, only 5 % α-helical content is calculated for the 12-mer. The high content of random coil impedes the detection of melting curves, therefore melting temperatures (T_m) have been determined by thermal-shift assay. Comparison of the melting behavior of 6-mer (T_m: 72-74 °C) and 12-mer (T_m: $\sim$ 65 °C) shows that the T_m of the hexameric state is considerably higher than that of the 12-mer. As higher-order oligomers are a transient phenomenon it is conclusive that these assemblies are less stable.

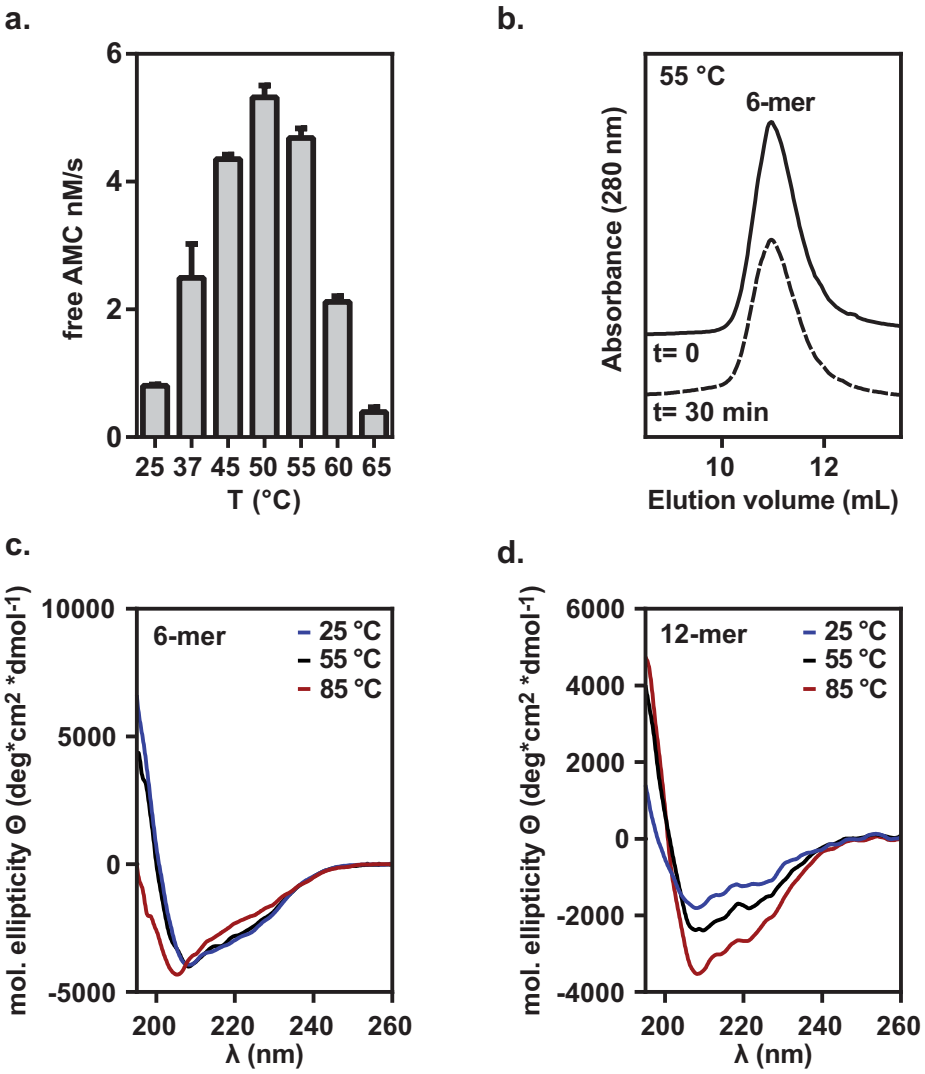

Figure 3.7: $HtrA_{Sn}$ is stable at elevated temperatures and shows high proteolytic activity. a) Monitoring the fluorogenic substrate cleavage of $HtrA_{Sn}$ 12-mer at increasing temperatures. At 50 °C the protease shows highest activity. b) Results from SEC for the $HtrA_{Sn}$ 6-mer before and after 30 minutes of incubation at 55 °C. There is no change detectable, the 6-mer is stable. c) CD spectra of the $HtrA_{Sn}$ 6-mer at 25 °C (blue), 55 °C (black) and 85 °C (red). Minor changes are visible between 25 °C and 55 °C whereas at 85 °C the curve shifted notably. d) CD spectra of the $HtrA_{Sn}$ 12-mer at 25 °C (blue), 55 °C (black) and 85 °C (red). CD signal decreases significantly with increasing temperature indicating disintegration of secondary structure elements.

3.2 Crystallization and structure elucidation of $HtrA_{Sn}$

3.2.1 Optimization of the crystallization condition of the $HtrA_{Sn}$ 6-mer and 12-mer and structure elucidation

First crystallization hits were obtained at acidic pH and near the theoretical isoelectric point of $HtrA_{Sn}$ by screening with commercial kits. The primary crystallization condition consisted of 0.1 M Mes pH 6.4, 0.7 M sodium potassium tartrate and 1 M lithium chloride. The protein crystallized usually within 18–24 hours. The diffraction data were collected to a resolution of 3.5 Å. The crystals belong to the space group $P2_1$ with large unit-cell parameters (a=144.53 Å, b= 143.61 Å, c= 200.75 Å, α, γ=90°, β=90.15°). Assuming a solvent content of ~50 % and a monomer molecular weight of 51 kDa, there are 12 molecules in the asymmetric unit (Matthews, 1986). A molecular replacement attempt with 12 monomeric protease domains and three single PDZ1 domains of 12-mer *E. coli* resulted in a cage-like 12-meric particle with refinement parameters of R_{work}=0.39 and R_{free}=0.45. Further improvement of this incomplete model by automated and manual model building was not successful due to the low resolution. The difficulties encountered in solving the protein structure of $HtrA_{Sn}$ was likely caused by the fast crystal growing leading to a disordered crystal lattice. Various optimization attempts were conducted at different temperatures to improve the quality of $HtrA_{Sn}$ crystals by slowing down the crystallization process. Finally, successful crystallization of $HtrA_{Sn}$ was achieved by using crystallization additives at low temperatures in a two-step incubation procedure. The first incubation period of two to three weeks at 4 °C without any visible nucleation was followed by a transfer to room temperature for another 7–14 days. Crystals growing in 0.1 M sodium acetate pH 4.7, 0.55 M potassium citrate tribasic monohydrate and 0.05 M sodium thiocyanate were obtained. The crystals formed hexagonal prisms with a pointed end (Fig. 3.8). X-ray diffraction data were collected to a resolution of 2.33 Å. The crystals were indexed in space group $P3_121$ with unit-cell parameters: a = 162.98 Å, b = 162.98 Å, c = 112.88 Å, α, β = 90°, γ = 120°. One asymmetric unit contains three monomers. Initial phases were calculated by molecular replacement using three individual protease domains of HtrA from *Arabidopsis thaliana* (PDB code:4ic5) as search model. An independent search of PDZ domains from *E. coli* DegQ 12-mer further completed the model. As not all PDZ domains were placed correctly the assumed monomer similarity enabled symmetry related positioning of the missing or misplaced PDZ domains. Iterative cycles of

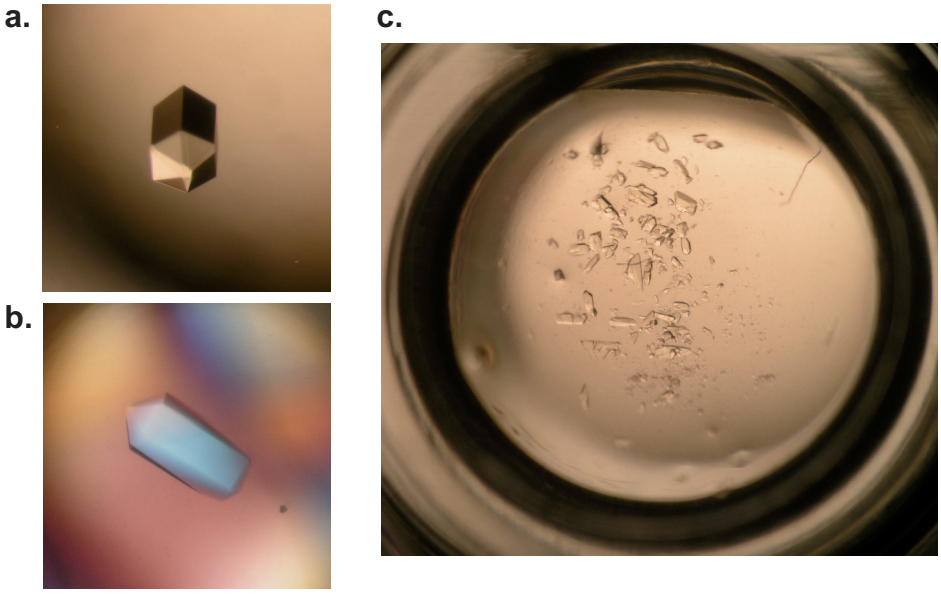

Figure 3.8: $HtrA_{Sn}$ crystals grown in 0.1 M sodium acetate pH 4.7, 0.55 M potassium citrate tribasic monohydrate and 0.05 M sodium thiocyanate. a) $HtrA_{Sn}$ 6-mer crystals form a hexagonal prism with a pointed end and b) polarize visible light. c) The presence of pept1 leads to a disruption of the crystal lattice and $HtrA_{Sn}$ 12-mer crystals form.

refinement alternating with model building lead to completion of the $HtrA_{Sn}$ 3-mer structure with a final R_{work} of 0.198 and an R_{free} of 0.237. Structure validation shows no Ramachandran outliers but 13 rotamer outliers out of 991 residues. The rotamer outliers are incorporated in hydrogen bonds or hydrophobic interactions which restricts the orientation of the amino acid side chain. Generation of symmetry mates enables the correct biological assembly of the 6-mer.

Besides $HtrA_{Sn}$, the refolded protein $HtrA_{Sn}{}^{\#}$ was crystallized in the same condition and the determined structure demonstrates a highly similar model with an overall root-mean-square devation (rmsd) of C_α-atoms of 0.625 Å. This validates the correct folding of $HtrA_{Sn}{}^{\#}$.

Soaking of $HtrA_{Sn}$ crystals with pept1 induced a change in the crystal lattice to lower symmetry. Diffraction data were collected to a resolution of 3.3 Å . The crystals belonged to space group ($P2_1$) with unit-cell parameters similar to the first successful data set (a = 142.15 Å, b = 142.62 Å, c = 203.43 Å, $\alpha = \beta = 90°$, $\gamma = 90.45°$). An initial structural model was determined by molecular replacement with the coordinates of the protease domain of the $HtrA_{Sn}$ 3-mer and individual PDZ domains and revealed a dodecameric sphere in the asymmetric unit. Refinement improved the model to an R_{work} of 0.20 and an R_{free} of 0.25, representing a three-dimensional model for an active $HtrA_{Sn}$ 12-mer. Structure validation shows 1.0 % ramachandran outliers and 1.9 % rotamer outliers of all 4878 residues which can mostly be traced back to the low res-

olution. Other crystallographic structures with the same resolution show comparable results. With the newly generated 12-mer model the first data set was reprocessed and also gave a quite similar 12-mer with an overall rmsd of C_α-atoms of 1.2 Å .

3.2.2 Crystal structure model of $HtrA_{Sn}$ 6-mer

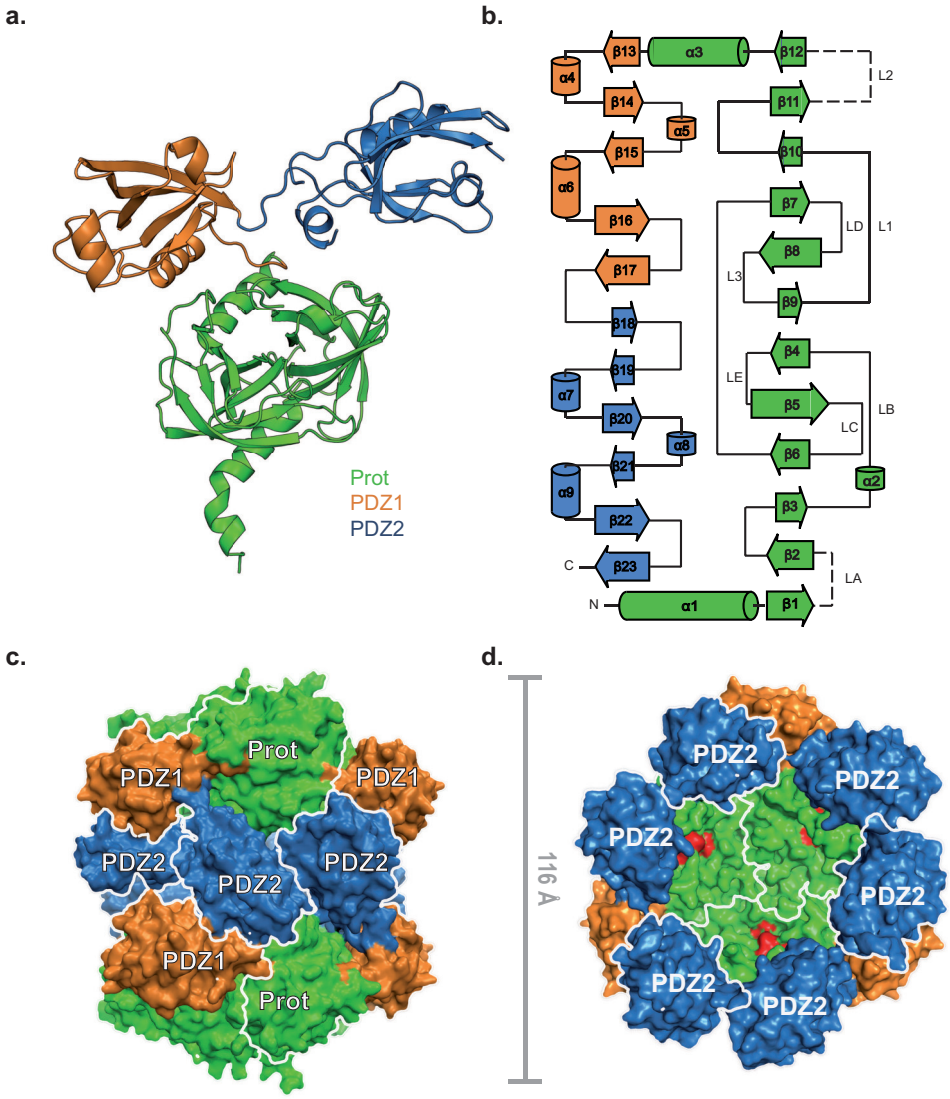

Figure 3.9: Crystal structure of the $HtrA_{Sn}$ 6-mer. a) Monomer consisting of a protease domain (green), a PDZ1 (orange) and a PDZ2 domain (blue). b) Topology model of secondary structure elements in the $HtrA_{Sn}$ monomer. c) View along the twofold axis of the $HtrA_{Sn}$ 6-mer at the intertrimeric PDZ2-interface. Individual monomers are separated by white contours. d) Sliced view of the 6-mer. Catalytic triade (red) lines the inner wall of the hollow sphere. The PDZ2 domains are forming a zipper-like ring, mediating intertrimeric contacts.

$HtrA_{Sn}$ 6-mer crystals consist of three molecules in the asymmetric unit with well-

defined electron densities for the protease domain, the PDZ1 and the PDZ2 domain (Fig. 3.9). Parts of the LA loop (71-85, 91-97) and the L2 loop (251-251) are too flexible to be traced. One monomer consists of 9 α-helices and 23 β-strands connected by loops with important regulatory functions labeled according to trypsin-protease nomenclature (e.g. L1-L3, LA-LE (Perona & Craik, 1995)). Two β-barrels enclosing the active proteolytic center and a helix at the N- and C-terminus are forming the protease domain. The PDZ1 domain consists of five antiparallel β-strands flanked by three α-helices with the peptide binding site located between β13 and α6 similar to other PDZ domains (Morais Cabral et al., 1996). The PDZ2 domain exhibits a six stranded β-barrel where bound peptide is mimicked by an additional antiparallel β-sheet (β18). The average B-factor of the protease domain (s. Tab. 3.1) is with 59.5 Å^2 significantly lower than the one for PDZ1 (71.9 Å^2) and the PDZ2 domain (124.3 Å^2). The latter two show high flexibility in contrast to the relatively rigid protease domain. The three molecules in the asymmetric unit reveal a very similar conformation with a low rmsd of C_α-atoms of 0.5 Å. They extensively interact with each other via protease domain contacts and thereby compose the basic building block of $HtrA_{Sn}$ oligomers (Fig. 3.9). A highly conserved residue D222 of the L1 loop seems to be involved in trimer stabilization as the residues of all three monomers are facing each other with a distance of $\sim$ 9 Å. Replacement of D222 by Asn reduces proteolytic activity of

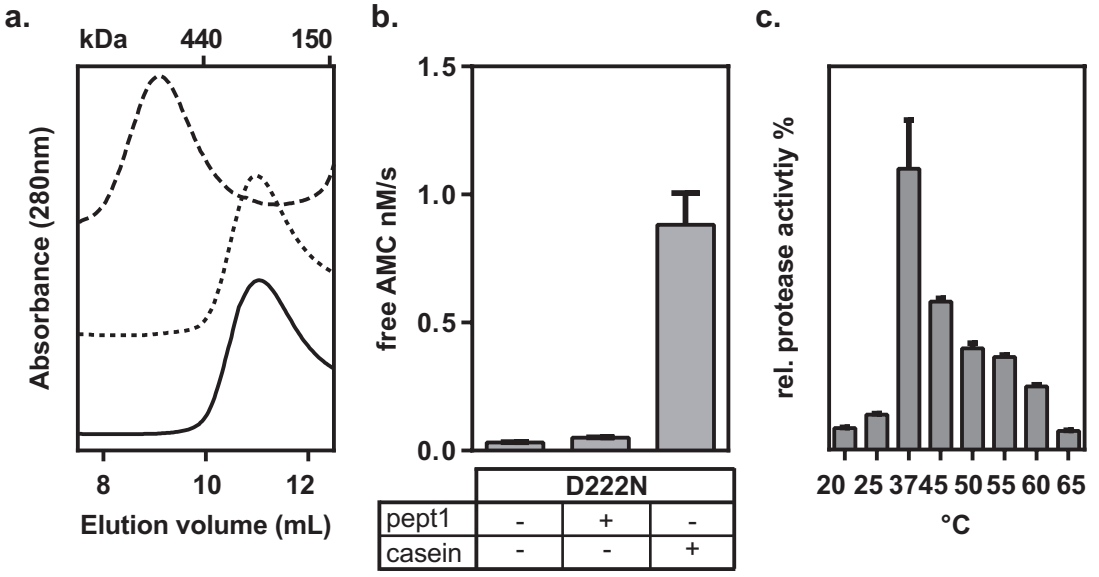

Figure 3.10: Biochemical characterization of $HtrA_{Sn}{}^{D222N}$. a) $HtrA_{Sn}{}^{D222N}$ forms higher-order oligomers in the presence of β-casein. b) The proteolytic activity of $HtrA_{Sn}{}^{D222N}$ is promoted by β-casein addition. The proteolytic activity is reduced in respect to $HtrA_{Sn}$. c) Temperature-dependent proteolytic activity of $HtrA_{Sn}{}^{D222N}$. Highest substrate cleavage rate is at 37 °C.

$HtrA_{Sn}{}^{D222N}$ but cage formation is still possible (Fig. 3.10). Intriguingly, the ability

to cleave substrate at high temperatures is severely reduced. Consequently, the D222 probably impedes the correct L1 loop orientation and proper folding of the oxyanion hole.

Two 3-mers are orientated in a face-to-face manner, forming a hollow sphere with an axial outer diameter of 116 Å and an axial width of 100 Å. At the interface between the two 3-mers, there are PDZ2 domains arranged in a zipper-like fashion (Fig. 3.9c). Two PDZ2 domains of one trimer enclose one PDZ2* domain of the opposite trimer (the asterisk denotes a contribution from a neighboring monomer). Additionally, the PDZ2 domain extensively interacts with the protease and PDZ1 domain of the adjacent trimer ensuring 6-mer stability. The α8-helix (PDZ2) contacts the stem of the LA* loop via hydrogen bonds between backbone amide of A428 to Q101 side chain and via main chain interactions between R429 and G67. The R429 side chain also forms ionic interactions with Q127 from the LB* loop. The C-terminal β23-sheet (PDZ2) is in close contact to residues of the PDZ1* domain of the opposite trimer forming a hydrophobic interface which is additionally stabilized by a hydrogen bond between Q290 and F477.

The catalytic triade is positioned at the inner wall of the protein shell in proximity to small pores (diameter: 12–13 Å) between the protease and PDZ1 domain ensuring limited entry of unfolded substrates. The PDZ1 domains poke out of the cage-like particle allowing extensive crystal contacts with the PDZ1 domain from the adjacent asymmetric unit. The active site residues (H121, D153, S230) adopt an inactive conformation with a blocked oxyanion hole and S1 specificity pocket. P227, a highly conserved residue, serves as a sensor for the active and inactive state of HtrA proteins (Wrase et al., 2011) as it performs a peptide flip upon activation.

3.2.3 Crystal structure of $HtrA_{Sn}$ 12-mer

The $HtrA_{Sn}$ 12-mer crystal contains twelve molecules in the asymmetric unit with a high similarity, as shown by an rmsd of C_α-atoms of approximately 0.6 Å. The electron density of the protease domain, PDZ1 and PDZ2 is well-defined and in contrast to the 6-mer model, the L2 loop is traceable and reduced in length. As a result, β11-strand is extended and exhibits 4 additional amino-acid residues. The LA loop (69–101) is not defined by electron density due to high flexibility. The proteolytic center adopts an active conformation with accessible oxyanion hole and S1 specificity pocket. The lateral pores show an increased diameter of 13 Å x 20 Å presumably facilitating

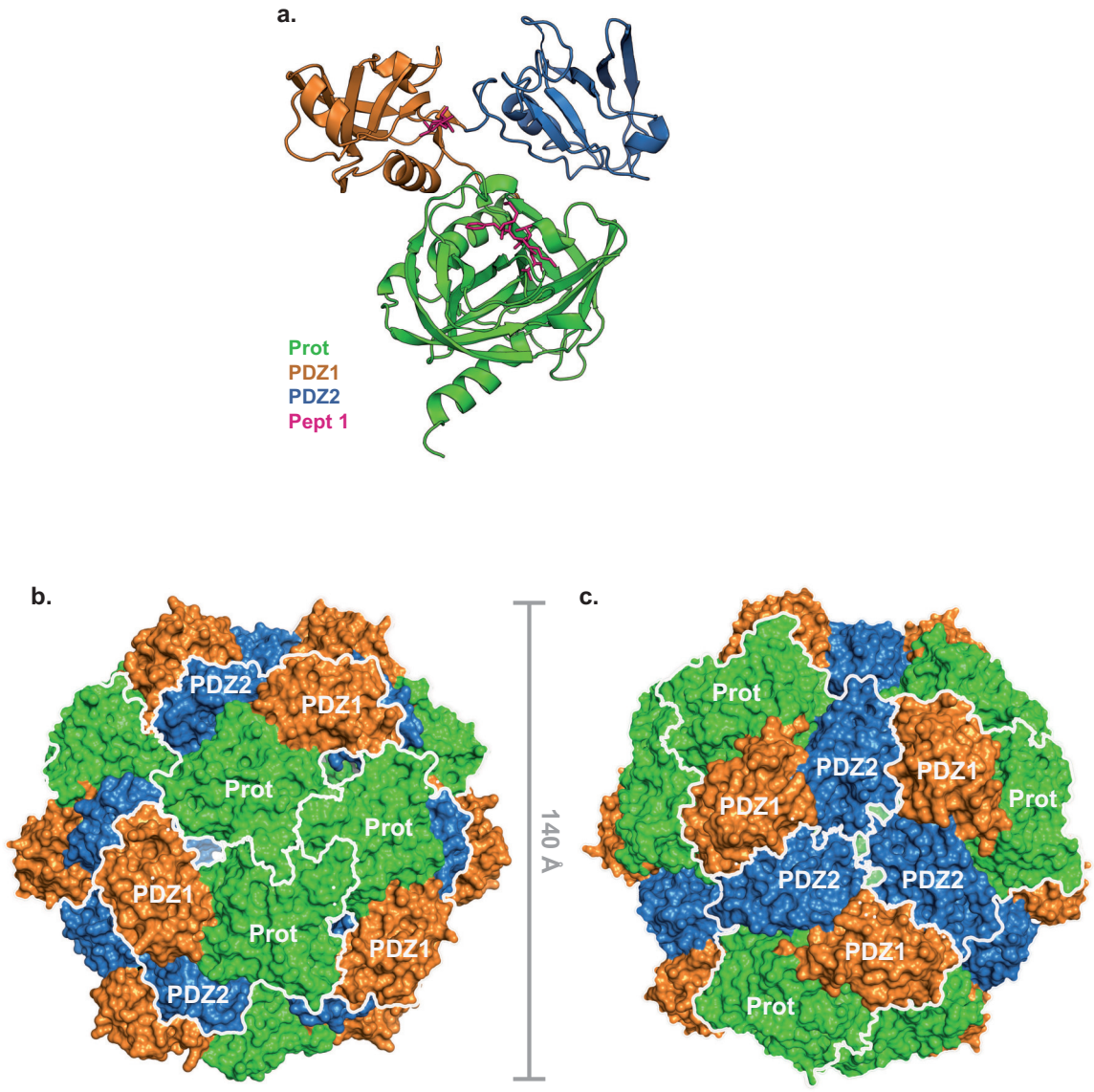

Figure 3.11: Crystal structure of the $HtrA_{Sn}$ 12-mer. a) One monomer with bound pept1 (magenta) at PDZ1 binding site and active site of the protease domain. The protease domain («Prot») is displayed in green, the PDZ1 domain in orange and the PDZ2 domain in blue. b) View along the threefold axis at the protease interface. Individual monomers are separated by white contours. c) View along the threefold axis at the PDZ2-interface. PDZ2 domains mediate intertrimeric contact to neighboring PDZ1 domains.

substrate access to the active site.

The $HtrA_{Sn}$ 12-mer displays a tetrahedral symmetry consisting of four homotrimers. Every trimer exhibits extensive protease-domain contacts. In contrast to the 6-mer

protease interface, all three L2 loops of one homotrimer in the 12-mer are in close interaction distance to each other (S252, Y255) conceivably stabilizing the active conformation. In $DegP_{Ec}$, a corresponding protein variant D232V corroborates this hypothesis, as replacement of a polar by an unpolar side chain increases proteolytic activity (Sobiecka-Szkatula et al., 2010). PDZ2 domains mediate interactions between 3-mers by forming an interface with two adjacent trimers. Additionally, a hydrophobic interface between PDZ2 and adjacent PDZ1* domain supports cage integrity.
The average temperature factor of $HtrA_{Sn}$ 12-mer is with 138 Å^2 quite high due to low resolution and high flexibility. Whereas the protease and PDZ1 domain show a B-factor of 108.4 Å2 and 111.5 Å^2, respectively, the PDZ2 domain has with 151.8 Å^2 a significantly higher delocalization of atoms (Tab. 3.1).

Table 3.1: B-factors in Å^2 of single domains of $HtrA_{Sn}$ monomer from 6- and 12-mer. (MC: Main chain/ SC: side chain/ Ov: Overall)

	MC	SC	Ov	MC	SC	Ov
	6-mer			**12-mer**		
Protease domain	56.8	55.2	59.5	107.3	96.8	108.4
PDZ1	69.5	66.3	71.9	109.8	102.1	111.5
PDZ2	125.9	113.9	124.3	151.2	140.8	151.8

Interestingly, in the PDZ1 domain and in the active site of each monomer, a peptide is bound to the $HtrA_{Sn}$ 12-mer (Fig. 3.11a). Similar to other PDZ domains, pept1 is located in the cleft between β13 and α6 of the PDZ1 domain (Doyle et al., 1996; Krojer et al., 2010; Wrase et al., 2011). Backbone amides of L285 and G286 from the carboxylate binding GLGF loop (FLGV in $HtrA_{Sn}$) are in hydrogen bonding distance to the C-terminus of the bound peptide (Fig. 3.13d). Additional hydrogen bonds by main chain contacts between Val287 and Leu289 (β13) are forming an antiparallel β-sheet. On the other side of the binding cleft, the substrate is fixed in position by highly conserved R345 (α6) side chain contacts to the backbone of the peptide. In the active site, pept1 binds via β-augmentation to the β11-sheet and is additionally stabilized by the L2 loop (Fig. 3.13d). A salt bridge between the backbone amide of G253 and the lysine side chain (P3) of the peptide stabilizes the large positively charged residue. Additional main chain contacts of I248 and S250 with P3 and P5 residue respectively, are fixing the position of the peptide. The side chain of I248 is oriented towards the S1 pocket forming hydrophobic contacts to the P1 residue side chain of the substrate and ensures the preference for small hydrophobic residues. Interestingly, there are amino-aromatic interactions from N209 of the L3 loop to a phenylalanine side chain (P4) of the substrate indicating a role of this loop in substrate binding.

The overall distance from the C-terminus of the peptide in PDZ1 binding site to the P1 site in the proteolytic center of the same protomer is around 42 Å. For $DegP_{Ec}$, a distance of 40 Å was assumed for substrate bound in the PDZ1 domain of one monomer and the protease* domain of the adjacent monomer as the distance to the same proteolytic site is with ∼ 55 Å significantly longer (Krojer et al., 2008a). In $HtrA_{Sn}$ this sort of cross-communication is not feasible as the distance to the neighboring proteolytic site is with >60 Å very large. Consequently, it is highly likely that the substrate binds in one protomer.

Table 3.2: Data collection and refinement statistics of $HtrA_{Sn}$ 6- and 12-mer crystal structure.

	$HtrA_{Sn}$ 6-mer	$HtrA_{Sn}$ 12-mer
Diffraction data statistics		
X-ray sourve	P11, PETRA III, DESY, Hamburg	
Wavelength (Å)	1.0332	1.0332
Resolution (Å)	48.23-2.32	49.25-3.3
Space group	$P3_121$	$P2_1$
Unit cell parameters (Å, °)	a=b=162.98, c=112.88	a=142.15, b=142.62, c=203.43 β=90.45
Molecules per asymmetric unit	3	12
Unique reflections	74245	121573
Multiplicity	10	3.4
Completeness (%)	98.8 (91.9)	99.5 (99.4)
R_{merge} [1]	0.085 (1.634)	0.064 (1.854)
R_{pim} [2]	0.028 (0.539)	0.041 (1.202)
$I/\sigma(I)$	16.1 (1.6)	11.6 (0.7)
$CC_{1/2}$ [3]	0.999 (0.516)	0.998 (0.293)
Wilson B factor (Å^2)	58	131.8
Refinement		
R_{work} [4]	0.198	0.20
R_{free} [4]	0.237	0.252
r.m.s.d. from ideal geometry		
Bonds (Å)	0.009	0.014
Angles (°)	1.049	1.599
Average B-factor (Å^2)	79	137
Ramachandran plot regions		
favored (%)	97.17	89.33
outlier (%)	0	1.00
PDB-Code		

Values for the highest resolution shell are shown in parenthesis

[1] $R_{merge} = \Sigma_{hkl}\Sigma_i \mid I(hkl)_i - < I(hkl) > \mid / \Sigma_{hkl}\Sigma_i I(hkl)_i$

[2] R_{pim} is the precision-indicating merging R factor (Weiss & Hilgenfeld, 1997)

[3] Correlation coefficient between two random-half data sets (Karplus & Diederichs, 2012)

[4] $R_{work} = \Sigma_{hkl} \mid F_0(hkl) - F_c(hkl) \mid / \Sigma_{hkl} F_0(hkl)$. R_{free} serves as cross-validation factor. A test set of reflections (5%) omitted from the refinement are used for calculation.

3.2.4 Comparison between the $HtrA_{Sn}$ 6-mer and 12-mer crystal structures

The structure of isolated domains in 6- and 12-mer reveals low deviation (protease domain: rmsd $\sim$ 0.8 Å, PDZ1: rmsd $\sim$ 0.6 Å, PDZ2: rmsd $\sim$ 0.9 Å. However, there are significant differences in position and orientation of surface loops in the protease domain and the entire PDZ2 domain takes a completely new position.
In the protease domain, flexible loops show a steric variation of up to 15 Å(L3 loop) between positions in 6- and 12-mer. Subsequently, the catalytic center is completely rearranged whereas the general fold is not affected. These conformational changes which might be induced by substrate binding and activate the protease, are therefore referred to as allosteric activation cascade (AAC).

Table 3.3: The RMSD of secondary structure elements in protease domain between 6- and 12-mer $HtrA_{Sn}$.

Loops	residues	rmsd (Å)	max. main chain distance (Å)
LA	66-102		
LB	124-127	1.274	1.4
LC	150-153	1.187	1.5
LD	189-195	4.431	5.7
LE	134-138	3.911	5.4
L1	222-232	1.415	2.2
L2*	247-250	(3.612)	5.1
L3	205-218	8.279	14.9

*As L2 is not completely resolved in 6-mer structure, the calculation of rmsd corresponds to the first residues which are present in both loops.

3.2.4.1 LA loop

An important regulatory element in the activation of proteolytic activity and oligomerization is the LA loop (Krojer et al., 2008a; Figaj et al., 2014). Due to its high flexibility, this loop is not fully resolved in any of the published HtrA crystal structures. In $DegP_{Ec}$, the stem of the LA loop is visible protruding from on monomer in the active site of the opposite monomer (Krojer et al., 2002).
Whereas in $HtrA_{Sn}$ 12-mer there is no well-defined electron density, in the 6-mer model the beginning (G67–D70) and end (P98–L102) of the LA loop are traceable which extends into the homotrimer not to the opposite site. G67 and Q101 are in hydrogen bonding distance to residues in PDZ2* domain (R429, A428) of the opposite trimer

suggesting a different stabilization mechanism than in $DegP_{Ec}$. Nearby, unidentified electron density is detected which could either be part of the LA loop or a co-purified peptide from *E. coli*. The latter is unlikely, as this electron density is also displayed in density maps of $HtrA_{Sn}{}^{\#}$. The electron density seems to fit two phenylalanine side chains with one enclosed other amino-acid residue (FXF motif). This motif exists in the LA loop and thereby the phenylalanines could be assigned to F76 and F78. The resolved residues in the LA loop are in hydrogen bonding distance to LB (R124), LC (T152), L2 (T246) and L3 (F218) loop. F76 forms a T-shaped aromatic-aromatic interaction with F218 from the L3 loop. It is the first time that interactions between LA and L3 loop could be visualized. Additionally, the F76 side chain forms hydrophobic interactions with I212, I248 and I262 with a maximal distance of 5 Å. These findings also underline the amino acid assignment of F76 as in *E. coli*, a bioinformatically calculated model also shows the interaction between F76 (*E. coli* equivalent F56) and I248 (*E. coli* equivalent I228) (Figaj et al., 2014). Besides, P75 is in hydrophobic interaction range (≤5 Å) to H121 from active center indicating a direct impact on proteolytic activity.

To further elucidate the binding events between LA and L3 loop, the corresponding

Table 3.4: Residues in interaction distance of ≤ 4–5 Å to the LA loop. Behind residues the belonging secondary structure element is named in parenthesis.(D/A: donor/acceptor, MC: main chain, SC: side chain, ASC: aromatic side chain)

Residue	D/A	Residue	D/A	residue	D/A	Residue	D/A
interactions with a distance of ≤ 4 Å							
6-mer				**12-mer**			
E66	O (MC)	Q127 (LB)	N (MC)	E66	O (MC)	Q127 (LB)	N (MC)
E66	O (MC)	R128 (β4)	N (MC)	G67	O (MC)	A126 (LB)	N (MC)
E66	O (SC)	R128 (β4)	N (SC)				
G67	O (MC)	A126 (LB)	N (MC)				
F76	ASC	R151 (LC)	N (SC)				
F76	ASC	F218 (L3)	ASC				
aromatic interactions with a distance of ≤ 5 Å							
F76	ASC	I212	L3				
F76	ASC	I248	L2				
F76	ASC	I262	β12				

amino acid F218 in the L3 loop has been replaced by alanine ($HtrA_{Sn}{}^{F218A}$). This drastically increases the distance to F76 and presumably weakens the hydrophobic interactions. $HtrA_{Sn}{}^{F218A}$ shows no proteolytic activity whereas oligomerization is still possible (Fig. 3.12a,b). In contrast to $HtrA_{Sn}$ (Fig. 3.6), $HtrA_{Sn}{}^{F218A}$ already assembles into mainly 12-mers at equimolar β-casein concentration. The presence of β-casein

in 5-fold excess results in 24-mer formation. Consequently, oligomerization occurs at lower substrate levels than for wildtype enzyme, indicating a destabilizing effect. As aromatic-aromatic interactions often play a crucial role in overall structure integrity, the interaction between F218 and F76 seems to be crucial for 6-mer stabilization and thereby, for regulated oligomerization. On the other hand, F218 is a highly conserved residue in L3 which is involved in contacts to the L3 loop itself, L2, β9 and β12. A substitution to alanine disrupts besides F76, two of three contacts to β12 (F260, I262) and weakens hydrophobic interactions to I212 (L3). As a result, it is difficult to pinpoint the destabilization only on the missing LA loop contact. For this reason a mutation to tyrosine has been introduced which preserves former contacts and has mainly an impact on F76. Whereas the T-shaped aromatic interaction can still take place, it pushes the LA loop from its former position. This mutant exhibits proteolytic activity with half the efficacy of $HtrA_{Sn}$ (Fig. 3.12) and is still able to from high-order oligomers. Similar to $HtrA_{Sn}{}^{F218A}$, $HtrA_{Sn}{}^{F218Y}$ oligomerizes at lower substrate concentrations. In the presence of equimolar amounts of β-casein almost half of F218Y is in 12-meric state whereas wild type $HtrA_{Sn}$ still shows mainly 6-mer cages ($\sim$85%). The amounts of oligomeric forms are quantified by peak height of SEC runs at same elution volumes (Fig.4.3). The oligomerization at lower substrate levels indicates a destabilization which can be addressed to the interaction of F218 with the LA loop.
Another interesting side effect of the $HtrA_{Sn}{}^{F218Y}$ variant is its pH sensitivity. Whereas $HtrA_{Sn}$ is stable at different pH values (Fig. 3.6), $HtrA_{Sn}{}^{F218Y}$ forms predominantly 6-mers at pH 8 and mainly 12-mers in acidic milieu (pH 4.5) (Fig. 4.3). As the LA loop contacts the H121 (L1 loop) from the active center in 6-mer state it is conceivable that protonation of the imidazole ring weakens these interactions. Taken together with the destabilizing effect of F218 replacement to tyrosine, 12-mer formation might occur in acidic milieu.

To further elucidate the importance of the LA loop for $HtrA_{Sn}$ 6-mer integrity, mutants were designed with LA-loop deletion (Δ69–100) and two ($HtrA_{Sn}{}^{\Delta 69-100/2G}$) or three glycines as linker region ($HtrA_{Sn}{}^{\Delta 69-100/3G}$). Unfortunately, the transformed *E. coli* cells showed atypical colony formation and did not produce the target protein. Either the deletion of LA loop impedes with correct folding of the protein or the manipulated protease is hyperactive which lead to cell toxicity. Consequently, the intact LA loop is required for $HtrA_{Sn}$ production.

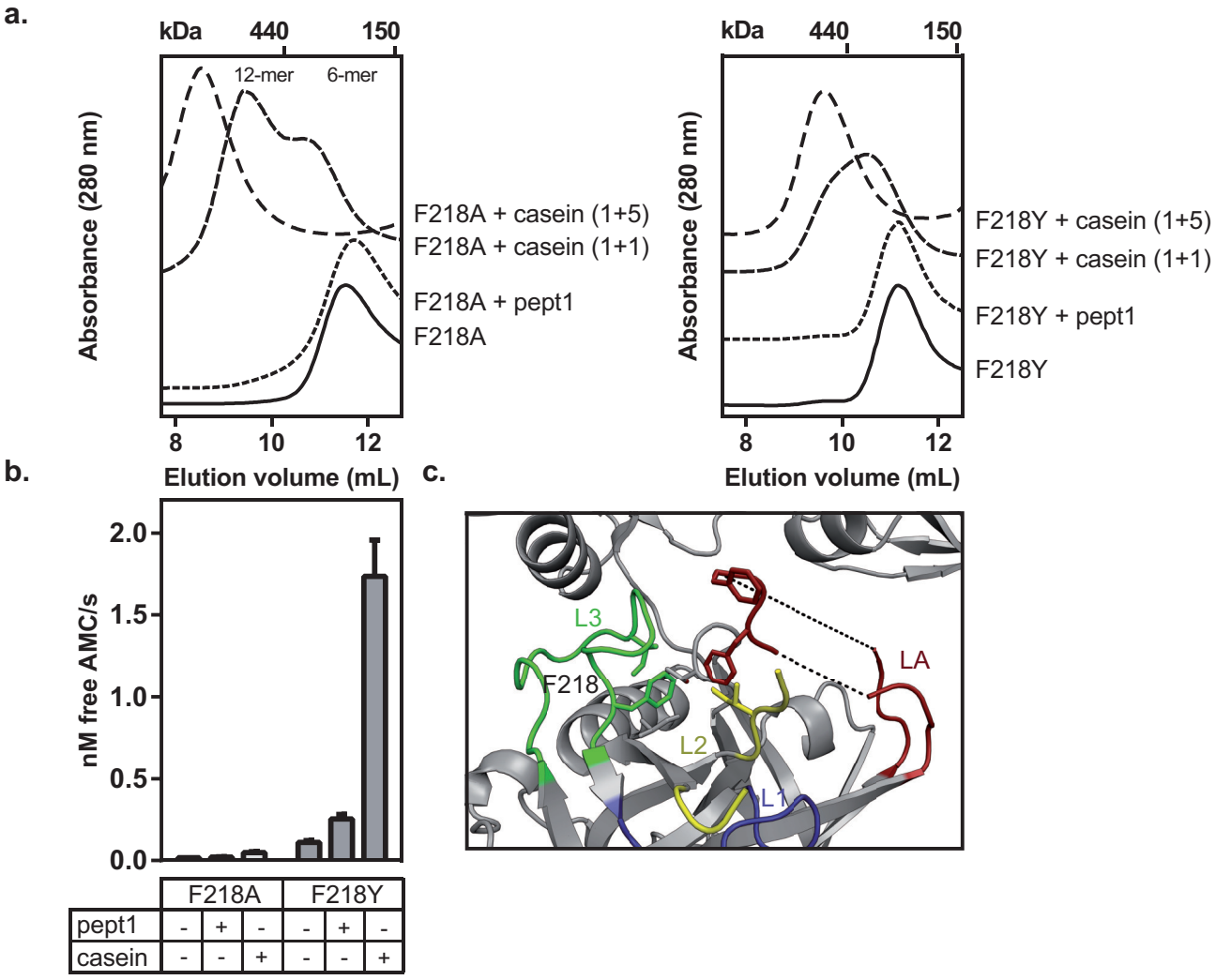

Figure 3.12: F218 of L3 loop stabilizes 6-mer assembly by interactions with LA loop. a) Results from SEC of $HtrA_{Sn}{}^{F218A}$ and $HtrA_{Sn}{}^{F218Y}$ show that both variants are able to form higher-order oligomers when β-casein is added. In contrast to $HtrA_{Sn}$, the oligomerization is induced at lower substrate concentration. b) Replacement of F218 by alanine renders protease inactive whereas $HtrA_{Sn}{}^{F218Y}$ still exhibits proteolytic activity. c) View at the defined parts of LA loop in 6-mer structure. Phenylalanine in LA loop interacts with F218 and I212 of L3 loop, with R151 (LC), I248 (L2) and I262 (β12).

3.2.4.2 LB loop

The shape of the LB loop is conserved in 6- and 12-mer state with an rmsd of 1.274 Å. This loop maintains interactions to the LC and LA loop. Oligomerization from 6- to 12-mer leads to an 1.4 Å shift of main chain atoms. The side chain amino group of R124, a residue forming hydrogen bonds to the LC loop and α2 helix moves 3.1 Å from previous position. Most interactions are conserved between both oligomeric states.

Table 3.5: Residues in interaction distance of ≤ 4 Å to the LB loop. Behind residues the belonging secondary structure element is named in parenthesis. (D/A: donor/acceptor, MC: main chain, SC: side chain)

Residue	D/A	Residue	D/A	residue	D/A	Residue	D/A
6-mer				**12-mer**			
R124	O (MC)	S69 (LA)	N (MC)	R124	N (MC)	Y120 (α2)	O (MC)
R124	N (MC)	Y120 (α2)	O (MC)	R124	N (SC)	D150 (LC)	O (SC)
R124	N (SC)	Y120 (α2)	O (SC)	A126	N (MC)	G67 (LA)	O (MC)
R124	N (SC)	D150 (LC)	O (SC)	Q127	N (MC)	E66 (LA)	O (MC)
A126	N (MC)	G67 (LA)	O (MC)				
Q127	N (MC)	E66 (LA)	O (MC)				
Q127	N (MC)	G67 (LA)	O (MC)				

3.2.4.3 LC loop

Table 3.6: Residues in interaction distance of ≤ 4 Å to the LC loop. Behind residues the belonging secondary structure element is named in parenthesis. (D/A: donor/acceptor, MC: main chain, SC: side chain, ASC: aromatic side chain)

Residue	D/A	Residue	D/A	residue	D/A	Residue	D/A
6-mer				**12-mer**			
D150	O (SC)	R124 (LB)	N (SC)	D150	O (SC)	R124 (LB)	N (SC)
R151	N (SC)	F76 (LA)	aromatic (SC)	R151	O (MC)	T213 (L3)	N (MC)
R151	N (SC)	I212 (L3)	O (MC)	R151	N (SC)	Y377	O (SC)
R151	N (SC)	Y377	O (SC)	D153	O (SC)	N119 (β3)	N (SC)
D153	O (SC)	Y120 (α2)	N (MC)	D153	O (MC)	N119 (β3)	N (SC)
D153	O (SC)	H121 (α2)	N (SC)	D153	O (SC)	Y120 (α2)	N (MC)
				D153	O (MC)	Y120 (α2)	N (MC)
				D153	O (SC)	H121 (α2)	N (SC)

The LC loop contains the aspartic acid D152 which interacts with H121 from α2. Both residues are part of the catalytic triade. Another residue which is incorporated in a lot of interactions is R151. This arginine, also found in $DegP_{Ec}$, is able to form hydrogen bonds to residues from LA, L3 and LB loop and interacts with Y377, a residue positioned in the linker region between PDZ1 and PDZ2 domain. Whereas the main chain of the LC loop shifts just maximal 1.5 Å from 6- to 12-mer, the amino group of the side chain of R151 moves around 5 Å and thereby partially changes interaction partner for hydrogen bonds. With an rmsd of 1.187 Å LC loop does not show large variations between 6-mer and 12-mer.

3.2.4.4 LD loop

The LD loop shows beside the L3 loop the biggest changes in shape and position between 6 and 12-mer which is proved by an rmsd of 4.431 Å. The main chain shifts up to 5.7 Å at the tip of the loop. Most parts of the LD loop are highly conserved among HtrA proteins indicating an important regulatory role for a functional protein. Interestingly, the LD loop interacts with loops of adjacent monomers and thereby allows intratrimeric information transfer. L193 and Q192 can both form hydrogen bonds to E216 from L3* loop in the 6-mer. Highly conserved N189 is able to interact with residues from L1 loop (G228), LE loop (H134) and β1 (Y62). The oligomerization from 6-mer to 12-mer rearranges the whole interface. In 12-mer extensive contacts to R207 (L3* loop) are mediated by L193, E194 and T196. F191 interacts via its aromatic side chain with the amino group of R251 from the L2* loop and forms an additional contact to P227 of the L1 loop.

Table 3.7: Residues in interaction distance of ≤ 4 Å to the LD loop. Behind residues the belonging secondary structure element is named in parenthesis. Residues marked by asterisks are from adjacent protomer.(D/A: donor/acceptor, MC: main chain, SC: side chain, ARS: aromatic side chain)

Residue	D/A	Residue	D/A	residue	D/A	Residue	D/A
6-mer				**12-mer**			
N189	O (SC)	Y62 (β 1)	N (MC)	N189	O (MC)	Q104 (β 2)	N (SC)
N189	O(SC)	H134 (LE)	N (SC)	N189	N (SC)	S106 (β 2)	O (SC)
N189	N (MC)	G228 (L1)	O (MC)	N189	N (MC)	S106 (β 2)	O (SC)
P190	N (MC)	G228 (L1)	O (MC)	N189	N (MC)	G228 (L1)	O (MC)
F191	ARS(SC)	Q220 (β9*)	N (SC)	F191	N (MC)	P227 (L1)	O (MC)
Q192	N (SC)	Y62 (β 1)	O (SC)	F191	ASC	R251 (L2)	N (SC)
Q192	O (SC)	K138 (LE)	N (SC)	L193	O (SC)	R207 (L3*)	N (SC)
Q192	N (SC)	E216 (L3*)	O(SC)	E194	O (SC)	H134 (LE)	N (SC)
L193	N (SC)	E216 (L3*)	O(SC)	E194	O (SC)	R207 (L3*)	N (SC)
				T196	O (SC)	R207 (L3*)	N (SC)
				T196	O (SC)	Q220 (β9*)	N (SC)

3.2.4.5 LE Loop

The LE loop is surface exposed and protrudes from the compact cage-like particle. There are significant changes in the position between 6- and 12-mer as the rmsd is with 3.911 Å quite high. Notably, this loop is longer in the 12-mer (133–140) than in the 6-mer (134–138). H134 interacts in both states with the LD loop but with different residues. In 12-mer, R139 is in hydrogen bonding distance to L302* and K303* of the

adjacent PDZ1 domain.

Table 3.8: Residues in interaction distance of ≤ 4 Å to the LE loop. Behind residues the belonging secondary structure element is named in parenthesis. Residues marked by asterisks are from adjacent protomer(D/A: donor/acceptor, MC: main chain, SC: side chain, ASC: aromatic side chain)

Residue	D/A	Residue	D/A	residue	D/A	Residue	D/A
6-mer				**12-mer**			
H134	N (SC)	T57 (α1)	O (MC)	H134	N (SC)	T57 (α1)	O (MC)
H134	N (SC)	V60 (β1)	O (MC)	H134	N (SC)	V60 (β1)	O (MC)
H134	N (SC)	N189 (LD)	O (SC)	H134	N (SC)	E172 (LD)	O (SC)
K138	N (SC)	Q192 (LD)	O (SC)	N136	N (SC)	P58 (α1)	O (MC)
				M137	O (MC)	Q162	N (SC)
				K138	N (MC)	Q162	O (SC)
				R139	N (SC)	L302*	O (MC)
				R139	N (SC)	K303*	O (MC)

3.2.4.6 L1 loop

Table 3.9: Residues in interaction distance of ≤ 4 Å to the L1 loop. Behind residues the belonging secondary structure element is named in parenthesis. Residues marked by asterisks are from adjacent protomer(D/A: donor/acceptor, MC: main chain, SC: side chain, ASC: aromatic side chain)

Residue	D/A	Residue	D/A	residue	D/A	Residue	D/A
6-mer				**12-mer**			
T221	O (MC)	G259 (β12)	N (MC)	D222	O (SC)	A199 (β8)	N (MC)
D222	O (SC)	I201 (β8)	N (SC)	D222	O (SC)	I201 (β8)	N (MC)
D222	N (MC)	S203 (β8)	O (SC)	D222	N (MC)	S203 (β8)	O (SC)
A224	N (MC)	T198 (β8)	O (SC)	A223	N (MC)	Y255 (L2)	O (SC)
A224	N (MC)	Y255 (L2)	O (SC)	A224	N (MC)	T198 (β8)	O (SC)
N226	N (SC)	M256* (L2)	O (MC)	N226	N (SC)	Y255 (L2)	N (MC)
G228	O (MC)	N189 (LD)	N (SC)	N226	N (SC)	M256 (L2*)	O (MC)
G228	O (MC)	P190 (LD)	N (MC)	P227	O (MC)	F191 (LD)	N (MC)
N229	O (MC)	N245 (β11)	N (SC)	G228	O (MC)	N189 (LD)	N (MC)
S230	O (SC)	N119 (β3)	N (SC)	S230	O (SC)	H121 (β2)	N (SC)
S230	O (SC)	A247 (L2)	N (MC)	G231	N (MC)	S106 (β2)	O (SC)
				G231	O (MC)	S106 (β2)	N (MC)
				G231	N (MC)	N119 (β3)	O (SC)
						pept1	
				G228	N (MC)	V(P1)	O (MC)
				S230	O (SC)	V(P1)	N (MC)
				S230	N (MC)	V(P1)	O (MC)

The L1 loop harbors the active serine S230, which in the 6-mer state interacts with highly conserved A247 from the L2 loop. It forms many interactions with the L2 loop (see subsection 3.2.4.7), also with neighboring L2* loop by salt bridges from N226 to M256*. Furthermore, L1 loop (G228) is able to interact with LD loop (N189, P190) in the 6-mer. These contacts are slightly changing in the $HtrA_{Sn}$ 12-mer, where P227 mediates contacts to F191 of the LD loop. In the 12-mer, S230 of the L1 loop interacts with H121 and thereby forms an active proteolytic center whereas in 6-mer both residues are 6 Å apart. Extensive contacts with β8 are preserved in both oligomeric forms problably enabling structure integration of the L1 loop. The overall position and shape of the loop stays the same (rmsd=1.415 Å).

3.2.4.7 L2 loop

Table 3.10: Residues in interaction distance of $\leq$ 4 Å to the L2 loop. Behind residues the belonging secondary structure element is named in parenthesis. Residues marked by asterisks are from adjacent protomer(D/A: donor/acceptor, MC: main chain, SC: side chain, ASC: aromatic side chain)

Residue	D/A	Residue	D/A	residue	D/A	Residue	D/A
6-mer				**12-mer**		**pept1**	
A247	O (MC)	S230 (L1)	N (MC)	G253	O (MC)	K (P3)	N (SC)
Y255	O (SC)	A224 (L1)	N (MC)	S250	O (MC)	M (P5)	N (MC)
12-mer				S250	N (MC)	M (P5)	O (MC)
R251	N (SC)	F191 (LD)	ASC	I248	O (MC)	K (P3)	N (MC)
Y255	O (SC)	A223 (L1)	N (MC)	I248	N (MC)	K (P3)	O (MC)
Y255	N (MC)	N226 (L1)	O (SC)				
M256	O (MC)	N226 (L1*)	N (SC)				

As the L2 loop in the 6-mer structure is not completely traceable by electron density, it is difficult to compare the loop in both states. For rmsd calculation, the first 4 residues have been used which differ significantly (rmsd= 3.612 Å). The L2 loop interacts extensively with the L1 loop. One important residue for these interactions is Y255 which is highly conserved in *Chlamydiae*. Y255 forms hydrogen bonds to A224 in 6-mer and to A223 and N226 in 12-mer. The proceeding residue M256 interacts with N226* of the adjacent L1* loop enabling information transfer from one monomer to another. The L2 loop is via R251 also in contact with the LD loop (F191). This interaction is unique to $HtrA_{Sn}$ as in other *Chlamydiae* species there is a glycine and in *E. coli* and *Legionella* a proline at the equivalent position. In 12-mer, the L2 loop interacts with the bound peptide. The highly conserved residues I248, S250 and G253 form hydrogen bonds to P3 (lysine) and P5 (methionine) of substrate mostly via main

chain interactions. G253 is in close contact to the side chain amino group of lysine and thereby stabilizes large polar residues.

3.2.4.8 L3 loop

Table 3.11: Residues in interaction distance of ≤ 4 Å to the L3 loop. Behind residues the belonging secondary structure element is named in parenthesis. Residues marked by asterisks are from adjacent protomer (D/A: donor/acceptor, MC: main chain, SC: side chain, ASC: aromatic side chain)

Residue	D/A	Residue	D/A	residue	D/A	Residue	D/A
6-mer				**12-mer**			
K205	N (SC)	D176	O (MC)	R207	N (SC)	L193 (LD*)	O (MC)
K205	N (SC)	V178	O (MC)	R207	N (SC)	E172 (LD*)	O (SC)
K205	N (MC)	E172 (LD*)	O (SC)	R207	N (SC)	T196 (β 8)	O (SC)
Q208	O (SC)	D176	N (MC)	R207	N (SC)	Q220 (β 9)	O (SC)
N209	N (SC)	N343 (α6)	O (SC)	Q208	O (SC)	N343 (α6)	N (SC)
Q211	O (SC)	R282	N (SC)	Q208	O (SC)	N346 (α6)	N (SC)
I212	O (MC)	R129 (LC)	N (SC)	N209	N (SC)	F (pept1)	ASC
E216	O (SC)	L193 (LD*)	N (MC)	T213	N (MC)	R129 (LC)	O (MC)
E216	O (SC)	Q192 (LD*)	N (MC)	D214	N (MC)	R129 (LC)	O (MC)
F218	ASC	F76 (LA)	ASC	D214	O (SC)	R282	N (SC)
F218	ASC	F260 (β 12)	ASC	L215	N (MC)	R129 (LC)	O (MC)
L219	N (MC)	E172 (LD*)	O (SC)	E216	O (SC)	R345 (α6)	N (SC)
L219	N (MC)	A261 (β 12)	O (MC)	E216	O (MC)	N346 (α6)	N (SC)
				F218	ASC	F260 (β 12)	ASC

The L3-loop changes show the largest deviation between 6-mer and 12-mer state with an rmsd of 8.279 Å. The main chain C_α of L210 moves 14.9 Å between the two oligomeric states.

This loop displays an interface between the protease and PDZ1 domain on the one hand and the adjacent protease* domains on the other hand. In 6-mer state there are extensive contacts between L3 (K205, E216, G219) and LD* loop (Q191, L193, E194). Upon 12-merization these interactions are rearranged. R207 contacts the LD* loop (L193, E194). N209 interacts in 6-mer with N343 and N346 from α6-helix of PDZ1 which is part of the substrate binding site via hydrogen bonds and electrostatic interactions, respectively. These interactions are preserved in the 12-mer, just the binding partners in the L3 loop become Q208 and E216. Additionally, E216 from $HtrA_{Sn}$ 12-mer forms contacts to R345, another residue from α6 (PDZ1). Interestingly, these highly conserved residues have a distance of 14 Å in the 6-mer state before oligomerization.

In the 12-mer, N209 interacts with peptide bound in the active site. The contacts are

mediated by the aromatic side chain of P4 phenylalanine and the positively charged asparagine side chain. Therefore, the L3 loop does not just interact indirectly with bound substrate in PDZ1 via α6 but also with bound peptide in the active site, emphasizing the unique role of this loop in HtrA proteases.

3.2.5 AAC of $HtrA_{Sn}$

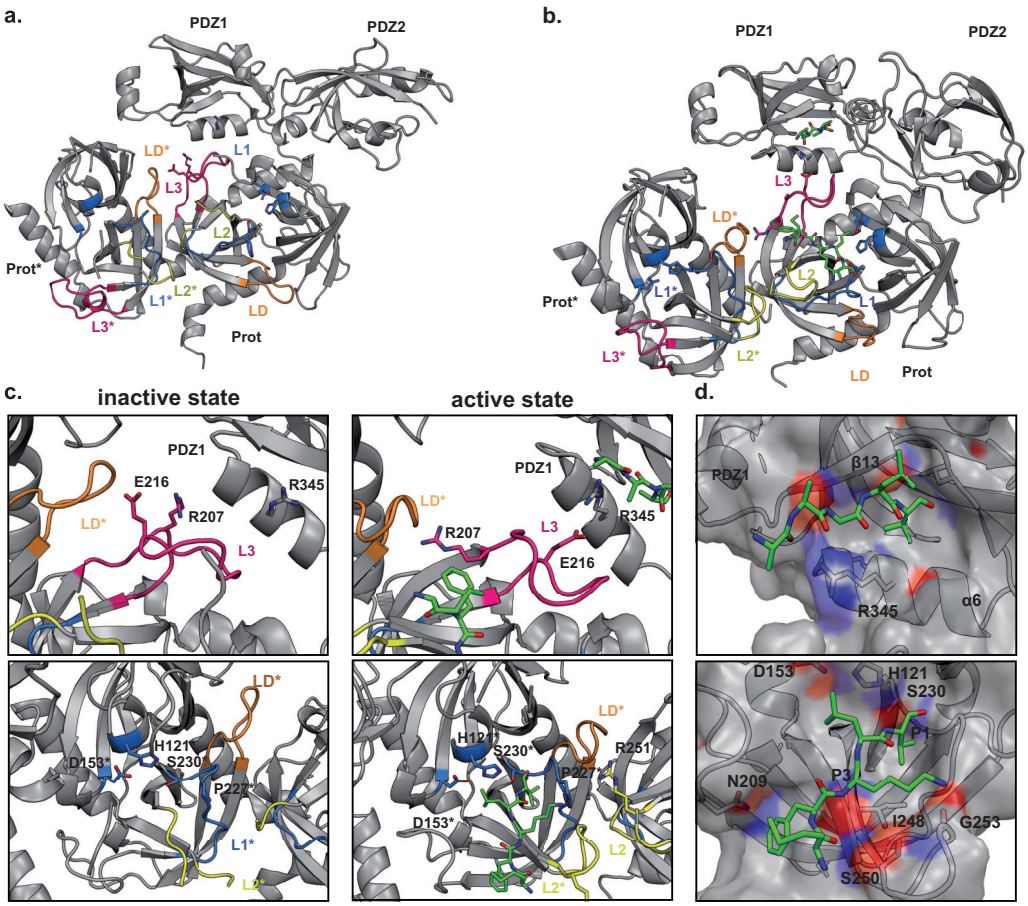

Figure 3.13: AAC of $HtrA_{Sn}$. a) Proteolytic inactive monomer from the $HtrA_{Sn}$ 6-mer with the adjacent protease domain (»Prot«). Structure elements from neighboring domains are marked by asterisks. b) One monomer of the $HtrA_{Sn}$ 12-mer with adjacent protease domain in active state with bound peptides in PDZ1 domain and in active center. c) PDZ1 interface with protease domain in active and inactive state. Peptide binding induces reorientation of the L3 loop and subsequently a LD* loop displacement. The LD* loop interacts with the L1* loop, unblocks the oxyanion hole and contacts to the L2 loop, which enables formation of the S1 binding pocket. After these conformational changes the protease is active. d) Pept1 in the PDZ1 domain and active site binding cleft. Positive charges are colored in blue, negative charges in red, visualizing interactions between peptides and the protease. In the PDZ1 domain, the peptide binds via β-augmentation. The peptide in the active center forms hydrogen bonds with residues from the L2 loop.

In the $HtrA_{Sn}$ 12-mer model, pept1 is bound to the PDZ1 binding site via β-augmentation (Fig 3.13d). On the opposite site of the binding cleft, the highly conserved R345 side chain (α6) is oriented towards the bound substrate and fixates its position by interactions with the carboxylate group of the peptide backbone (Fig 3.13a,c). For $DegP_{Ec}$, this arginine has been reported as a trigger for AAC by reorientation of the PDZ1 domain (Krojer et al., 2002). Indeed in $HtrA_{Sn}$, the position of R345 switches between the 6- and 12-mer state upon substrate binding, unblocks the PDZ1 binding site and is able to mediate contacts to the highly conserved E216 in the L3 loop. Rearrangement of the L3 loop enables interactions between R207 (L3) to the backbone amide of E216* and the side chain of T196* of adjacent LD* loop leading to a conformational change. Subsequently, the remodeled LD* loop leads to changes in L1* and intriguingly in adjacent L2 loop. A newly formed contact between F191* (LD*-loop) to P227* (L1*-loop) induces a proline peptide switch freeing the blocked oxyanion hole. Additional contacts between F191* and R251 from L2 loop which in turn interacts with S252* from opposite L2* loop facilitates the formation of S1 specificity pocket, enabling substrate binding. The extensive cross-talk between adjacent monomers is essential for the correct folding of proteolytic active centers.

3.2.6 The interaction between Q290 and F477 stabilizes cages

The position and orientation of the PDZ domains in $HtrA_{Sn}$ 6- and 12-mer changes upon oligomerization. A detailed analysis of PDZ-PDZ interactions between two adjacent homotrimers is conducted to shed light on the assembly mode of $HtrA_{Sn}$.
Upon substrate binding, the secondary structure elements α6 and β13 near the PDZ1 binding site show a shift in their position (Fig. 3.15a) between 6-mer and 12-mer. Consequently, they induce rotation and translation of adjacent elements like, e.g. α5 which moves around 9 Å from its former position in the 6-mer. The PDZ1 and PDZ2* domains from the opposite trimer form a hydrophobic interface in the 6-mer which is preserved in the 12-mer. In contrast, the PDZ2 domain switches around ~ 50 ° from 6- to 12-mer, repositioning the whole domain. The PDZ2 domain in the 12-mer is in closer contact to the PDZ1 and protease domain of the same monomer. The exact mechanism which rearranges the PDZ2 domain completely is not clear.

A closer look at the PDZ1-PDZ2* interface reveals interactions between the C-terminus of $HtrA_{Sn}$ (β23*) and residues from β13-α4 in the PDZ1 domain. For $DegQ_{Lf}$, the last nine residues of the C-terminus are crucial for higher-order oligomer assembly (Wrase

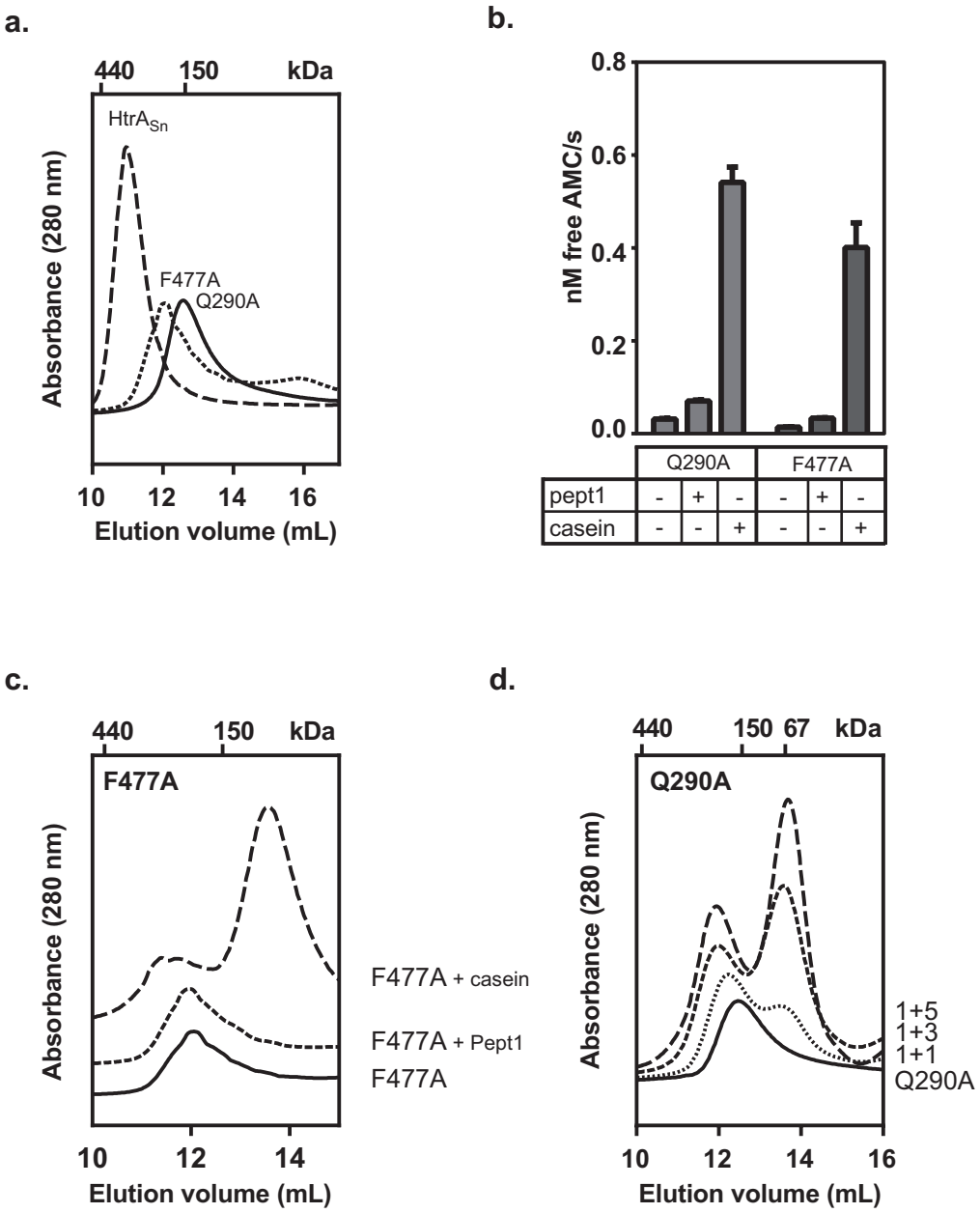

Figure 3.14: Biochemical analysis of $HtrA_{Sn}{}^{F477A}$ and $HtrA_{Sn}{}^{Q290A}$. a) $HtrA_{Sn}{}^{F477A}$ and $HtrA_{Sn}{}^{Q290A}$ elute as 3-mers in SEC. b) In the presence of β-casein both variants show proteolytic activity. c) $HtrA_{Sn}{}^{F477A}$ is not able to form higher-order oligomers. The presence of β-casein leads to a small shift which occurs probably due to substrate binding. c) $HtrA_{Sn}{}^{Q290A}$ binds to β-casein and thereby, the apparent molecular weight increases stepwise. No cage assembly is visible.

et al., 2011). Sequence alignment of these residues shows genus-specific conservation of residues. Within the chlamydial family F477 is conserved, in *E. coli* and *Legionella* this residues is a tyrosine. The *E. coli* $DegP_{Ec}{}^{Y444A}$ variant appears mainly as trimer corroborating the importance of this residue for oligomerization (Kim & Sauer, 2012). In $HtrA_{Sn}$, replacement of F477 with an alanine ($HtrA_{Sn}{}^{F477A}$) predominantly leads to

3-mer formation without the ability to form cages (Fig. 3.14c). Nevertheless, F477A shows basal proteolytic activity in the presence of β-casein (s. Fig3.14b). As part of β23, the F477 side chain forms a hydrophobic interface with L309-V311 and G327 of the PDZ1 domain. This interface could be important for 12-merization as alanine replacement disrupts these contacts and no higher-order oligomer was detectable. In the 12-mer, F477 is in hydrophobic interaction distance to L309 and V311 and to a highly conserved L296 in the α4-helix of PDZ1 domain. The latter is a unique contact only occurring in 12-mer assembly. However, the *E. coli* equivalent $DegP_{Ec}^{L276A}$ is still able to form higher-order oligomers (Kim & Sauer, 2012), thereby indicating no essential role for the oligomerization mechanism. Interestingly, F477 forms one hydrogen bond to the side chain of Q290 (β13) which is stable in 6- and 12-mer and exhibits the only hydrogen bond in the PDZ1-PDZ2* interface. An exchange of Q290 to alanine prevents the formation of hydrogen bonds.

The $HtrA_{Sn}^{Q290A}$ variant elutes exclusively as a trimer in SEC (Fig. 3.14c). The presence of β-casein increases the molecular weight in a concentration-dependent manner but without the formation of cages (Fig. 3.14). The same dose-dependent increase in size has been observed for $HtrA_{Sn}$ (Fig. 3.6). In this study a mechanism has been proposed in which the substrate binds stepwise and thereby increases the molecular weight, or alternatively an intermediate 9-mer state is formed. The inability of $HtrA_{Sn}^{Q290A}$ to form higher-order oligomers excludes the possibility of an intermediate state. These experiments substantiate the hypothesis of a stepwise binding mechanism.
The $HtrA_{Sn}^{Q290A}$ variant shows a similar proteolytic rate to $HtrA_{Sn}^{F477A}$. Taken together, these results indicate that the hydrogen bond between Q290 (PDZ1) and F477 (PDZ2*) is an essential contact in the PDZ1-PDZ2*-interface stabilizing both 6- and 12-mer oligomeric state. As main chain interactions of F477 form the hydrogen bond, the alanine substitution should not influence this contact. Nevertheless, $HtrA_{Sn}^{F477A}$ shows only trimeric assembly indicating that besides the hydrogen bond, the aromatic side chain interactions of the phenylalanine are important for the structural integrity of the PDZ1-PDZ2*-interface.

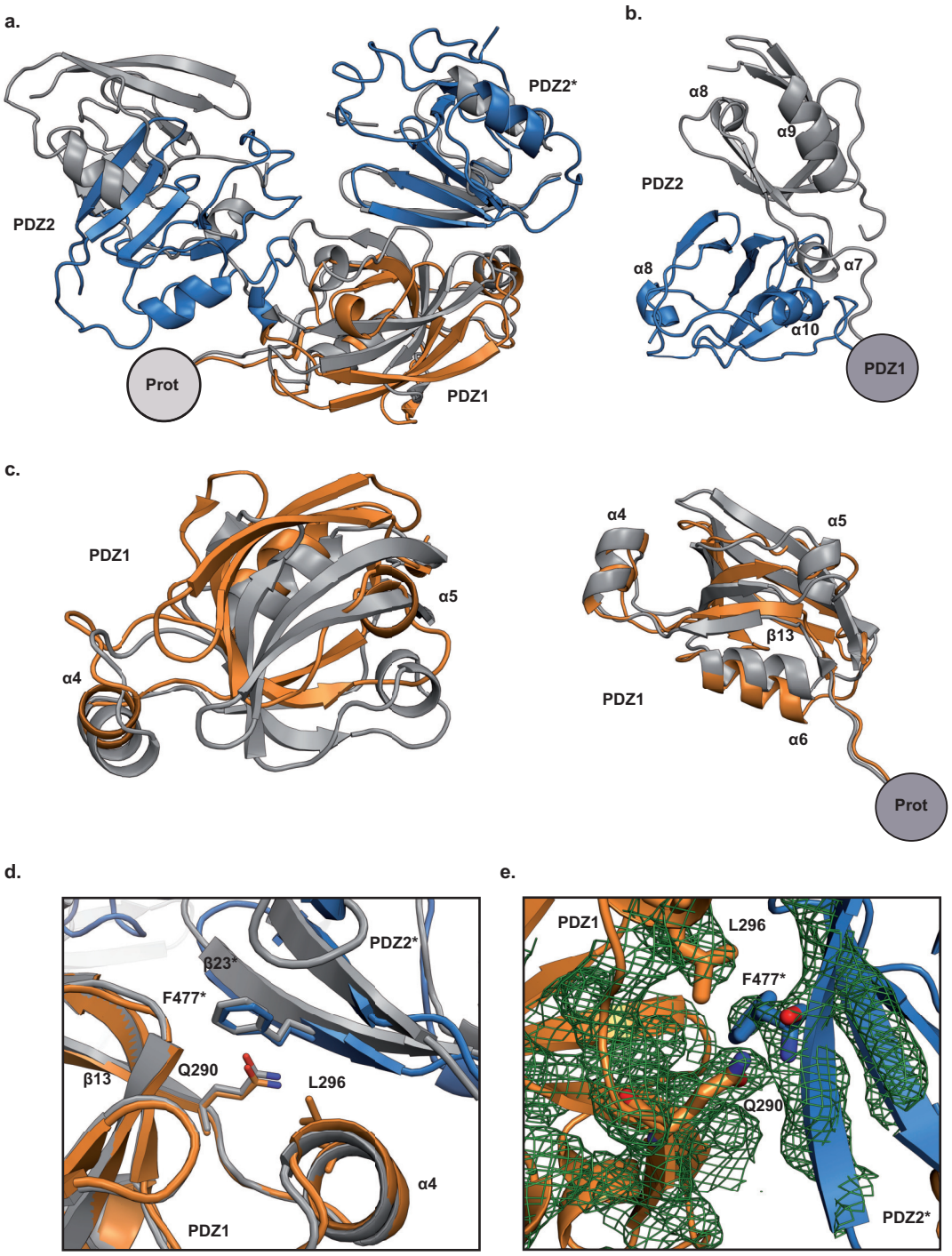

Figure 3.15: Comparison of the PDZ1 and PDZ2 domain positions in 6- and 12-mer. a) Overlay of the PDZ1 (6-mer: grey, 12-mer: orange) and the PDZ2 (6-mer: grey, 12-mer: blue) domains of one $HtrA_{Sn}$ monomer and the adjacent PDZ2* domain. In the $HtrA_{Sn}$ 12-mer, the PDZ2 domain is in close proximity with the protease and PDZ1 domain of the same monomer. b) Overlay of the PDZ2 domains from 6-mer and 12-mer aligned in PDZ1. The 12-mer PDZ2 domain is reoriented around 50° and rotated in contrast to position in 6-mer. c) Overlay of the PDZ1 domains from 6-mer and 12-mer from the side and from above, aligned in the protease domain. Secondary structure elements are shifted up to ~ 9 Å($\alpha 5$). d) Overlay of the hydrophobic PDZ1-PDZ2*domain interface in 6- and 12-mer aligned in the PDZ1 domain with important residues depicted as sticks. e) Electron density map of the hydrogen bond between Q290 and F477* in $HtrA_{Sn}$ 6-mer.

3.2.7 $HtrA_{Sn}$ 6- and 12-mer crystal structures reveal a unique architecture

$DegP_{Ec}$ and DegQ proteins from *Legionella* show a similar structural assembly to the three-dimensional models of $HtrA_{Sn}$ 6- and 12-mer. An alignment of the crystal structures of $DegP_{Ec}$ 6-mer (PDB code: 1KY9), 12-mer (PDB code: 3OTP), and $DegQ_{Lf}$ (PDB code: 3PV2) with $HtrA_{Sn}$ allows the comparison of the overall protein architecture. Despite their high amino acid sequence identity of around 40 %, the geometry of the $HtrA_{Sn}$ 6-mer and 12-mer differs significantly from $DegP_{Ec}$ and $DegQ_{Lf}$ which is due to the deviations in the positioning of the PDZ1 and PDZ2 domain.

The $HtrA_{Sn}$ 6-mer is a condensed spherical particle with an axial diameter of $\sim$ 116 Å. In contrast the $DegP_{Ec}$ 6-mer axial diameter is with $\sim$ 85 Å significantly shorter and the whole particle is arranged in a different fashion (Fig. 3.16). When aligned separately the rmsd of the C_α atoms of the protease domain of the $HtrA_{Sn}$ and $DegP_{Ec}$ 6-mer is low (rmsd $\sim$ 0.9 Å Å). The comparison of the PDZ1 domains also shows a very similar fold (rmsd $\sim$ 1.2 Å). Only the helix α4 is shifted $\sim$ 8 Å in contrast to the $HtrA_{Sn}$ PDZ1 domain (Fig. 3.16a). As the PDZ2 domain is the most flexible domain within the 6-meric particle the rmsd shows with 2.18 Å the biggest difference but the overall fold is quite comparable. Interestingly, $DegP_{Ec}$ comprises two different conformations within the asymmetric unit of the protein crystals. These crystal structures differ significantly in their PDZ1-domain position and are referred to as »open« and »closed« forms (Fig. 3.16) (Krojer et al., 2002).
An overlay of the C_α atoms of the protease domain of the $HtrA_{Sn}$ and $DegP_{Ec}$ 6-mer shows different positions of the PDZ1 and PDZ2 domains (Fig. 3.17a). The PDZ1 domain of the closed $DegP_{Ec}$ is tilted away 45° in comparison to the position of the PDZ1 domain of the $HtrA_{Sn}$ 6-mer (Fig. 3.17b) whereas the PDZ1 domain of the open $DegP_{Ec}$ shows a completely different orientation (Fig. 3.17b). Big lateral apertures are formed between the PDZ1 and the protease domain of the $DegP_{Ec}$ 6-mer. Consequently, the access to the substrate binding cleft of the PDZ1 domain differs between the $HtrA_{Sn}$ and the $DegP_{Ec}$ 6-mer.
The $DegP_{Ec}$ PDZ1 domain stabilizes the cage-like formation by interactions with the opposite PDZ1* and PDZ2* domains. Loop interactions between the PDZ1 and the PDZ2* domain of the opposite protomer are forming the PDZ1-PDZ2* domain interface. The PDZ2 domain of the $DegP_{Ec}$ 6-mer is in close proximity to the protease domain of the same monomer. These interactions might stabilize the proteolytic inactive state of $DegP_{Ec}$ which is in accordance with the proposed inhibitory role of the PDZ2 domain (Jiang et al., 2008). Extensive LA loop interactions support the struc-

tural integrity of the 6-mer (Fig. 3.16b) and keep the protease inactive (Figaj et al., 2014).

In the $HtrA_{Sn}$ 6-mer, the PDZ2 domains are the key players in mediating the interactions between opposite monomers and thereby providing structural integrity. The PDZ2 domain of one monomer is enclosed by two PDZ2* domains of the opposite trimeric building block, and interacts additionally with the protease* and PDZ1* domain of one opposite monomer (Fig. 3.9c, 3.16a). The PDZ1-PDZ2* interface is maintained by interactions between β13-α4 (PDZ1) and β23 (PDZ2*)(Fig. 3.15d). A compact and stable 6-mer is formed. The PDZ2 domain of one $HtrA_{Sn}$ protomer is not in interaction distance to the protease domain of the same monomer and the LA loop does not protrude into the opposite trimer. This suggests that the more condensed architecture of the $HtrA_{Sn}$ 6-mer with very small entry pores is sufficient to regulate proteolytic activity.

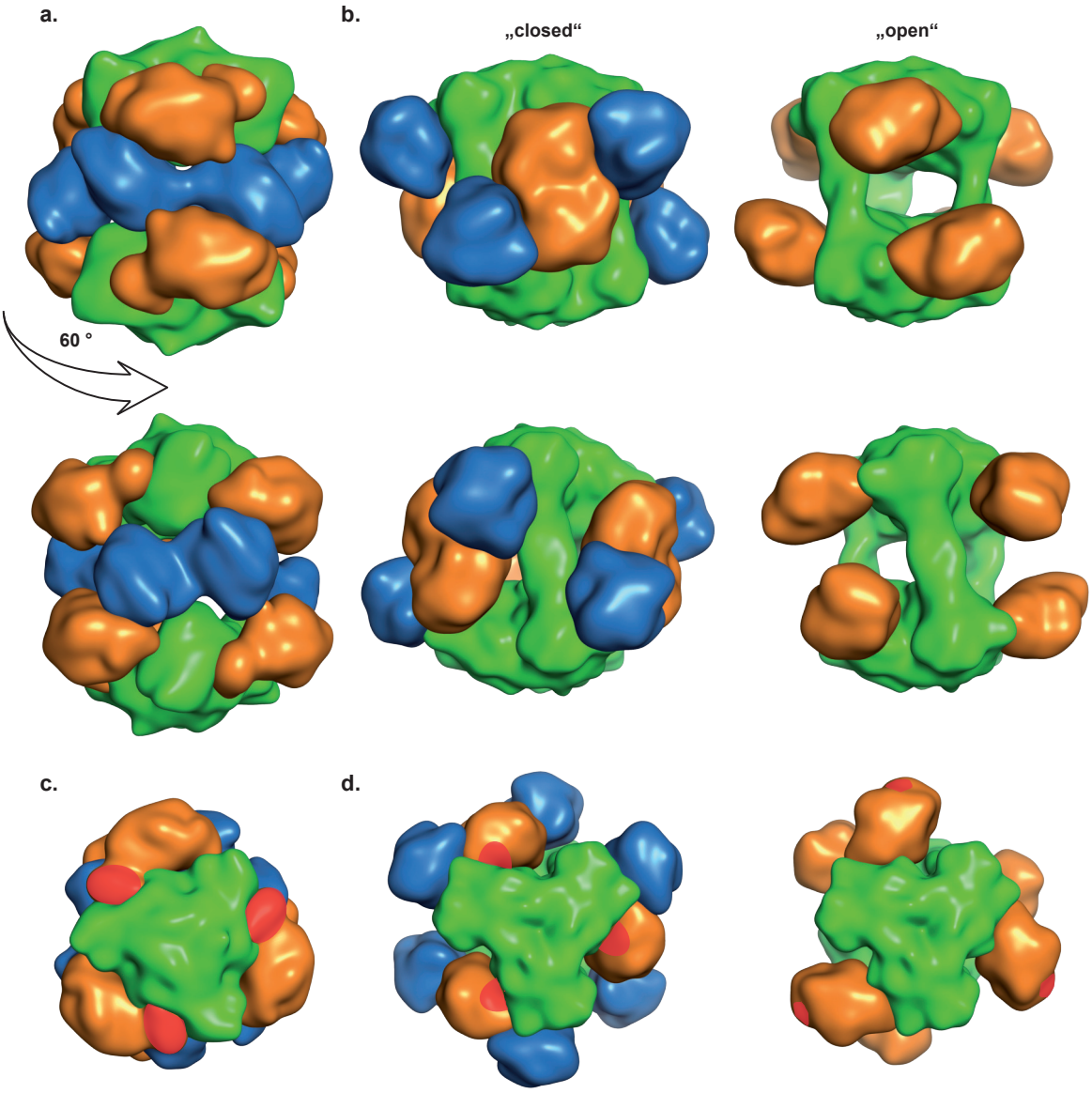

Figure 3.16: Unique architecture of the $HtrA_{Sn}$ 6-mer. a) Side view of the $HtrA_{Sn}$ 6-mer with the protease (green) interface on top. The PDZ2 domains (blue) are stabilizing the intertrimeric interface by interactions with the opposite protease*, PDZ1* (orange) and PDZ2* domain. One PDZ2 domain is flanked by two PDZ2* domains of the opposite trimer in a zipper-like-fashion. b) Side view of the $DegP_{Ec}$ 6-mer in open and closed conformation aligned in protease domain with $HtrA_{Sn}$. The PDZ1 domain interacts with the PDZ1* and PDZ2* domain of the opposite trimer in closed state. LA loop interactions stabilize the $DegP_{Ec}$ 6-mers in both conformations. In the open conformation, the PDZ2 domains are missing due to high flexibility. c) Top view on the protease interface of the $HtrA_{Sn}$ 6-mer shows a compact particle. Marked in red is the substrate binding site of the PDZ1 domain. d) Top view on the protease interface of the $DegP_{Ec}$ 6-mer. The PDZ2 domains are exposed to the environment in closed state. Depicted in red is the PDZ1 binding site.

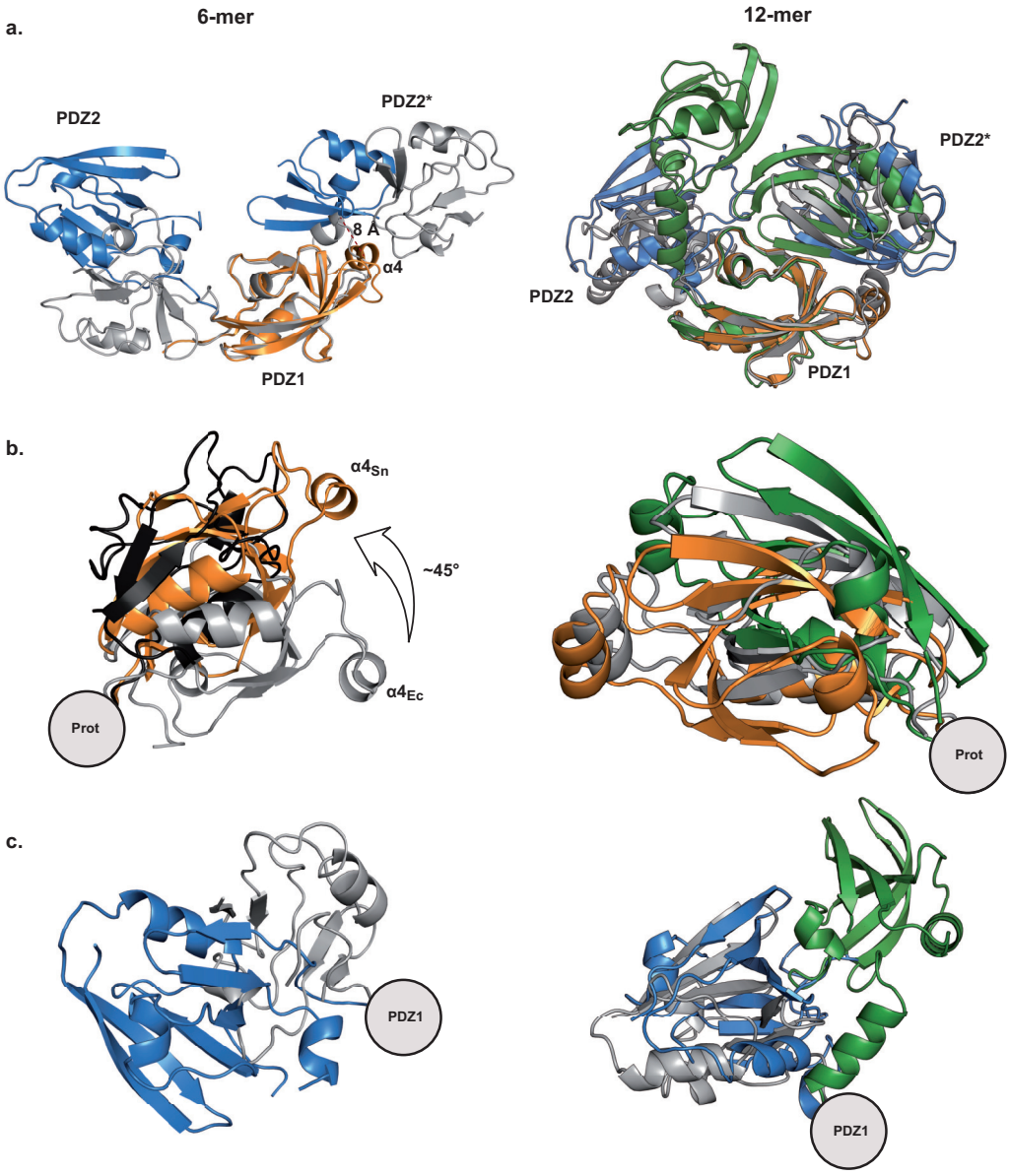

Figure 3.17: The PDZ1 and PDZ2 domains of the 6 and 12-mer HtrA crystal structures (HtrASn: PDZ1 - orange, PDZ2 - blue, $DegP_{Ec}$: grey (closed form) black (open form), $DegQ_{Lf}$: green). a) PDZ1-PDZ2* interface of $HtrA_{Sn}$, $DegP_{Ec}$ and $DegQ_{Lf}$ aligned in PDZ1 domain. In the 6-mer crystal structures of $HtrA_{Sn}$ and $DegP_{Ec}$ (»closed« conformation) the PDZ1-PDZ2* interface differs significantly whereas in the 12-mer, there are just small changes. b)PDZ1 domains aligned in the protease domain for the $HtrA_{Sn}$ 6- and 12-mer crystal structures in comparison to $DegP_{Ec}$ and $DegQ_{Lf}$. c) Comparison of PDZ2 domains of $HtrA_{Sn}$, $DegP_{Ec}$and $DegQ_{Lf}$ in 6-mer and 12-mer structure aligned in the PDZ1 domain.

The HtrA 12-mer structures are huge spherical particles with the same dimension in all three organisms (Fig. 3.18). The $HtrA_{Sn}$ 12-mer forms a compact cage with a convex protease interface. Whereas the $DegP_{Ec}$ 12-mer shows a similar curved protease interface, the $DegQ_{Lf}$ 12-mer reveals an almost planar protease interface.
The alignment of separate domains shows a high similarity between all three crystal structures (Tab. 3.12).

Table 3.12: The RMSD of the C_α-atoms of the separate domains from model structures of $HtrA_{Sn}$ 12-mer in comparison with the $DegP_{Ec}$ and $DegQ_{Lf}$ 12-mer.

Domain	**$DegP_{Ec}$ 12-mer**	**$DegQ_{Lf}$ 12-mer**
Protease	0.576	0.813
PDZ1	0.719	0.985
PDZ2	2.056	1.577

The $HtrA_{Sn}$ PDZ1 domains are surface-exposed and facilitate substrate binding. Based on the protease domain, the $DegP_{Ec}$ PDZ1 domain is shifted ∼3–4 Å (α6) and rotated around α6 (35-40°) compared to the $HtrA_{Sn}$ 12-mer PDZ1 domain. The PDZ1 domain of the $DegQ_{Lf}$ 12-mer is 45° rotated around the α6-helix compared to the PDZ1 domain of $HtrA_{Sn}$ (Fig. 3.18b). Interestingly, they are all forming hydrophobic PDZ1-PDZ2* domain interfaces indicating the importance of these contacts for oligomer stability.
In comparison to the PDZ2 domain of $HtrA_{Sn}$, the $DegQ_{Lf}$ PDZ2 domain is shifted ∼ 20 Å and slightly rotated. The PDZ2 domain of $DegP_{Ec}$ shows a rotation of ∼100° around α9 with respect to the $HtrA_{Sn}$ PDZ2 domain. The PDZ2 domain of one monomer forms an interface with two adjacent PDZ2* domains (Fig. 3.18b,c). The different orientations and positions of the PDZ2 domains form diverse PDZ2-domain interfaces. In the $HtrA_{Sn}$ 12-mer, loop interactions (loop between α7 and β20) are maintaining the PDZ2-domain interface. Additional contacts to the protease domain of the same monomer and one PDZ1* domain of the neighboring monomer stabilize the 12-mer cage. The interactions with the protease domain position the PDZ2 domains towards the inner cavity lead to the formation of a funnel-like shape. This shape restricts the inner cavity of the $HtrA_{Sn}$ 12-mer. The inner distance (11–14 Å) between two PDZ2-domain interfaces is a third of the inner distance between two PDZ2-domain interfaces of $DegQ_{Lf}$ (45 Å). In $DegQ_{Lf}$, β18-sheets are forming the PDZ2-domain interface. One PDZ2 domain interacts with two neighboring PDZ2* domains, one PDZ1* domain and one protease* domain in the adjacent trimer. In the $DegP_{Ec}$ 12-mer, the distances between adjacent PDZ2 domains are very large which lead to a more open PDZ2-domain interface. This allows close interactions of the PDZ2 domains with the PDZ1* domains of the neighboring trimer. The different positioning and interaction profiles

of the PDZ2 domains of each HtrA protein lead to distinct features in the structural architecture. The position of the PDZ2 domain is limited by the length of the flexible linker region between the PDZ1 and PDZ2 domain. For $DegP_{Ec}$ it has been described that changes in the linker region result in different oligomeric forms (Jiang et al., 2008).

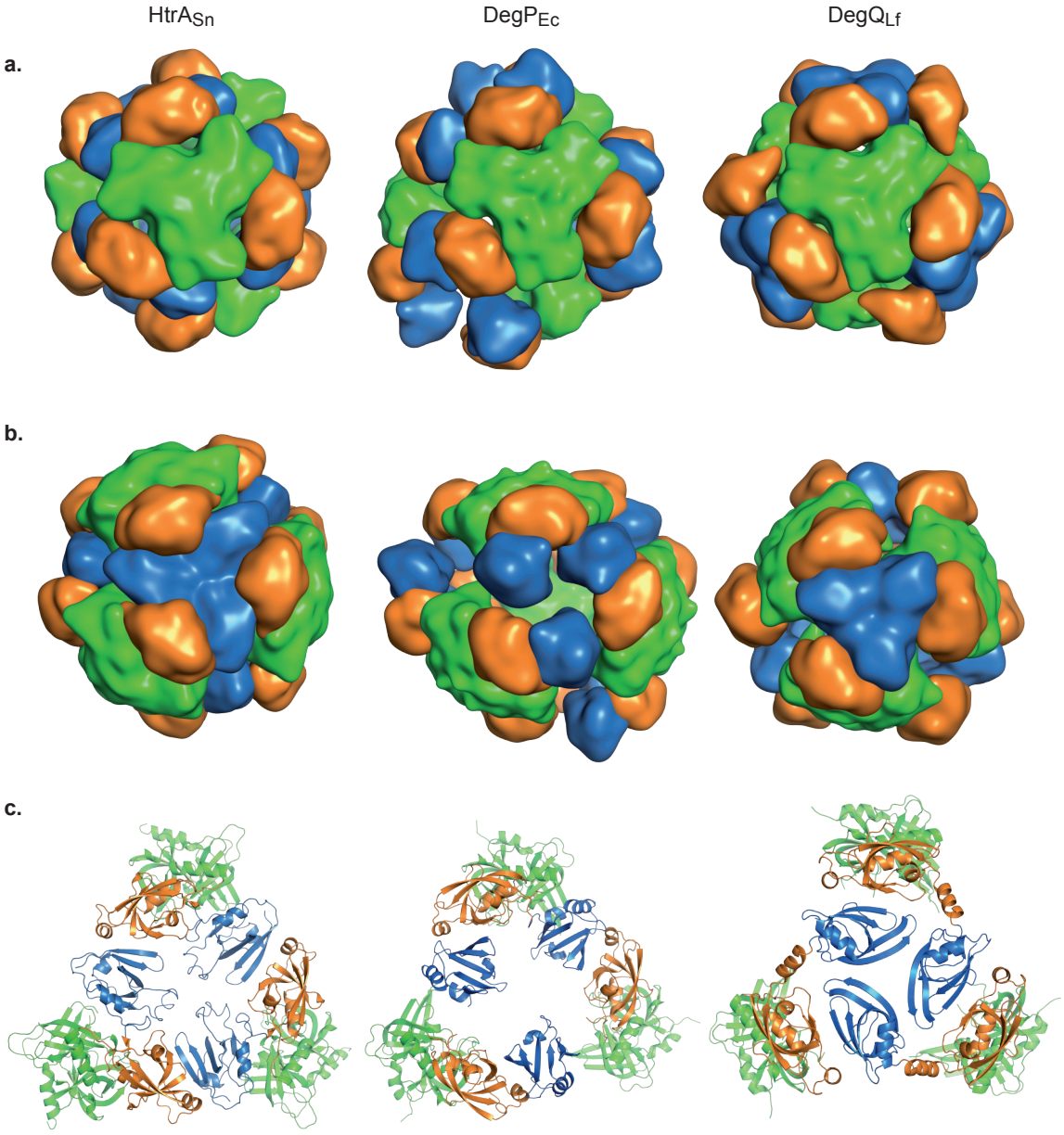

Figure 3.18: Geometry of the HtrA 12-mer structures. a) View on the protease (green) domain of $HtrA_{Sn}$, $DegP_{Ec}$and $DegQ_{Lf}$ 12-mer crystal structure. The PDZ1 domains are represented in orange, the PDZ2 domains in blue. b) View on the PDZ2 interface of the $HtrA_{Sn}$, $DegP_{Ec}$ and $DegQ_{Lf}$ 12-mer crystal structures. In the $HtrA_{Sn}$ 12-mer, PDZ2 domains contact each other extensively and form a funnel-like structure. c) Cartoon representation of the PDZ2-domain interfaces. The interface in $HtrA_{Sn}$ is mediated via loop interactions (loop between $\alpha 7$ and $\beta 20$), in $DegQ_{Lf}$ $\beta 18$ sheets are facing each other.

3.2.8 SAXS

SAXS offers complementary information to crystallographic studies about protein folding, aggregation, shape and assembly in low resolution range of 50-10 Å (Putnam et al., 2007). The biggest obstacle is the preparation of a monodisperse protein sample without aggregates.

SAXS data for $HtrA_{Sn}$ proteins in different conditions at increasing concentrations were measured. Samples with a low protein concentration are important for data collection in low q-range. The variable q is described as the scattering vector and depends on the scattering angle and the incoming wavelength λ ($q = \frac{4*\pi*\sin\theta}{\lambda}$). Similar to the reciprocal lattic in X-ray crystallography, the unit parameter of q is nm^{-1}. Therefore, the low q-range yields information about long distances, the overall particle shape and the molecular weight unbiased by aggregation. Samples with higher protein concentrations give rise to better signal-to-noise ratios in greater q-ranges containing details about shorter distances. To preserve information, curves at high and low concentrations are merged. $HtrA_{Sn}$ shows a slight concentration dependency of the radius of gyration (R_G) which increases at higher concentrations. This effect is due to intermolecular interactions of protein particles and a typical effect of concentration-dependent oligomerization (Blobel et al., 2009). Nevertheless, the data was analyzed (s. Tab.) and averaged (s. Tab.3.13). $HtrA_{Sn}{}^{\#}$ serves as control sample as it displays predominantly 6-mers. In comparison to the $HtrA_{Sn}$ 6-mer, there are small differences in curve progression visible which result in higher R_G values for $HtrA_{Sn}$ (Fig. 3.19a). Interestingly, the addition of pept1 does not change the scattering curve shape at all, and R_G is also in similar range (Fig.3.19b) whereas a buffer exchange to acidic milieu has a relatively big impact on the curve. The scattering curve of $HtrA_{Sn}$ 12-mer shows a shift towards the lower q-range which is induced by the bigger scope of the protein and the curve progression is more similar to a sphere. With the extrapolated value

Table 3.13: Scattering curve analysis of $HtrA_{Sn}$ in different conditions by PRIMUS (Konarev et al., 2003) yields the R_G, D_{max} and Porod volume. DLS measurement enable the determination of hydrodynamic radius (R_h) which is proportional to R_G.

protein	$\mathbf{R_h}$ **(nm)**	$\mathbf{R_G}$ **(nm)**	$\frac{R_G}{R_h}$	$\mathbf{D_{max}}$ **(nm)**	**PV**
$HtrA_{Sn}$ 6-mer	6.25	5.29	0.85	16.21	748
$HtrA_{Sn}$ 12-mer	7.75	6.28	0.81	18.09	1505
$HtrA_{Sn}{}^{\#}$ (Tris 8)	5.72	4.82	0.84	14.57	622
$HtrA_{Sn}{}^{\#}$ (NaAc 4.5)	6.08	5.2	0.86	15.48	833
$HtrA_{Sn}$ + pept1	5.76	5.23		16.24	735

of I(0), it is possible to draw conclusions about the molecular weight of the protein

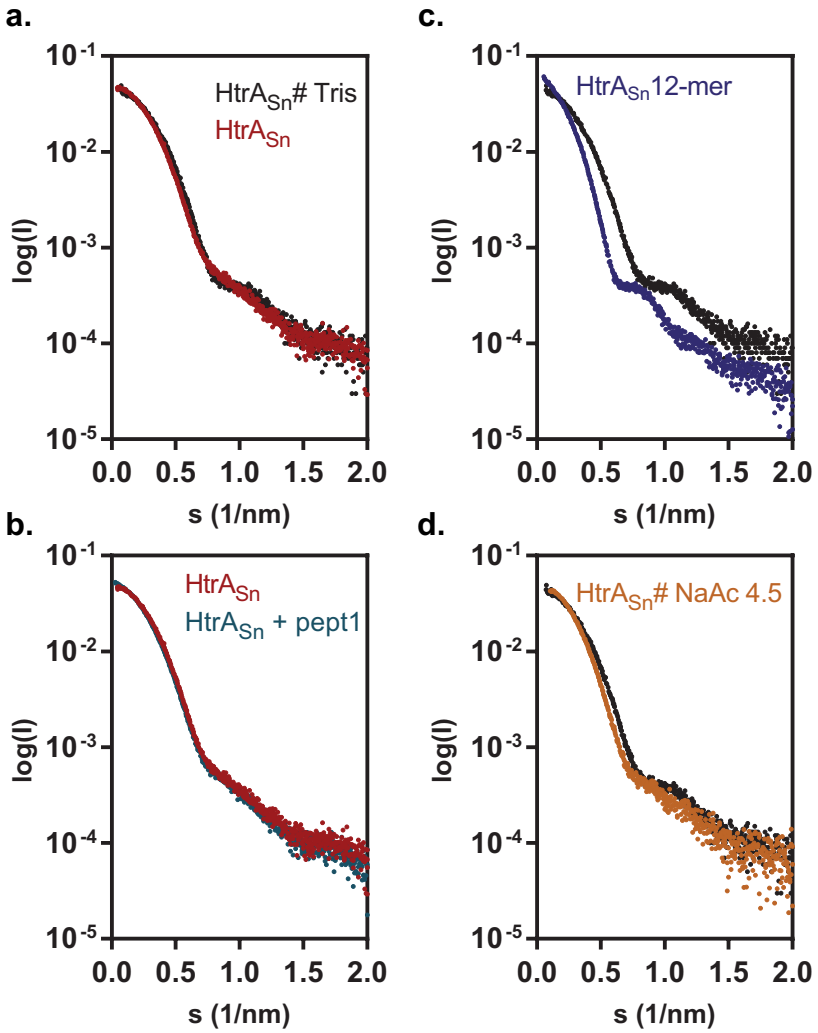

Figure 3.19: SAXS curves of $HtrA_{Sn}$ allow to distinguish between different states and oligomeric forms. a) SAXS curve of $HtrA_{Sn}$ wild type (red) shows small differences to $HtrA_{Sn}{}^{\#}$ (black) due to the bigger 12-meric volume fraction. Curve progression indicates a spheric particle. b) Addition of pept1 (blue) displays the same curve progression as for wild type indicating no oligomerization due to heptapeptide binding. c) SAXS curve of $HtrA_{Sn}$ 12-mer differs significantly from 6-mer curve exhibiting a higher I(0) and R_G. d) $HtrA_{Sn}{}^{\#}$ scatters differently in acidic range because of the higher amount of 12-mer state.

sample (s. Tab. 3.14). For spherical samples, half of the Porod volume (PV) also gives a good approximation of the molecular weight. For $HtrA_{Sn}$ and $HtrA_{Sn}{}^{\#}$, the values are alternating around $\sim$ 300 kDa fitting the size of a 6-mer. However, the calculated molecular mass for the $HtrA_{Sn}$ 12-mer differs significantly between both methods which is an indicator for low quality data. A little controversial is also the behavior of D_{max} which is quite high for the $HtrA_{Sn}$ 6-mer. A conclusive explanation gives the program OLIGOMER from the ATSAS package (Konarev et al., 2003). It calculates the volume fractions of a multicomponent mixture of proteins for an experimental scattering

curve when the crystal structures of the individual components are given. OLIGOMER shows (s. Tab. 3.14) that the analyzed samples are not monodisperse in regard to their oligomeric state but mixtures of 6-mer and 12-mers and even 3-mers. These results complicate the data analysis as the mixture is not in equilibrium and the oligomerization is concentration-dependent. To reconstruct a three-dimensional envelope with an *ab initio* model building approaches a deconvolution of the SAXS curves is necessary to extract curves for the 6- and 12-mer state. As these mathematic operating are not yet customized, this would be a bioinformatic project for future research.

Table 3.14: Scattering curve analysis by OLIGOMER (Konarev et al., 2003) shows that the samples are forming a mixture of different oligomeric states. Molecular weight calculation by SAXS is enabled by I(0) or Porod volume. For $HtrA_{Sn}$ 6-mer the MW alternates around 300 kDa, matching the expected mass. The 12-mer shows a big discrepancy between both MWs which is an indicator for low quality data.

	MW (kDa)		**Oligomer**		
protein	**PV**	**I(0)**	**3-mer**	**6-mer**	**12-mer**
$HtrA_{Sn}$	374	264	0.04	0.73	0.24
$HtrA_{Sn}$ 12-mer	753	391	0.00	0.29	0.71
$HtrA_{Sn}^{\#}$ (Tris 8)	311	246	0.12	0.77	0.11
$HtrA_{Sn}^{\#}$ (NaAc 4.5)	416	308	0.00	0.77	0.23
$HtrA_{Sn}$ +pept1	368	241	0.04	0.72	0.24

3.3 HtrA from *C. trachomatis* - $HtrA_{Ct}$

Previous studies highlight $HtrA_{Ct}$ as a potential new therapeutic target to battle chlamydia infections (Marsh et al., 2017). *In vitro* and *in vivo* experiments show that bacterial HtrA proteins are functionally distinct and do not conform in all aspects to the *E. coli* DegP model. $HtrA_{Sn}$ exhibits a higher sequence identity to $HtrA_{Ct}$ than $DegP_{Ec}$ and is likewise a member of the bacterial order *Chlamydiales*. Therefore, it is conceivable that $HtrA_{Sn}$ represents a more suitable model for HtrA proteins in *Chlamydiae*. To further investigate this hypothesis, biochemical and structure-biological studies of $HtrA_{Ct}$ have been performed and compared to $HtrA_{Sn}$.

3.3.1 Purification of $HtrA_{Ct}$

$HtrA_{Ct}$ with an N-terminal His-tag has been successfully produced in *E. coli* Ku98 cells and purified by affinity chromatography (Fig. 3.20a) with a yield of $\sim$ 50 mg/ 2 L cell culture. A second purification step by preparative SEC shows two oligomeric forms of $HtrA_{Ct}$ (P1+P2) (Fig. 3.20b). SDS-PAGE analysis reveal a prominent protein band at 50 kDa which is in accordance with the monomer size of $HtrA_{Ct}$ (Fig. 3.20d). For molecular weight determination and investigation of the oligomeric states of $HtrA_{Ct}$ P1 and P2, analytical SEC analysis was conducted. Results (Fig. 3.20c) for P2 show a very broad peak with an apparent molecular weight of 370 kDa. This indicates a multicomponent mixture containing predominantly 6-mers. P1 contains at least three oligomeric forms with a large peak at the void volume of the column probably consisting of 24-mers and higher-order oligomers, a peak at 8.95 mL with an apparent molecular mass of 660 kDa (12-mer) and a third peak at 10.16 mL with a mass of 385 kDa (6-mer). Higher-order oligomer assembly is probably induced by co-purified peptides from *E. coli*.

To diminish the impact of co-purified peptides, $HtrA_{Ct}$ has been purified under denaturing conditions and successfully refolded ($HtrA_{Ct}{}^{\#}$). Results from preparative SEC shows two peaks (Fig. 3.21a). The first peak is probably a mixture of 6- and 12-mers. The second peak elutes later and contains thereby proteins with a lower molecular weight (P3). Further analysis of P3 reveal a mixture of at least three oligomeric forms (s. Fig 3.21b). The elution peak in analytical gelfiltration is broadened and shows a maximum at 11.3 mL matching an apparent molecular mass of 270 kDa and two shoulders at 10.6 mL ($\sim$370 kDa) and 9.3 mL ($\sim$ 520 kDa). The peak at 11.3 mL is very close to the protein standard of the BSA dimer (MW: 130 kDa) with an appar-

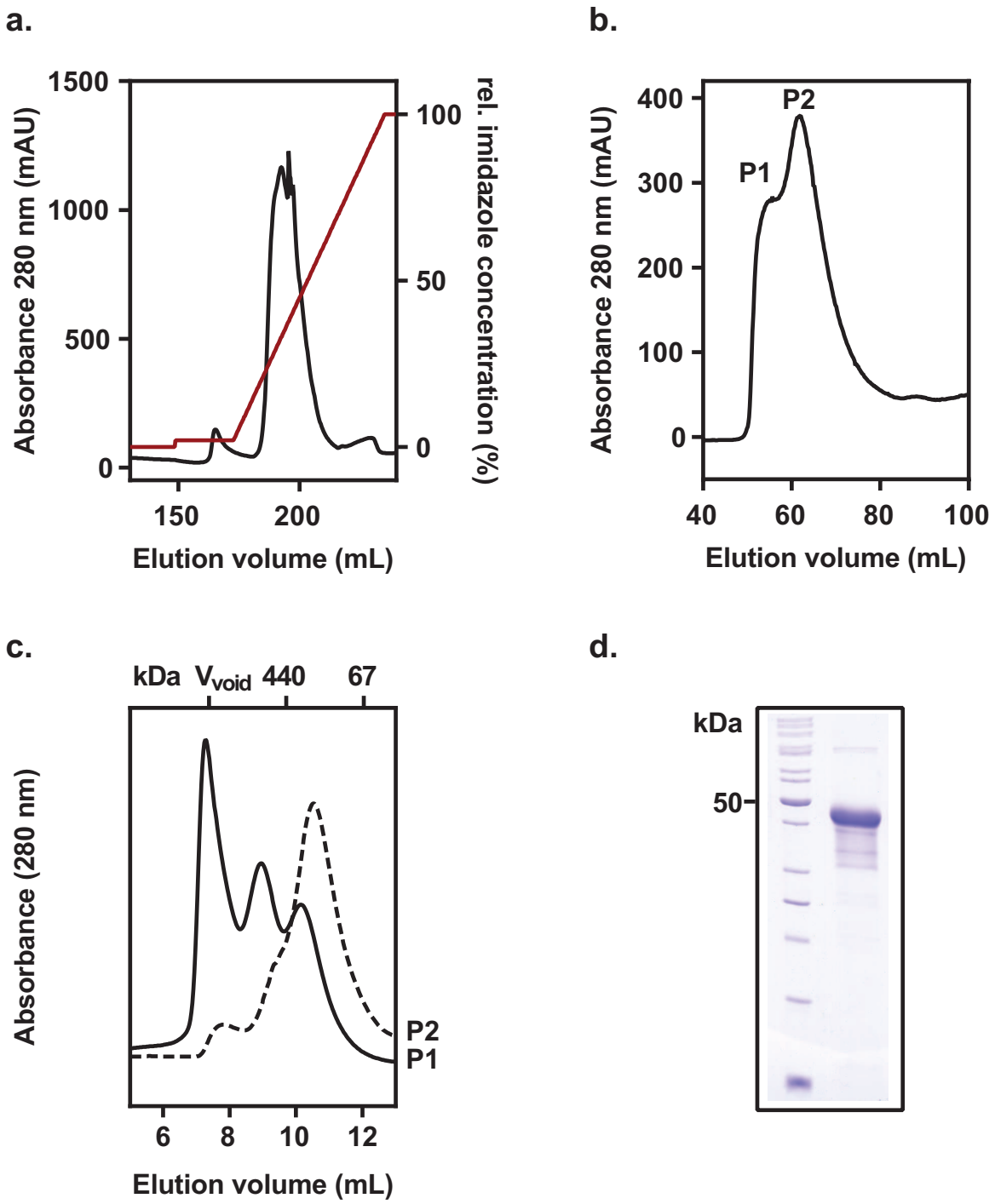

Figure 3.20: Purification of $HtrA_{Ct}$. a) Purification of $HtrA_{Ct}$ via affinity chromatography yields high amounts of recombinantly produced target protein. b) In preparative SEC $HtrA_{Ct}$ elutes in two oligomeric forms (P1+P2). c) Results from analytical SEC of P1 reveal a mixture of oligomeric forms whereas P2 elutes in a broad peak with an apparent molecular weight of 370 kDa corresponding to 6-meric assembly. d) SDS-PAGE results display a prominent band at around 50 kDa matching the monomer size of $HtrA_{Ct}$.

ent molecular weight of 230 kDa. These discrepancies in molecular weight reveal the limited accuracy of analytical SEC in high molecular range. Thereby, it is assumed that the first peak corresponds to a 3-meric assembly whereas the shoulders consist of 6-mer and 12-mer, respectively.
Replacement of the active-site serine (S247) with an alanine, the proteolytic inactive $HtrA_{Ct}{}^{0}$ variant was generated and successfully purified. After affinity chromatography, a preparative SEC was conducted to increase purity. The protein elutes in two peaks (Fig.3.21a). The bigger peak elutes between P1 and P2 probably consisting of a 6-mer/12-mer mixture. The smaller peak (P3) shows an apparent molecular weight of 320 kDa which also implicates 6-mer formation (Fig. 3.21c). As for $HtrA_{Ct}{}^{\#}$ a peak at the same elution volume in preparative SEC shows a mixture of 3-, 6- and 12-mer with predominantly 3-mer it is conceivable that $HtrA_{Ct}{}^{0}$ P3 also displays a mixture of 3- and 6-mers.

3.3.2 Biochemical characterization of $HtrA_{Ct}$

3.3.2.1 Proteolytic activity of $HtrA_{Ct}$

Proteolytic activity of $HtrA_{Ct}$ and $HtrA_{Ct}{}^{\#}$ have been measured to verify functionality (Fig. 3.22a,b). To ensure comparability, the same assay conditions as for $HtrA_{Sn}$ were applied. Both protein variants show a low basal proteolytic activity rate of 0.08 ($HtrA_{Ct}{}^{\#}$) and 0.10 $\frac{nM}{s}$ ($HtrA_{Ct}$), respectively. Addition of pept1 increases substrate cleavage for $HtrA_{Ct}$ around 10-fold (0.96 $\frac{nM}{s}$). $HtrA_{Ct}{}^{\#}$ displays with 0.13 $\frac{nM}{s}$ almost no activation effect. The presence of β-casein induces a dramatic increase in proteolytic activity in both proteins to ~ 5 $\frac{nM}{s}$ which is comparable to the $HtrA_{Sn}$ activity in the presence of the same amount of β-casein.
Denatured BSA and lysozyme are other reported protease substrates for HtrA proteins (Krojer et al., 2008b). Both proteins increase proteolytic activity of $HtrA_{Ct}{}^{\#}$ significantly. Unfolded BSA leads to a release of 0.93 $\frac{nM}{s}$ free AMC, lysozyme to 1.13 $\frac{nM}{s}$, representing less efficient activators than β-casein. $HtrA_{Ct}$ degrades denatured BSA visibly whereas unfolded lysozyme shows very slow decay. Consequently, the activation of proteolytic cleavage is not necessarily associated with the degradation of the activator.
Experiments at different pH values show that $HtrA_{Ct}$ is proteolytically active over a wide range of pH from 5-9 with an optimum at physiological pH (Fig. 3.24a).
In a fluorescence assay with 1 μM protease and increasing reporter-peptide concentrations, the enzyme kinetics of $HtrA_{Ct}{}^{\#}$ were further investigated. The proteolytic

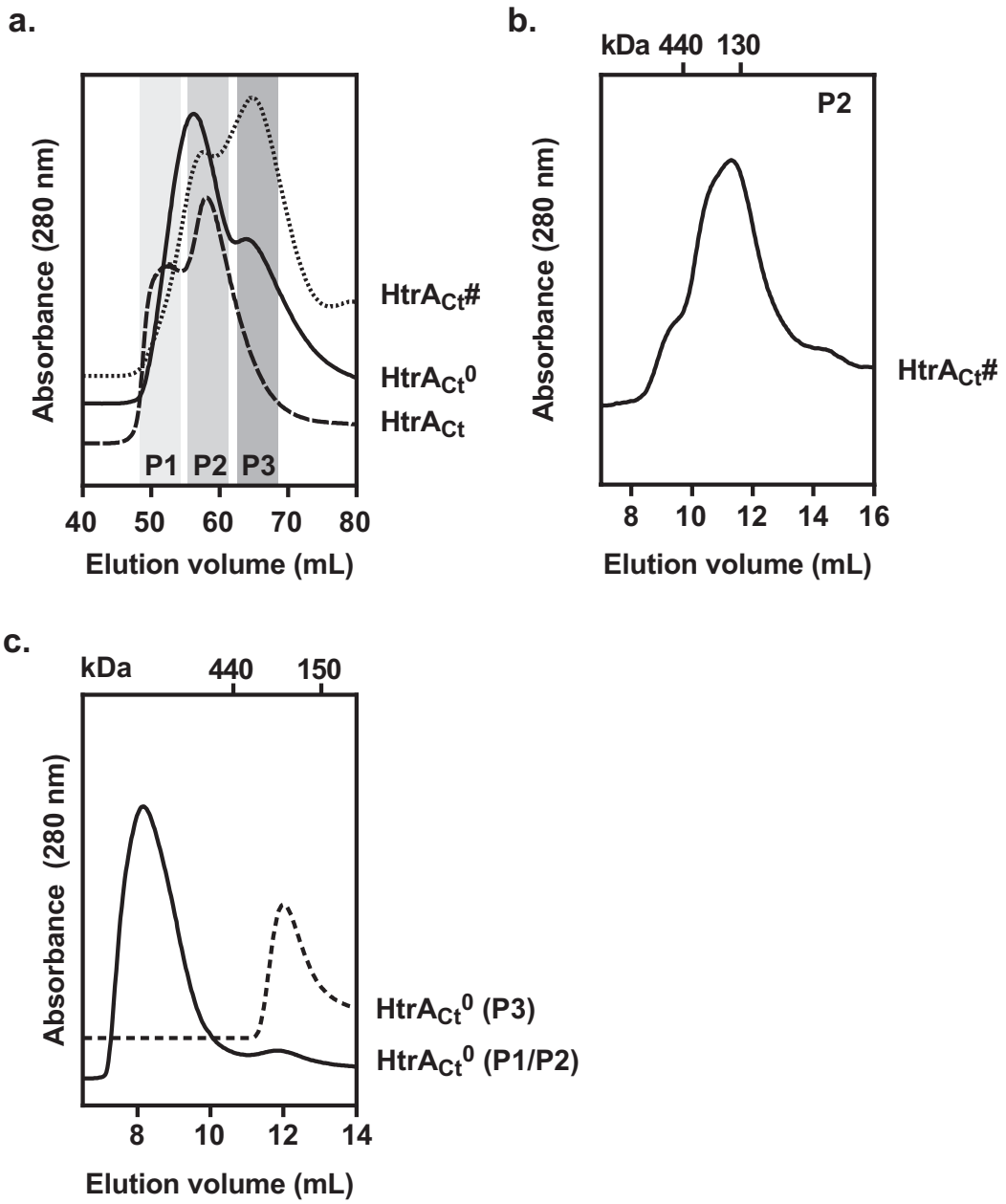

Figure 3.21: Purification of HtrA$_{Ct}$$^{\#}$ and HtrA$_{Ct}$^{0}. a) Results from preparative SEC of HtrA$_{Ct}$$^{\#}$ and HtrA$_{Ct}$^{0} in comparison with HtrA$_{Ct}$. Three different elution peaks are obtained (P1-P3). b) Results from analytical gelfiltration of HtrA$_{Ct}$$^{\#}$ P3 reveals a mixture of 3-, 6- and 12-mer with predominantly 3-mer. c) Results from analytical SEC of HtrA$_{Ct}$^{0}. P3 elutes as predominantly 3-mer whereas the second peak contains a mixture of HtrA$_{Ct}$ P1+P2.

activity of HtrA$_{Ct}$$^{\#}$ increases linear with increasing substrate concentrations but is in contrast to HtrA$_{Sn}$ very low. Even at 800-fold substrate excess, the proteolytic rate of 0.22 $\frac{nM}{s}$ is almost negligible. This implies that the typically *E. coli*-substrate is not optimal for HtrA$_{Ct}$. In (Huston et al., 2011), they identified with MFKLI a peptide with a 4.5-fold higher K_{cat}/K_M rate than DPMFKLV. For future experiments it would

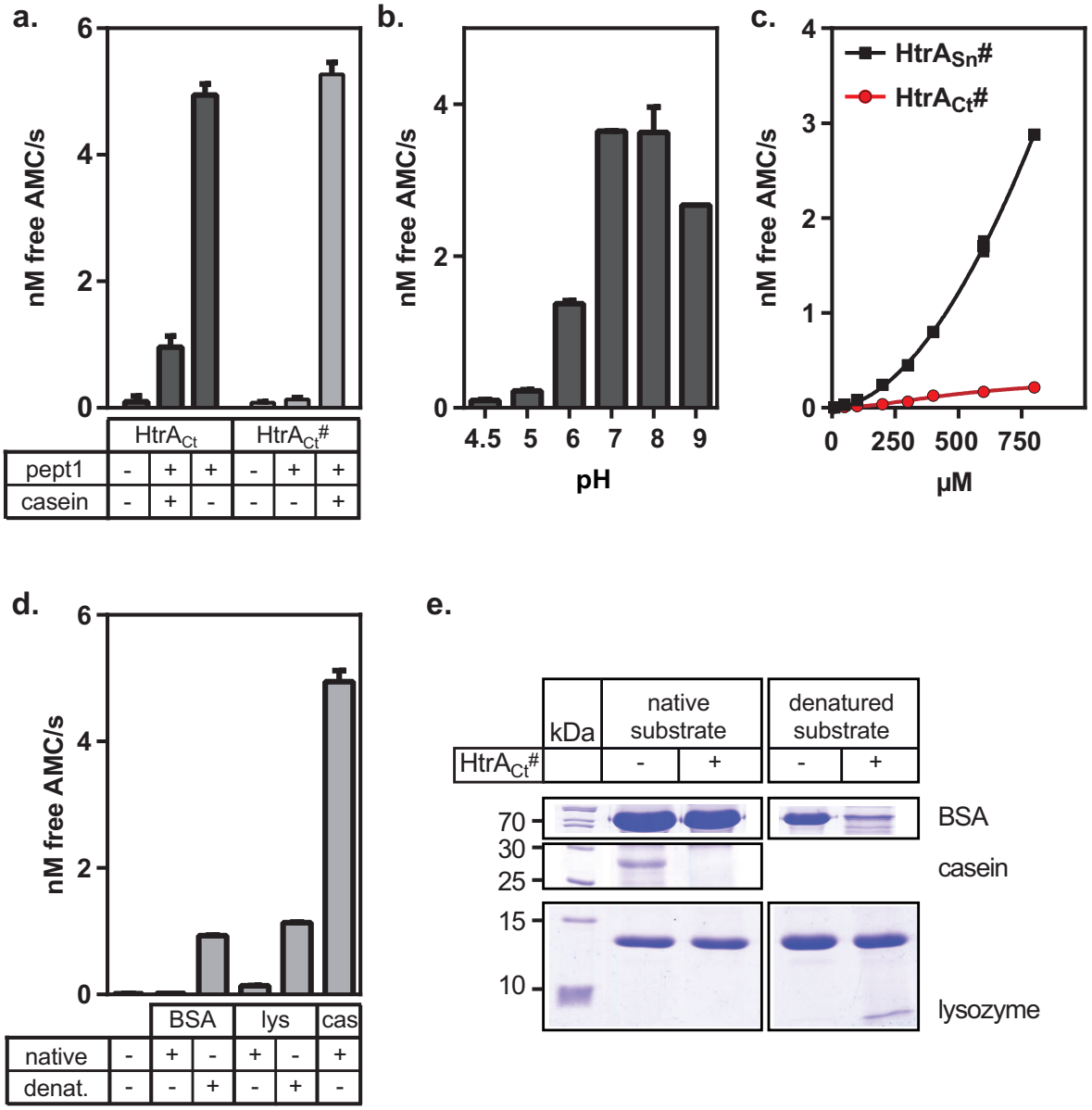

Figure 3.22: Protein activity assay of $HtrA_{Ct}$ and $HtrA_{Ct}{}^{\#}$. a) $HtrA_{Ct}$ is proteolytically active in the presence of pept1 and β-casein. $HtrA_{Ct}{}^{\#}$ shows no proteolytic activity in the absence of substrates. Whereas pept1 addition leads to a basal substrate cleavage, the presence of β-casein dramatically increases protease activity. b) $HtrA_{Ct}$ is proteolytically active over a wide pH range with highest free AMC release at pH 7-8. c) Cleavage rate of DPMFKLV-AMC by $HtrA_{Ct}{}^{\#}$ and $HtrA_{Sn}{}^{\#}$ at increasing substrate concentrations. The proteolytic activity of $HtrA_{Ct}\#$ is linear to the substrate concentration. d) Denatured lysozyme and BSA activate proteolytic activity of $HtrA_{Ct}{}^{\#}$. e) Denatured BSA and β-casein are degraded by $HtrA_{Ct}{}^{\#}$ to a higher extend than unfolded lysozyme.

be interesting to test MFKLI in homolog HtrA proteins such as $HtrA_{Sn}$.

3.3.2.2 Oligomerization behaviour of $HtrA_{Ct}$

A distinct feature of HtrA proteins is the oligomerization into higher-order oligomers. $HtrA_{Ct}$ has previously been described to occur as 6-mer in solution (Huston et al., 2007). As already mentioned (Fig. 3.20c), $HtrA_{Ct}$ possesses the ability to adopt different oligomeric states such as 6-mers, 12-mers and even higher-order oligomers. In contrast to $HtrA_{Sn}$, even the refolded protein shows more than one oligomeric form and occurs as a mixture of 3-mer, 6-mer and 12-mer (s.Fig. 3.21b).
$HtrA_{Ct}$ and $HtrA_{Ct}{}^{\#}$ 3- and 6-mers (Fig.3.23a,b) assemble into higher-order oligomers in the presence of β-casein. The oligomerization is substrate-concentration dependent (Fig.3.23a) A 5-fold excess leads to mainly 12-mer cages whereas a 20-fold β-casein excess promotes assembly of higher-order oligomers such as 24-mers (Fig. 3.23a).

In the $HtrA_{Sn}$ 6-mer, the presence of pept1 has no effect on oligomer assembly. The same was observed for $HtrA_{Ct}$ in 6-mer state (Fig. 3.23a). Interestingly, $HtrA_{Ct}{}^{0}$ shows a shift in elution volume and an additional peak representing a small 12-mer fraction in the presence of pept1 (Fig. 3.23d).
Oligomerization is assumed to be a transient process. A $HtrA_{Ct}$ sample containing three oligomeric forms (6-mer, 12-mer, higher-order oligomer) was incubated with β-casein (Fig. 3.23d). Immediately after substrate addition, the $HtrA_{Ct}$ 6-mer peak vanishes completely and the peak in the void volume increases. Analytical gelfiltration after 2 days of incubation at 37 °C reveal no changes in the oligomeric states. There are still no 6-mers detectable. Full-length β-casein was degraded but there are still degradation byproducts visible in SEC and SDS-PAGE analysis. It is conceivable that the presence of degradation fragments impedes with the disintegration of higher-order oligomers.

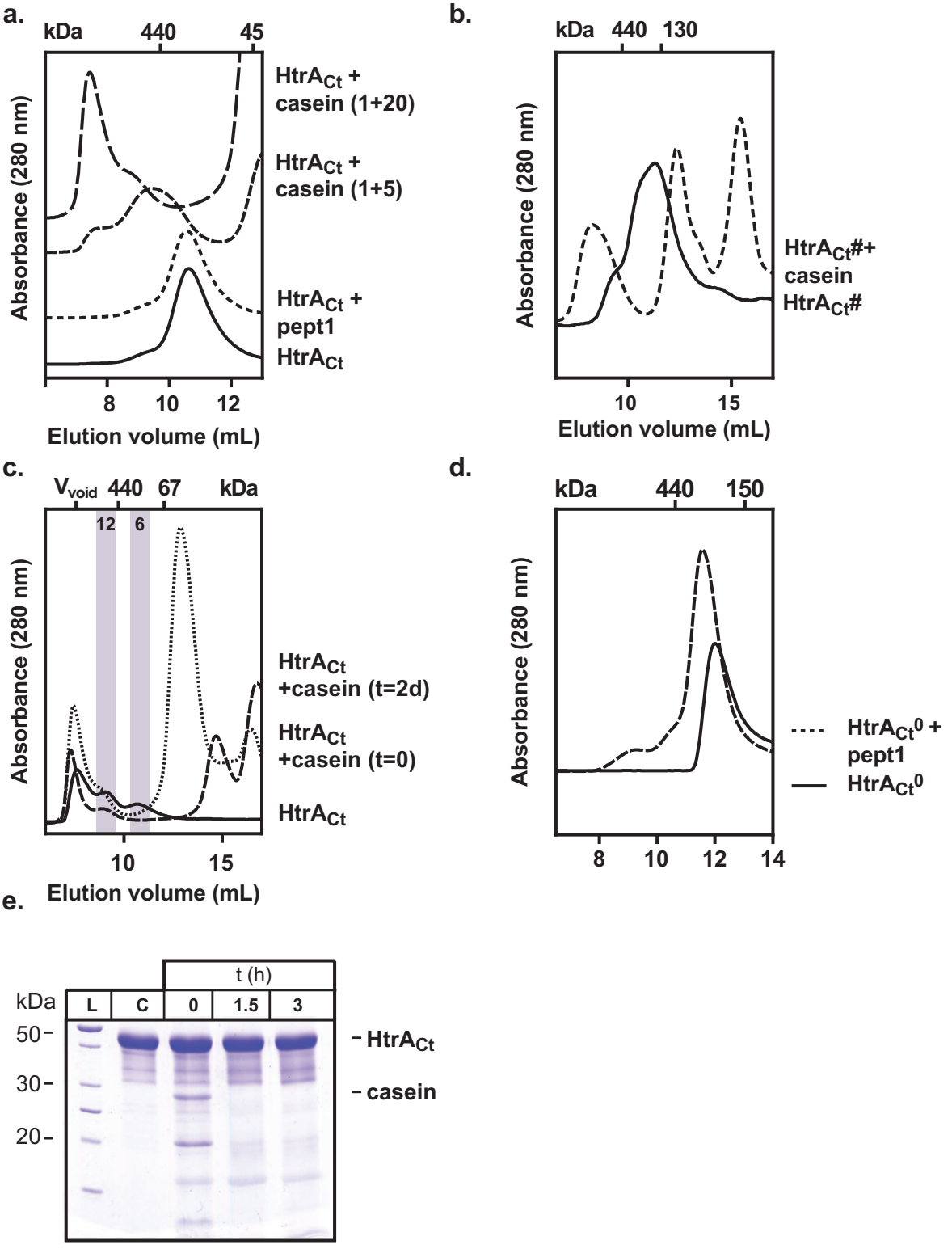

Figure 3.23: Oligomerization behavior of $HtrA_{Ct}$ protein variants. a) $HtrA_{Ct}$ forms higher-order oligomers in a dose-dependent manner in the presence of β-casein . Pept1 does not effect the oligomeric state. b) $HtrA_{Ct}{}^{\#}$ forms higher-order oligomers in the presence of β-casein. c) $HtrA_{Ct}{}^{0}$ shows a higher molecular weight in the presence of pept1 and an additional small peak appears at 9.3 mL ($\sim$ 600 kDa) representing a 12-mer. d) Time-dependent β-casein degradation by $HtrA_{Ct}$. In the presence of β-casein the 6-mer peak vanishes. After two days of incubation, there is still no 6-mer peak detectable. e) SDS-PAGE analysis of β-casein digested by $HtrA_{Ct}$. After 1.5h, β-casein is depleted but there are still degradation by-products present.

3.3.2.3 Temperature dependency

HtrA proteins manage heat stress response and exhibit thereby full functionality at high temperatures. Similar to $HtrA_{Sn}$, $HtrA_{Ct}$ exhibits proteolytic activity over a wide temperature range with highest cleavage efficacy at 50 °C (Fig. 3.24). Even at 65°C, the protease still retains the ability for substrate cleavage.
CD spectra for $HtrA_{Ct}$ recorded at 25 and 55 °C are quite similar with minima at 210, 217 and 221 nm. At 85 °C changes in secondary structure become evident indicating disintegration of the protein structure. K2D3 analysis of secondary structure content results in 1 % α-helix, 27 % β-strand and 72 % random coil at 25 °C. At 85 °C there is only 20 % β-strand content left but the CD spectrum still looks like the protein is mostly folded. A melting curve at 218 nm reveals a T_m of 72 °C which is similar to 6-mer results from $HtrA_{Sn}$.
As $DegP_{Ec}$ disassembles at higher temperatures (Krojer et al., 2008b), $HtrA_{Ct}$ in different oligomeric states were incubated for 1h at 55 °C. Whereas a mixture of 3- and 6-mers shows a slight increase in 3-mer volume fraction, the oligomeric form in void volume (probably a 24-mer) precipitates partly and there is a disintegration to 6- and 12-mers detectable. Consequently, the smaller oligomeric states such as 3- and 6-mers show a higher stability than higher-order oligomers.

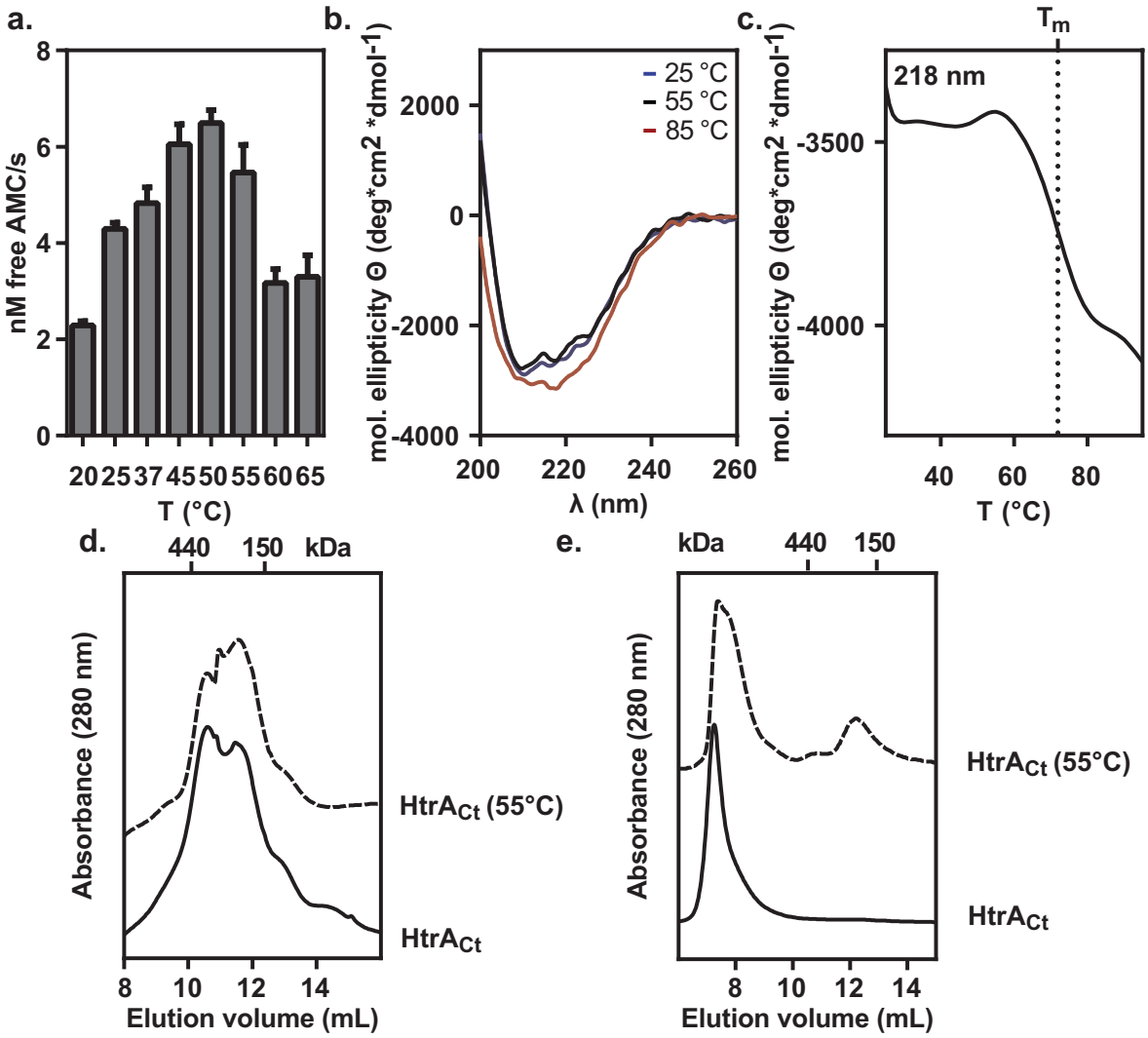

Figure 3.24: $HtrA_{Ct}$ is active at high temperatures. a) Substrate cleavage at elevated temperatures shows a maximum efficacy at 50 °C. $HtrA_{Ct}$ has been activated in the presence of β-casein. b) CD spectra of $HtrA_{Ct}$ 6-mer at 25 °C (blue), 55 °C (black) and 85 °C (red). At 25 °C, the secondary structure content exhibits 27 % β-sheet and 1 % α-helix. At 85 °C, the β-sheet fraction is diminished to 20 % but the protein is still mostly folded. c) A temperature curve measured by CD reveals a T_m at 72 °C. d) Incubation of $HtrA_{Ct}$ 3-/6-mer mixture at 55 °C for 1h leads to a slow decay of 6-mers to 3-mers. e) A higher-order oligomeric form of $HtrA_{Ct}$ disintegrates to smaller oligomers upon incubation at 55 °C.

3.3.2.4 Crystallization of $HtrA_{Ct}$

First attempts to crystallize $HtrA_{Ct}$ stored in 20 mM Tris (pH 7.4), 150 mM NaCl with commercial screening kits like PegIon™ and Index™ from Hampton Research and Structure and PACT *premier*™ from Molecular Dimensions were not successful. A buffer test with DLS shows the best spectrum at 50 mM sodium citrate (pH 5), 150 mM NaCl and 5 mM TCEP (Fig. 3.25a). The change in storage buffer seems to stabilize the oligomeric composition and thereby, facilitates crystal formation. With $HtrA_{Ct}$ in acidic storage buffer over 30 initial crystal conditions could be identified. The most promising ones were optimized (crystallisation conditions: 0.2 M magnesium formate (pH 7) 18% PEG 3350; 0.2 M sodium formate (pH 8) 18% PEG 3350) (Fig. 3.25b) and measured at the synchrotron. Unfortunately, none of these crystals diffracted X-ray radiation. As various optimization attempts did not improve the crystal quality, other $HtrA_{Ct}$ variants were cloned, purified and tried to crystallize.

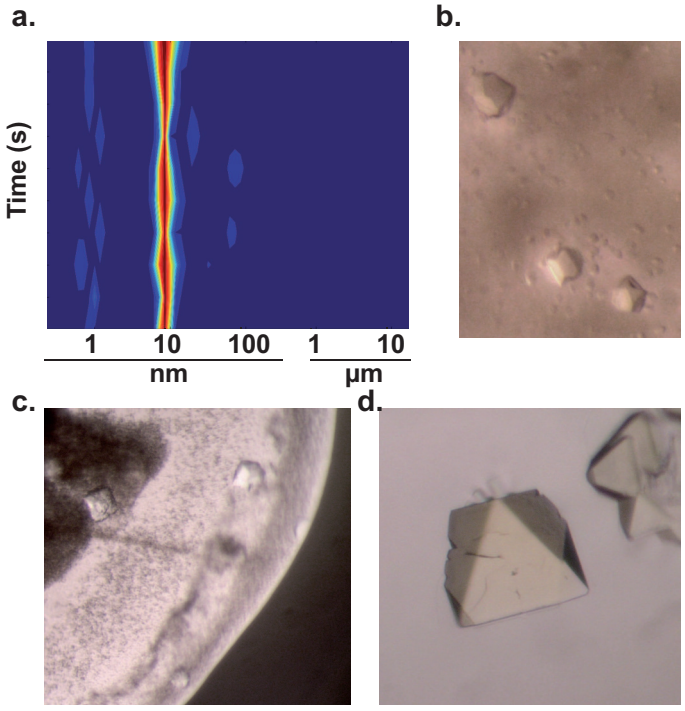

Figure 3.25: $HtrA_{Ct}$ crystallizes when the protein is transferred into acidic storage buffer. a) DLS spectrum of $HtrA_{Ct}$ in 50 mM sodium citrate (pH 5), 150 mM NaCl and 5 mM TCEP. b) $HtrA_{Ct}$ crystals grown in 0.2 M magnesium formate (pH 7) and 18% PEG 3350. c) $HtrA_{Ct}$ crystals grown in 0.2 M sodium formate (pH 8) and 18% PEG 3350. d) $HtrA_{Ct}{}^{0}\Delta N34^{\#}$ crystal grown in 0.1 M sodium citrate pH 5 and 2.5 M sodium formate diffract to a resolution of $\sim$ 3.5 Å.

$HtrA_{Ct}{}^{0}\Delta N34^{\#}$, a proteolytic inactive variant (S247A) where the beginning of the N-

terminus is deleted (starts at amino acid 35) forms diamond-shaped crystals in 0.1 M sodium citrate and 2.5 M sodium formate (Fig. 3.25d). The diffraction pattern shows a resolution limit of $\sim$ 3.5 Å. Unfortunately, the data set seems to be twinned and thereby, space group determination was difficult. Different attempts of molecular replacement did not give a definite solution and thereby, it was not possible to solve the three-dimensional structure of $HtrA_{Ct}$.

3.3.2.5 SAXS

To gather structural informations about $HtrA_{Ct}$, SAXS data at increasing concentrations with and without addition of pept1 were collected (Fig. 3.26). The R_G of $HtrA_{Ct}$

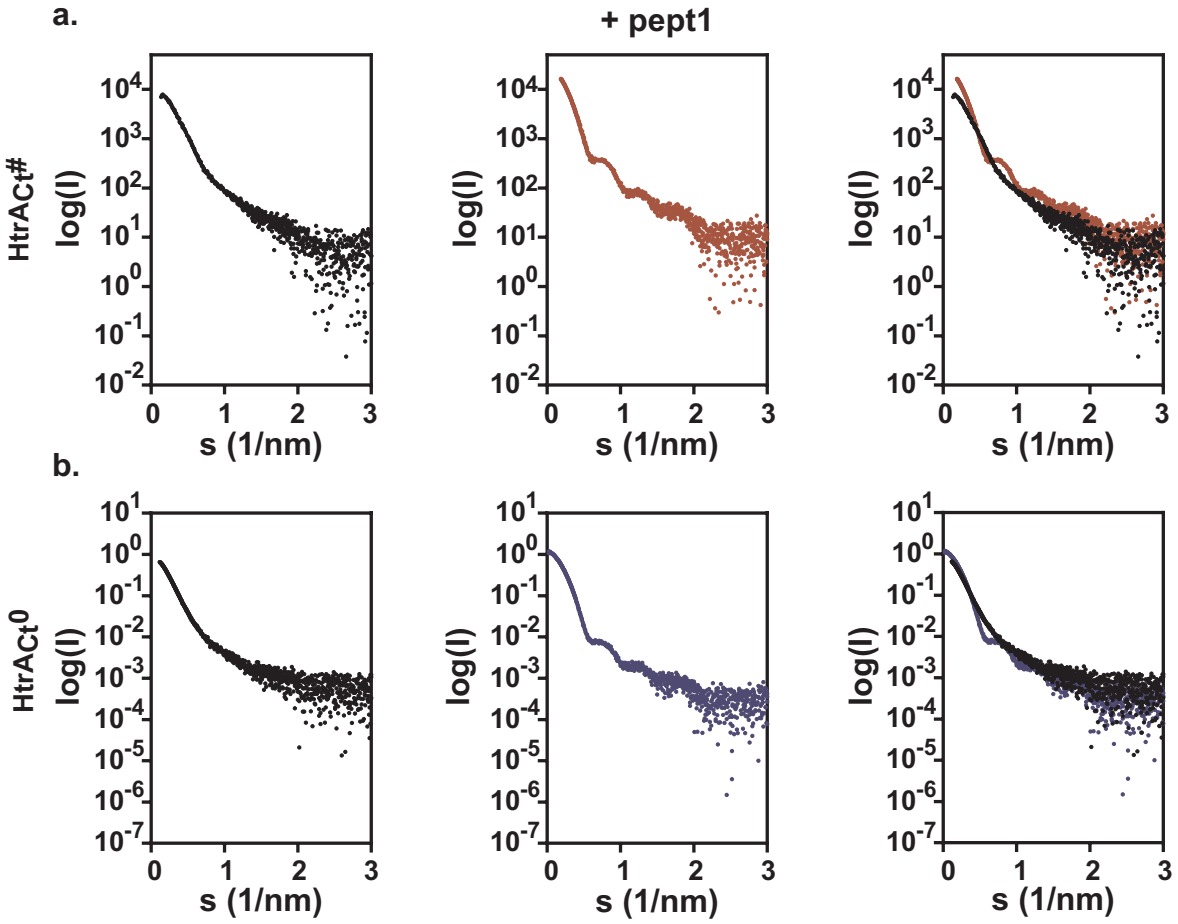

Figure 3.26: $HtrA_{Ct}$ underdoes structural changes in the presence of pept1. a) Scattering curves of $HtrA_{Ct}$ with and without pept1 differ significantly due to the different compositions of oligomeric states in the particular sample. b) Scattering curves of $HtrA_{Ct}{}^0$ with and without pept1 behave similar to $HtrA_{Ct}$.

increases with higher concentrations (s. Tab. 4.2) similar to $HtrA_{Sn}$ displaying the

influence of intermolecular interactions between particles. Molecular mass determination via I(0) and PV differs significantly. Extrapolated I(0) results in an averaged MW of ~ 265 kDa whereas calculation via PV yields a MW of 421 kDa. These discrepancies can be explained by the sample composition. Analysis by OLIGOMER (Konarev et al., 2003) shows that $HtrA_{Ct}$ is a mixture of 3-, 6- and 12-mer with preferences for 3-mers in lower concentration range (Tab. 3.15). These results fit the analytical SEC data (Fig. 3.20c). As the MW calculation based on PV assumes a spherical particle, the trimeric fraction impedes with the approximation. The oligomerization behavior of $HtrA_{Ct}$ seems to be concentration-dependent as with increasing protein amount the proportions between 3-, 6- and 12-mers shift towards larger oligomers.

Table 3.15: Scattering curve analysis of $HtrA_{Ct}$ and $HtrA_{Ct}{}^{0}$ with and without pept1 addition by PRIMUS (Konarev et al., 2003) yields R_G, D_{max} and PV. The volume fractions of 3-, 6- and 12-mer have been determined by OLIGOMER (Konarev et al., 2003).

protein	R_G	D_{max}	PV	MW_{PV} (kDa)	$MW_{I(0)}$ (kDa)	Oligomer 3-mer	6-mer	12-mer
$HtrA_{Ct}$	5.86	18.81	660	330	264.5	0.459	0.347	0.193
$HtrA_{Ct}$ + pept1	6.18	18.18	1160	580	410.7	0.000	0.463	0.537
$HtrA_{Ct}{}^{0}$	6.79	20.02	963	482	381	0.484	0.000	0.561
$HtrA_{Ct}{}^{0}$ + pept1	7.44	22.87	2200	1100	577	0.000	0.146	0.854

Interestingly, the addition of pept1 had a huge impact on the scattering curve of $HtrA_{Ct}$ (Fig. 3.26). The radius of gyration and the PV increases and results from OLIGOMER reveal a change in oligomer composition with a clear increase in 12-mer fraction. As a result, the presence of pept1 might promote higher-order oligomer assembly. The same effect could be observed for $HtrA_{Ct}{}^{0}$ (Fig. 3.26b). The inactive variant consists of a 3-mer/12-mer mixture with a higher R_G than $HtrA_{Ct}$. The curve progression is similar to $HtrA_{Ct}$. Addition of pept1 changes scattering profile dramatically and also increases R_G and PV. These findings do not match the $HtrA_{Sn}$ results. For $DegP_{Ec}$ (Merdanovic et al., 2010) and $DegQ_{Lp}$ (Schubert et al., 2015), oligomerization in the presence of peptides was described. As depicted in Fig. 4.5, $DegQ_{Lp}{}^{\#}$ at pH 7.5 shows similar scattering curves as $HtrA_{Ct}$. $DegQ_{Lp}\Delta PDZ2$ variant forms exclusively trimers without the cage forming abilities and thereby, the scattering curve is a good example for trimer assembly. The curve profile of $DegQ_{Lp}\Delta PDZ2$ resembles $DegQ_{Lp}{}^{\#}$ and $HtrA_{Ct}$, indicating mainly 3-meric content. The $DegQ_{Lp}{}^{\#}$ scattering curve changes completely upon peptide addition due to mainly 12-mer formation (s. Tab. 4.3) whereas the $DegQ_{Lp}\Delta PDZ2$ curve stays the same. As a conclusion, $HtrA_{Ct}$ behaves in SAXS more

like $DegQ_{Lp}$ than $HtrA_{Sn}$.

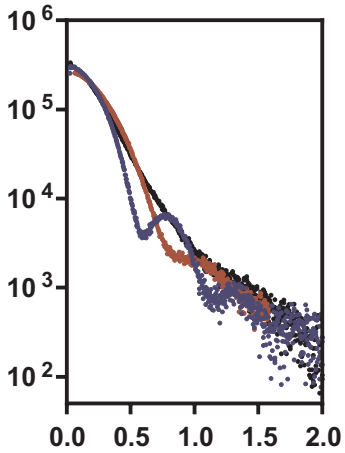

Figure 3.27: SAXS enables the identification of oligomeric state of HtrA proteins as the scattering curves of 3-mer (black, $DegQ_{Lp}\Delta PDZ2$), 6-mer (red, $HtrA_{Sn}$) and 12-mer (blue, $DegQ_{Lp}$+pept1) show a distinct pattern.

SAXS measurements enable the identification of oligomeric forms of HtrA proteins by scattering curve comparison. In Fig. 3.27 the curves of samples containing predominantly 3-mer, 6-mer and 12-mer are depicted and they differ significantly from each other. With these preliminary results, it is possible to immediately draw conclusions about the oligomeric state of HtrA proteins by looking at the raw data.

3.4 Interactions between major outer membrane proteins (MOMPs) and HtrA

For $DegP_{Ec}$ and $HtrA_{Ct}$, interactions with outer membrane β-barrels have been identified (Krojer et al., 2008a; Huston et al., 2011), indicating a potential *in vivo* substrate. $DegP_{Ec}$ stabilizes folded outer-membrane proteins (OMPs) (Krojer et al., 2008b) and prevents accumulation of un- or misfolded OMPs in the periplasmic space by degradation (Ge et al., 2014). In $HtrA_{Ct}$, MOMP as a fusion protein with an MBP-tag induces proteolytic activity (Huston et al., 2011) and the formation of higher-order oligomers. These results suggest a general link between OMPs and HtrA which is further investigated for $HtrA_{Sn}$. As a positive control, the same experiments were also conducted with $HtrA_{Ct}$.

3.4.1 Purification of $MOMP_{Sn}$-MBP

MOMPs are very hydrophobic molecules, therefore the solubility is an issue that has to be considered during protein purification. As previously described for $MOMP_{Ct}$ (Huston et al., 2011), the attachment of a 43 kDa MBP-tag enables soluble protein synthesis. Recombinant $MOMP_{Sn}$-MBP has been successfully produced in *E. coli* BL21Gold cells and resided in the supernatant. By affinity chromatography, a high yield of the target protein could be obtained (Fig. 3.28a). SDS-PAGE analysis shows a double-band after elution at around 70 kDa. A second purification step by anion exchange chromatography separated these two proteins and the free MBP, and therefore lead to a successfull protein extraction.
The $MOMP_{Sn}$-MBP fusion protein has a molecular weight of 72 kDa. Various attempts to cleave MBP-tag by factor X were not successful as $MOMP_{Sn}$ precipitates immediately. Thereby, the following experiments were carried out with the fusion protein. As a control, all biochemical characterizations were also conducted with MBP alone.
Besides $MOMP_{Sn}$-MBP, the corresponding construct of *Chlamydia trachomatis* $MOMP_{Ct}$-MBP (85 kDa) was successfully purified as previously described (Huston et al., 2011).

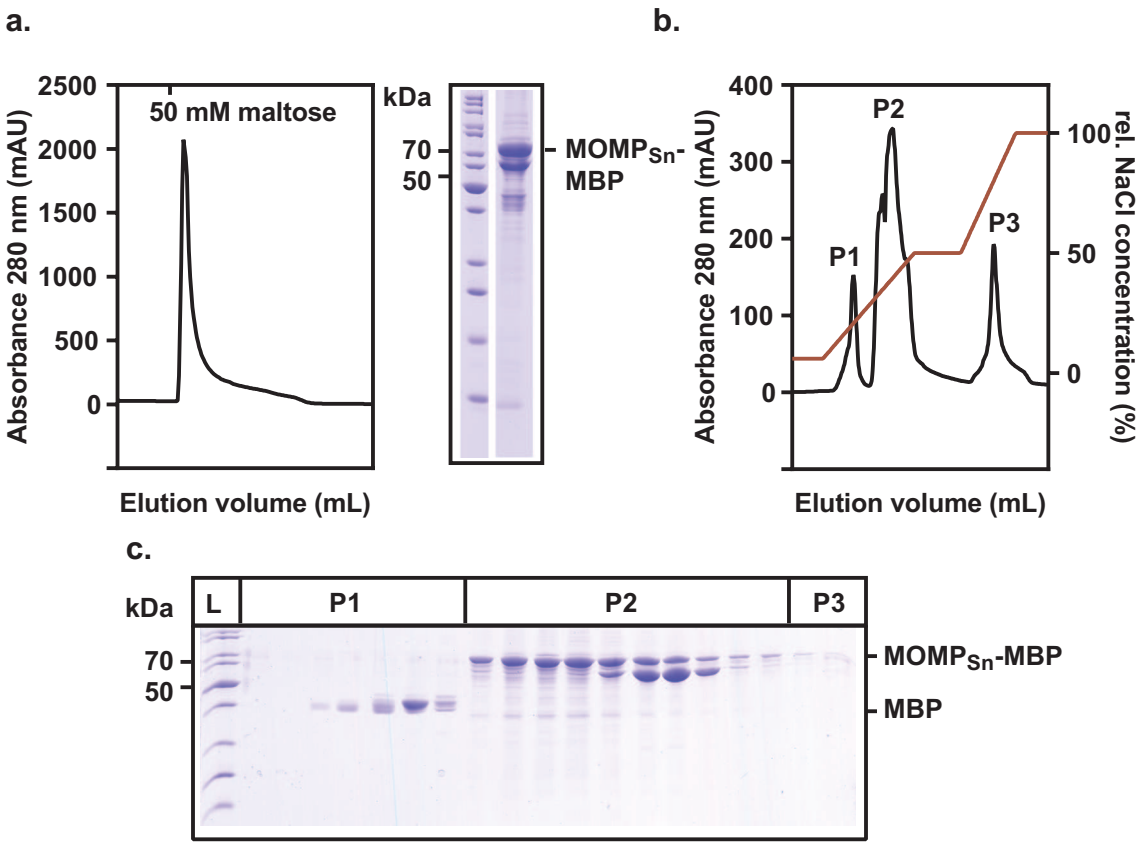

Figure 3.28: Purification of $MOMP_{Sn}$-MBP. a) First purification step via MBP-affinity chromatography yields high amounts of the target protein which occurs as a double-band in SDS-PAGE analysis. b) By anion exchange chromatography, the double bands and the free MBP are separated, increasing purity of $MOMP_{Sn}$-MBP. c) SDS-PAGE results of the anion exchange chromatography of $MOMP_{Sn}$-MBP.

3.4.2 Biochemical characterization of interactions between MOMP-MBP and HtrA

To investigate the influence of MOMP-MBP on the HtrA oligomerization state, analytical SEC experiments were conducted. $MOMP_{Sn}$-MBP and $MOMP_{Ct}$-MBP, both eluted in the void volume of the column, indicating oligomerization or aggregation. The incubation of $MOMP_{Sn}$-MBP with $HtrA_{Sn}$ does not change this elution profile. However, SDS-PAGE analysis reveals the co-existence of $HtrA_{Sn}$ with $MOMP_{Sn}$-MBP in the void volume of the column (Fig. 3.29a). The same was observed for $HtrA_{Ct}$ and $MOMP_{Ct}$-MBP. In this case, the $HtrA_{Ct}$ peak vanishes completely indicating oligomerization into a higher-order oligomer which interacts with $MOMP_{Ct}$-MBP.

Both MBP-fusion proteins induce proteolytic activity of HtrA proteins to a similar extend, releasing $\sim 2\ \frac{nM}{s}$ of free AMC. Thus, the results match the reported ones for

$HtrA_{Ct}$ (Huston et al., 2011). For $HtrA_{Sn}$ it could also be shown that it slowly degrades $MOMP_{Sn}$-MBP (s. Fig. 3.29e). This result is controversial to findings for $DegP_{Ec}$ where only degradation of unfolded OMPs was observed. This put the folding state of MOMP-MBPs into question. As both target proteins appear in the void volume, there is a strong possibility that partly unfolded protein is linked to correctly folded MBP leading to aggregation. CD spectra show a typical α-helical fold with minima at 209 and 220 nm (s. Fig. 3.29d) which is inconclusive as MOMPs form mainly β-barrels. Thereby, the results are ambiguous.

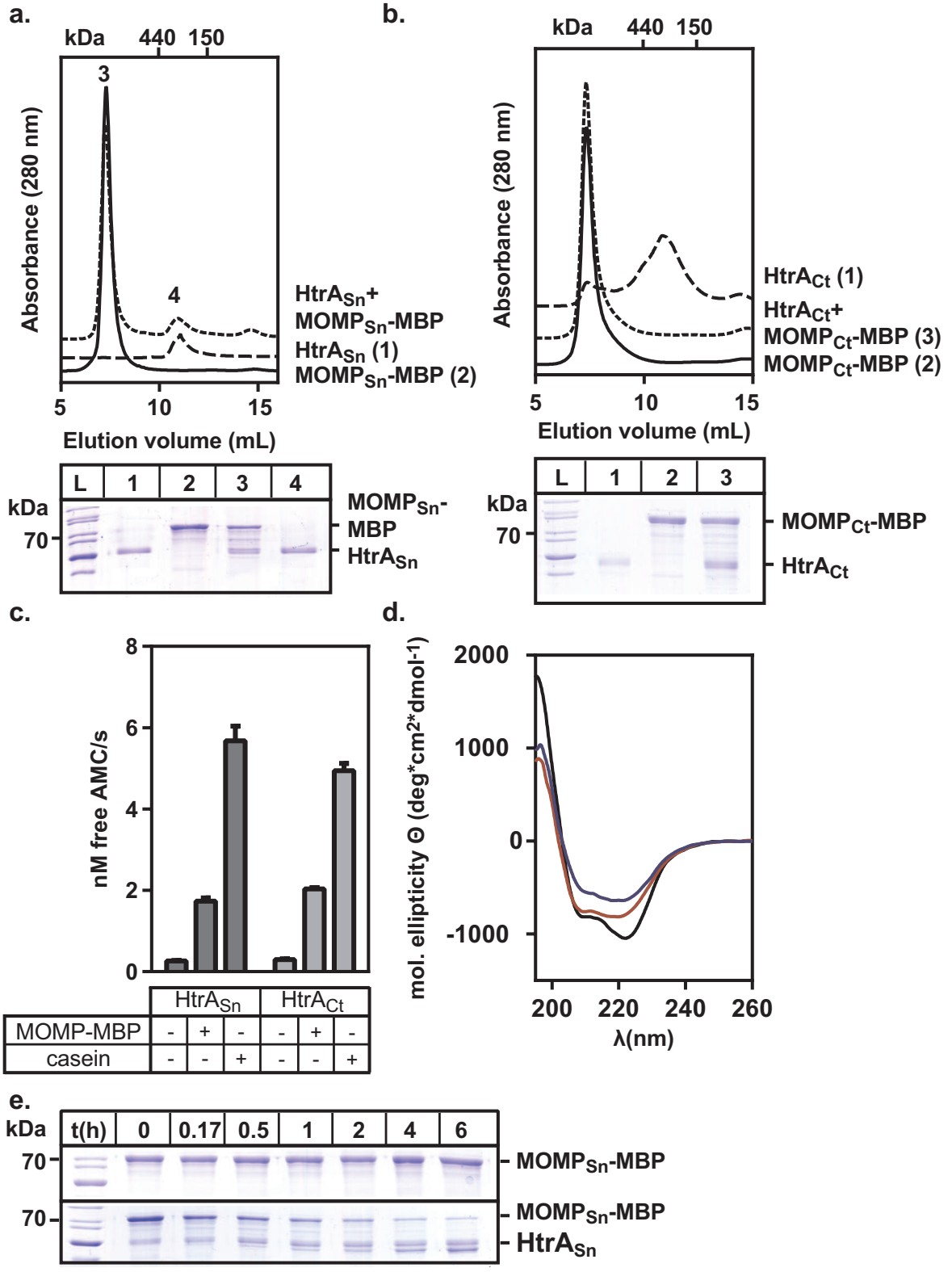

Figure 3.29: The presence of MOMP-MBP promotes oligomerization and proteolytic activation of HtrA proteins. a) Incubation of MOMP$_{Sn}$-MBP and HtrA$_{Sn}$ leads to an accumulation of HtrA$_{Sn}$ together with MOMP$_{Sn}$-MBP in the void volume as SDS-PAGE analysis reveal. b) HtrA$_{Ct}$ accumulates with MOMP$_{Ct}$-MBP in void volume and HtrA$_{Ct}$ peak disappears completely. c) Proteolytic activity of HtrA$_{Sn}$ and HtrA$_{Ct}$ is increased in the presence of MOMP-MBP. d) CD-Spectra of MOMP$_{Sn}$-MBP (blue), MOMP$_{Ct}$-MBP(red) and free MBP(black) reveal a typical α-helical fold with minima at 220 and 209 nm. e) MOMP$_{Sn}$-MBP is degraded slowly by HtrA$_{Sn}$.

3.4.3 Purification of $MOMP_{Sn}$ and $MOMP_{Ct}$

Another approach was taken, purifying MOMPs without MBP-tag as membrane proteins. For $MOMP_{Ct}$, this was already done by a series of washing steps with follow-up SEC and anion exchange chromatography (Wen et al., 2016). To simplify this protocol, $MOMP_{Sn}$ and $MOMP_{Ct}$ constructs were cloned with N-terminal His-tag. Both proteins were successfully produced in *E. coli* BL21Gold and the membrane was isolated. Solubilization was done by 1% sarkosyl and 10 mM DTT. As sarkosyl is a very harsh detergent which impedes with HtrA proteolytic activity, $MOMP_{Sn}$ was eluted with 0.2 % DDM and $MOMP_{Ct}$ with 1 % from the affinity column (Fig. 3.30). As both protein preparations show a very low yield, only one purification step was performed.

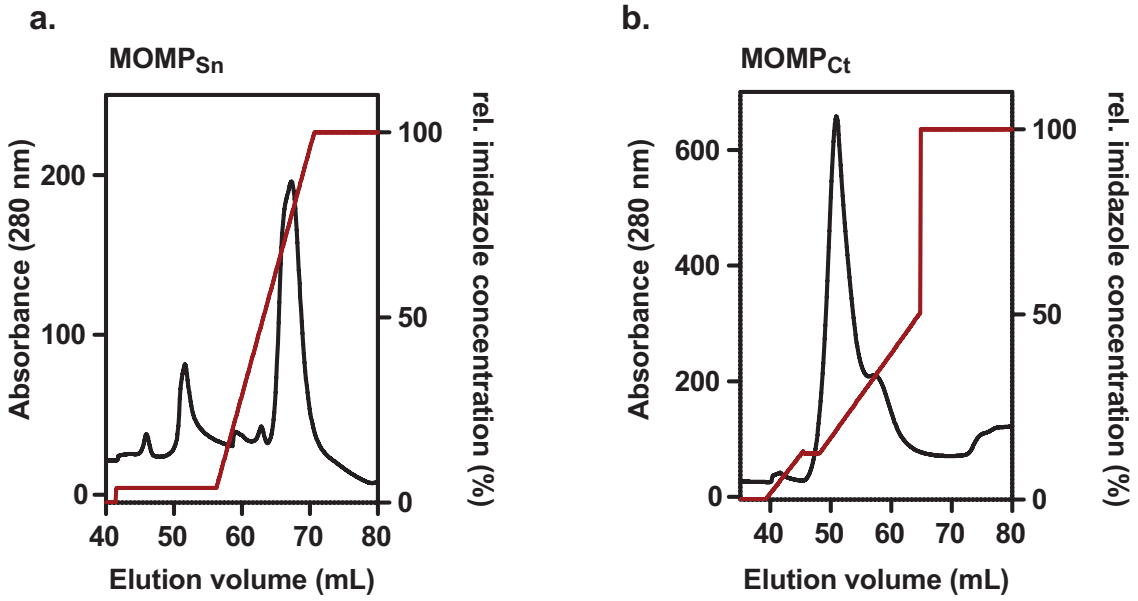

Figure 3.30: Purification of $MOMP_{Sn}$ and $MOMP_{Ct}$ with N-terminal His-tag. Affinity chromatography results of $MOMP_{Sn}$ (a) and $MOMP_{Ct}$ (b). The elution buffer contained 0.2 % DDM or 1 % OG, respectively.

3.4.4 Biochemical characterization of interactions between MOMP-His_6 and HtrA

The difficulty in experiments with membrane proteins is the impact of detergents on the performed method. The problem already starts at protein concentration determination, as the detergent micelles interfere with UV/Vis spectroscopy and also with colorimetric

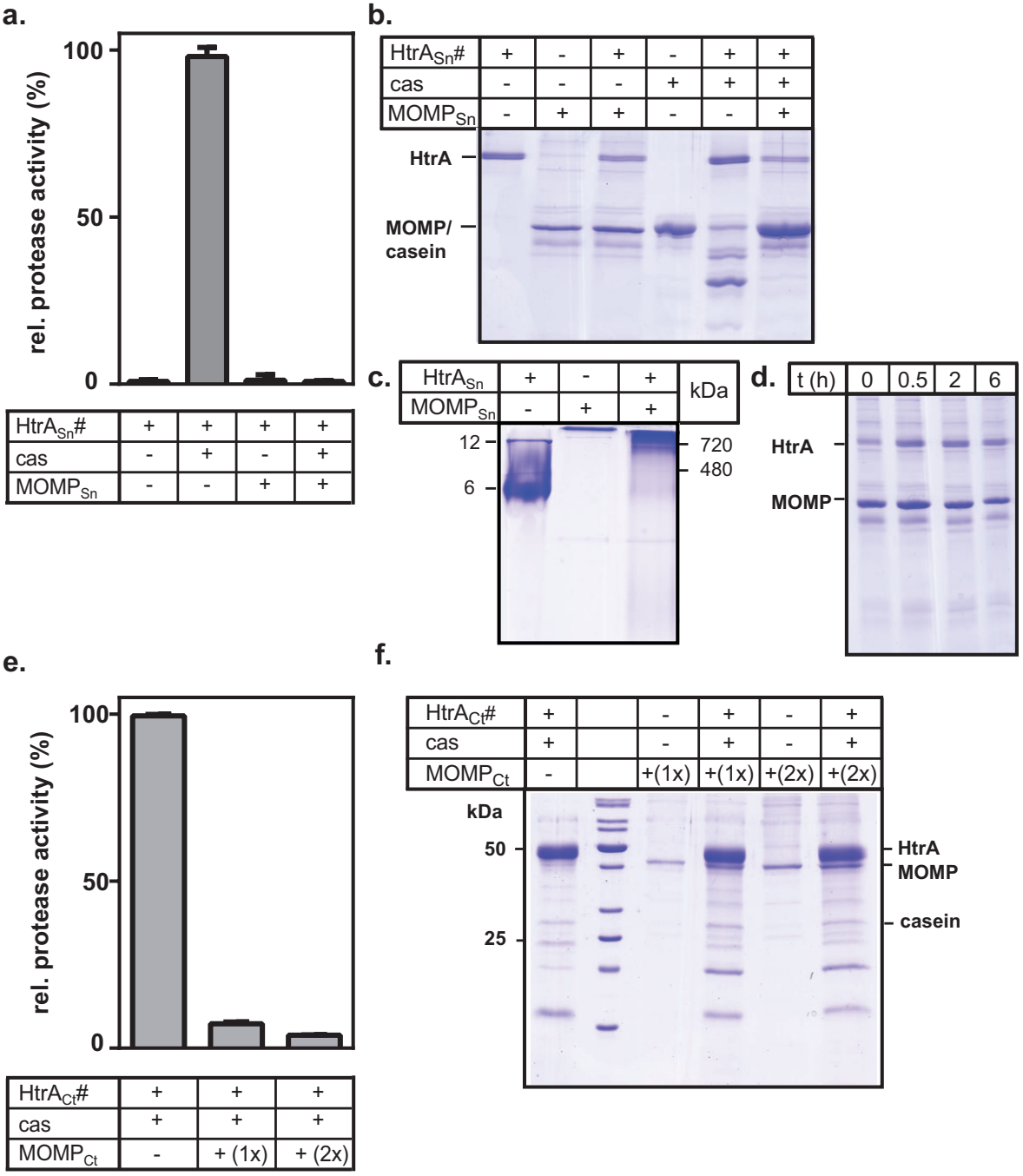

Figure 3.31: MOMPs have an inhibitory effect on the proteolytic activity of HtrA proteins. a) Impact of $MOMP_{Sn}$ on proteolytic activity of $HtrA_{Sn}$ in 0.1% DDM buffer. $MOMP_{Sn}$ inhibits fluorogenic reporter cleavage significantly even in the presence of β-casein. b) SDS-PAGE analysis of protease assay samples reveals that β-casein digestion is hindered by $MOMP_{Sn}$ addition. c) $MOMP_{Sn}$ is stable for at least 6 h when exposed to $HtrA_{Sn}$. e) $MOMP_{Ct}$ inhibits proteolytic activity of $HtrA_{Ct}$ in a concentration-dependent manner. The assay buffer contains 1% OG. f) SDS-PAGE analysis of protease assay samples shows that β-casein digestion is slowed down due to $MOMP_{Ct}$ addition.

assay methods like Bradford or biuret reaction. Therefore, the determination of the protein concentration could only be estimated by UV/Vis spectroscopic measurement and evaluated by SDS-PAGE analysis.
Interestingly, $MOMP_{Sn}$ and $MOMP_{Ct}$ show a completely different behaviour than the MBP-fusion proteins. Both have an inhibitory effect on proteolytic activity of HtrA proteins (s. Fig. 3.31a,e). Even β-casein digestion is slowed down significantly (s. Fig. 3.31b,f) when both substrates are added. MOMP itself is not degraded (s. Fig. 3.31c) by HtrA proteins matching $DegP_{Ec}$ results (Ge et al., 2014).
To investigate the influence of MOMP on the oligomerization state of HtrA proteins, native PAGE analysis was used because analytical SEC runs are disturbed by detergent addition. Results suggest the formation of higher-order oligomers as the 6-mer band of $HtrA_{Sn}$ completely disappears (Fig. 3.31d) and many prominent bands in high molecular range are detected.
Taken together, these preliminary results show that *in vitro* $HtrA_{Sn}$ and $HtrA_{Ct}$ interact with MOMPs in folded and probably unfolded state (MOMP-MBPs). Further analysis is required to investigate the relevance of these results *in vivo*.

4 Discussion

Protein-quality control prevents excessive protein aggregation in living cells by sophisticated molecular mechanisms which ensure cellular survival under harsh conditions. Key players in the ATP-independent quality control are members of the HtrA protein family. Their unique architecture enables controlled proteolysis and chaperone-like functions. Several prokaryotic HtrA proteins have been associated with infectious diseases and consequently represent potential targets for antibacterial therapy.
$HtrA_{Ct}$ has been identified as one virulence factor essential for bacterial survival (Gloeckl et al., 2013) in *C. trachomatis* infections, the leading cause of preventable blindness and the most commonly reported sexually transmitted disease (Rajeeve et al., 2018). The rise of antibiotic resistance impedes conventional treatment and emphasizes the demand for new antibacterial therapeutics (Mestrovic & Ljubin-sternak, 2018). Crystal structures allow rational drug design and facilitate the development of new chemical agents specifically targeting, e.g. the active site of proteases.
In this study, crystal structures for a close relative of $HtrA_{Ct}$, $HtrA_{Sn}$ from *S. negevensis* a potential new human pathogen associated with pneumonia and bronchiolitis (Vouga et al., 2017) were determined and revealed a unique architecture among HtrA proteins. Based on the structural data as a framework, new protein variants were designed and subsequently characterized with the focus on oligomerization behavior and proteolytic activity.

4.1 $HtrA_{Sn}$ - a self-compartimentizing protease

Proteins from the prokaryotic HtrA family occur as homooligomers in solution. Homooligomerization is a mechanism to increase functional diversity in the cellular environment without increasing the genome size. The transition between different oligomeric states is a common process to regulate enzymatic activity which is also used by e.g. caspases in apoptosis (Chang et al., 2003) or ATPases in transcription (De Carlo et al., 2006).

For HtrA proteins from *E. coli* a two-state model mechanism was proposed. The binding of misfolded proteins transforms proteolytic inactive hexamers into large proteolytic active higher-oder oligomers (Krojer et al., 2008b). Results from this study show that $HtrA_{Sn}$ usually forms 6-mer in solution. In contrast to *E. coli* HtrA proteins, these 6-mers are not fully inactive. The $HtrA_{Sn}$ 6-mers are able to cleave substrate at a basal rate. Protein variants ($HtrA_{Sn}{}^{Q290A}$, $HtrA_{Sn}{}^{F477A}$) which exclusively form 3-mers also retain their ability for substrate cleavage. Consequently, higher-order oligomerization of $HtrA_{Sn}$ is not an absolute requisite for proteolytic activity.

The substrate cleavage efficacy of the $HtrA_{Sn}$ 3- and 6-mer is quite low compared to the cleavage rate of the $HtrA_{Sn}$ 12-mer. The proteolytic activity of $HtrA_{Sn}$ increases in a concentration-dependent manner in the presence of unfolded protein substrates and shows positive cooperativity. The protease-substrate ratio with the highest proteolytic activity coincides with the complete reorganization from 6- to 12-mers.

Intriguingly, the molecular weight of the $HtrA_{Sn}$ oligomers continuously increases with rising substrate concentration until 12-mers are the most prevalent molecular species. According to the two state model established for the *E. coli* HtrA proteins, we expected the presence of two distinct states in SEC experiments (Krojer et al., 2008b). There are two ways to interpret these results. Either the substrate binding is a stepwise process which induces oligomerization at a critical concentration. Alternatively, an intermediate state assembles with a molecular weight of $\sim$ 450 kDa (9-mer) and the SEC results are based on a shift in the equilibrium between 6-, 9- and 12-mer. Experiments with the $HtrA_{Sn}{}^{Q290A}$ variant which is unable to form cages also show a continuous molecular weight shift. This supports the theory of stepwise substrate binding. Thus, the two state model established for the *E. coli* HtrA proteins also applies to $HtrA_{Sn}$ with little adjustments. Without external stress conditions, the $HtrA_{Sn}$ 6-mer maintains cellular survival by cleavage of unfolded or misfolded proteins at low concentrations. If the amount of unfolded protein exceeds a critical concentration, oligomerization into a more active 12-mer is required to remove the high amount of unfolded protein. It is conceivable that the substrate binds with a higher affinity to the 12-meric state allowing faster substrate cleavage.

In proteolytic-activity assays of $HtrA_{Sn}$, the cleavage rate of the fluorogenic substrate could be drastically increased by the addition of unfolded proteins. Interestingly, there are two different types of protease activators for $HtrA_{Sn}$. Substrates like β-casein increase proteolytic activity and are rapidly degraded. On the other hand, unfolded lysozyme also activates the proteolytic activity of $HtrA_{Sn}$ but is not degraded to the same extent. It acts as allosteric activator. The denaturation by addition of DTT probably does not allow complete unfolding. For $DegP_{Ec}$, there are similar results published depending on the mode of denaturation. Carboxy-methylated lysozyme is

cleaved efficiently (Kim et al., 2011) whereas denaturation of lysozyme with DTT leads to a slow degradation process (Jomaa et al., 2007).
Previous studies investigated the allosteric activation of $DegP_{Ec}$ by specifically engineered peptides. These peptides can bind the PDZ1 binding site but the cleavage motif was removed. Instead of an expected inhibitory effect, the proteolytic activity was increased (Krojer et al., 2008a). $DegQ_{Lp}$ shows a similar behavior, as the presence of pept1 increases proteolytic activity (Schubert et al., 2015). In contrast, $HtrA_{Sn}$ could not be activated by pept1 addition. An explanation for this phenomenon based on structural data is described in section 4.1.1.

Based on the structural data, the catalytic center of the $HtrA_{Sn}$ adopts an active (12-mer) and an inactive conformation (6-mer). In the inactive state, accessibility of the oxyanion hole and the S1 specificity pocket is not enabled. A cascade of conformational changes in the L3, LD*, L2 and L1* loops leads to an activated proteolytic center. The cross communication between monomers of one homotrimer is essential for proteolytic activation and facilitates substrate binding by unblocking the neighboring monomer. The L3 loop is in direct interaction distance to the PDZ1 binding pocket and the bound substrate in the active site of one monomer and therefore, changes in these areas have an impact on the position and conformation of the L3 loop. The changes in the L3 loop are sensed by the adjacent LD* loop which undergoes big conformational changes. Interestingly, the LD loop conformation from $DegP_{Ec}$ is identical in the inactive and active state (Figaj et al., 2016) and is already oriented as in the $HtrA_{Sn}$ active state. Thereby, different structural reorganizations lead to the same outcome - an active proteolytic center. This kind of allosteric activation cascade has been described for other HtrA proteins (Wrase et al., 2011; Wilken et al., 2004; Krojer et al., 2010), suggesting a general mechanism for activation. It is assumed that the cascade starts with substrate binding to the PDZ1 domain as mutations in the PDZ1 binding pocket leave the protease inactive (Schubert et al., 2015; Merdanovic et al., 2010; Krojer et al., 2010). For $DegP_{Ec}$ it has been proposed that the bound substrate in one PDZ1 domain could be cleaved by the protease domain of the same and the neighboring monomer (hold-and-bite mechanism) (Krojer et al., 2008a). The shortest distance to the catalytic center of the same protomer is with $\sim$55 Å considerably longer than the distance to the neighboring catalytic center (40 Å). These distances could be bridged by peptides with 16 to 12 residues, respectively, which is in accordance with the mean cleavage product size of 13-15 residues of $DegP_{Ec}$ (Krojer et al., 2008a). In the $HtrA_{Sn}$ 12-mer, the mechanism seems to be reversed as the distance between the PDZ1 domain and the catalytic center of one monomer is with 42 Å shorter than the distance to the adjacent proteolytic center (60 Å).

4.1.1 The importance of the PDZ2-PDZ1* interface in oligomer stabilization of HtrA proteins

In solution, $HtrA_{Sn}$ forms exceptional stable 6-mers which are not influenced by pH or temperature changes in contrast to $DegP_{Ec}$ (Krojer et al., 2008b) and $DegQ_{Lf}$ (Wrase et al., 2011). This study reveals that one reason for this stability are extensive PDZ2-domain interactions between the opposite trimers. The PDZ2 domains of one trimer interact with the opposite site protease*, PDZ1* and PDZ2* domains which is the first time that these contacts are described for prokaryotic HtrA 6-mers. Two PDZ2* domains of the adjacent trimer enclose one PDZ2 domain in a zipper-like fashion. Thus, a tightly interconnected cage is formed that is fundamentally different from the $DegP_{Ec}$ 6-mer (Krojer et al., 2002) where PDZ1-domain and LA-loop interactions are the main stabilizers for the structural integrity of 6-mers. In the $HtrA_{Sn}$ 6-mer, the PDZ2 domains form a hydrophobic interface with the PDZ1* domains of the opposite monomer in a pairwise manner. Based on the structural data, the interactions in this interface were analyzed and together with a sequence alignment, a highly conserved residue Q290 was identified. Q290 forms a hydrogen bond to the backbone amide of F477* from the opposite trimer. Mutational analysis of both residues reveals two protein variants which are unable to form cages. This highlights the importance of the PDZ2-PDZ1* interface for 6-mer stability. Interestingly, the same interface is found in $HtrA_{Sn}$ 12-mer and also in $DegP_{Ec}$ 12- and 24-mer (Krojer et al., 2008b; Jiang et al., 2008). This indicates that not only 6-mer stability but also higher-order oligomer stability is achieved by this PDZ2-PDZ1* interface. In $DegP_{Ec}$, the formation of this interface was attributed to stabilization effects (Kim et al., 2011; Krojer et al., 2010) and to an increase in substrate binding affinity (Kim & Sauer, 2012) in higher-order oligomers. Similar to $HtrA_{Sn}$, Deg_{Ec} variants with mutations in the PDZ1-PDZ2* interface assemble exclusively as 3-mers. For these mutants the substrate affinity was significantly lower than for the wildtype enzyme but could be increased in the presence of isolated PDZ2 domains. The authors concluded that substrate binding affinity is increased by the interaction of the PDZ1 with the PDZ2* domain of the adjacent trimer. As in $HtrA_{Sn}$ the interface stays the same for 6- and 12-mer it is unlikely that these interactions increase substrate affinity. Interestingly, the position of the PDZ2 in respect to the PDZ1 domain of the same monomer changes dramatically from 6- to 12-mer. In the HtrA 6-mer, the PDZ2 domain of one monomer does not interact with other domains of this monomer due to the long linker between the PDZ1 and PDZ2 domain. However, in the $HtrA_{Sn}$ 12-mer the PDZ2 domain can contact the protease domain of the same monomer. Consequently, it is tempting to speculate that substrate

bound in the PDZ1 and the protease domain interacts directly with the PDZ2 domain. As a result, the changes in the orientation of the PDZ2 domain could increase substrate affinity similar to the $DegP_{Ec}$ 12-mer by a different mechanism.
Another interesting aspect of the stabilizing PDZ2-PDZ1* interface is the question what happens during the process of oligomerization. The current model for $DegP_{Ec}$ suggests a transient disassembly into trimers after substrate binding which subsequently assembles into higher-order oligomers. For the $DegP_{Ec}$ 12-mer it was reported that the cage integrity is maintained as long as uncleaved substrate is available (Kim et al., 2011). Consequently, disassembly is not necessary for substrate entry into the cage. Due to the high stability of the $HtrA_{Sn}$ 6-mer even at harsh conditions, a high amount of energy is required to destabilize this assembly. Thus, it seems highly unlikely that this assembly disintegrates upon substrate binding. Based on these results, a working model of oligomerization is proposed (Fig. 4.1).

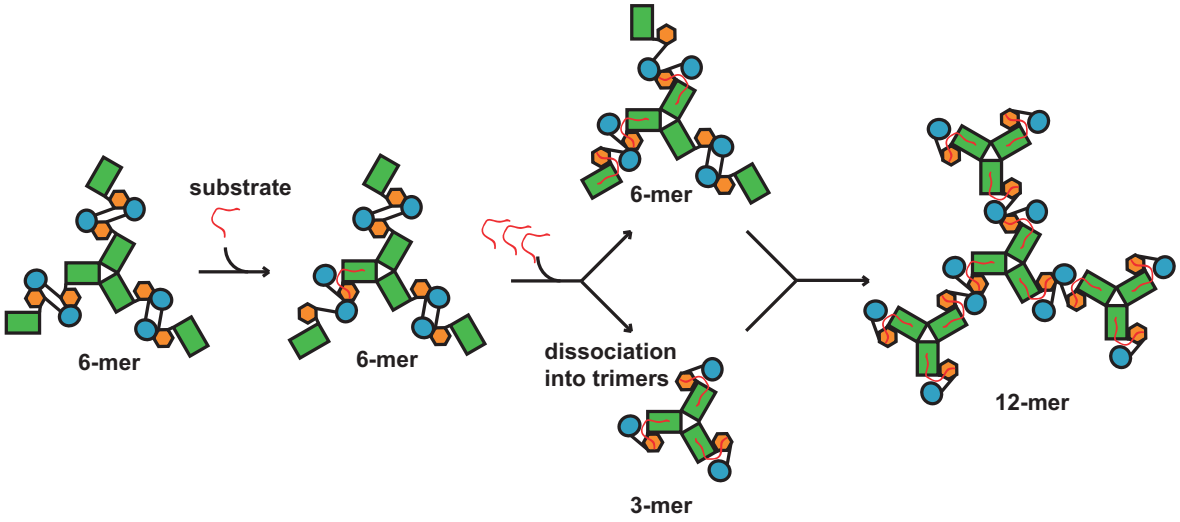

Figure 4.1: Model for $HtrA_{Sn}$ oligomerization. Inactive 6-mers form stable PDZ1-PDZ2*/PDZ2-PDZ1* interfaces with the opposite monomer. Substrate binds to the PDZ1 domain of one monomer inducing a shift in the PDZ2* domain's position. The PDZ2* domain of the opposite monomer now stabilizes the bound substrate. As a result, the PDZ2-PDZ1* interface is disrupted and the 6-mer engages in a more open conformation. Stepwise substrate binding destabilizes the 6-mer by further disintegrations of PDZ2-PDZ1* interfaces which at a critical concentration either promotes further cage opening or trimer dissociation and a subsequent assembly into 12-mers. (protease domain - green, PDZ1 - orange, PDZ2 - blue)

$HtrA_{Sn}$ forms a stable compact 6-mers in solution with extensive PDZ2 interactions to the opposite site trimer. In the presence of substrate with a sufficient length to bind in the PDZ1 and protease domain simultaneously, the PDZ2 domain swings in to interact directly with the substrate like a hatch. This additionally fixes the substrate in its position and thereby increases substrate binding affinity. The PDZ1-PDZ2* interface

of the two monomers remains stable whereas the PDZ2-PDZ1* interface is disrupted by the movement of the PDZ2 domain towards the bound substrate. This opening of the 6-mer cage allows facilitated substrate entry but its structural integrity is still intact as one of the two PDZ interfaces persists. It is tempting to speculate that during the entire oligomerization process at least one PDZ2-PDZ1* interface stays intact and prevents a complete 6-mer disassembly. The released PDZ1* domain is now able to bind substrate, recruit another trimer and generate a new PDZ1-PDZ2* interface and the $HtrA_{Sn}$ 6-mer assembles into a 12-mer. An important requisite for this theory is the length of the substrate. To induce the conformational change in the PDZ2 domain, interactions between substrate and the PDZ2 domain are required. β-casein with a molecular weight of 25 kDa could bind in the proteolytic center and the PDZ1 domain simultaneously, leading to interactions with the PDZ2 domain. The heptapeptide pept1 on the other hand is also able to bind in the PDZ1 and protease domain but without a covalent linkage region which can interact with the PDZ2 domain. As a result, β-casein induces oligomerization in the $HtrA_{Sn}$ 6-mer whereas pept1 does not. Interestingly, in $DegP_{Ec}$ (Merdanovic et al., 2010) and $DegQ_{Lp}$ (Schubert et al., 2015), the heptapeptide operates as an allosteric activator for proteolytic activity and oligomerization as in $DegP_{Ec}$ 6-mer the PDZ2 domain is in close contact to the protease and PDZ1 domain and can sense even short substrates. The positioning of the PDZ2 domain in respect to the PDZ1 domain is dependent on the loop length between both domains. Different studies for $DegP_{Ec}$ show that deletion of this linker region leads to exclusively 12-mer assembly whereas a prolonged linker supports 6-mer formation (Iwanczyk et al., 2007; Kim & Sauer, 2012). The $DegP_{Ec}$ 6-mer variants with prolonged linker between the PDZ1 and PDZ2 domain do not oligomerize in the presence of peptides similar to $HtrA_{Sn}$. Consequently, the linker length and the resulting position of the PDZ2 domain determines the oligomeric state. $HtrA_{Sn}$ (residues: 374–387) and $DegP_{Ec}$ (residues: 357–364) (Iwanczyk et al., 2007) have a similar loop length. Thus, both HtrA proteins appear mainly as 6-mers. In DegQ from *Legionella*, there is an additional α-helix between the PDZ1 and PDZ2 domain which shortens the loop region dramatically. Thereby no hexameric assembly was observed (Wrase et al., 2011; Schubert et al., 2015). Based on the structural data, R151 of the LC loop (harboring the active site aspartate D153) is in close interaction distance to Y377 of the linker region between the PDZ1 and PDZ2 domain in $HtrA_{Sn}$ (Fig. 4.2). Consequently, changes in the PDZ domain position have a direct impact on the proteolytic center not only via L3 loop interactions but also by the LC loop. Corroborating this statement, replacement of the equivalent residue of R151 in $HtrA_{Ct}$ (K160) with valine led to reduced proteolytic activity (Marsh et al., 2013).

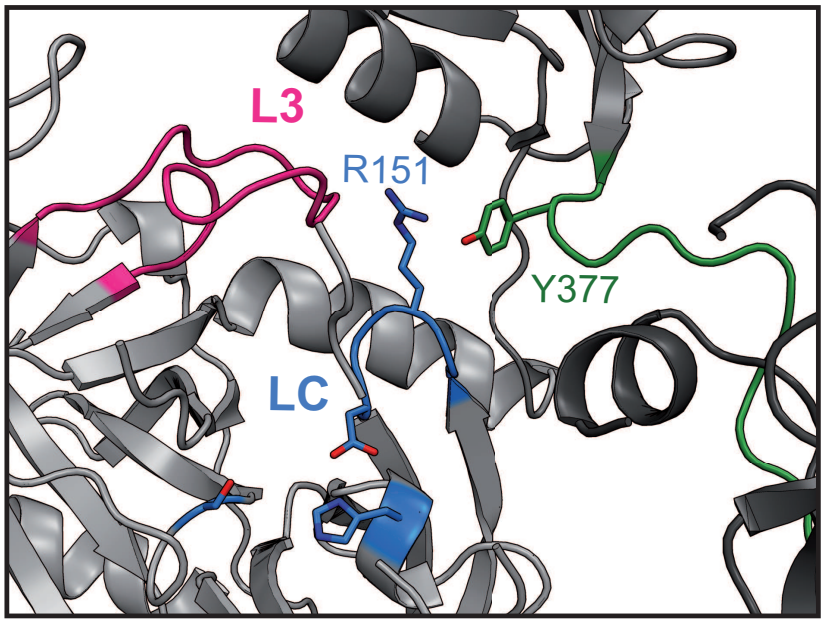

Figure 4.2: In the $HtrA_{Sn}$ 6-mer, the linker region between the PDZ1 and PDZ2 domain (orange) is in close contact (Y377) to the R151 of the LC loop (blue). Thus, changes in the linker region directly effect the active site of the protease domain. The L3 loop is shown in pink.

4.1.2 The importance of the regulatory LA-loop in $HtrA_{Sn}$

Previous studies have shown the importance of the regulatory LA loop as a stabilizer for the proteolytic inactive $DegP_{Ec}$ 6-mer by interactions with the L1* and L2* loop of the opposite site trimer. The LA loops form pillar-like structures by extensive interactions with each other which protrude in the active site of the adjacent trimer (Krojer et al., 2002). However, structural information of major parts of the loop are not provided by the available crystal structures of HtrA proteins. A theoretical model for the $DegP_{Ec}$ LA loop has been proposed and supported by mutational analysis (Figaj et al., 2014). This model enables the identification of important residues which interact with the LA loop. Hydrophobic interactions between the LA loop of one monomer with the L1* loop of the opposite monomer are thought to be critical for maintaining the proteolytic inactive conformation (Figaj et al., 2014). As the LA loop sequence alignment shows only a few preserved amino acids between chlamydial HtrA proteins and $DegP_{Ec}$ (s. Fig. 4.4) the relevance of the generated model for $HtrA_{Sn}$ is questionable.
Interestingly, short protein sequences belonging to the LA loop were identified in the $HtrA_{Sn}$ 6-mer crystal structure. The beginning and end of the loop point in the direction of the catalytic center of the same protomer and are stabilized by interactions with the PDZ2* domain of the opposite trimer. These contacts might provide structure integrity of the 6-mer by cross communication between trimers and simultaneously

regulate proteolytic activity as the LA loop is thought to operate as inhibitory loop (Figaj et al., 2014). The LA loop of $HtrA_{Sn}$ is reduced in length in contrast to $DegP_{Ec}$. Thus, it is conceivable that the LA-PDZ2*-interactions perform the same task of 6-mer stabilization as the pillar-like LA-LA* loop interactions in $DegP_{Ec}$.
In contrast to the $DegP_{Ec}$ 6-mer, the LA loop in the $HtrA_{Sn}$ 6-mer reaches into the proteolytic center of the same monomer. It is tempting to speculate that the LA loops of one trimer interact with each other and stabilize the trimeric assembly. Interestingly, the role of the regulatory LA loop differs in the HtrA protein family. The deletion of the LA loop leads in the $DegP_{Ec}$ 6-mer to mainly monomer and trimer assembly (Jomaa et al., 2007) whereas the $DegQ_{Lf}$ 12-mer still assembles predominantly as 12-mer with low percentage of trimers and monomers (Wrase et al., 2011). $HtrA_{Sn}{}^{\Delta LA}$ was not possible to purify which might be due to a hyperactive protease or misfolding of the protein.

Another short sequence of the LA loop was identified in the $HtrA_{Sn}$ 6-mer which is in interaction distance to F218 of the L3 loop. Replacement of F218 by alanine and tyrosine destabilizes the 6-meric state and readily assembles into 12-mers at low substrate concentrations. This reveals that besides the interactions to the L1 and L2 loop also the regulatory L3 loop is in contact to the inhibitory LA loop which has an impact on the oligomerization behavior of $HtrA_{Sn}$. Interestingly, the facilitated assembly of higher-order oligomers is not accompanied by an increase in proteolytic activity. As F218 is a highly conserved residue, alterations might disturb the tightly regulated allosteric activation cascade and lead to reduced substrate cleavage. This is the first time that structural evidence of interactions between the LA and the L3 loop are reported.

4.1.3 $HtrA_{Sn}$ reveals a unique architecture

Proteolytic activity for protein-quality control has to be balanced to maintain cellular fitness during stress situations (oxidative stress, inflammation, protein aggregation, metabolic stress, etc.). Whereas *E. coli* developed an elaborated system to avoid aggregation of un- or misfolded proteins that involves three members of the HtrA family in chlamydial species just one HtrA protein is present. Consequently, *Chlamydiae* evolved other regulatory mechanisms to ensure cell viability.
$HtrA_{Sn}$ reveals a unique architecture for the 6- and 12-mers despite the high amino acid sequence homology to other HtrA proteins. It is the second prokaryotic 6-meric crystal structure in the RCSB Protein Data Bank (Berman et al., 2000) with two PDZ

domains and differs significantly from the $DegP_{Ec}$ 6-mer. The $HtrA_{Sn}$ 6-mer forms a highly symmetric condensed spherical particle which is mainly stabilized by PDZ2 domain interactions. Small apertures near the catalytic center might allow limited entry of unfolded protein substrate. The $DegP_{Ec}$ 6-mer is less compact with big lateral pores and shows other stabilizing mechanisms via PDZ1 domain and LA loop interactions. Experiments at elevated temperatures reveal the stability of the $HtrA_{Sn}$ 6-mer which in contrast to the $DegP_{Ec}$ 6-mer does not dissociate into trimers at 42 °C (Krojer et al., 2008b).

Cage assembly seems to protect cells from excessive or inappropriate proteolysis (Kim & Sauer, 2012) and simultaneously shields them from misfolded proteins by encapsulation. An increase in protein aggregates is accompanied by the formation of larger cages like 12- or 24-mers. The cage architecture is determined by the orientation of the PDZ2 domains of the HtrA proteins. As the position of the PDZ2 domains varies in all three analyzed HtrA proteins from *S. negevensis*, *E. coli* and *L. fallonii*, the 12-mer structures show a surprising diversity.

The $HtrA_{Sn}$ 12-mer preserves the stabilizing PDZ1-PDZ2* interface of the $HtrA_{Sn}$ 6-mer but instead of a zipper-like arrangement, the PDZ2 domains form a unique trimeric funnel-like interface. This emargination might present a niche for interactions with unfolded substrate or a docking station for protein-membrane attachment. This inward orientation of the PDZ2 domain arises by the change in position towards the protease domain and decreases the inner cave size in comparison to e.g. $DegQ_{Lf}$. Therefore, close interactions between adjacent trimers are possible but this also limits the amount of encapsulated substrate.

The conformational changes in the L3 loop between 6- and 12-mer state leads to an increase in pore size which facilitates substrate entry. This phenomenon is observed for all 12-mer structures.

Although the overall function for prokaryotic HtrA proteins is quite similar, different mechanisms have been adopted to achieve the same outcome. For example, extensive LA loop interactions between both trimers stabilize the $DegP_{Ec}$ 6-mer whereas in $HtrA_{Sn}$ the LA loop is reduced in length and contacts the PDZ2* domain of the opposite trimer and has thereby a stabilization effect. Also, the LD loop in $HtrA_{Sn}$ undergoes a conformational change between the active and inactive state whereas in $DegP_{Ec}$ the loop is already in an active conformation and the proteolytic inactivity is maintained by other mechanisms. Consequently, every species developed a perfectly adapted protein quality control system dependent on their particular environment.

4.1.4 $HtrA_{Ct}$ - a virulence factor with many faces

$HtrA_{Ct}$, an essential virulence factor required for *C. trachomatis* chlamydial survival in cells (Gloeckl et al., 2013) is a promising target for antibacterial therapeutics. Secretion into the host cell cytoplasm was reported (Wu et al., 2011) but its cellular targets and virulence mechanism are still under investigation. As there are no crystal structures available for $HtrA_{Ct}$, $DegP_{Ec}$ with a sequence identity of 40 % is used as a model protein. Recent studies show that members of the HtrA protein family do not conform in all aspects to the *E. coli* DegP model (Marsh et al., 2017). The results of this study reveal with $HtrA_{Sn}$ a close relative to $HtrA_{Ct}$ (sequence identity of 54 %) which may represent a more suited model protein for chlamydial HtrAs.

As described in previous studies, $HtrA_{Ct}$ is a serine protease (Huston et al., 2007) which shows the same AAC (Huston et al., 2011) as other HtrA proteins. In contrast to $HtrA_{Sn}$, the basal proteolytic activity of $HtrA_{Ct}$ is almost negligible and even at high concentration of the fluorogenic reporter peptide which was used for the functional protein assay, the cleavage rate is low in the absence of activators. The presence of unfolded proteins induces proteolytic activity of $HtrA_{Ct}$. As described for other prokaryotic HtrA proteins (Pallen & Ponting, 1997), β-casein is an effective activator for proteolytic activity of $HtrA_{Ct}$. BSA and lysozyme in denatured state also promote proteolytic activity. Similar to $HtrA_{Sn}$, β-casein and unfolded BSA are degraded rapidly whereas for reduced lysozyme only very slow degradation is detectable. Consequently, the same mode of function as for $HtrA_{Sn}$ is assumed. More precisely, the unfolded C-terminus of the substrate binds in the PDZ1 domain of $HtrA_{Ct}$, to induce the AAC and subsequently, to enables proteolytic activity. Cleavage site accessibility is dependent on the unfolded state of the substrate and thereby, degradation efficacy varies.

$HrtA_{Ct}$ occurs in different oligomeric forms (3-, 6-, 12-mer and higher-order oligomers) dependent on buffer conditions, concentration and age of the sample. This complicates experiments as dependent on oligomer assembly the protein behaves in different ways. For example, a protein sample consisting of mainly 6-mer assembly is not affected by the presence of pept1 (Fig. 3.23) whereas SAXS data reveal that $HtrA_{Ct}$ and $HtrA_{Ct}{}^{0}$ 3-mers form 12-mers in the presence of pept1 similar to $DegQ_{Lp}$ (Schubert et al., 2015). It is conceivable that the 6-mer state resembles the $HtrA_{Sn}$ 6-mer and therefore needs larger substrates to oligomerize such as β-casein whereas the trimeric assembly promotes oligomerization even for short substrates. In $HtrA_{Ct}$ 3-mers, the proteolytic active sites are exposed and might degrade proteins excessively when activated by sub-

strate binding. To regulate the proteolytic activity, 3-mers readily oligomerize into 12-mer cages with protease domains at the inner wall of the cage and limited substrate entry.

Based on SAXS data, an interesting phenomenon for $HtrA_{Ct}$ was discovered. The proportions of different oligomeric forms are concentration-dependent. Whereas $HtrA_{Ct}$ 3-mers dominate at low protein amounts, higher concentrations lead to mainly 6- and 12-mer assembly. During stress conditions, the $HtrA_{Ct}$ level increases in cells (Huston et al., 2008) which shifts the equilibrium towards cage assembly which might in turn facilitate unfolded substrate cleavage. For $DegP_{Ec}$ it was shown that an increase in protein concentration subsequently boosts proteolytic activity even when inactive variants are added (Jiang et al., 2008).

For $HtrA_{Sn}$ and $DegP_{Ec}$, it was shown that oligomerization is a transient process (Krojer et al., 2008b) which is reversed when substrate is depleted. The presence of β-casein induces higher-order oligomerization in $HtrA_{Ct}$ which immediately starts degrading β-casein. After a few hours, there is no full length β-casein left but the oligomerization state of $HtrA_{Ct}$ is unchanged. Even after two days of incubation time, there is no reorganization into 6- or 3-mers visible. SDS-PAGE analysis reveals degradation byproducts which obviously are not degraded by $HtrA_{Ct}$. Thus, $HtrA_{Ct}$ might not fully degrade unfolded protein substrates preventing higher-order oligomer disassembly or the higher-order oligomeric states are more stable under the tested conditions. The latter was observed for $DegQ_{Lf}$ which show mainly 12-mer assembly in solution at physiological pH independent of substrate presence which implies a biological function for the higher-order oligomer (Wrase et al., 2011).

Based on these results, a working model is proposed which may explain the function and regulation of $HtrA_{Ct}$. In the absence of substrates, $HtrA_{Ct}$ forms 3- and 6-mers in a concentration-dependent manner. Upon substrate binding or a further increase in protein concentration, 3-mer and 6-mer oligomerize into higher-order cages. This process is accompanied by a dramatic increase in proteolytic activity. The active 12-mers and 24-mers are stable and do not disassemble into smaller oligomers. The proteolytic activity is controlled by the accessibility of unfolded substrates. When there is no substrate available it is tempting to speculate that the cage-like particles slowly degrades themselves by autoproteolysis. A similar behavior has been reported for $DegP_{Ec}$ (Jomaa et al., 2009).

Taken together, $HtrA_{Ct}$ on the one hand combines features from $HtrA_{Sn}$ in 6-mer state, DegQ from *Legionella* in 3- and 12-mer state and on the other hand shows unique properties which are not observed in other HtrA proteins such as concentration-

dependent oligomerization.

4.2 Interactions between chlamydial HtrA proteins and MOMPs

For various members of the HtrA protein family interactions with membrane proteins have been reported. For $DegP_{Ec}$, a role in OMP biogenesis is proposed, as there are Cryo-EM structures revealing a 24-mer cage with an encapsulated folded OMP which is not degraded (Krojer et al., 2008b). The folded fusion protein MBP-$MOMP_{Ct}$ promotes proteolytic activity of $HtrA_{Ct}$ and thereby indicates a potential *in vivo* substrate (Huston et al., 2011). In this study, the interactions of $HtrA_{Sn}$ and $HtrA_{Ct}$ with $MOMP_{Sn}$ and $MOMP_{Ct}$, respectively, have been analyzed to investigate if there is a general link between HtrA proteins and outer membrane proteins in prokaryotic species and to gain new insights into the interaction between both protein families.

For $HtrA_{Ct}$, MBP fusion proteins were used to obtain soluble MOMP proteins which demonstrably function as an proteolytic activator of $HtrA_{Ct}$ (Huston et al., 2011). This results could be reproduced in this study and the same activation effect was seen for $HtrA_{Sn}$ and MBP-$MOMP_{Sn}$. The fusion proteins were slowly degraded by HtrA proteases which implies a potential *in vivo* substrate. These results are regarded controversially, as these effects are expected for mis- or unfolded proteins. Both fusion proteins elute in the void volume of the SEC column suggesting protein aggregation. Protein aggregation due to mis- or unfolding is a common problem when purifying membrane proteins with the MBP-tag. As there was no validation method to doubtlessly prove that the MBP-MOMPs are correctly folded, the same experiments were conducted with MOMPs without tag, solubilized by detergent micelles.
Interestingly, $MOMP_{Sn}$ and $MOMP_{Ct}$ exhibit the opposite effect and inhibit proteolytic activity of HtrA proteins. A similar behavior has been observed for $DegP_{Ec}$ and the lipoprotein Lpp (Kim & Sauer, 2014). It is conceivable that the hydrophobic surface of the membrane protein leads to encapsulation by HtrA proteins and blocks the proteolytic sites for other substrates. The folded state of MOMP prevents the protein from degradation. HtrA proteins bind membranes (Shen et al., 2009) which might indicate a transporter role to the outer membrane. As the exact interaction mechanisms are still unclear it is also possible, that $HtrA_{Sn/Ct}$ is attached to the outer membrane via interactions with MOMP and kept in a proteolytic inactive state until a stress response is required.

These preliminary results reveal new interesting aspects of the function of the HtrA protein family which could be addressed in future experiments.

4.3 Concluding remarks and future perspectives

The structural and biochemical data provided in this study reveal further insights into the variety of HtrA proteins. The $HtrA_{Sn}$ 6- and 12-mer crystal structures are the first models for chlamydial HtrA proteins. The unique architecture shed new light on the role of the PDZ2 domain in oligomer stabilization as its interface with the PDZ1* domain of a neighboring monomer is already found in 6-mers and not only in higher-order oligomers. Important interactions in this interface have been revealed which are presumably relevant for other family members, too.
Although in recent years many questions concerning HtrA proteins have been answered certain aspect of their molecular architecture and function are still not well understood. The exact mechanism of oligomerization and also of the proposed chaperone-like function of HtrA proteins still awaits characterization. The diversity of structural features which in most cases lead to the same functions are astonishing and indicate a perfect adaption of each specimen to the particular environment. As a result, several inhibitors of bacterial HtrAs which have been shown to be effective against one protease are suboptimal against other homologs. This makes these proteins very interesting targets for various therapeutic approaches.

Appendix

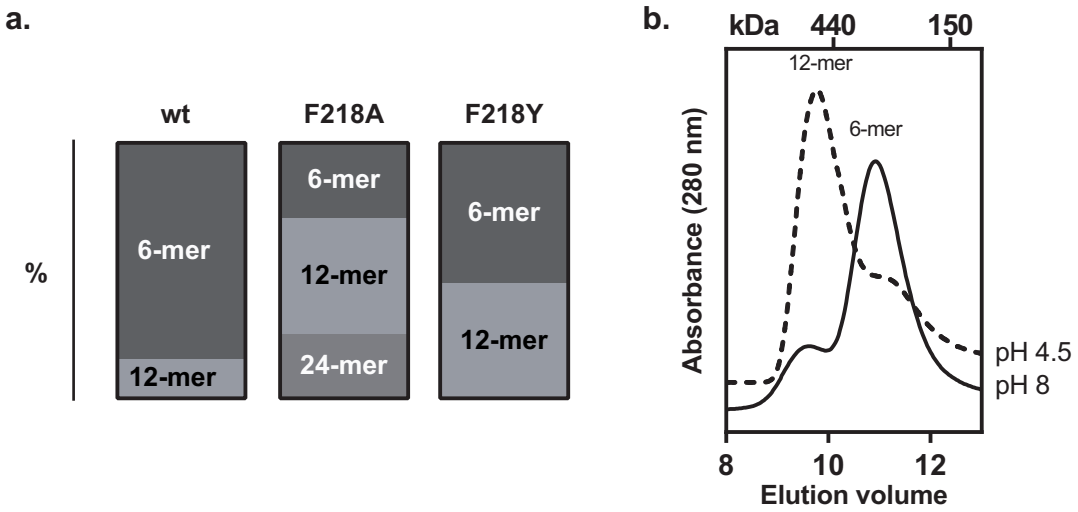

Figure 4.3: Oligomerization studies of F218A and F218Y show the disposition to form higher-order oligomers at lower substrate levels than wild type and at different pH. a)Percentage of oligomeric forms of $HtrA_{Sn}$ wild type, F218A and F218Y when β-casein is added in equimolar amounts (1+1) determined by SEC result analysis. At distinct elution volumes for 6-mer, 12-mer and 24-mer, respectively, the absorbance (mAU at 280 nm) was correlated to the amount of the corresponding oligomeric form. Wild type $HtrA_{Sn}$ shows mainly hexameric form with just $\sim$ 15 % 12-mer whereas F218A is mainly 12-meric with approximately same amount of 6- and 24-mer. For F218Y, 6-mer and 12-mer are present in almost equal amounts.b) pH sensitivity of F218Y. SEC results show that F218Y forms predominantly 6-mers at pH 8 whereas in acidic milieu it assembles mainly as 12-mer.

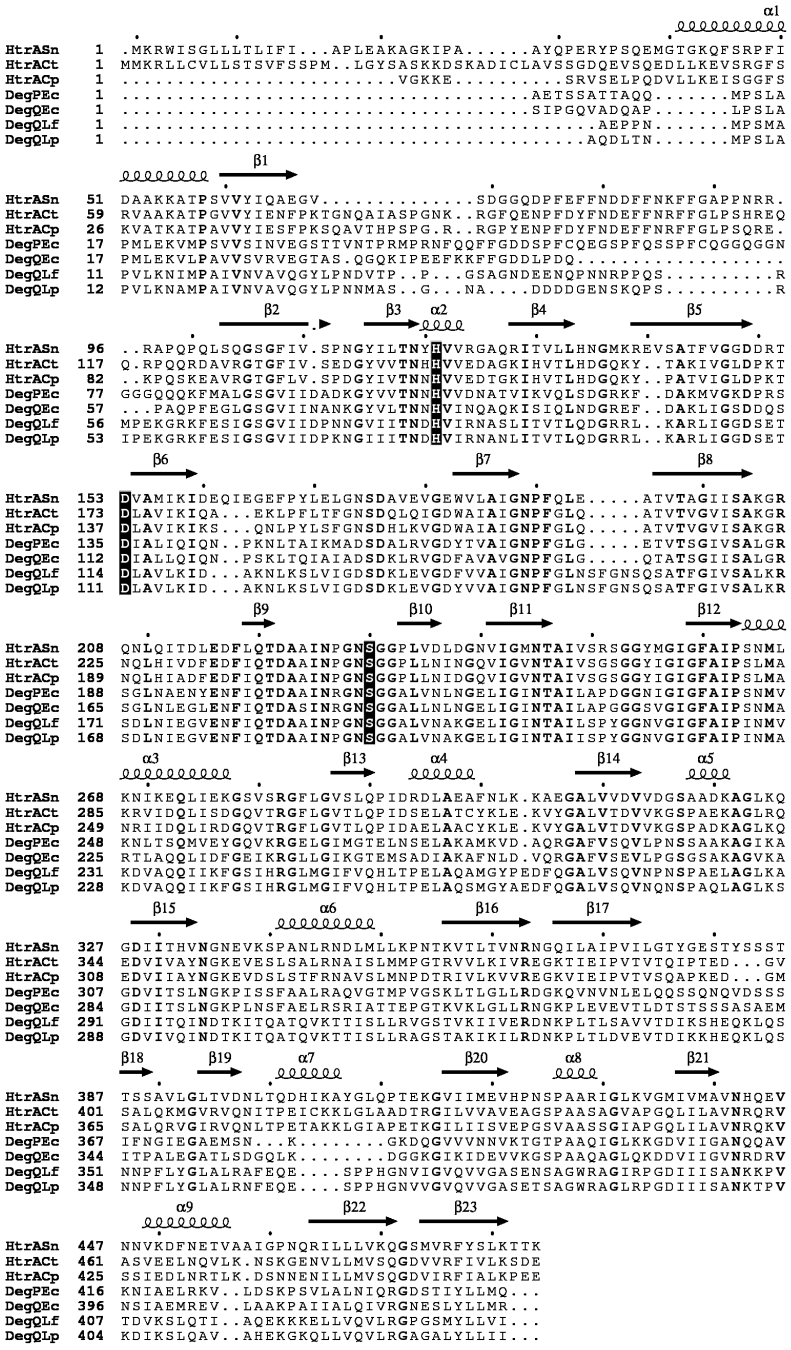

Figure 4.4: Amino acid sequence alignment of HtrA_{Sn} with DegP and DegQ from *E. coli*, HtrA from *C. trachomatis* and *C. pneumoniae* and DegQ from *L. fallonii* and *L. pneumophila*. Highly conserved amino acid residues are displayed in bold letters. The catalytic triade is emphasized by a black background. The secondary structure elements of HtrA_{Sn} were determined by DSSP Kabsch & Sander (1983); Touw et al. (2015) and is shown above the sequence.

Table 4.1: $HtrA_{Sn}$ SAXS sample data analysis by PRIMUS and OLIGOMER. For every scattering curve PRIMUS calculates the Guinier radius (R_G), D_{max} and Porod volume whereas OLIGOMER tries to estimate the volume fractions of a multicomponent protein mixture based on crystal structures. The quality of fit is given by χ^2, which is 1 for a perfect match(Konarev et al., 2003).

	c (mg/mL)	R_G (nm)	D_{max} (nm)	PV	I(0)	MW (kDa) PV	MW (kDa) I(0)	data quality (%)	Oligomer 3-mer	Oligomer 6-mer	Oligomer 12-mer	χ^2
$HtrA_{Sn}$# (Tris 8)												
1	0.32	4.74	14.95	592	0.045	296	180	90	0.00	0.96	0.04	0.76
2	0.97	4.78	14.39	613	0.19	307	251	86	0.10	0.72	0.18	3.32
3	1.51	4.85	14.57	629	0.3	315	254	68	0.17	0.72	0.11	
4	1.65	4.84	14.48	633	0.34	316	264	69	0.17	0.72	0.11	7.00
5	2.00	4.88	14.44	645	0.44	322	282	68	0.16	0.73	0.12	7.18
		4.82	**14.57**	**622**		**311**	**246**		**0.12**	**0.77**	**0.11**	12.57
$HtrA_{Sn}$# (NaAc 4.5)												
1	1.14	5.2	15.45	817	0.28	409	314	92	0.00	0.79	0.22	12.33
2	2.04	5.2	15.5	848	0.48	424	301	90	0.00	0.75	0.25	13.34
		5.2	**15.48**	**833**		**416**	**308**		**0.00**	**0.77**	**0.23**	
$HtrA_{Sn}$												
1	0.28	5.08	15.20	702	49440	351	254	93	0.07	0.72	0.21	4.53
2	0.59	5.22	16.50	733	107600	367	263	77	0.06	0.72	0.23	16.03
3	1.25	5.35	16.70	765	230600	383	266	70	0.02	0.73	0.24	32.67
4	3.00	5.49	16.43	792	569200	396	273	60	0.00	0.73	0.27	34.40
		5.29	**16.21**	**748**		**374**	**264**		**0.04**	**0.73**	**0.24**	
$HtrA_{Sn}$ + pept1												
1	0.28	5.08	16.14	702	44460	351	229	96	0.06	0.73	0.21	3.34
2	0.59	5.24	16.39	742	101900	371	249	89	0.04	0.72	0.24	11.28
3	1.25	5.36	16.2	762	214300	381	247	60	0.01	0.72	0.27	41.16

	c (mg/mL)	R_G (nm)	D_{max} (nm)	PV	I(0)	MW (kDa) PV	MW (kDa) I(0)	data quality (%)	Oligomer 3-mer	Oligomer 6-mer	Oligomer 12-mer	χ^2
		5.23	**16.24**	**735**		**368**	**241**		**0.04**	**0.72**	**0.24**	
$HtrA_{Sn}$ 12-mer												
1	0.52	6.29	17.56	1490	0.15	745	369	83	0.00	0.16	0.84	2.81
2	1.18	6.40	18.80	1480	0.33	740	358	81	0.00	0.24	0.77	9.90
3	2.25	6.19	17.50	1450	0.71	725	404	73	0.00	0.32	0.68	36.17
4	4.30	6.23	18.50	1600	1.46	800	435	78	0.00	0.44	0.56	47.45
		6.28	**18.09**	**1505**		**753**	**391**		**0.00**	**0.29**	**0.71**	

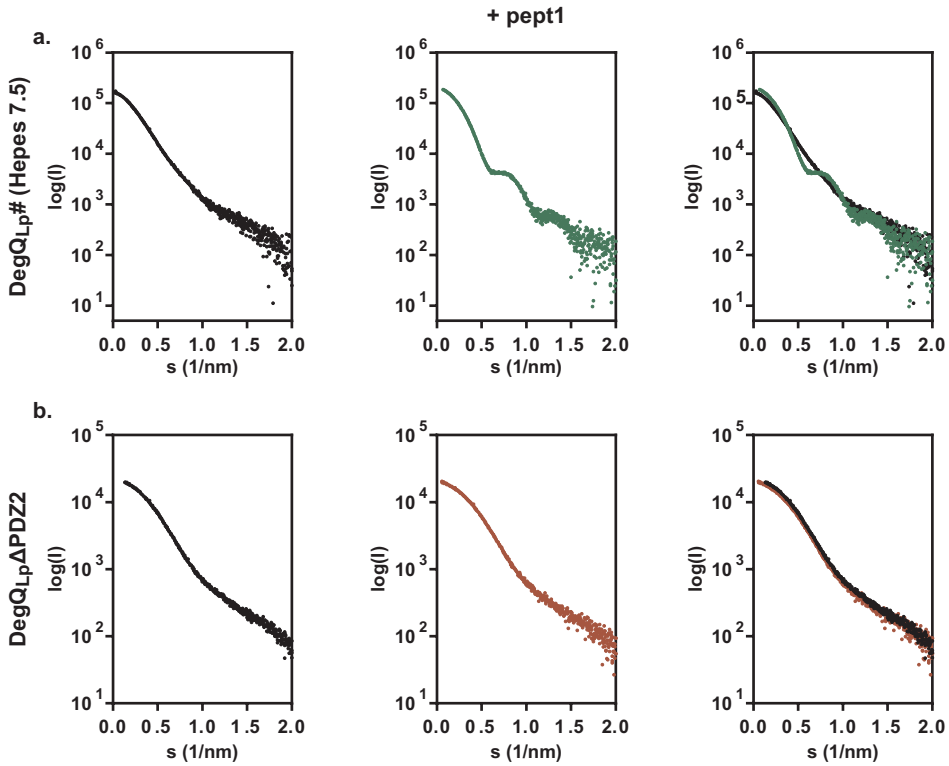

Figure 4.5: $DegQ_{Lp}$ undergoes conformational changes when pept1 is added. a) Scattering curve of $DegQ_{Lp}{}^{\#}$ measurd by SAXS with and without pept1 differ significantly due to different amounts of oligomeric states. $DegQ_{Lp}{}^{\#}$ forms mainly 3-mers. The addition of pept1 leads to 12-mer assembly. b) $DegQ_{Lp}\Delta PDZ2$ only occurs as 3-mer. Addition of pept1 does not change scattering curve, no oligomerization is induced.

Table 4.2: $HtrA_{Ct}$ SAXS sample data analysis by PRIMUS and OLIGOMER. For every scattering curve PRIMUS calculates the Guinier radius (R_G), D_{max} and Porod volume whereas OLIGOMER tries to estimate the volume fractions of a multicomponent protein mixture based on crystal structures. The quality of fit is given by χ^2, which is 1 for a perfect match(Konarev et al., 2003).

	c (mg/mL)	**R_G (nm)**	**D_{max} (nm)**	**PV**	**I(0)**	**MW (kDa) PV**	**MW (kDa) I(0)**	**data quality (%)**	**Oligomer 3-mer**	**Oligomer 6-mer**	**Oligomer 12-mer**	**χ^2**
$HtrA_{Ct}$												
1	0.39	5.66	18.69	675	10480	338	187	85	0.375	0.363	0.272	3.32
2	0.81	6.10	18.86	735	26510	368	229	86	0.289	0.454	0.257	96.76
3	1.69	6.60	20.63	898	74720	449	307	88	0.204	0.401	0.395	136.95
4	3.62	7.26	23.49	1060	174000	530	335	77	0.162	0.300	0.538	158.70
merge		5.86	18.81	660		330		89	0.459	0.347	0.193	14.66
$HtrA_{Ct}$+pept1												
2.1	0.65	6.24	18.50	1180	25940	590	280	89	0.000	0.239	0.761	12.33
3.1	1.35	6.70	20.42	1560	84930	780	437	74	0.000	0.127	0.873	109.54
4.1	2.89	7.35	25.78	1960	214100	980	515	82	0.000	0.107	0.893	639.00
merge		6.18	18.18	1160		580		91	0.000	0.463	0.537	25.48
$HtrA_{Ct}{}^0$												
1	0.29	6.69	18.73	935	0.06	468	278	91	0.430	0.000	0.570	1.99
2	0.55	6.90	19.81	987	0.11	494	256	89	0.407	0.000	0.593	2.71
3	1.03	7.38	23.18	1130	0.27	565	337	86	0.403	0.000	0.597	8.76
4	1.13	7.70	25.41	1190	0.36	595	408	81	0.396	0.000	0.604	12.79
5	1.74	7.96	25.45	1300	0.61	650	449	76	0.391	0.000	0.609	18.54
6	2.51	7.30	22.05	1240	0.84	620	428	89	0.150	0.348	0.502	27.31
7	4.29	8.37	26.88	1490	1.71	745	511	82	0.066	0.465	0.469	6.72
merge		6.79	20.02	963		482		90	0.484	0.000	0.561	4.81
$HtrA_{Ct}{}^0$+10x pept1												
	2.44	7.44	22.87	2200	1.10	1100	577	70	0.000	0.146	0.854	69.37

Table 4.3: $DegQ_{Lp}$ SAXS sample data analysis by PRIMUS and OLIGOMER. For every scattering curve PRIMUS calculates the Guinier radius (R_G), D_{max} and Porod volume whereas OLIGOMER tries to estimate the volume fractions of a multicomponent protein mixture based on crystal structures. The quality of fit is given by χ^2, which is 1 for a perfect match(Konarev et al. (2003)).

	c (mg/mL)	**R_G (nm)**	**D_{max} (nm)**	**PV**	**I(0)**	**MW (kDa) PV**	**I(0)**	**data quality (%)**	**Oligomer 3-mer**	**6-mer**	**12-mer**	χ^2
$DegQ_{Lp}\Delta PDZ2$												
1	0.20	3.72	10.53	197	21590	98	155	84				
2	0.45	3.85	12.43	203	45160	101	144	91				
3	0.60	3.80	11.53	205	67110	103	161	90				
4	0.97	3.88	12.55	210	111900	105	166	88				
merge		3.86	13.26	207		104		92				
$DegQ_{Lp}\Delta PDZ2$+pept1												
1	0.13	3.77	12.27	195	25530	98	283	88				
2	0.35	3.78	11.32	200	51930	100	214	88				
3	1.01	4.04	14.26	221	136300	111	195	79				
merge		3.75	11.67	204		102		89				
$DegQ_{Lp}$# (50 mM Hepes 7.5. 500 mM NaCl)												
1	0.35	5.05	14.34	408	33260	204	137	85	0.674	0.241	0.085	3.290
2	0.63	6.03	20.06	513	89890	256	205	79	0.543	0.280	0.178	13.510
3	0.91	6.54	22.80	603	157700	301	249	77	0.433	0.318	0.248	34.700
4	1.20	6.97	25.00	696	234400	348	282	74	0.338	0.354	0.308	53.070
$DegQ_{Lp}$#+pept1 (50 mM Hepes 7.5. 500 mM NaCl)												
1	0.33	5.63	17.27	573	45980	286	204	90	0.381	0.300	0.320	2.930
2	0.59	5.88	17.70	734	119000	367	290	91	0.108	0.385	0.508	7.710
3	0.85	6.00	19.25	810	194400	405	329	88	0.000	0.417	0.583	16.120

List of Figures

1.1 Phylogenetic tree of the *Chlamydiales* order. 2
1.2 Life cycle of *C. trachomatis* 4
1.3 Allosteric activation cascade of *E.coli*-HtrA proteins. 9
1.4 Three-dimensional crystal structures of prokaryotic HtrA proteins. . . . 11

2.1 Calibration curves of Superdex 200 10/300. 31
2.2 Calibration curve for RFU/AMC correlation coefficient and preliminary detergent test. 37

3.1 Purification of $HtrA_{Sn}$. 42
3.2 Refolded $HtrA_{Sn}{}^{\#}$ essentially shows 6-mer assembly. 43
3.3 Proteolytic activity of $HtrA_{Sn}$. 44
3.4 The influence of unfolded proteins on proteolytic activity of $HtrA_{Sn}$. . . 46
3.5 $HtrA_{Sn}$ and $HtrA_{Sn}{}^{0}$ form higher-order oligomers in the presence of unfolded proteins. 47
3.6 Higher-order oligomer assembly is a substrate-concentration dependent transient process. 48
3.7 Temperature dependency of $HtrA_{Sn}$ 50
3.8 $HtrA_{Sn}$ Crystals 52
3.9 Crystal structure of the $HtrA_{Sn}$ 6-mer. 53
3.10 Biochemical characterization of $HtrA_{Sn}{}^{D222N}$. 54
3.11 Crystal structure of the $HtrA_{Sn}$ 12-mer. 56
3.12 F218 of L3 loop stabilizes 6-mer assembly by interactions with LA loop. 62
3.13 AAC of $HtrA_{Sn}$. 68
3.14 Biochemical analysis of $HtrA_{Sn}{}^{F477A}$ and $HtrA_{Sn}{}^{Q290A}$. 70
3.15 Comparison of the PDZ1 and PDZ2 domain positions in 6- and 12-mer 72
3.16 Unique architecture of the $HtrA_{Sn}$ 6-mer. 75
3.17 PDZ1 and PDZ2 domains of the 6 and 12-mer HtrA crystal structures. 76
3.18 Geometry of the HtrA 12-mer structures. 79
3.19 SAXS curves of $HtrA_{Sn}$ allow to distinguish between different states and oligomeric forms. 81
3.20 Purification of $HtrA_{Ct}$. 84
3.21 Purification of $HtrA_{Ct}{}^{\#}$ and $HtrA_{Ct}{}^{0}$. 86
3.22 Protein activity assay of $HtrA_{Ct}$ and $HtrA_{Ct}{}^{\#}$. 87
3.23 Oligomerization behavior of $HtrA_{Ct}$ protein variants. 89
3.24 $HtrA_{Ct}$ is active at high temperatures. 91
3.25 $HtrA_{Ct}$ crystallizes when the protein is transferred into acidic storage buffer. 92
3.26 $HtrA_{Ct}$ underdoes structural changes in the presence of pept1. 93
3.27 SAXS enables the identification of oligomeric state of HtrA proteins. . . 95

3.28 Purification of $MOMP_{Sn}$-MBP. 97
3.29 The presence of MOMP-MBP promotes oligomerization and proteolytic activation of HtrA proteins. 99
3.30 Purification of $MOMP_{Sn}$ and $MOMP_{Ct}$ with N-terminal His-tag. 100
3.31 MOMPs have an inhibitory effect on the proteolytic activity of HtrA proteins. 101

4.1 Model for $HtrA_{Sn}$ oligomerization. 107
4.2 In the $HtrA_{Sn}$ 6-mer, the linker region between the PDZ1 and PDZ2 domain (orange) is in close contact (Y377) to the R151 of the LC loop (blue). Thus, changes in the linker region directly effect the active site of the protease domain. The L3 loop is shown in pink. 109

4.3 Oligomerization studies of F218A and F218Y show the disposition to form higher-order oligomers at lower substrate levels than wild type and at different pH. 117
4.4 Amino acid sequence alignment of $HtrA_{Sn}$ with DegP and DegQ from *E. coli*, HtrA from *C. trachomatis* and *C. pneumoniae* and DegQ from *L. fallonii* and *L. pneumophila*. 118
4.5 $DegQ_{Lp}$ undergoes conformational changes when pept1 is added. 121

List of Tables

2.1 Primers for cloning and mutagenesis. 26
2.2 Optimized conditions for recombinant protein production. 28
2.3 Standard proteins for calibration of the analytic gel-filtration column. . 30
2.4 Optimized conditions for recombinant protein purification. 31
2.5 MW and theoretical absorption coefficient determined by ExPASy ProtParam. 34
2.6 Buffer composition for SDS-PAGE analysis. 34
2.7 Gel casting instruction for 15% separating polyacrylamide gels with 5% stacking gels. 35
2.8 Instrument settings of Jasco J-715 for CD spectra measurement (wavelength scan). 36
2.9 SAXS settings for diffraction data collection. 38

3.1 B-factors in Å^2 of single domains of $HtrA_{Sn}$ monomer from 6- and 12-mer. (MC: Main chain/ SC: side chain/ Ov: Overall) 57
3.2 Data collection and refinement statistics of $HtrA_{Sn}$ 6- and 12-mer crystal structure. 58
3.3 The RMSD of secondary structure elements in protease domain between 6- and 12-mer $HtrA_{Sn}$. 59
3.4 Residues in interaction distance of $\leq$ 4–5 Å to the LA loop. Behind residues the belonging secondary structure element is named in parenthesis.(D/A: donor/acceptor, MC: main chain, SC: side chain, ASC: aromatic side chain) 60
3.5 Residues in interaction distance of $\leq$ 4 Å to the LB loop. Behind residues the belonging secondary structure element is named in parenthesis. (D/A: donor/acceptor, MC: main chain, SC: side chain) 63
3.6 Residues in interaction distance of $\leq$ 4 Å to the LC loop. Behind residues the belonging secondary structure element is named in parenthesis. (D/A: donor/acceptor, MC: main chain, SC: side chain, ASC: aromatic side chain) 63
3.7 Residues in interaction distance of $\leq$ 4 Å to the LD loop. Behind residues the belonging secondary structure element is named in parenthesis. Residues marked by asterisks are from adjacent protomer.(D/A: donor/acceptor, MC: main chain, SC: side chain, ARS: aromatic side chain) 64

3.8 Residues in interaction distance of $\leq$ 4 Å to the LE loop. Behind residues the belonging secondary structure element is named in parenthesis. Residues marked by asterisks are from adjacent protomer(D/A: donor/acceptor, MC: main chain, SC: side chain, ASC: aromatic side chain) 65
3.9 Residues in interaction distance of $\leq$ 4 Å to the L1 loop. Behind residues the belonging secondary structure element is named in parenthesis. Residues marked by asterisks are from adjacent protomer(D/A: donor/acceptor, MC: main chain, SC: side chain, ASC: aromatic side chain) 65
3.10 Residues in interaction distance of $\leq$ 4 Å to the L2 loop. Behind residues the belonging secondary structure element is named in parenthesis. Residues marked by asterisks are from adjacent protomer(D/A: donor/acceptor, MC: main chain, SC: side chain, ASC: aromatic side chain) 66
3.11 Residues in interaction distance of $\leq$ 4 Å to the L3 loop. Behind residues the belonging secondary structure element is named in parenthesis. Residues marked by asterisks are from adjacent protomer (D/A: donor/acceptor, MC: main chain, SC: side chain, ASC: aromatic side chain) 67
3.12 The RMSD of the C_α-atoms of the separate domains from model structures of $HtrA_{Sn}$ 12-mer in comparison with the $DegP_{Ec}$ and $DegQ_{Lf}$ 12-mer. 77
3.13 Scattering curve analysis of $HtrA_{Sn}$ in different conditions by PRIMUS (Konarev et al., 2003) yields the R_G, D_{max} and Porod volume. DLS measurement enable the determination of hydrodynamic radius (R_h) which is proportional to R_G. 80
3.14 Scattering curve analysis by OLIGOMER (Konarev et al., 2003) shows that the samples are forming a mixture of different oligomeric states. Molecular weight calculation by SAXS is enabled by I(0) or Porod volume. For $HtrA_{Sn}$ 6-mer the MW alternates around 300 kDa, matching the expected mass. The 12-mer shows a big discrepancy between both MWs which is an indicator for low quality data. 82
3.15 Scattering curve analysis of $HtrA_{Ct}$. 94

4.1 $HtrA_{Sn}$ SAXS sample data analysis. 119
4.2 $HtrA_{Ct}$ SAXS sample data analysis. 122
4.3 $DegQ_{Lp}$ SAXS sample data analysis. 123

Abbreviations

AAC	allosteric activation cascade
ADH	alcohol dehydrogenase
AMC	7-amino-4-methylcoumarin
AmyAC	amylose affinity chromatography
APS	ammonium persulfate
ASC	aromatic side chain
ATP	adenosine triphosphate
B. anthracis	*Bacillus anthracis*
BSA	bovine serum albumin
C. jejeuni	*Campylobacter jejeuni*
CatIEx	cation exchange chromatography
CD	circular dichroism
COPD	chronic obstructive pulmonary disease
CPAF	chlamydial protease-like activating factor
C. trachomatis / Ct	*Chlamydia trachomatis*
CV	column volume
D/A	donor/aceptor
DLS	dynamic light scattering
DNA	desoxyribonucleic acid
DTT	dithiothreitol
EB	elementary bodies
E. coli / Ec	*Escherichia coli*
EDTA	Ethylendiamintetraacetat
ER	endoplasmic reticulum
FPR2	formyl peptide receptor 2
GTPase	guanosine triphosphatase
HCl	Salzsäure
HEp-2	human epithelial cells type 2
H. pylori	*Heliobacter pylori*
HSP	heat shock protein
HtrA	High temperature requirement A
IMAC	immobilized metal ion affinity chromatography
IPTG	isopropyl β-D-1-thiogalactopyranoside
LPS	lipopolysaccharide
L. fallonii / Lf	*Legionella fallonii*
L. pneumophila / Lf	*Legionella pneumophila*
LGV	lymphogranuloma venerum
MBP	maltose-binding protein
MC	main chain

MES	2-(*N*-morpholino)ehtanesulfonic acid
MRW	mean residue weight
MOMP	major outer membrane protein
MW	molecular weight
NaAc	sodium acetate
NaCl	sodium chloride
NaOH	sodium hydroxide
OG	Octyl β-D-glucopyranoside
OMP	outer membrane protein
OMPdb	outer membrane β-barrel data base
OMV	outer-membrane vesicle
Ov	overall
PAGE	polyacrylamide gel electrophoresis
PCR	polymerase chain reaction
PDI	protein disulfide isomerase
PDZ	post synaptic density protein (PSD95), Drosophila disc large tumor suppressor (I
pept1	DPMFKLV
PV	Porod volume
RB	reticulate bodies
RFU	relative fluorescence units
rmsd	root-mean-square deviation
SAXS	small angle X-ray scattering
SC	side chain
SDS-PAGE	sodium dodecyl sulfate-polyacrylamide gel electrophoresis
SEC	size-exclusion chromatography
S. flexneri	*Shigella flexneri*
S. negevensis /Sn	*Simkania negevensis*
Std	standard
TCEP	Tris(2-carboxyethyl)phosphine hydrochloride
T_m	melting temperature
TRIS	Tris (hydroxymethyl)aminomethane
TSA	thermal shift assay
YT	Yeast extract tryptone
TEMED	tetramethylethylenediamine
UV	ultraviolet
VD	variable domains

Bibliography

C. M. Abfalter, M. Schubert, C. Götz, T. P. Schmidt, G. Posselt & S. Wessler: HtrA-mediated E-cadherin cleavage is limited to DegP and DegQ homologs expressed by gram-negative pathogens. *Cell Commun. Signal.* **14**, 1–12. 2016.

S. Abromaitis & R. S. Stephens: Attachment and entry of *chlamydia* have distinct requirements for host protein disulfide isomerase. *PLoS Pathog.* **5**, 1–12. 2009.

P. V. Afonine, R. W. Grosse-Kunstleve, N. Echols, J. J. Headd, N. W. Moriarty, M. Mustyakimov, T. C. Terwilliger, A. Urzhumtsev, P. H. Zwart & P. D. Adams: Towards automated crystallographic structure refinement with phenix.refine. *Acta Crystallogr. Sect. D Biol. Crystallogr.* **68**, 352–367. 2012.

Y. Akiyama, K. Kanehara & K. Ito: RseP (YaeL), an *Escherichia coli* RIP protease, cleaves transmembrane sequences. *EMBO J.* **23**, 4434–4442. 2004.

B. M. Alba, J. A. Leeds, C. Onufryk, C. Z. Lu & C. A. Gross: DegS and YaeL participate sequentially in the cleavage of RseA to activate the ζ^{E}-dependent extracytoplasmic stress response. *Genes Dev.* **16**, 2156–2168. 2002.

D. J. Augustine: Modelling *Chlamydia*-koala interactions: Coexistence, population dynamics and conservation implications. *J. Appl. Ecol.* **35**, 261–272. 1998.

S. Backert, S. Bernegger, J. Skórko-Glonek & S. Wessler: Extracellular HtrA serine proteases: An emerging new strategy in bacterial pathogenesis. *Cell. Microbiol.* **20**, 1–9. 2018.

X. C. Bai, X. J. Pan, X. J. Wang, Y. Y. Ye, L. F. Chang, D. Leng, J. Lei & S. F. Sui: Characterization of the structure and function of *Escherichia coli* DegQ as a representative of the DegQ-like proteases of bacterial HtrA family proteins. *Structure* **19**, 1328–1337. 2011.

E. Bartolini, E. Ianni, E. Frigimelica, R. Petracca, G. Galli, F. B. Scorza, N. Norais, D. Laera, F. Giusti, A. Pierleoni, M. Donati, R. Cevenini, O. Finco, G. Grandi & R. Grifantini: Recombinant outer membrane vesicles carrying *Chlamydia muridarum* HtrA induce antibodies that neutralize chlamydial infection in vitro. *J. Extracell. Vesicles* **2**, 1–14. 2013.

R. J. Bastidas, C. A. Elwell, J. N. Engel & R. H. Valdivia: Chlamydial intracellular survival strategies. *Cold Spring Harb. Perspect. Med.* **3**, 1–20. 2013.

D. Baud & G. Greub: Intracellular bacteria and adverse pregnancy outcomes. *Clin. Microbiol. Infect.* **17**, 1312–1322. 2011.

W. L. Beatty: Trafficking from CD63-positive late endocytic multivesicular bodies is essential for intracellular development of *Chlamydia trachomatis*. *J. Cell Sci.* **119**, 350–359. 2006.

S. Bedson & J. Bland: A morphological study of psittacosis virus, with the description of a developmental cycle. *Br. J. Exp. Pathol.* 461. 1932.

R. J. Belland, S. P. Ouellette, J. Gieffers & G. I. Byrne: *Chlamydia pneumoniae* and atherosclerosis. *Cell. Microbiol.* **6**, 117–127. 2004.

L. Berger, K. Volp, S. Mathews, R. Speare & P. Timms: *Chlamydia pneumoniae* in a free-ranging giant barred frog (*Mixophyes iteratus*) from Australia. *J. Clin. Microbiol.* **37**, 2378–2380. 1999.

H. M. Berman, J. Westbrook, Z. Feng, G. Gilliland, T. N. Bhat, H. Weissig, I. N. Shindyalov & P. E. Bourne: The Protein Data Bank **28**, 235–242. 2000.

J. Blobel, P. Bernado, D. I. Svergun, R. Tauler & M. Pons: Low-Resolution Structures of Transient Protein - Protein Complexes Using Small-Angle X-ray Scattering. *J. Am. Chem. Soc.* 4378–4386. 2009.

M. Boehm, B. Hoy, M. Rohde, N. Tegtmeyer, K. T. Bæk, O. A. Oyarzabal, L. Brøndsted, S. Wessler & S. Backert: Rapid paracellular transmigration of *Campylobacter jejuni* across polarized epithelial cells without affecting TER: Role of proteolytic-active HtrA cleaving E-cadherin but not fibronectin. *Gut Pathog.* **4**, 1–12. 2012.

S. Bøje, A. W. Olsen, K. Erneholm, J. S. Agerholm, G. Jungersen, P. Andersen & F. Follmann: A multi-subunit *Chlamydia* vaccine inducing neutralizing antibodies and strong IFN-γ + CMI responses protects against a genital infection in minipigs. *Immunol. Cell Biol.* **94**, 185–195. 2016.

N. Borel, R. Thoma, P. Spaeni, R. Weilenmann, K. Teankum, E. Brugnera, D. R. Zimmermann, L. Vaughan & A. Pospischil: *Chlamydia*-related abortions in Cattle from Graubunden, Switzerland. *Vet. Pathol.* **43**, 702–708. 2006.

R. A. Carabeo, C. A. Dooley, S. S. Grieshaber & T. Hackstadt: Rac interacts with Abi-1 and WAVE2 to promote an Arp2/3-dependent actin recruitment during chlamydial invasion. *Cell. Microbiol.* **9**, 2278–2288. 2007.

R. A. Carabeo, S. S. Grieshaber, A. Hasenkrug, C. A. Dooley & T. Hackstadt: Requirement for the Rac GTPase in *Chlamydia trachomatis* invasion of non-phagoycytic cells. *Traffic* **5**, 418–425. 2004.

R. A. Carabeo, D. J. Mead & T. Hackstadt: Golgi-dependent transport of cholesterol to the *Chlamydia trachomatis* inclusion. *Proc. Natl. Acad. Sci. U. S. A.* **100**, 6771–6. 2003.

R. Chaba, B. Alba, M. Guo, J. Sohn, N. Ahuja, R. Sauer & C. Gross: Signal integration by DegS and RseB governs the σ^{E}-mediated envelope stress response in *Escherichia coli*. *Proc. Natl. Acad. Sci. U. S. A.* **108**, 2106–2111. 2011.

D. W. Chang, D. Ditsworth, H. Liu, S. M. Srinivasula, E. S. Alnemri & X. Yang: Oligomerization is a general mechanism for the activation of apoptosis initiator and inflammatory procaspases. *J. Biol. Chem.* **278**, 16466–16469. 2003.

Z. Chang: The function of the DegP (HtrA) protein: Protease versus chaperone. *IUBMB Life* **68**, 904–907. 2016.

T. Chitlaru, G. Zaide, S. Ehrlich, I. Inbar, O. Cohen & A. Shafferman: HtrA is a major virulence determinant of *Bacillus anthracis*. *Mol. Microbiol.* **81**, 1542–1559. 2011.

I. Choroszy-Król, M. Frej-Mądrzak, M. Hober, J. Sarowska & A. Jama-Kmiecik: Infections Caused by *Chlamydophila pneumoniae*. *Adv. Clin. Exp. Med.* **23**, 123–126. 2014.

L. Cislakova, M. Stanko, J. Fricova, L. Mosansky, M. Travnicek, M. Halanova, S. Mardzinova & A. Stefancikova: Small mammals (*Insectivora, Rodentia*) as a potential source of Chlamydial infection in East Slovakia. *Ann. Agric. Environ. Med.* **11**, 139–143. 2004.

T. Clausen, M. Kaiser, R. Huber & M. Ehrmann: HTRA proteases: Regulated proteolysis in protein quality control. *Nat. Rev. Mol. Cell Biol.* **12**, 152–162. 2011.

T. Clausen, C. Southan & M. Ehrmann: The HtrA family of proteases: Implications for protein composition and cell fate. *Mol. Cell* **10**, 443–455. 2002.

J. L. Cocchiaro & R. H. Valdivia: New insights into *Chlamydia* intracellular survival mechanisms. *Cell. Microbiol.* **11**, 1571–1578. 2009.

D. Corsaro & G. Greub: Pathogenic Potential of Novel *Chlamydiae* and Diagnostic Approaches to Infections Due to These Obligate Intracellular Bacteria. *Society* **19**, 283–297. 2006.

R. Cosentini, P. Tarsia, C. Canetta, G. Graziadei, A. M. Brambilla, S. Aliberti, M. Pappalettera, F. Tantardini & F. Blasi: Severe asthma exacerbation: Role of acute *Chlamydophila pneumoniae* and *Mycoplasma pneumoniae* infection. *Respir. Res.* **9**, 1–6. 2008.

P. N. Danese, W. B. Snyder, C. L. Cosma, L. J. Davis & T. J. Silhavy: The Cpx two-component signal transduction pathway of *Escherichia coli* regulates transcription of the gene specifying the stress-inducible periplasmic protease, DegP. *Genes Dev.* **9**, 387–398. 1995.

C. Dartigalongue, D. Missiakas & S. Raina: Characterization of the *Escherichia coli* σE Regulon. *J. Biol. Chem.* **276**, 20866–20875. 2001.

A. Dautry-Varsat, A. Subtil & T. Hackstadt: Recent insights into the mechanisms of *Chlamydia* entry. *Cell. Microbiol.* **7**, 1714–1722. 2005.

S. De Carlo, B. Chen, T. R. Hoover, E. Kondrashkina, E. Nogales & B. T. Nixon: The structural basis for regulated assembly and function of the transcriptional activator NtrC. *Genes Dev.* **20**, 1485–1495. 2006.

A. De Las Peñas, L. Connolly & C. A. Gross: The σ^{E}-mediated response to extracytoplasmic stress in *Escherichia coli* is transduced by RseA and RseB, two negative regulators of σ^{E}. *Mol. Microbiol.* **24**, 373–385. 1997.

D. Dean, R. J. Suchland & W. E. Stamm: Evidence for long-term cervical persistence of *Chlamydia trachomatis* by omp1 genotyping. *J. Infect. Dis.* **182**, 909–916. 2000.

I. Derré, R. Swiss & H. Agaisse: The lipid transfer protein CERT interacts with the *Chlamydia* inclusion protein IncD and participates to ER-*Chlamydia* inclusion membrane contact sites. *PLoS Pathog.* **7**. 2011.

D. A. Doyle, A. Lee, J. Lewis, E. Kim, M. Sheng & R. MacKinnon: Crystal structures of a complexed and peptide-free membrane protein- binding domain: Molecular basis of peptide recognition by PDZ. *Cell* **85**, 1067–1076. 1996.

A. Elmi, F. Nasher, H. Jagatia, O. Gundogdu, M. Bajaj-Elliott, B. Wren & N. Dorrell: *Campylobacter jejuni* outer membrane vesicle-associated proteolytic activity promotes bacterial invasion by mediating cleavage of intestinal epithelial cell E-cadherin and occludin. *Cell. Microbiol.* **18**, 561–572. 2016.

C. A. Elwell, S. Jiang, J. H. Kim, A. Lee, T. Wittmann, K. Hanada, P. Melancon & J. N. Engel: *Chlamydia trachomatis* co-opts GBF1 and CERT to acquire host sphingomyelin for distinct roles during intracellular development. *PLoS Pathog.* **7**. 2011.

P. Emsley, B. Lohkamp, W. G. Scott & K. Cowtan: Features and development of Coot. *Acta Crystallogr. Sect. D Biol. Crystallogr.* **66**, 486–501. 2010.

P. R. Evans: An introduction to data reduction: Space-group determination, scaling and intensity statistics. *Acta Crystallogr. Sect. D Biol. Crystallogr.* **67**, 282–292. 2011.

S. Fadel & A. Eley: *Chlamydia trachomatis* OmcB protein is a surface-exposed glycosaminoglycan-dependent adhesin. *J. Med. Microbiol.* **56**, 15–22. 2007.

A. J. Ferreri, M. Guidoboni, M. Ponzoni, C. De Conciliis, S. Dell'Oro, K. Fleischhauer, L. Caggiari, A. A. Lettini, E. Dal Cin, R. Ieri, M. Freschi, E. Villa, M. Boiocchi & R. Dolcetti: Evidence for an association between *Chlamydia psittaci* and ocular adnexal lymphomas. *J. Natl. Cancer Inst.* **96**, 586–594. 2004.

B. S. Fields, R. F. Benson & R. E. Besser: *Legionella* and Legionnaires' Disease: 25 Years of Investigation. *J. Clin. Microbiol.* **15**, 506–526. 2002.

D. Figaj, A. Gieldon, M. Bartczak, T. Koper, U. Zarzecka, A. Lesner, B. Lipinska & J. Skórko-Glonek: The LD loop as an important structural element required for transmission of the allosteric signal in the HtrA (DegP) protease from *Escherichia coli*. *FEBS J.* **283**, 3471–3487. 2016.

D. Figaj, A. Gieldon, A. Polit, A. Sobiecka-Szkatula, T. Koper, M. Denkiewicz, B. Banecki, A. Lesner, J. Ciarkowski, B. Lipinska & J. Skórko-Glonek: The LA loop as an important regulatory element of the HtrA (DegP) protease from *Escherichia coli* structural and functional studies. *J. Biol. Chem.* **289**, 15880–15893. 2014.

J. M. Flynn, I. Levchenko, R. T. Sauer & T. A. Baker: Modulating substrate choice: The SspB adaptor delivers a regulator of the extracytoplasmic-stress response to the AAA+ protease ClpXP for degradation. *Genes Dev.* **18**, 2292–2301. 2004.

E. Gasteiger, C. Hoogland, A. Gattiker, S. Duvaud, M. R. Wilkins, R. D. Appel & A. Bairoch: Protein Identification and Analysis Tools on the ExPASy Server. *Proteomics Protocols Handbook* 571–608. 2005.

X. Ge, R. Wang, J. Ma, Y. Liu, A. N. Ezemaduka, P. R. Chen, X. Fu & Z. Chang: DegP primarily functions as a protease for the biogenesis of β-barrel outer membrane proteins in the Gram-negative bacterium *Escherichia coli*. *FEBS J.* **281**, 1226–1240. 2014.

H. C. Gérard, U. Dreses-Werringloer, K. S. Wildt, S. Deka, C. Oszust, B. J. Balin, W. H. Frey, E. Z. Bordayo, J. A. Whittum-Hudson & A. P. Hudson: *Chlamydophila (Chlamydia) pneumoniae* in the Alzheimer's brain. *FEMS Immunol. Med. Microbiol.* **48**, 355–366. 2006.

S. Gloeckl, V. A. Ong, P. Patel, J. D. A. Tyndall, P. Timms, K. W. Beagley, J. A. Allan, C. W. Armitage, L. Turnbull, C. B. Whitchurch, M. Merdanovic, M. Ehrmann, J. C. Powers, J. Oleksyszyn, M. Verdoes, M. Bogyo & W. M. Huston: Identification of a serine protease inhibitor which causes inclusion vacuole reduction and is lethal to *Chlamydia trachomatis*. *Mol. Microbiol.* **89**, 676–689. 2013.

S. S. Grieshaber, N. A. Grieshaber & T. Hackstadt: *Chlamydia trachomatis* uses host cell dynein to traffic to the microtubule-organizing center in a p50 dynamitin-independent process. *J. Cell Sci.* **116**, 3793–3802. 2003.

L. Halberstadter & S. Prowazek: Über zelleinschlüsse parasitärer natur beim trachom. *Arbeiten aus dem kaiserlichen Gesundheitsamte* **26**. 1907.

T. Harkinezhad, T. Geens & D. Vanrompay: *Chlamydophila psittaci* infections in birds: A review with emphasis on zoonotic consequences. *Vet. Microbiol.* **135**, 68–77. 2009.

M. Harnasch, S. Grau, C. Behrends, S. L. Dove, A. Hochschild, M. K. Iskandar, W. Xia & M. Ehrmann: Characterization of presenilin-amyloid precursor interaction using bacterial expression and two-hybrid systems for human membrane proteins. *Mol. Membr. Biol.* **21**, 373–383. 2004.

P. Hauske, N. Mamant, S. Hasenbein, S. Nickel, C. Ottmann, T. Clausen, M. Ehrmann & M. Kaiser: Peptidic small molecule activators of the stress sensor DegS. *Mol. Biosyst.* **5**, 980–985. 2009.

R. W. Hepler, D. D. Nahas, B. Lucas, R. Kaufhold, J. A. Flynn, J. D. Galli, R. Swoyer, J. M. Wagner, A. Espeseth, J. G. Joyce, J. C. Cook & E. Durr: Spectroscopic Analysis of Chlamydial Major Outer Membrane Protein in Support of Structure Elucidation. *Protein Sci.* 2018.

J. A. Herweg, V. Pons, D. Becher, M. Hecker, G. Krohne, J. Barbier, H. Berger, T. Rudel & A. Mehlitz: Proteomic analysis of the *Simkania*-containing vacuole: The central role of retrograde transport. *Mol. Microbiol.* **99**, 151–171. 2016.

D. Heuer, A. R. Lipinski, N. Machuy, A. Karlas, A. Wehrens, F. Siedler, V. Brinkmann & T. F. Meyer: *Chlamydia* causes fragmentation of the Golgi compartment to ensure reproduction. *Nature* **457**, 731–735. 2009.

R. J. Hogan, S. A. Mathews, S. Mukhopadhyay, J. T. Summersgill & P. Timms: Chlamydial Persistence: Beyond the Biphasic Paradigm. *Infect. Immun.* **72**, 1843–1855. 2004.

B. Hoy, T. Geppert, M. Boehm, F. Reisen, P. Plattner, G. Gadermaier, N. Sewald, F. Ferreira, P. Briza, G. Schneider, S. Backert & S. Wessler: Distinct roles of secreted HtrA proteases from gram-negative pathogens in cleaving the junctional protein and tumor suppressor E-cadherin. *J. Biol. Chem.* **287**, 10115–10120. 2012.

B. Hoy, M. Löwer, C. Weydig, G. Carra, N. Tegtmeyer, T. Geppert, P. Schröder, N. Sewald, S. Backert, G. Schneider & S. Wessler: *Helicobacter pylori* HtrA is a new secreted virulence factor that cleaves E-cadherin to disrupt intercellular adhesion. *EMBO Rep.* **11**, 798–804. 2010.

Z. Huang, M. Chen, K. Li, X. Dong, J. Han & Q. Zhang: Cryo-electron tomography of *Chlamydia trachomatis* gives a clue to the mechanism of outer membrane changes. *J. Electron Microsc. (Tokyo).* **59**, 237–241. 2010.

E. S. Hughes, K. M. Shaw & R. H. Ashley: Mutagenesis and Functional Reconstitution of Chlamydial Major Outer Membrane Proteins: VS4 Domains Are Not Required for Pore Formation but Modify Channel Function. *Infect. Immun.* **69**, 1671–1678. 2001.

W. M. Huston, J. E. Swedberg, J. M. Harris, T. P. Walsh, S. A. Mathews & P. Timms: The temperature activated HtrA protease from pathogen *Chlamydia trachomatis* acts as both a chaperone and protease at 37 °C. *FEBS Lett.* **581**, 3382–3386. 2007.

W. M. Huston, C. Theodoropoulos, S. A. Mathews & P. Timms: *Chlamydia trachomatis* responds to heat shock, penicillin induced persistence, and IFN-gamma persistence by altering levels of the extracytoplasmic stress response protease HtrA. *BMC Microbiol.* **8**, 1–16. 2008.

W. M. Huston, J. D. Tyndall, W. B. Lott, S. H. Stansfield & P. Timms: Unique residues involved in activation of the multitasking protease/chaperone HtrA from *Chlamydia trachomatis*. *PLoS One* **6**, 1–10. 2011.

K. Hybiske & R. S. Stephens: Exit strategies of intracellular pathogens. *Nat. Rev. Microbiol.* **6**, 99–110. 2008.

H. Ingmer & L. Brøndsted: Proteases in bacterial pathogenesis. *Res. Microbiol.* **160**, 704–710. 2009.

J. Iwanczyk, D. Damjanovic, J. Kooistra, V. Leong, A. Jomaa, R. Ghirlando & J. Ortega: Role of the PDZ domains in *Escherichia coli* DegP protein. *J. Bacteriol.* **189**, 3176–3186. 2007.

J. Iwanczyk, V. Leong & J. Ortega: Factors defining the functional oligomeric state of *Escherichia coli* DegP protease. *PLoS One* **6**. 2011.

C. J. Jeffery: Molecular mechanisms for multitasking: Recent crystal structures of moonlighting proteins. *Curr. Opin. Struct. Biol.* **14**, 663–668. 2004.

F. Jeleń, A. Oleksy, K. Śmietana & J. Otlewski: PDZ domains - Common players in the cell signaling. *Acta Biochim. Pol.* **50**, 985–1017. 2003.

J. Jiang, X. Zhang, Y. Chen, Y. Wu, Z. H. Zhou, Z. Chang & S.-F. Sui: Activation of DegP chaperone-protease via formation of large cage-like oligomers upon binding to substrate proteins. *Proc. Natl. Acad. Sci.* **105**, 11939–11944. 2008.

A. Jomaa, D. Damjanovic, V. Leong, R. Ghirlando, J. Iwanczyk & J. Ortega: The inner cavity of *Escherichia coli* DegP protein is not essential for molecular chaperone and proteolytic activity. *J. Bacteriol.* **189**, 706–716. 2007.

A. Jomaa, J. Iwanczyk, J. Tran & J. Ortega: Characterization of the autocleavage process of the *Escherichia coli* HtrA Protein: Implications for its physiological role. *J. Bacteriol.* **191**, 1924–1932. 2009.

W. Kabsch: XDS. *Acta Crystallogr. Sect. D Biol. Crystallogr.* **66**, 125–132. 2010.

W. Kabsch & C. Sander: Dictionary of Protein Secondary Structure: Pattern Recognition of Hydrogen-Bonded and Geometrical Features. *Biopolymers* **22**, 2577–2637. 1983.

S. Kahane, N. Kimmel & M. G. Friedman: The growth cycle of *Simkania negevensis*. *Microbiology* **148**, 735–742. 2002.

L. Kari, W. M. Whitmire, D. D. Crane, N. Reveneau, H. John & H. D. Caldwell: *Chlamydia trachomatis* Native Major Outer Membrane Protein Induces Partial Protection in Non-Human Primates: Implication for a Trachoma Transmission Blocking Vaccine. *J. Immunol.* **182**, 8063–8070. 2009.

P. A. Karplus & K. Diederichs: Linking crystallographic model and data quality. *Science* **336**, 1030–1033. 2012.

K. Karunakaran, A. Mehlitz & T. Rudel: Evolutionary Conservation of Infection-Induced Cell Death Inhibition among *Chlamydiales* **6**. 2011.

D. Y. Kim: Two stress sensor proteins for the expression of σ^{E} regulon: DegS and RseB. *J. Microbiol.* **53**, 306–310. 2015.

D. Y. Kim & K. K. Kim: Structure and function of HtrA family proteins, the key players in protein quality control. *J. Biochem. Mol. Biol.* **38**, 266–274. 2005.

S. Kim, R. A. Grant & R. T. Sauer: Covalent linkage of distinct substrate degrons controls assembly and disassembly of DegP proteolytic cages. *Cell* **145**, 67–78. 2011.

S. Kim & R. T. Sauer: Cage assembly of DegP protease is not required for substrate-dependent regulation of proteolytic activity or high-temperature cell survival. *Proc. Natl. Acad. Sci.* **109**, 7263–7268. 2012.

S. Kim & R. T. Sauer: Distinct regulatory mechanisms balance DegP proteolysis to maintain cellular fitness during heat stress. *Genes Dev.* **28**, 902–911. 2014.

R. Koebnik, K. P. Locher & P. Van Gelder: Structure and function of bacterial outer membrane proteins: barrels in a nutshell. *Mol. Microbiol.* **37**, 239–253. 2000.

H. Kolmar, P. R. Waller & R. T. Sauer: The DegP and DegQ periplasmic endoproteases of *Escherichia coli*: Specificity for cleavage sites and substrate conformation. *J. Bacteriol.* **178**, 5925–5929. 1996.

P. V. Konarev, V. V. Volkov, A. V. Sokolova, M. H. Koch & D. I. Svergun: PRIMUS: A Windows PC-based system for small-angle scattering data analysis. *J. Appl. Crystallogr.* **36**, 1277–1282. 2003.

V. Kozjak-Pavlovic, J. A. Herweg & T. Rudel: The role of host cell organelles in the development of *Simkania negevensis*. *Int. J. Med. Microbiol.* 0–1. 2017.

T. Krojer, M. Garrido-Franco, R. Huber, M. Ehrmann & T. Clausen: Crystal structure of DegP (HtrA) reveals a new protease-chaperone machine. *Nature* **416**, 455–459. 2002.

T. Krojer, K. Pangerl, J. Kurt, J. Sawa, C. Stingl, K. Mechtler, R. Huber, M. Ehrmann & T. Clausen: Interplay of PDZ and protease domain of DegP ensures efficient elimination of misfolded proteins. *Proc. Natl. Acad. Sci.* **105**, 7702–7707. 2008a.

T. Krojer, J. Sawa, R. Huber & T. Clausen: HtrA proteases have a conserved activation mechanism that can be triggered by distinct molecular cues. *Nat. Struct. Mol. Biol.* **17**, 844–852. 2010.

T. Krojer, J. Sawa, E. Schäfer, H. R. Saibil, M. Ehrmann & T. Clausen: Structural basis for the regulated protease and chaperone function of DegP. *Nature* **453**, 885–890. 2008b.

Y. Kumar, J. Cocchiaro & R. H. Valdivia: The Obligate Intracellular Pathogen *Chlamydia trachomatis* Targets Host Lipid Droplets. *Curr. Biol.* **16**, 1646–1651. 2006.

A. Lawrence, T. Fraser, A. Gillett, J. D. Tyndall, P. Timms, A. Polkinghorne & W. M. Huston: Chlamydia Serine Protease Inhibitor, targeting HtrA, as a New Treatment for Koala *Chlamydia infection*. *Sci. Rep.* **6**, 1–12. 2016.

S. Lima, M. S. Guo, R. Chaba, C. A. Gross & R. T. Sauer: Dual molecular signals mediate the bacterial response to outer-membrane stress. *Science* **340**, 837–841. 2013.

B. Lipinska, S. Sharma & C. Georgopoulos: Sequence analysis and regulation of the *htrA* gene of *Escherichia coli*: a σ32-independent mechanism of heat-inducible transcription. *Nucleic Acids Res.* **16**, 10053–10067. 1988.

D. Longbottom, M. Russell & G. E. Jones: Molecular Cloning and Characterization of the Genes Coding for the Highly Immunogenic Cluster of 90-Kilodalton Envelope Proteins from the *Chlamydia psittaci* subtype that causes abortion in sheep. *Microbiology* **66**, 1317–1324. 1998.

C. Louis-Jeune, M. A. Andrade-Navarro & C. Perez-Iratxeta: Prediction of protein secondary structure from circular dichroism using theoretically derived spectra. *Proteins* 374–381. 2011.

D. C. W. Mabey, A. W. Solomon & A. Foster: Trachoma. *Lancet* **362**, 223–9. 2003.

T. Madden: Chapter 16 : The BLAST Sequence Analysis Tool. In NCBI Handbook, 1–15. 2003.

H. Malet, F. Canellas, J. Sawa, J. Yan, K. Thalassinos, M. Ehrmann, T. Clausen & H. R. Saibil: Newly folded substrates inside the molecular cage of the HtrA chaperone DegQ. *Nat. Struct. Mol. Biol.* **19**, 152–157. 2012.

J. W. Marsh, W. B. Lott, J. D. A. Tyndall & W. W. M. Huston: Proteolytic activation of *Chlamydia trachomatis* HTRA is mediated by PDZ1 domain interactions with protease domain loops L3 and LC and beta strand β5. *Cell. Mol. Biol. Lett.* **18**, 522–537. 2013.

J. W. Marsh, V. A. Ong, W. B. Lott, P. Timms, J. D. A. Tyndall & W. M. Huston: CtHtrA : the lynchpin of the chlamydial surface and a promising therapeutic target. *Future Microbiol.* **12**. 2017.

B. Matthews: Solvent content of protein crystals. *J Mol Biol.* **2**. 1986.

A. J. McBroom & M. J. Kuehn: Release of outer membrane vesicles by Gram-negative bacteria is a novel envelope stress response. *Mol. Microbiol.* **63**, 545–558. 2007.

A. J. McCoy, R. W. Grosse-Kunstleve, P. D. Adams, M. D. Winn, L. C. Storoni & R. J. Read: Phaser crystallographic software. *J. Appl. Crystallogr.* **40**, 658–674. 2007.

M. McKuen, K. E. Mueller, Y. Bae & K. Fields: FRAEM reveals a role for *C. trachomatis* TmeA in invasion that is independent of host AHNAK. *Infect. Immun.* **85**, 1–18. 2017.

F. D. Menozzi, K. Pethe, P. Bifani, F. Soncin, M. J. Brennan & C. Locht: Enhanced bacterial virulence through exploitation of host glycosaminoglycans. *Mol. Microbiol.* **43**, 1379–1386. 2002.

M. Merdanovic, N. Mamant, M. Meltzer, S. Poepsel, A. Auckenthaler, R. Melgaard, P. Hauske, L. Nagel-Steger, A. R. Clarke, M. Kaiser, R. Huber & M. Ehrmann: Determinants of structural and functional plasticity of a widely conserved protease chaperone complex. *Nat. Struct. Mol. Biol.* **17**, 837–843. 2010.

J. E. Messinger, E. Nelton, C. Feeney & D. C. Gondek: *Chlamydia* Infection Across Host Species Boundaries Promotes Distinct Sets of Transcribed Anti-Apoptotic Factors. *Front. Cell. Infect. Microbiol.* **5**, 1–9. 2015.

T. Mestrovic & S. Ljubin-sternak: Molecular mechanisms of *Chlamydia trachomatis* resistance to antimicrobial drugs . *Frontiers In Bioscience* 656–670. 2018.

R. Michel, K. D. Müller, L. Zöller, J. Walochnik, M. Hartmann & E. N. Schmid: Free-living amoebae serve as a host for the *Chlamydia*-like bacterium *Simkania negevensis*. *Acta Protozool.* **44**, 113–121. 2005.

S. Montigiani, F. Falugi, M. Scarselli, O. Finco, R. Petracca, G. Galli, M. Mariani, R. Manetti, M. Agnusdei, R. Cevenini, M. Donati, R. Nogarotto, N. Norais, I. Garaguso, S. Nuti, G. Saletti, D. Rosa, G. Ratti & G. Grandi: Genomic approach for analysis of surface proteins in *Chlamydia pneumoniae*. *Infect. Immun.* **70**, 368–79. 2002.

J. H. Morais Cabral, C. Petosa, M. J. Sutcliffe, S. Raza, O. Byron, F. Poy, S. M. Marfatia, A. H. Chishti & R. C. Liddington: Crystal structure of a PDZ domain. 1996.

R. J. Morris, A. Perrakis & V. S. Lamzin: ARP/wARP's model-building algorithms. I. The main chain. *Acta Crystallogr. Sect. D Biol. Crystallogr.* **58**, 968–975. 2002.

S. Nyari, S. A. Khan, G. Rawlinson, C. A. Waugh, A. Potter, V. Gerdts & P. Timms: Vaccination of koalas (*Phascolarctos cinereus*) against *Chlamydia pecorum* using synthetic peptides derived from the major outer membrane protein. *PLoS One* **13**, 1–15. 2018.

P. O'Byrne, P. MacPherson, S. DeLaplante, G. Metz & A. Bourgault: Approach to lymphogranuloma venereum. *Can. Fam. Physician* **62**, 554–558. 2016.

A. W. Olsen, F. Follmann, K. Erneholm, I. Rosenkrands & P. Andersen: Protection Against *Chlamydia trachomatis* Infection and Upper Genital Tract Pathological Changes by Vaccine-Promoted Neutralizing Antibodies Directed to the VD4 of the Major Outer Membrane Protein. *J. Infect. Dis.* **212**, 978–989. 2015.

S. P. Ouellette & R. A. Carabeo: A functional slow recycling pathway of transferrin is required for growth of *Chlamydia*. *Front. Microbiol.* **1**, 1–12. 2010.

S. P. Ouellette, F. C. Dorsey, S. Moshiach, J. L. Cleveland & R. A. Carabeo: *Chlamydia* species-dependent differences in the growth requirement for lysosomes. *PLoS One* **6**, 1–16. 2011.

S. Pal, E. M. Peterson & L. M. De La Maza: Vaccination with the *Chlamydia trachomatis* major outer membrane protein can elicit an immune response as protective as that resulting from inoculation with live bacteria. *Infect. Immun.* **73**, 8153–8160. 2005.

S. Pal, I. Theodor, E. M. Peterson & L. M. De la Maza: Immunization with the *Chlamydia trachomatis* mouse pneumonitis major outer membrane protein can elicit a protective immune response against a genital challenge. *Infect. Immun.* **69**, 6240–6247. 2001.

M. J. Pallen & C. P. Ponting: PDZ domains in bacterial proteins. *Mol. Microbiol.* **26**, 411–413. 1997.

A. M. Perna, F. Reisen, T. P. Schmidt, T. Geppert, M. Pillong, M. Weisel, B. Hoy, P. C. Simister, S. M. Feller, S. Wessler & G. Schneider: Inhibiting *Helicobacter pylori* HtrA protease by addressing a computationally predicted allosteric ligand binding site. *Chem. Sci.* **5**, 3583–3590. 2014.

J. J. Perona & C. S. Craik: Structural basis of substrate specificity in the serine proteases. *Protein Sci.* **4**, 337–360. 1995.

F. Petrovay & E. Balla: Two fatal cases of psittacosis caused by *Chlamydophila psittaci*. *J. Med. Microbiol.* **57**, 1296–1298. 2008.

T. Pillonel, C. Bertelli, N. Salamin & G. Greub: Taxogenomics of the order *Chlamydiales*. *Int. J. Syst. Evol. Microbiol.* **65**, 1381–1393. 2015.

A. Pospischil: From disease to etiology: historical aspects of Chlamydia-related diseases in animals and humans. *Drugs of Today* **45**, 141–146. 2009.

T. B. Poston, S. L. Gottlieb & T. Darville: Status of vaccine research and development of vaccines for *Chlamydia trachomatis* infection. *Vaccine* 2017.

G. E. Purdy, C. R. Fisher & S. M. Payne: IcsA surface presentation in *Shigella flexneri* requires the periplasmic chaperones DegP, Skp, and SurA. *J. Bacteriol.* **189**, 5566–5573. 2007.

C. D. Putnam, M. Hammel, G. L. Hura & J. A. Tainer: X-ray solution scattering (SAXS) combined with crystallography and computation: Defining accurate macromolecular structures, conformations and assemblies in solution, volume 40. 2007.

K. Rajeeve, S. Das, B. K. Prusty & T. Rudel: *Chlamydia trachomatis* paralyses neutrophils to evade the host innate immune response. *Nat. Microbiol.* **3**, 824–835. 2018.

R. Regan, J. Dathan & J. Treharne: Infective endocarditis with glomerulonephritis associated with cat chlamydia (*C. psittaci*) infection. *Br. Heart J.* **42**, 349–352. 1979.

A. Rejman Lipinski, J. Heymann, C. Meissner, A. Karlas, V. Brinkmann, T. F. Meyer & D. Heuer: Rab6 and Rab11 regulate *Chlamydia trachomatis* development and golgin-84-dependent Golgi fragmentation. *PLoS Pathog.* **5**. 2009.

V. A. Rhodius, W. C. Suh, G. Nonaka, J. West & C. A. Gross: Conserved and variable functions of the σ^{E}-stress response in related genomes. *PLoS Biol.* **4**, 0043–0059. 2006.

T. M. Russell, M. J. Delorey & B. J. Johnson: *Borrelia burgdorferi* BbHtrA degrades host ECM proteins and stimulates release of inflammatory cytokines in vitro. *Mol. Microbiol.* **90**, 241–251. 2013.

T. M. Russell & B. J. B. Johnson: Lyme disease spirochaetes possess an aggrecan-binding protease with aggrecanase activity. *Mol. Microbiol.* **90**, 228–240. 2013.

K. A. Rzomp, A. R. Moorhead & M. A. Scidmore: The GTPase Rab4 interacts with *Chlamydia trachomatis* inclusion membrane protein CT229. *Infect. Immun.* **74**, 5362–5373. 2006.

K. A. Rzomp, L. D. Scholtes, B. J. Briggs, G. R. Whittaker & M. A. Scidmore: Rab GTPases are recruited to chlamydial inclusions in both a species-dependent and species-independent manner. *Infect. Immun.* **71**, 5855–5870. 2003.

J. Sawa, H. Malet, T. Krojer, F. Canellas, M. Ehrmann & T. Clausen: Molecular adaptation of the DegQ protease to exert protein quality control in the bacterial cell envelope. *J. Biol. Chem.* **286**, 30680–30690. 2011.

A. Schaeffer & B. Henrich: Rapid detection of *Chlamydia trachomatis* and typing of the lymphogranuloma venereum associated L-Serovars by TaqMan PCR. *BMC Infect. Dis.* **8**, 1–10. 2008.

A. Schubert, R. Wrase, R. Hilgenfeld & G. Hansen: Structures of DegQ from *Legionella pneumophila* Define Distinct on and off States. *J. Mol. Biol.* **427**, 2840–2851. 2015.

S. Sela-Abramovich, T. Chitlaru, O. Gat, H. Grosfeld, O. Cohen & A. Shafferman: Novel and unique diagnostic biomarkers for *Bacillus anthracis* infection. *Appl. Environ. Microbiol.* **75**, 6157–6167. 2009.

Q.-T. Shen, X.-C. Bai, L.-F. Chang, Y. Wu, H.-W. Wang & S.-F. Sui: Bowl-shaped oligomeric structures on membranes as DegP's new functional forms in protein quality control. *Proc. Natl. Acad. Sci.* **106**, 4858–4863. 2009.

B. Sixt, R. Valdivia & G. Kroemer: *Chlamydia trachomatis'* struggle to keep its host alive. *Microb. Cell* **4**, 101–104. 2017.

J. G. Sklar, T. Wu, D. Kahne & T. J. Silhavy: Defining the roles of the periplasmic chaperones SurA, Skp, and DegP in *Escherichia coli*. *Genes Dev.* **21**, 2473–2484. 2007.

J. Skórko-Glonek, D. Zurawa, E. Kuczwara, M. Wozniak, Z. Wypych & B. Lipinska: The *Escherichia coli* heat shock protease HtrA participates in defense against oxidative stress. *Mol. Gen. Genet.* **262**, 342–350. 1999.

A. Sobiecka-Szkatula, A. Gieldon, A. Scire, F. Tanfani, D. Figaj, T. Koper, J. Ciarkowski, B. Lipinska & J. Skorko-Glonek: The role of the L2 loop in the regulation and maintaining the proteolytic activity of HtrA (DegP) protein from *Escherichia coli*. *Arch. Biochem. Biophys.* **500**, 123–130. 2010.

G. Soldati, Z. H. Lu, L. Vaughan, A. Polkinghorne, D. R. Zimmermann, J. B. Huder & A. Pospischil: Detection of mycobacteria and chlamydiae in granulomatous inflammation of reptiles: A retrospective study. *Vet. Pathol.* **41**, 388–397. 2004.

C. Spiess, A. Beil & M. Ehrmann: A temperature-dependent switch from chaperone to protease in a widely conserved heat shock protein. *Cell* **97**, 339–347. 1999.

J. Storz & L. a. Page: Taxonomy of the Chlamydiae: Reasons for Classifying Organisms of the Genus *Chlamydia*, Family *Chlamydiaceae*, in a Separate Order, *Chlamydiales* ord. nov. *Int. J. Syst. Bacteriol.* **21**, 332–334. 1971.

K. L. Strauch, K. Johnson & J. Beckwith: Characterization of *depP*, a gene required for proteolysis in the cell envelope and essential for growth of *Escherichia coli* at high temperature. *J Bacteriol.* **171**, 2689–2696. 1989.

H. Su, L. Raymond, D. D. Rockey, E. Fischer, T. Hackstadt & H. D. Caldwell: A recombinant *Chlamydia trachomatis* major outer membrane protein binds to heparan sulfate receptors on epithelial cells. *Proc. Natl. Acad. Sci. U. S. A.* **93**, 11143–8. 1996.

K. H. Swamy, C. H. Chung & A. L. Goldberg: Isolation and characterization of protease Do from *Escherichia coli*, a large serine protease containing multiple subunits. *Arch. Biochem. Biophys.* **224**, 543–554. 1983.

K. A. Swanson, L. D. Taylor, S. D. Frank, G. L. Sturdevant, E. R. Fischer, J. H. Carlson, W. M. Whitmire & H. D. Caldwell: *Chlamydia trachomatis* polymorphic membrane protein D is an oligomeric autotransporter with a higher-order structure. *Infect. Immun.* **77**, 508–516. 2009.

L. Tang, J. Chen, Z. Zhou, P. Yu, Z. Yang & G. Zhong: Chlamydia-secreted protease CPAF degrades host antimicrobial peptides. *Microbes Infect.* **17**, 402–408. 2015.

N. Tegtmeyer, S. Wessler, V. Necchi, M. Rohde, A. Harrer, T. T. Rau, C. I. Asche, M. Boehm, H. Loessner, C. Figueiredo, M. Naumann, R. Palmisano, E. Solcia, V. Ricci & S. Backert: *Helicobacter pylori* Employs a Unique Basolateral Type IV Secretion Mechanism for CagA Delivery. *Cell Host Microbe* **22**, 552–560.e5. 2017.

T. C. Terwilliger, R. W. Grosse-Kunstleve, P. V. Afonine, N. W. Moriarty, P. H. Zwart, L. W. Hung, R. J. Read & P. D. Adams: Iterative model building, structure refinement and density modification with the PHENIX AutoBuild wizard. *Acta Crystallogr. Sect. D Biol. Crystallogr.* **64**, 61–69. 2007.

D. Theegarten, K. Sachse, B. Mentrup, K. Fey, H. Hotzel & O. Anhenn: *Chlamydophila spp.* infection in horses with recurrent airway obstruction: Similarities to human chronic obstructive disease. *Respir. Res.* **9**, 1–9. 2008.

N. Thomson, M. Holden, C. Carder, N. Lennard, S. Lockey, P. Marsh, P. Skipp, I. Goodhead, H. Norbertzcak, B. Harris, D. Ormond, R. Rance, M. a. Quail, J. Parkhill, R. S. Stephens & I. N. Clarke: *Chlamydia trachomatis*: genome sequence analysis of lymphogranuloma venereum isolates. *Genome Res* **18**, 161–171. 2008.

J. Tommassen: Assembly of outer-membrane proteins in bacteria and mitochondria. *Microbiology* **156**, 2587–2596. 2010.

W. G. Touw, C. Baakman, J. Black, T. A. Te Beek, E. Krieger, R. P. Joosten & G. Vriend: A series of PDB-related databanks for everyday needs. *Nucleic Acids Res.* **43**, D364–D368. 2015.

K. D. Tsirigos, P. G. Bagos & S. J. Hamodrakas: OMPdb: A database of β-barrel outer membrane proteins from Gram-negative bacteria. *Nucleic Acids Res.* **39**, 324–331. 2011.

D. Vanrompay, A. A. Andersen, R. Ducatelle & F. Haesebrouck: Serotyping of European isolates of *Chlamydia psittaci* from poultry and other birds. *J. Clin. Microbiol.* **31**, 134–137. 1993.

M. Vouga, D. Baud & G. Greub: *Simkania negevensis* may produce long-lasting infections in human pneumocytes and endometrial cells. *Pathog. Dis.* **75**, 1–10. 2017.

M. Vouga, J. Liénard, L. Baskin, D. Baud & G. Greub: What is the true clinical relevance of *Simkania negevensis* and other emerging *Chlamydiales* members ? *New Microbes New Infect.* **23**, 1–5. 2018.

P. R. H. Waller & R. T. Sauer: Encoding Homologs of the DegP Protease **178**, 1146–1153. 1996.

S. P. Wang & J. T. Grayston: Three new serovars of *Chlamydia trachomatis*:Da,Ia and L2a. *J. Infect. Dis.* **163**, 403–405. 1991.

Y. Wang: Etiology of trachoma: a great success in isolating and cultivating *Chlamydia trachomatis*. *Chinese Medical Journal* **112**, 938–941. 1999.

E. Weir: Upsurge of genital *Chlamydia trachomatis* infection. *Can. Med. Assoc. J.* **51**, 171. 2004.

M. S. Weiss & R. Hilgenfeld: On the use of the merging R factor as a quality indicator for X-ray data. *J. Appl. Crystallogr.* **30**, 203–205. 1997.

Z. Wen, M. A. Boddicker, R. M. Kaufhold, P. Khandelwal, E. Durr, P. Qiu, B. J. Lucas, D. D. Nahas, J. C. Cook, S. Touch, J. M. Skinner, A. S. Espeseth, C. T. Przysiecki & L. Zhang: Recombinant expression of *Chlamydia trachomatis* major outer membrane protein in *E. coli* outer membrane as a substrate for vaccine research. *BMC Microbiol.* **16**, 1–13. 2016.

C. Wilken, K. Kitzing, R. Kurzbauer, M. Ehrmann & T. Clausen: Crystal Structure of the DegS Stress Sensor. *Cell* **117**, 483–494. 2004.

M. D. Winn, C. C. Ballard, K. D. Cowtan, E. J. Dodson, P. Emsley, P. R. Evans, R. M. Keegan, E. B. Krissinel, A. G. Leslie, A. McCoy, S. J. McNicholas, G. N. Murshudov, N. S. Pannu, E. A. Potterton, H. R. Powell, R. J. Read, A. Vagin & K. S. Wilson: Overview of the CCP4 suite and current developments. *Acta Crystallogr. Sect. D Biol. Crystallogr.* **67**, 235–242. 2011.

R. Wrase, H. Scott, R. Hilgenfeld & G. Hansen: The *Legionella* HtrA homologue DegQ is a self-compartmentizing protease that forms large 12-meric assemblies. *Proc. Natl. Acad. Sci. U. S. A.* **108**, 10490–10495. 2011.

X. Wu, L. Lei, S. Gong, D. Chen, R. Flores & G. Zhong: The chlamydial periplasmic stress response serine protease cHtrA is secreted into host cell cytosol. *BMC Microbiol.* **11**, 22–31. 2011.

T. Y. Yen, S. Pal & L. M. De La Maza: Characterization of the disulfide bonds and free cysteine residues of the *Chlamydia trachomatis* mouse pneumonitis major outer membrane protein. *Biochemistry* **44**, 6250–6256. 2005.

Acknowledgements

At first I would like to thank Prof. Dr. rer. nat. Dr. h.c. Rolf Hilgenfeld who gave me the opportunity to do my PhD thesis in his institute. I really appreciate the good working atmosphere at the institute, the good laboratory infrastructure and the possibility to regularly use the P11 beamline at DESY in Hamburg.

My deepest gratitude goes to my direct supervisor Dr. Guido Hansen for his constant support especially regarding crystallography. He was always an excellent discussion partner and listened to all my scientific problems. A big thank you for that, Guido!
I would also like to give many thanks to Britta Schwarzloh, Walter Verheyen and Achim Kraus who gave me constant support in and out of the lab and became real friends over the years (over a lot of excellent coffee). Thank you!
Special thanks to Antje Lindae for the many fruitful discussions, the proofreading of this thesis and the good times we had together.

I would also like to thank Dr. Jeroen R. Mesters for the many good advices regarding crystallography and structure elucidation. Equally important, I appreciated the help, discussions and suggestions from my colleagues: Prof. Dr. Stefan Anemüller, Dr. Jian Lei, Susanne Zoske, Silke Schmidtke, Raffaele Ciriello, Mia Lahey-Rudolph, Jens Klingenbeil and the entire staff of the biochemistry department.
Furthermore, I acknowledge the outstanding preliminary work of Robert Wrase.

I thank the *Deutsche Forschungsgesellschaft* for the financial support.

Finally, my very special thanks are for my husband Friedemann and his unlimited love and support in every situation of my life, and for my parents who were always encouraging and supporting me during this challenging time!